N64-27870
(ACCESSION NUMBER)
350
(PAGES)
CR-55893
(NASA CR OR TMX OR AD NUMBER)
(THRU)
1
(CODE)
06
(CATEGORY)
FACILITY FORM 602

NASA CR-55893
EOS Report

FINAL REPORT

STUDY OF A FLIGHT EXPERIMENT OF SOLAR-CONCENTRATOR REFLECTIVE SURFACES

prepared for

NATIONAL AERONAUTICS AND SPACE ADMINISTRATION

by

The Staff of the Optics Division and the Aerospace Electronics Division

1 November 1963

Contract NAS 1-2880

This report is reproduced photographically
from copy supplied by the contractor.

OTS PRICE

XEROX $ 19.75 ph

MICROFILM $ _____

ELECTRO-OPTICAL SYSTEMS, INC.
300 N. HALSTEAD ST., PASADENA, CALIFORNIA

NOTICE

This report was prepared as an account of Government-sponsored work. Neither the United States, nor the National Aeronautics and Space Administration (NASA), nor any person acting on behalf of NASA:

a. Makes any warranty or representation expressed or implied with respect to the accuracy, completeness, or usefulness of the information contained in this report, or that the use of any information, apparatus, method, or process disclosed in this report may not infringe privately-owned rights; or

b. Assumes any liabilities with respect to the use of, or for damages resulting from the use of any information, apparatus, method, or process disclosed in this report.

As used above, "person acting on behalf of NASA" includes any employee or contractor of NASA, or employee of such contractor, to the extent that such employees or contractor of NASA, or employee of such contractor prepares, disseminates, or provides access to, any information pursuant to his employment or contract with NASA, or his employment with such contractor.

Requests for copies of this report should be referred to:

National Aeronautics and Space Administration
Office of Scientific and Technical Information
Washington, 25, D.C.

Attention: AFSS-A

FOREWORD

This final report covers the study program conducted from June 1963 to November 1963 on contract NAS 1-2880. The work was performed at Electro-Optical Systems, Inc. by the staff of the Optics Division and the Aerospace Electronics Division. The Project Manager was P. A. Button; the Associate Project Manager was D. E. McDowell. The following persons assisted in the program and the preparation of this report: J. T. Arnold; M. L. Dalton; D. P. Foote; H. D. Goodman; G. R. Griffin; P. L. Johnson; B. E. Kalensher; D. G. Marlow; D. H. McClelland; C. W. Reed; A. Schaffer; R. D. Villwock; and E. Zeiner. The program was under the direction of the Technical Monitor, Mr. Atwood Heath, Jr., of the NASA-Langley Research Center.

Reviewed and approved by

Peter A. Button
Project Manager

Approved by

Russell A. Temple for
Charles W. Stephens
Manager, Optics Division

ABSTRACT

27870

Final report on a study program involving a flight experiment for the determination of the effects of space environment on the performance of solar concentrator reflective surfaces. The program included definition of the factors in space that will affect concentrator surfaces, the selection of concentrator surface samples for evaluation, and the analysis and prediction of the effects of a space environment on concentrator surfaces. Also reported, is the work on the simulation of a space environment for ground tests, and the designs of two complete satellite systems for testing concentrator samples in space.

Author

CONTENTS

1. INTRODUCTION 1-1

2. EXPERIMENT DEFINITION 2-1

2.1 Space Environment Definition 2-2

2.1.1 Introduction 2-2

2.1.2 Temperature 2-4

2.1.3 Pressure-Density 2-5

2.1.4 Meteoroids 2-8

2.1.5 Electromagnetic Radiations 2-12

2.1.6 Geomagnetic Field 2-20

2.1.7 Charged Particle Radiations 2-22

2.2 Sample Selection 2-35

2.2.1 Possible Surface Sample Materials 2-35

2.2.2 Suggested Surface Sample Selection for Flight Experiment 2-42

2.3 Analysis and Prediction of the Effects of the Space Environment on Reflective Surfaces 2-44

2.3.1 Thermal Behavior of Mirrors in Space 2-44

2.3.2 Degradation of Reflecting Surfaces by Micrometeoroids 2-52

2.3.3 Effect of Charged Particles on Reflective Surfaces 2-60

2.3.4 Nonthermal Effects of Solar Ultraviolet Radiation 2-61

2.3.5 Other Causes of Mirror Degradation 2-62

2.4 Experiment Requirements 2-64

2.4.1 Experimental Operational Philosophy 2-64

2.4.2 Sample Exposure 2-66

2.4.3 Measurements 2-70

CONTENTS (contd)

2.4.4 Separation of Effects 2-77

2.4.5 Instrumentation Operational Philosophy 2-79

2.4.6 Ground Simulation 2-81

3. PREFERRED AND MINIMUM FLIGHT EXPERIMENT LAUNCH VEHICLE 3-1

3.1 Orbital Analysis 3-1

3.1.1 Payload/Orbit Altitude Study 3-1

3.1.2 Passage Through Earth's Shadow 3-5

3.1.3 Time Spent in Earth's Shadow 3-9

3.1.4 Direct Ascent Trajectory versus "Parking Orbit 3-9

3.2 Preferred and Minimum Flight Experiment Launch Vehicle Recommendations 3-12

3.2.1 The Scout Vehicle 3-14

3.2.2 The P-11 Vehicle 3-15

4. PREFERRED FLIGHT EXPERIMENT 4-1

4.1 Measurements 4-1

4.1.1 Reflectivity Measurements 4-4

4.1.2 Temperature Measurements 4-9

4.1.3 Space Environment 4-13

4.1.4 Samples and Separation of Effects 4-15

4.2 Instrumentation 4-19

4.2.1 Reflectivity 4-19

4.2.2 Instrumentation for Temperature Measurements on Samples 4-43

4.2.3 Space Environment 4-44

4.3 Orientation System 4-48

4.3.1 Perturbing Torques 4-48

4.3.2 Spin Damping 4-58

4.3.3 Impulse Budget 4-60

4.3.4 Orientation Control 4-60

4.3.5 Orientation Control Analysis 4-72

4.3.6 Propellant Requirement 4-80

4.3.7 Propellant System 4-80

4.3.8 Balanced vs Unbalanced Torquing 4-81

CONTENTS (contd)

4.4 Satellite Power System Design 4-84

4.4.1 Selection of Storage Battery Type 4-84

4.4.2 Probable Orbit and Solar Panel Power Output 4-85

4.4.3 The +13-Volt Regulator 4-85

4.4.4 The +28-Volt Regulator 4-86

4.4.5 The Storage Battery and Constant Current Charger 4-86

4.4.6 Power Supply Housekeeping 4-88

4.4.7 Summary 4-88

4.5 Telemetry and Command System 4-90

4.5.1 Functions of Telemetry and Command Subsystem 4-90

4.5.2 Constraints on Experiment Telemetry 4-91

4.5.3 Design of Telemetry 4-93

4.5.4 Synthesis and Design of Command Subsystem 4-107

4.5.5 Selection of Components for a Functional Telemetry and Command System 4-111

4.6 Preferred Experiment System Operation 4-114

4.7 Ground Support Program 4-115

4.7.1 Prelaunch Check 4-115

4.7.2 Countdown Check 4-115

4.7.3 Post Launch Data Acquisition and Tracking Ground Support Program 4-116

4.8 Systems Design 4-121

4.8.1 Systems Performance Requirements 4-121

4.8.2 Interface Parameters 4-125

4.8.3 Reliability Considerations 4-148

5. MINIMUM FLIGHT EXPERIMENT 5-1

5.1 Minimum Reflectivity Experiment 5-2

5.2 Orientations and Orbits 5-4

5.3 Additional Instrumentation 5-4

5.4 Telemetry and Command 5-5

5.5 Power System 5-7

CONTENTS (contd)

6. SUBTASK 3.1 - GROUND SIMULATION TEST DEFINITION 6-1

6.1 Introduction 6-1

6.2 General Discussion 6-2

6.2.1 Samples to be Tested 6-2

6.2.2 Space Environment Definition 6-2

6.2.3 Thermal Considerations 6-3

6.2.4 Pressure Considerations 6-3

6.2.5 Micrometeoroid Investigation 6-4

6.2.6 Ground Simulation Testing Philosophy 6-6

6.3 Test Program 6-9

6.3.1 Thermal Study 6-9

6.3.2 Electromagnetic Radiation 50 Å - 23,000 Å 6-17

6.3.3 Charged Particles 6-35

6.3.4 Combined EMR and Charged Particles 6-44

6.4 Summary and Conclusion 6-49

7. FABRICATION PROGRAM 7-1

7.1 Preferred Flight Experiment 7-1

7.2 Minimum Flight Experiment 7-1

8. SUMMARY OF RECOMMENDATIONS 8-1

REFERENCES

APPENDIX A — SOLAR COLLECTOR TEST SATELLITE

APPENDIX B — ELECTRICAL INTERCONNECTIONS BETWEEN SUBSYSTEMS

ILLUSTRATIONS

Figure		Page
2-1	Kinetic temperature as a function of altitude (Ref. 1)	2-6
2-2	Atmospheric pressure as a function of altitude (Ref. 1)	2-6
2-3	Atmopsheric density as a function of altitude (Ref. 4)	2-7
2-4	Density of the upper atmosphere (Ref. 5)	2-7
2-5	Distribution of corrected velocities for 285 sporadic and 74 shower meteors (Refs. 7,29)	2-11
2-6	Distribution of visual sporadic meteor-radiants in ecliptic latitude (Ref. 7)	2-13
2-7	Cumulative meteoroid impact rates near the earth (Ref. 8)	2-13
2-8	Solar electromagnetic radiation, at earth's distance from the sun (Ref. 2)	2-16
2-9	Albedo and earth radiation variation with altitude (Ref. 3)	2-16
2-10	Solar spectral energy distribution from 2000 Å to x-rays (Ref. 9)	2-19
2-11	The geomagnetic field and the cavity boundary configuration when acted upon by the solar wind (Ref. 12)	2-23
2-12	Galactic cosmic particles vs energy per nucleon (Ref. 14)	2-25
2-13	Intensity of the various primary components of the galactic cosmic radiation as a function of geomagnetic latitude (Ref. 14)	2-25
2-14	Quiet day flux (electrons/cm^2/sec) contours of electrons with energies greater than 20 kev which form the electron belt of the Van Allen radiation belt. The high energy photon flux contours of $E \geq 30$ Mev are also shown for reference (Refs. 16,17)	2-29
2-15	Quiet day low energy electron and photon flux contours as approximated by Van Allen (Ref. 18)	2-29

ILLUSTRATIONS (contd)

Figure		Page
2-16	Electron flux distribution of the magnetosphere as a function of geocentric radial distance on the geomagnetic equator	2-32
2-17	Proton flux distribtuion of the magnetosphere as a function of geocentric radial distance	2-32
2-18	Integral electron and proton spectra on the geomagnetic equator at various geocentric radial distances	2-33
2-19	Summary of observed omnidirectional intensities of electrons ($E \geq 40$ kev) in the magnetic equatorial plane obtained from approximately twenty complete orbits of Explorer 14 during October-December 1962 and from Explorer 12 during August-December 1961 (Ref. 26)	2-34
2-20	Various satellite configurations	2-68
2-21	Typical reflectance coefficients R_s and R_p as a function of angle of incidence	2-74
2-22	Solar irradiance as modified by reflectivity characteristics	2-74
3-1	Transfer ellipse from initial to final orbit	3-4
3-2	Payload in elliptical orbit vs altitude of apogee, for several booster combinations (fixed perigee altitude = 300 N. Mi.)	3-4
3-3	Cross section of earth's shadow (not drawn to scale)	3-6
3-4	Definition of γ, λ, i	3-10
3-5	Orbit period and maximum time spent in earth's shadow vs orbit altitude (circular orbit)	3-10
3-6	Apogee vs payload weight for Scout and P-11 vehicles	3-13
4-1	Preferred flight experiment	4-2
4-2	Various reflectometer systems	4-5
4-3	Reflectometer optical schematic	4-20
4-4	Dispersing system schematic	4-24
4-5	Beam divergence schematic	4-24
4-6	Relative output of tungsten at 2800°K as a function of wavelength	4-27

ILLUSTRATIONS (contd)

Figure		Page
4-7	Solar spectrum	4-27
4-8	Solar spectral irradiance outside the earth's atmosphere after Stair and Johnson, and Dunkelman and Scolnik	4-27
4-9	Geometry of spherical reflector	4-29
4-10	Detectivity as a function of wavelength for lead sulfide with a cutoff of 2.5 microns at 25°C	4-33
4-11	Detector and high input impedance amplifier	4-33
4-12	Orbit in ecliptic plane	4-51
4-13	Orbit normal to ecliptic plane	4-51
4-14	Arbitrary orbit orientation	4-51
4-15	Equivalent sphere for satellite	4-54
4-16	Satellite attitude control system	4-62
4-17	Sun sensor	4-64
4-18	Sun sensor mask	4-64
4-19	Schematic of attitude correction electronics	4-69
4-20	Body-fixed coordinate system	4-73
4-21	Relation of body-fixed to inertial system	4-73
4-22	Path of $\vec{\omega}$ in body-fixed coordinates	4-73
4-23	Dampers	4-75
4-24	Coordinate system	4-77
4-25	Motion of Z and H in inertial coordinates	4-77
4-26	Initial motion of Z and H	4-77
4-27	Precession of Z-axis following impulse	4-79
4-28	Motion of Z and H with repeated torquing	4-79
4-29	Motion in dead zone	4-79
4-30	Effect of damping on motion in dead zone	4-79
4-31	Block diagram, power subsystem	4-89
4-32	Reflectometer detector output wave form	4-94
4-34	Pulse code modulation data processing format	4-98
4-35	Block diagram of telemetry system data processor	4-98

ILLUSTRATIONS (contd)

Figure		Page
4-36	Antenna equivalent noise temperature as a function of frequency	4-104
4-37	Approximate orbit of satellite	4-104
4-38	Telemetry subsystem functional block diagram	4-106
4-39	System power programmer and cutoff timer	4-110
4-40	Satellite automatic test system	4-117
4-41	Electrical block diagram of the solar collector test satellite	4-126
4-42	Power profile	4-127
5-1	Minimum flight experiment	5-3
5-2	Block diagram of P-11 telemetry and command system	5-6
6-1	Tentative ground simulation test schedule	6-10
6-2	Measurement of thermal conductivity	6-12
6-3	Measurement of $\frac{\alpha}{E}$ of reflective surfaces	6-12
6-4	Measurement of effective emissivity (E) of reflective surfaces	6-12
6-5	Schematic of carbon arc refractive radiative transfer system	6-20
6-6	Solar ultraviolet filter configurations for xenon and mercury xenon compact arcs	6-26
6-7	Schematic for xenon arc reflective radiative transfer system	6-26
6-8	Schematic of xenon arc catadioptric radiative transfer system	6-26
6-9	Typical particle accelerator equipment and insulation	6-42
6-10	Charged particle sample irradiation test setup schematic	6-45
6-11	Combined EMR charged particle test setup (plan view)	6-45
7-1	Solar concentrator reflective surface flight experiment schedule (preferred flight experiment)	7-2
A-1	Solar collector test satellite engineering drawing	A-1

TABLES

Number		Page
2-1	Atmospheric pressure, temperature, particle density and composition at selected altitudes (Ref. 2)	2-9
2-2	Cumulative energy distribution in sunlight, at earth's distance from the sun (Ref. 2)	2-15
2-3	Intensity at 1 astronomical unit produced by the strongest solar emission lines (Ref. 9)	2-18
2-4	Electron and proton fluxes measured by Explorer 14 near the equatorial plane (Ref. 22)	2-30
2-5	Possible surface sample materials	2-43
2-6	Fortran program for mirror temperature calculation	2-47
2-7	Earth emission and albedo view factor	2-48
2-8	Mirror temperatures under various conditions	2-49
2-9	Physical properties of mirror substrate materials	2-55
2-10	Target constants for mirror substrate materials	2-56
2-11	Fractional surface area loss per year for mirror substrate materials	2-57
2-12	Fractional surface area loss per year for mirror substrate materials based on new Whipple estimate	2-58
2-13	Comparison of preferred and minimum experiments to optimum	2-65
4-1	Preferred experiment sample selection and separation of effects	4-17
4-2	Characteristics of photoelectric detectors	4-30
4-3	Flight experiment - radiation detection instrument	4-45
4-4	Impulse budget for one year	4-61
4-5	Attitude control propellant mass and storage volume	4-66

TABLES (contd)

Number		Page
4-6	Typical weight and power required of various submultiplexer combinations	4-95
4-7	Telemetry and command subsystem component parts list	4-112
4-8	Satellite weight breakdown	4-138
4-9	Calculated thermal history of vehicle	4-146
4-10	Chart form of the exponential failure	4-150
6-1	Charged particles, energies, and flux level summary	6-35
6-2	Energy and flux output capabilities	6-41
7-1	Preferred flight experiment cost	7-3
7-2	Minimum flight experiment cost	7-5

1. INTRODUCTION

It is rapidly becoming apparent that the development of space power systems for advanced space missions will be one of the most critical problem areas in space technology during the next one or two decades. The only two basic energy sources which presently appear capable of meeting the requirements of these missions are solar energy and nuclear energy. Up to certain power levels solar energy systems are lighter, safer to operate and less expensive. A solar energy system consists of the solar concentrator, the absorber, and the energy conversion device. Thus, the overall system performance is a function of the performance of these three subsystems.

The performance of a solar concentrator is dependent on the geometrical accuracy and spectral/specular reflectivity of the concentrator surface. Considerable effort has been, and is being, directed at developing fabrication techniques for obtaining the required geometrical accuracies and in investigating materials which, in ground tests, demonstrate high spectral reflectivity. One area in which data are critically weak, however, is that of performance and life of highly reflective surfaces in the space environment. This results from two factors: uncertainty of the space environment and the difficulty to simulate effectively those characteristics known to be present. The problems of simulation become particularly difficult when the necessity for long duration tests and combinations of physical effects are considered.

ABST

The subject of this report is a feasibility study of a flight experiment for accurate determination of the performance of the reflective properties of solar concentrators in space. This study

includes a definition of the basic experiment which involves an evaluation of the space environment as it is presently known, a selection of the solar concentrator samples to be tested, an analysis and prediction of the performance of the samples in the space environment and the generation of the experiment requirements. A preferred and minimum flight experiment with respect to meaningful results and cost are given. Both flight experiments are described with respect to the instrumentation, satellite attitude control, power, telemetry and command systems, operation, ground support equipment, and general systems design. The instrumentation includes not only the basic reflectivity measurement but other complementary measurements (temperature and space environment). Techniques of separating and identifying the specific causes of sample degradation are included. Recommendations for a program to simulate the effects of the space environment to supplement any already performed are discussed. Finally, the estimated cost and time for detailed design, fabrication and checkout of the preferred and minimum flight experiments is given.

AUTHOR

The study program was organized into four major tasks each of which have subtasks. These are:

Task 1 - Space Environment and Effects Study
- Subtask 1.1 - Environment Definition
- Subtask 1.2 - Reflective Sample Selection
- Subtask 1.3 - Analysis and Prediction

Task 2 - Instrument Design
- Subtask 2.1 - Experiment Definition
- Subtask 2.2 - Instrument Design

Task 3 - Ground Simulation Test Study
- Subtask 3.1 - Test Definition
- Subtask 3.2 - Test Equipment

Task 4 - Systems Study
- Subtask 4.1 - Systems Analysis
- Subtask 4.2 - Structures and Packaging

Subtask 4.3 - Power System

Subtask 4.4 - Thermal Control

Subtask 4.5 - Orientation System

Subtask 4.6 - Orbital Analysis

Subtask 4.7 - Telemetry System

Subtask 4.8 - Ground Support Equipment

Subtask 4.9 - System Integration

Subtask 4.10 - Quality Assurance

Subtask 4.11 - Fabrication Program

The duration of the study program was about four months starting in July 1963. This report contains information presented in the monthly reports and can be considered as being a complete description of the program. The organization of the report includes the experiment definition, the preferred and minimum flight experiment launch vehicle, the preferred flight experiment, the minimum flight experiment, the ground simulation test study and the fabrication program.

2. EXPERIMENT DEFINITION

The objective definition of a space experiment and the execution of its detailed design are somewhat difficult and complex. The number of variables involved in designing a space flight experiment for solar-concentrator reflector surfaces is very large and most of them are interrelated. This section is an attempt to define an experiment that will answer questions regarding the performance of solar-concentrator reflective surfaces in space. The point of view of this section is that of the experimenter although, it must be admitted, the known requirements of space systems and subsystems such as launch vehicle orbit capability, telemetry and power systems have influenced the experiment definition to some degree (and rightly so for practical purposes).

This section describes the space environment as it is presently known. In addition, a general discussion of the various samples which might and should be tested is presented. Based upon the above, an analysis and prediction task was undertaken to attempt to predict the behavior of the reflective samples in space. This prediction is used for the experiment definition and requirements. The experiment requirements include the experimental orbital philosophy, sample exposure, the individual measurements that should be performed, the necessary separation of effects, the instrument operational philosophy and the correlation of the flight experiment with the ground simulation tests.

2.1 Space Environment Definition

2.1.1 Introduction

Engineering assessment and evaluation of the behavior of materials in space requires complete knowledge of the space environment in the regions to be encountered by these materials. A survey of the current state of knowledge of space physics reveals many wide gaps in the data and many variations in models set forth to explain and correlate scattered data collected in space explorations with terrestrial and astronomical observations. It is, therefore, difficult to conclude with precision the environments a particular earth satellite or planetary probe will encounter during a planned mission. This section attempts to summarize the current knowledge of the space environment in order to provide guidelines for analysis and engineering efforts in planning a meaningful flight test. The material provided in this section is quantitative wherever possible, but in many instances where data are inconclusive, questionable, or lacking, the best estimates of recognized experts have been provided.

Environments to which materials in space will be exposed have been classified for the purposes of our study into the following headings:

1. Temperature
2. Pressure
3. Meteoroids
4. Electromagnetic Radiations
5. Geomagnetic Fields
6. Charged Particles

In the present study program we are primarily concerned with effects of the environment on solar-concentrator reflective surfaces. Since reflection is primarily a surface characteristic we are particularly sensitive to aspects of the environment that might not ordinarily pose much of a hazard to materials or structures in which mechanical strength, chemical or electrical characteristics alone are the

prime considerations. An example is the damaging effect to surfaces resulting from exposure to low energy charged particles as opposed to the more penetrating charged particle and electromagnetic radiations. Unfortunately, it is the low energy charged particle of space of which the least is known. Most of the early space exploratory satellites and probes have contained simple detectors that were selective for high energy radiations to the exclusion of the low energy particles. Recent data, from Explorers 12 and 14 with more sophisticated equipment, indicate that high levels of the lower energy particles exist in the Van Allen Belt regions. Another region of which little is known is the area immediately in the vicinity of the magnetopause and the regions of interplanetary space. Another cause for uncertainty arises from temporal variations due to solar storms of varying intensities that distort the geomagnetic trapping areas causing unpredictable and wide fluctuations in intensity, energy, and spatial distribution of the charged particles. Certainly the space "weather" is very difficult if not impossible to predict with a high degree of accuracy.

The region of space considered, for purposes of this study, is bounded by the minimum altitude suitable to an earth satellite out to the outer limits of the magnetopause. This is approximately equivalent to altitudes lying between 100 miles to 10 to 12 earth radii, or about 40,000 to 48,000 miles altitude. Of principal concern then, are the trapped radiations occurring within the magnetosphere; the changes in these belts resulting from solar flares; and the cosmic and solar emissions in the form of electromagnetic and charged particle radiations penetrating this region.

Treatment of cosmic radiation has been limited to basic data sufficient to indicate the relative effectiveness, or ineffectiveness, of damage from this source of radiation. More complete treatises are readily available in the literature and standard reference books. For the purposes of this study, cosmic rays are a negligible factor in materials degradations.

The subjects of temperature and pressure as a function of altitude has been included to be complete. However, at the altitudes under consideration, we are primarily concerned with the atomic density or the number of particles per unit volume found in space and the speed of these particles (their kinetic temperature). These data may be of importance when considering the relative speed of a satellite and slowly, or swiftly, moving uncharged atomic particles on collision with the surfaces of the satellite.

In the case of micrometeoroids, the potential physical damage possible to surfaces of the satellite from these bits of matter can be easily appreciated. In some cases, there can be actual penetration of the surface by swift, dense meteoroids. These cases are somewhat a matter of chance and the degree of risk can be inferred.

The extremely high levels of electromagnetic radiant energy in the ultraviolet region of the spectrum originating with the sun combined with the earth's albedo, cause a good deal of attention to be focused on this subject. In particular, the existing intensities and spectral distributions of these electromagnetic radiations are of concern when studying materials effects because of the possible selective absorption or sensitivity of the material to particular wavelengths. Degradation of spectral reflectance with excess absorptivity of the reflecting surface following prolonged exposure is of concern to the optical engineer. The damaging effect of the combined environment or reflecting surfaces exposed in space missions is certain to be more apparent than for other satellite structures.

2.1.2 Temperature

From a practical point of view the conditions of temperature in space are somewhat paradoxical. Temperature, being defined in terms of the average random kinetic energy of the molecules or translational motion, is determined from the following equation:

$$\frac{mv^2}{2} = \frac{3kT}{2}$$

where

v = average molecular velocity

k = Boltzmann constant

m = particle mass

T = temperature

From this it can be seen that temperature is proportional to the mass and the square of the velocity of the molecule or particle. As can be noted from Fig. 2-1 (Ref. 1) the kinetic temperature rises rapidly at altitudes above 100 km, which means that the particle is moving at very high speeds. At altitudes of 400 km and greater, the kinetic temperature is approximately 1500°K but here the atomic density is only about 10^7 atoms/cm^3. This low density of high temperature molecules or atoms will not greatly affect the temperature of the satellite. At these and higher altitudes the vehicle achieves a thermal balance between the sun (6000°K), earth (288°K blackbody), moon (123-400°K blackbody), its own internal heat sources, and space (4°K blackbody). Even at a pressure of 10^{-5} mm Hg (~100 km) and an assumed vehicle temperature of 300°K, the ratio of heat transfer by conductive means is about 10^{-3} of the radiative process. Heat transfer effects may usually be adequately simulated by testing pressures of 10^{-5} mm Hg.

2.1.3 Pressure-Density

Atmospheric pressure decreases from 760 mm Hg at sea level to a figure of less than 10^{-12} mm Hg beyond 4000 miles altitude (approximately one earth radius). (Refs. 1, 2, and 3). Figure 2-2 (Ref. 1) charts pressure as a function of altitude. As the pressure changes with altitude, there is also a change in the relative concentrations or densities of the constituent molecules or atoms, Fig. 2-3 (Ref. 4). At lower altitudes the N_2 molecule is predominant. At about 200 km altitude O_2 molecules dissociate into single neutral atoms and predominate. At altitudes above 1000 km He atoms begin to predominate. Above about 2500 km, H atoms predominate as noted from Fig. 2-4, (Ref. 5), which gives atmospheric and constituent

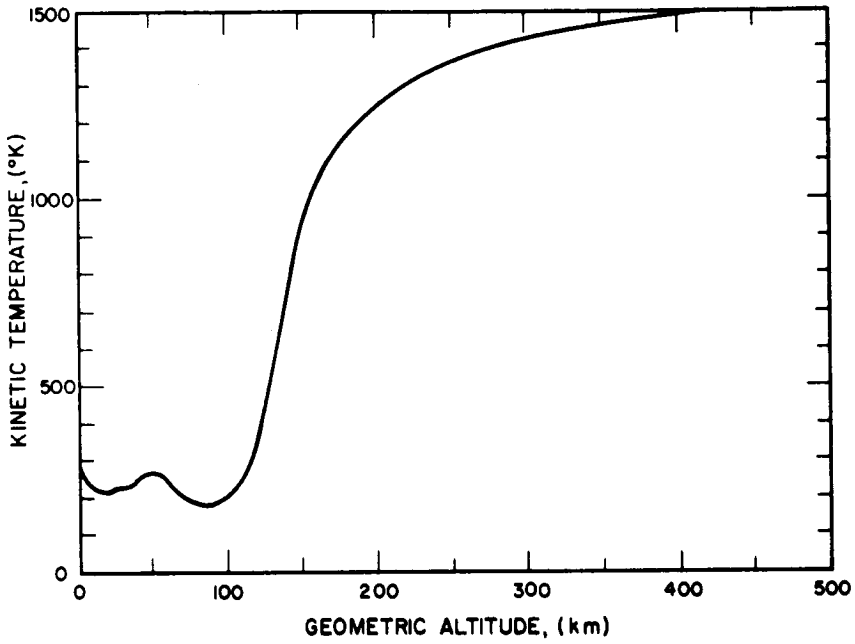

FIG. 2-1

KINETIC TEMPERATURE AS A FUNCTION OF ALTITUDE (Ref. 1)

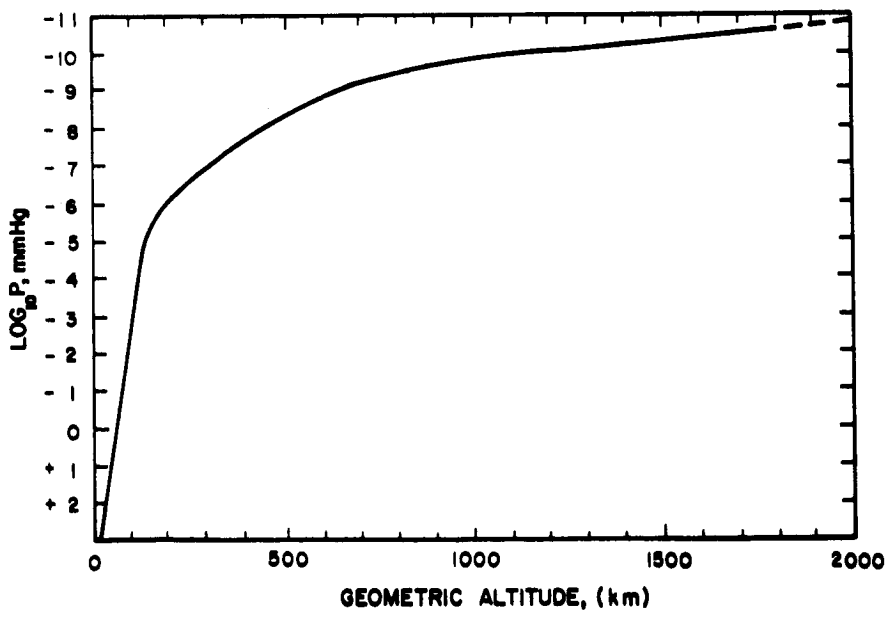

FIG. 2-2

ATMOSPHERIC PRESSURE AS A FUNCTION OF ALTITUDE (Ref. 1)

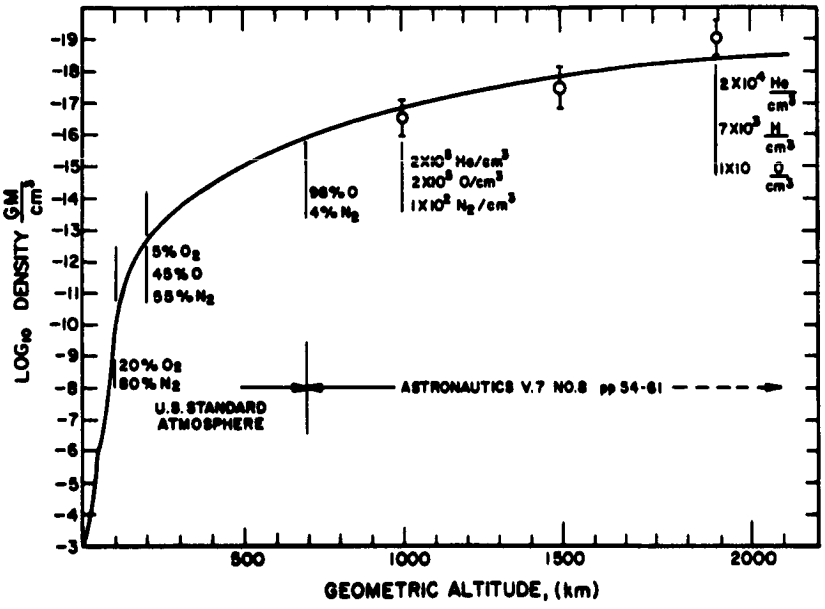

FIG. 2-3

ATMOSPHERIC DENSITY AS A FUNCTION OF ALTITUDE (Ref. 4)

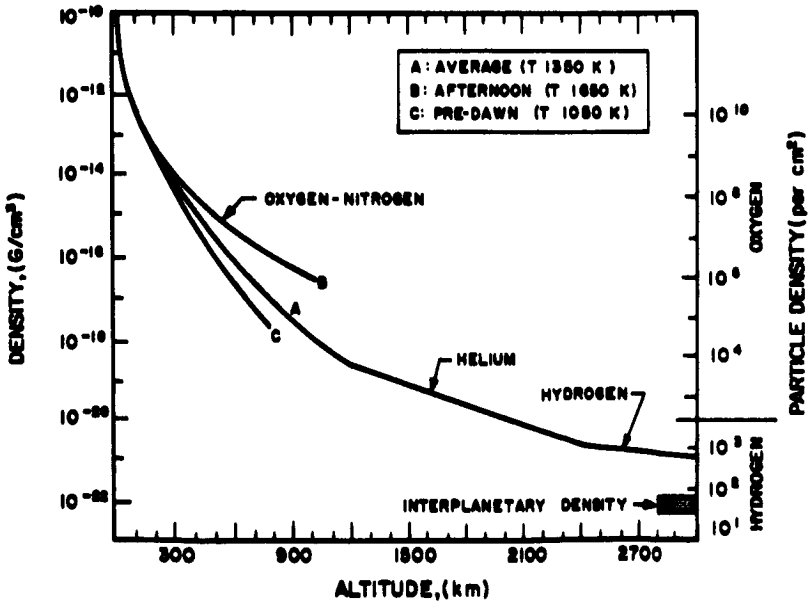

FIG. 2-4

DENSITY OF THE UPPER ATMOSPHERE (Ref. 5)

particle density as a function of altitude. Table 2-1 (Ref. 2) tabulates atmospheric pressure, temperature, particle density, concentration, and ionic composition at selected altitudes.

Singer (Ref. 6) defines the base of the exosphere as the level above which one half of the escaping atoms will undergo a collision. From this base at the top of the atmosphere, molecules may escape into space. At lower altitudes molecules are prevented from escaping by collisions with other molecules in the overlying atmosphere. The exosphere is, therefore, the fringe of the atmosphere that extends into space. This altitude is calculated to be 530 km which is equivalent to a geocentric radius of 6900 km. In the absence of collisions above the base of the exosphere, there will be no thermodynamic equilibrium and, in general, no Maxwellian distribution of velocities of the particles. Therefore, the concept of temperature cannot be used above this altitude.

2.1.4 Meteoroids

Damage to materials can result from meteoroids by erosion, perforation, spallation, and pressure shocks. The extent of damage is related to the flux rate, particle size and density, and impact speed. As is generally true of other elements of the space environment these data are not yet too accurately defined with respect to spatial distribution and are variable with time. Meteoroids may be classified as meteorites, meteors, and micrometeoroids or dust. These differ as to mass, density, orbit, and origin.

Meteorites

Masses of stone or metal reaching the earth from outer space, are believed to be of asteroidal origin and orbit the sun not far from the ecliptic. Their masses are often above 1 gram with densities of 3 to 3.5 gm/cm^3; about 10 percent are iron-nickel fragments with densities of 7 to 8 gm/cm^3. Their velocities are usually about 20 km/sec though they may have velocities of a maximum of 72 km/sec. They do not concentrate around the earth so that their flux in the vicinity of the earth is so low that collision with an earth satellite is highly improbable.

TABLE 2-1 ATMOSPHERIC PRESSURE, TEMPERATURE, PARTICLE DENSITY AND COMPOSITION AT SELECTED ALTITUDES (Ref. 2)

Altitude	Pressure, mm Hg	Temperature		Concentration molecules, atoms, or ions/cm^3	Composition
		°C	°F		
Sea level	$760 \simeq 10^3$	-40 to +40	-40 to +105	2.5×10^{19}	78% N_2, 21% O_2, 1% A
30 km (100,000 ft)	$90 \simeq 10^2$	-40	-40	4×10^{17}	N_2, O_2, A
200 km (125 mile)	10^{-6}	10^3	10^3	10^{10}	N_2, O, O_2, O^+
800 km (500 mile)	10^{-9}	10^3	10^3	10^6	O, O^+, H
6500 km (4000 mile)	10^{-13}	10^3	10^3	10^3	H^+, H
Above 22,000 km (14,000 mile)	$< 10^{-12}$	10^3 to 10^5	10^3 to 10^5	10^1 to 10^2	85% H^+, 15% He^{++}

Meteors

Visual flashes are caused by the entrance of meteoric particles into the earth's atmosphere. The majority of these particles, detectable visually or by radio, radar, or photography, are presumed to come from comet debris. They are mostly porous dust balls with a very low overall density, probably near 0.1 gm/cm^2 with a mass generally less than 1 gm down to the limit of detectability of 10^{-5} gm. Orbits are elliptic, mostly with high eccentricities, and occur at all angles to the plane of the ecliptic. These meteoric particles do not concentrate around the earth. Their velocities relative to the earth or a satellite range from a few km/sec outside the earth's gravitational field up to about 72 km/sec and average about 30 km/sec. Close to the earth the minimum velocity is increased by the earth's gravitational field to 11 km/sec. Closer to the sun, velocities increase. Some of the meteors are associated in showers moving together in elliptic orbits which the earth may intersect once or twice a year. Figure 2-5 gives the distribution of velocities for sporadic and shower meteors (Ref. 7). Figure 2-6 charts the number of particles as a function of ecliptic latitude, (Ref. 7).

Micrometeoroids

The fine dust particles are believed by some to be of the same cometary origin as the visible meteors. Density of the particles, or porous aggregates of dust, range from 0.05 to 3.5 g/cm^3. Minimum masses vary from about 4×10^{-10} g, at a density of 0.05 g/cm^3, to about 7×10^{-14} g, at a density of 3.5 g/cm^3. The maximum size approaches 10^{-5} g. Dust orbits around the sun are, in general, nearly circular and are near the plane of the ecliptic. Relative velocities are mostly under 20 km/sec. Predictions of increased dust concentration around the earth are confirmed by examination of the altitude dependence of micrometeoroid flux as measured by sounding rockets, satellites, and space probes. Attempts to quantitate the data indicate flux variation with a power of

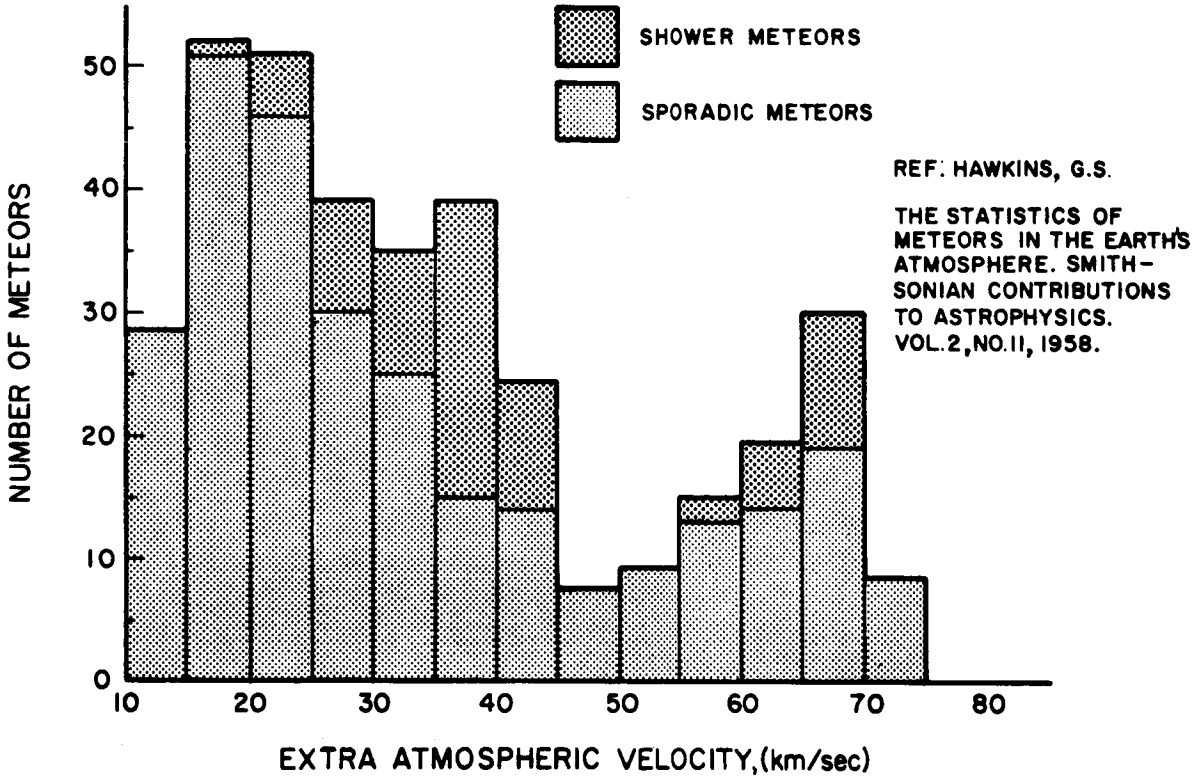

FIG. 2-5 DISTRIBUTION OF CORRECTED VELOCITIES FOR 285 SPORADIC AND 74 SHOWER METEORS (Refs. 7, 29)

R_e of between R_e^{-1} and R_e^{-2} where R_e is the geocentric radius. The dust cloud around the earth extends out about 10^6 km. The particles composing it are either spiralling in toward the earth or orbiting around it. Velocities relative to the earth probably average 7 to 15 km/sec at low altitudes, and 3 to 10 km/sec at higher altitudes. The dust cloud is held by gravitation. Atmospheric drag, including electrostatic drag, and interactions with solar radiation pressure may play a part in the earth's capture of this dust from the heliocentric orbits. In interplanetary space, the dust concentration increases toward the sun at about the 3/2 power of solar distance.

The chart given in Fig. 2-7 (Ref. 8) gives a comparison of data on cumulative meteoroid impact rates near the earth estimated by various workers. Whipple's curve, labeled 1963A, Fig. 2-7 represents the most recent estimation of influx rate by an expert in this field of study. This curve and the curve labeled "B" in the figure have been calculated for an average particle density, ρ, of 0.44 g/cm^3.

2.1.5 Electromagnetic Radiations

2.1.5.1 Infrared, Visible, Near Ultraviolet (λ>3000Å)

The total flux of solar electromagnetic radiation per unit area at 1 AU (astronomical unit) from the sun is known as the solar constant. The solar constant is given as follows:

$$2.0\ (\pm\ .04)\ \text{calories/cm}^2\text{/min}$$

$$\text{or}\quad 1.4\ (\pm\ .028) \times 10^6\ \text{erg/cm}^2\text{/sec}$$

The greatest bulk, or approximately 98.7% of electromagnetic energy existing within our solar system emanates from the sun in the spectral range above 3000 Å in the region between 0.3 and 7 microns.

The sun's energy spectrum is given in Fig. 2-8 for altitudes greater than 100 km (Ref. 2). The spectrum closely approximates the emission of a theoretical blackbody solar disk at a temperature of 6000°K, a commonly accepted figure used in calculations

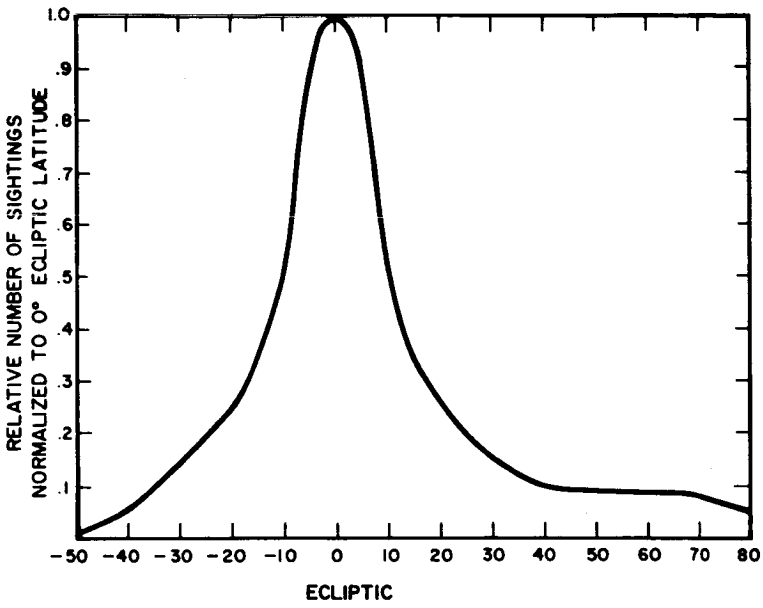

FIG. 2-6

DISTRIBUTION OF VISUAL SPORADIC METEOR-RADIANTS IN ECLIPTIC LATITUDE (Ref. 7)

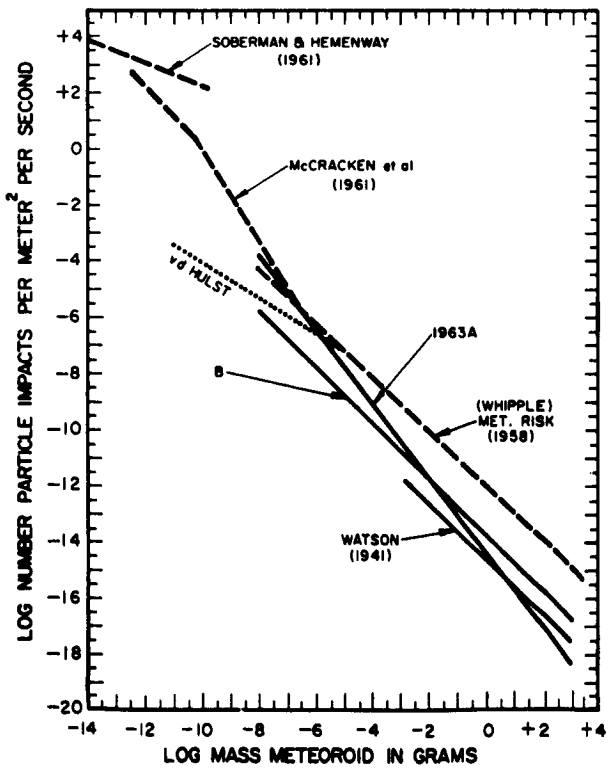

FIG. 2-7

CUMULATIVE METEOROID IMPACT RATES NEAR THE EARTH (Ref. 8)

involving solar energy. At distances large with respect to the sun's diameter, the irradiance may be considered to vary in accordance with the inverse square of the distance to the sun.

The sun's energy output remains very constant. Variations caused by sun spots and solar flares cause less than 0.4% change in output. Most of this change occurs at the short wavelengths. This is further discussed in Section 2.1.5.2. Table 2-2 (Ref. 2) gives a breakdown of the fraction of total energy and the total energy on a cumulative basis with increasing wavelength values.

Important to satellites is the effect of the atmosphere's reflectance and scattering properties, or albedo radiation, which causes an increase in the radiant energy to which the vehicle surfaces are exposed. The earth's hemispherical reflectance (albedo) averages 0.36 to 0.39 at visible wavelengths, with seasonal changes from about 0.3 to 0.5. Estimates for the near infrared are about 0.3; for the near ultraviolet about 0.5 (Ref. 2). For a 100-mile earth orbit and an assumed albedo of 0.36 the maximum radiant energy per unit area on a spherical vehicle is 400 watts/meter^2. Figure 2-9 shows the energy per unit area of spherical and flat surfaces as a function of altitude resulting from the earth's albedo and the earth's thermal radiant energy (Ref. 3).

Besides reflected sunlight, there will also be thermal emission from planets at far-infrared wavelengths. Close to the earth, this amounts to about 2×10^5 erg/cm^2/sec, peaking at 120,000 Å (12 microns). Much less than 0.1% of this radiation is at visible and ultraviolet wavelengths. The same is true of the radiation from the other planets. These radiations, as well as the zodiacal light caused by scattering of solar radiation by interplanetary dust particles of the order of 10^{-3} cm in size distributed throughout interplanetary space, are of negligible energy when compared to the direct solar radiation.

TABLE 2-2 CUMULATIVE ENERGY DISTRIBUTION IN SUNLIGHT, AT EARTH'S DISTANCE FROM THE SUN (Ref. 2)

Up to wavelength, Å	Fraction of total energy	Energy, at sunspot maximum (including flares) erg/cm^2-yr
0.1	10^{-11}	10^2 - 10^*
1	10^{-11}	10^2 - 10^3
10	10^{-8}	10^5 - 10^6
100	10^{-6}	10^7 - 10^8
500	10^{-6}	10^8
1,000	10^{-5}	10^8
1,500	10^{-5}	10^9
2,000	10^{-4}	4×10^9
2,500	1.3×10^{-3}	6×10^{10}
3,000	1.2×10^{-2}	5×10^{11}
4,000	9×10^{-2}	4.0×10^{12}
5,000	0.24	1.1×10^{13}
6,000	0.37	1.6×10^{13}
7,000	0.49	2.2×10^{13}
8,000	0.58	2.6×10^{13}
9,000	0.65	2.9×10^{13}
10,000	0.71	3.2×10^{13}
15,000	0.88	3.9×10^{13}
20,000	0.94	4.2×10^{13}
30,000	0.98	4.3×10^{13}
70,000	0.999	4.4×10^{13}

*10^9 to 10^{10} photons/cm^2-yr shorter than 0.1 Å.

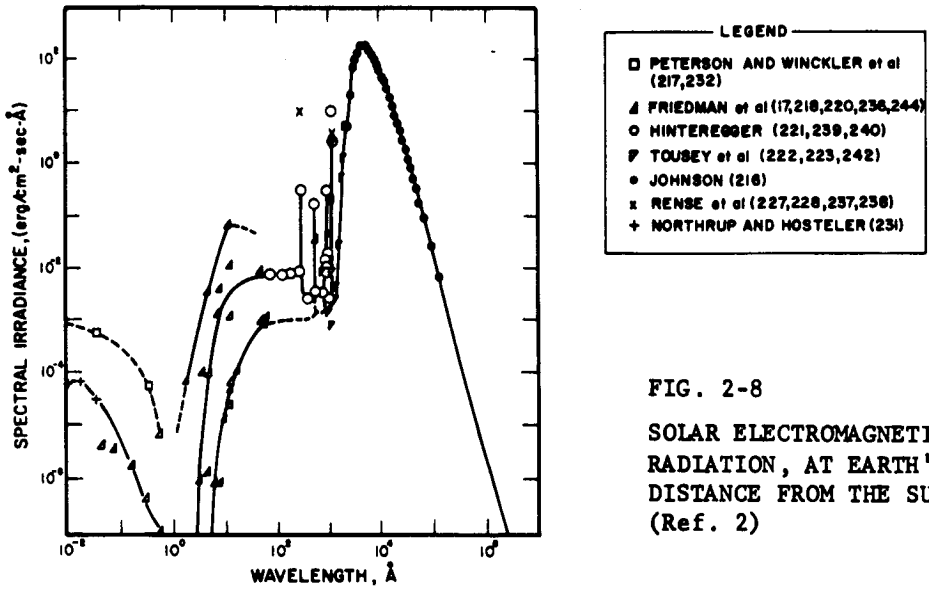

FIG. 2-8

SOLAR ELECTROMAGNETIC RADIATION, AT EARTH'S DISTANCE FROM THE SUN (Ref. 2)

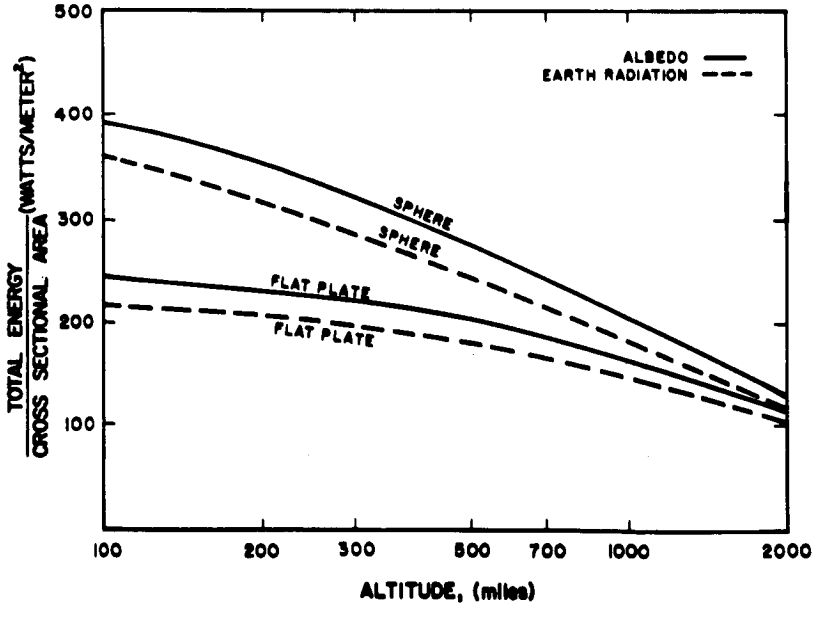

FIG. 2-9

ALBEDO AND EARTH RADIATION VARIATION WITH ALTITUDE (Ref. 3)

2.1.5.2 Ultraviolet X-Rays (λ less than 3000 Å)

As noted from Table 2-2 the fraction of total radiant energy below 3000 Å is about 1.2% of the sun's energy amounting to about 1.7×10^2 erg/cm^2/sec. Principal lines are given in Table 2-3. A chart of the solar ultraviolet spectrum is given in Fig. 2-10 (Ref. 9). During periods of solar flares the levels can be increased by several orders of magnitude for periods of a few hours. (Ref. 10).

The main reason for interest in these uv and x-ray emissions is because the photon energies are sufficiently high to initiate chemical reactions and ionization of materials. Such reactions can begin at wavelengths below 3000 Å in the near ultraviolet. Again, because of concern with surface effects these radiations are of more than usual interest even though their intensity levels are low. In view of transient nature of sunspots and solar flares the most practical presentation of data is in terms of yearly averages since a test vehicle would almost certainly be in orbit for a fair fraction of a year for a meaningful test of space environmental effects on materials.

Figure 2-10 (Ref. 9) summarizes results of rocket measurements of solar spectral energy distribution above the atmosphere. This chart gives data obtained during sunspot minimum in 1953 and 1954, marked A-16, and during sunspot maximum in 1956, marked A-43. They represent the minimum and maximum fluxes observed during a sunspot cycle. The shaded region added to the A-16 curve is the increment of flux measured below 20 Å and attributed to localized hot spots at 2 million degrees K. Near sunspot minimum in 1953 and 1954 the rocket measurements indicated a marked reduction in x-ray

TABLE 2-3 INTENSITY AT 1 ASTRONOMICAL UNIT PRODUCED BY THE STRONGEST SOLAR EMISSION LINES (Ref. 9)

λ(Å)	Identification	Erg/cm²/sec
1892.03	Si III (1)	0.10
1817.42 *	Si II (1)	0.45
1808.01		0.15
1670.81	Al II (2)	0.08
1657.00 *	C I (2)	0.16
1640.47	He II (12)	0.07
1561.40 *	C I (3)	0.09
1550.77	C IV (1)	0.06
1548.19	C IV (1)	0.11
1533.44	Si II (2)	0.041
1526.70	Si II (2)	0.038
1402.73	Si IV (1)	0.013
1393.73	Si IV (1)	0.030
1335.68	C II (1)	0.050
1334.51	C II (1)	0.050
1306.02	O I (2)	0.025
1304.86	O I (2)	0.020
1302.17	O I (2)	0.013
1265.04	Si II (4)	0.020
1260.66 *	Si II (4)	0.010
1242.78 *	N V	0.003
1238.80	N V	0.004
1215.67	H Ly-α	5.1
1206.52	Si III (2)	0.030
1175.70 *	C III (4)	0.010
1139.89 *	C I (20–23)	0.003
1085.70 *	N II (1)	0.006
1037.61 *	O VI (1)	0.025
1031.91	O VI (1)	0.020
1025.72	H Ly-β	0.060
991.58 *	N III (1)	0.010
989.79 *	N III (1)	0.006
977.03	C III (1)	0.050
949.74	H Ly	0.010
937.80	H Ly	0.005
835 *	O II, III	0.010

The value for Lyman-α applies to the intensity within the 1-Å wide central part of the line (based on an ion-chamber reading of 6.0 erg/cm²/sec).

* Indicated that the line is a blend of lines of other elements or is an unresolved multiplet.

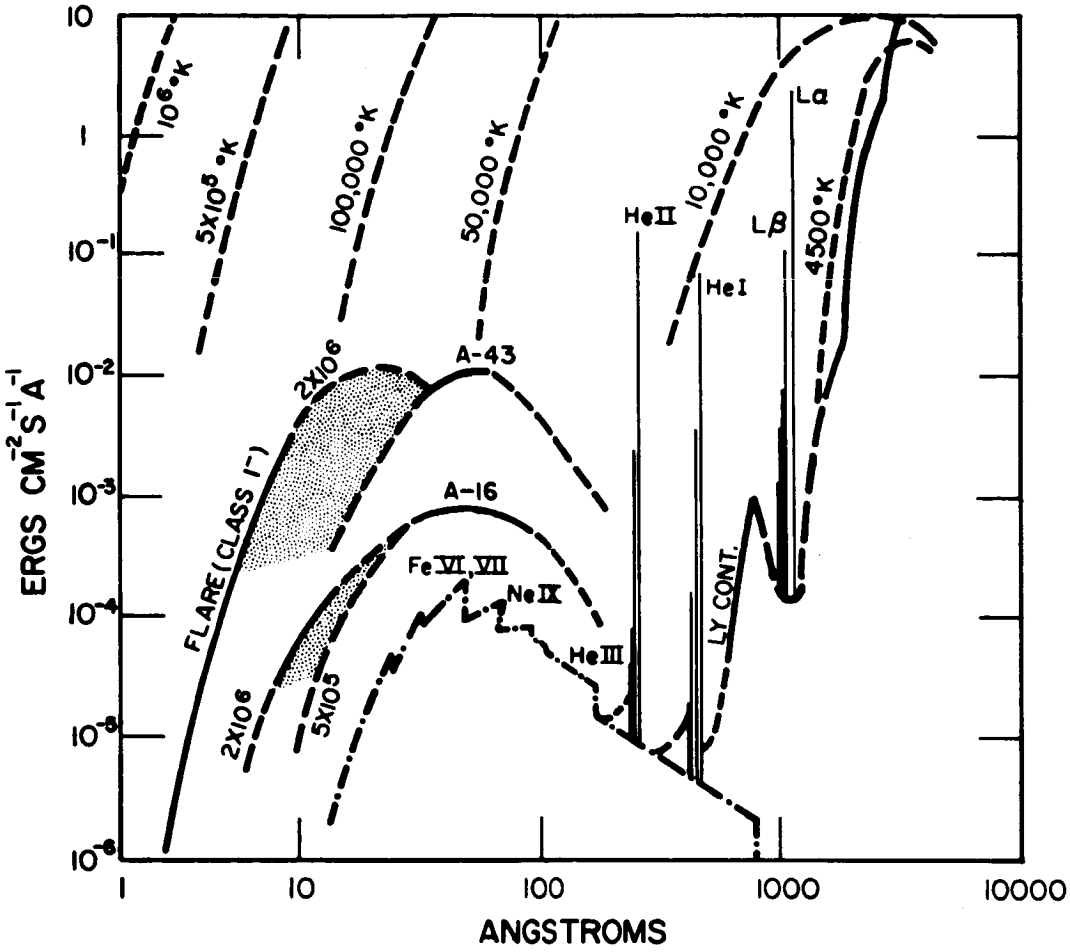

FIG. 2-10 SOLAR SPECTRAL ENERGY DISTRIBUTION FROM 2000 Å TO X-RAYS (Ref. 9)

emission below 20 Å. In some experiments no emission at all was detected below 10 Å. With the approach to solar maximum, the overall x-ray flux increased, especially at the shorter wavelengths. In the 2 to 8 Å band the minimum to maximum variation was a factor of several hundred; from 8 to 20 Å, at least a factor of 45; in the 44 to 60 Å. band, the variation was approximately sevenfold. Assuming that the x-ray spectrum had a gray-body distribution it was not possible to fit the measurements in these three wavelength intervals by a single temperature. The longer wavelength emission could be adequately described by a temperature between 0.5 to 1.0 x 10^6 degrees K, but the shorter wavelength range, below 20 Å required a temperature closer to 2 x 10^6 degrees K.

Rocket measurements have shown that the entire night sky as seen from 100 km is aglow with a diffuse Lyman α radiation which produces an illumination of 10^{-2} ergs/cm^2/sec for the entire hemisphere. The intensity drops to a minimum in the direction opposite to the sun and it is concluded that most of the radiation is solar radiation scattered by neutral hydrogen. While much of this hydrogen is probably associated with the earth, part of the scattered radiation may originate from neutral atoms in interplanetary space.

2.1.6 Geomagnetic Field

Since the earth's magnetic field plays such an important part in shielding the earth from interstellar and particularly solar charged particle radiations a clear model of the geomagnetic field and its relationship with the solar and/or galactic magnetic fields would be of great value. Unfortunately, this subject is still in the early stages of study. Therefore, a discussion of the geomagnetic field must remain qualitative in most respects.

Of particular interest, is the effect of the geomagnetic field in shielding or trapping charged particles. This

subject is more fully covered in Section 2.1.7. The earth's magnetic field approximates that of a dipole at the earth's center and is inclined about 11 degrees to the earth's rotational axis. At the earth's surface the intensity varies from 0.3 gauss horizontal at geomagnetic equator to 0.6 gauss vertical at the poles.

It has been estimated that 99% of the field at the surface of the earth originates from sources within the earth. The source of the magnetic field is believed to arise from an electric current system flowing in a molten metallic core within the earth. Large departures in the field strength at certain points about the earth are believed to exist and are probably caused by irregularities or eddies in the internal current system. Smaller deviations are believed to be caused by deposits of ferromagnetic material in the crust of the earth. In general, the intensity decreases with the cube of the radius; consequently, at distances from the earth's surface the effect of the surface variations is quite small. At distances of 100,000 feet the small deviations are almost completely eliminated. At greater distances the earth's field resembles that of a dipole.

Time variations of the earth's magnetic field are from two sources; external variations caused by solar storms are quite rapid and may last from a few seconds to a few days; much slower variations are caused by changes in the current in the earth's core. These secular changes indicate that the rates of rotation of the earth and its core are not the same; however, these changes are not entirely predictable.

Knowledge of the interplanetary magnetic field is highly speculative. The Pioneer 5 space probe measured a fairly stable and uniform field of about 10^{-4} gauss that is believed to be a galactic field. Theories predicting a radial field from the sun caused by the solar wind have not as yet been substantiated (Ref. 3).

The latest conception of the geomagnetic field is that it is compressed on the daytime side of the earth by the pressure effect of the solar wind, and on the night side the magnetic field is stretched out or tailed out by the solar wind. The model contemplates a shock wave front occurring about 10 to 12 earth radii in the direction of the sun. (Ref. 11).

Downstream the field is stretched out to about 60 earth radii, Figure 2-11 (Ref. 12). Within this region of the magnetosphere, a ring current caused by the solar wind is visualized. In this region, fluxes of protons and electrons exist flowing in opposite directions. As described in Section 2.1.7.1 changes in galactic cosmic ray intensity are noted as a result of magnetic storms. The changing solar wind and the increasing magnetic field intensities carried in the plasma resulting from a solar flare cause increased deflection of the primary charged particles from interstellar space with the result that some of the lower energy particles are deflected away from the earth. Only those with sufficient magnetic rigidity will penetrate to the region of the earth.

Most of the data from satellites have applied to the daylight side of the earth's geomagnetic field. Data for the night side of the earth are scarce and inconclusive. Early reports of data from Explorer 14 (Ref. 13) still do not clarify the geomagnetic field on the night side although this mission should be accomplished by the end of this year (1963) or early in 1964, barring any difficulties with function of the satellite equipment.

2.1.7 Charged Particle Radiations

2.1.7.1 Galactic Cosmic Rays

Interstellar, or galactic, cosmic rays, as distinguished from solar cosmic rays, are of extremely high energy, arriving isotropically and at relatively low intensity originating in interstellar space outside the solar system where they are accelerated by processes as yet not understood. The primary radiations are positively

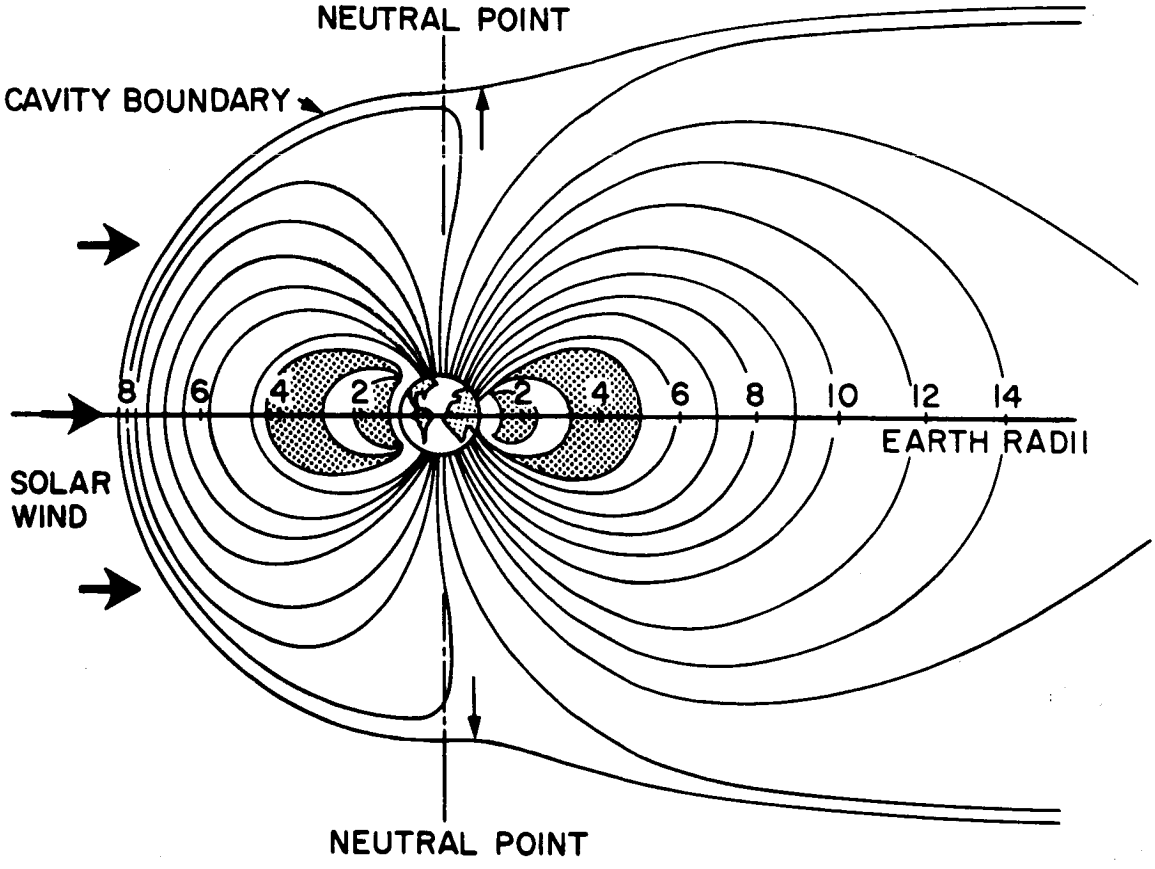

FIG. 2-11 THE GEOMAGNETIC FIELD AND THE CAVITY BOUNDARY CONFIGURATION WHEN ACTED UPON BY THE SOLAR WIND (Ref. 12)

charged particles composed chiefly of hydrogen ions or protons (75 to 80 percent) together with lesser quantities of positively charged (15 to 19 percent) helium atoms. The remaining 1-3 percent consists of carbon, nitrogen, oxygen, and other elements with iron as the highest atomic number element known to exist in these primary radiations. The chart of Fig. 2-12 (Ref. 14) gives the flux levels of the various components of the primary radiation as a function of energy. The energy ranges between 10^8 and 10^{19} ev with an average of about 3.5×10^9. The free space flux rate ranges between 2.2 particles/cm^2/sec at solar maximum to about 4 particles/cm^2/sec at solar minimum.

Intensity of the various components as a function of geomagnetic latitude is given by Fig. 2-13 (Ref. 14). In the chart, L is for atomic numbers of Z between 3 and 5; M is for atomic numbers from 6 to 9; and H for Z equal to or greater than 10. During periods of magnetic storms, there are frequently very pronounced decreases in the primary cosmic ray intensity. This is called the Forbush-type decrease. This amounts to an average intensity decrease of about 5 to 10 percent with occasional changes to 30%. The recovery time is in the order of one to two days and sometimes longer (Ref. 14). All of the cosmic ray intensity changes associated with magnetic storms appear to be caused by the deflection of primary particles in the energy interval 0 to 5 Bev/nucleon of the solar corpuscular beam. In addition, this beam is responsible for sweeping out many of the electrons in the Heaviside layer and disrupting the structure in the outer Van Allen radiation belts. These electrons are driven into the earth's atmosphere causing the well-known aurorae at both poles. There are numerous other data available in the literature concerning cosmic radiation temporal variations, but these are lower order effects of relatively little importance to the present study.

2.1.7.2 Solar Cosmic Rays

The solar wind consists of more or less steady streams of plasma flowing from the corona approximately radially outward

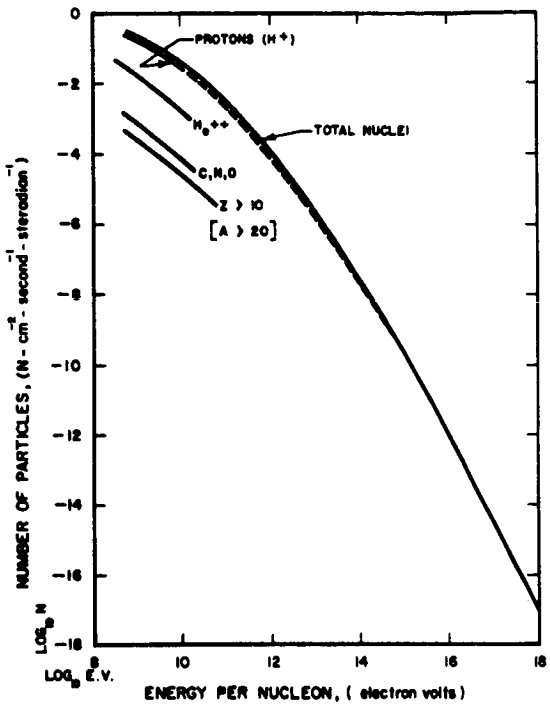

FIG. 2-12

GALACTIC COSMIC PARTICLES VS ENERGY PER NUCLEON (Ref. 14)

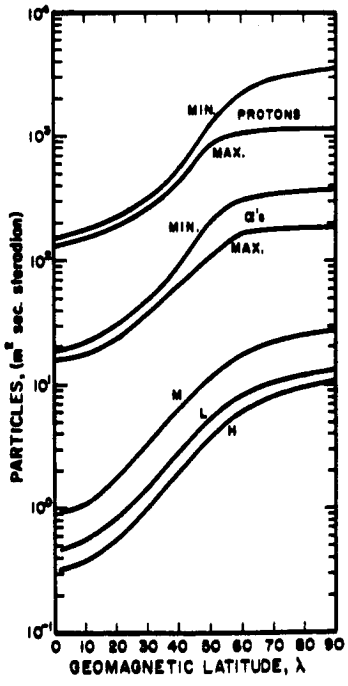

FIG. 2-13

INTENSITY OF THE VARIOUS PRIMARY COMPONENTS OF THE GALACTIC COSMIC RADIATION AS A FUNCTION OF GEOMAGNETIC LATITUDE (Ref. 14)

from the sun. The study of plasmas in space is closely connected with the study of interplanetary magnetic fields. In fact, it is preferable to think of a plasma measurement and magnetic field measurement as two aspects of a single experiment. The high electrical conductivity of the plasma causes the magnetic flux lines to be effectively frozen into the plasma. In the normal case in interplanetary space, the kinetic energy density of the plasma is greater than the magnetic energy density, so that the magnetic field is carried along by the plasma motion. Near the earth the situation is reversed, and the solar plasma is excluded from regions where the geomagnetic energy density is greater than the energy density in the plasma, so that a cavity (the magnetosphere) is formed.

This plasma consists primarily of protons; heavier ions are expected to be present in about the ratios found in the solar atmosphere: about 15 percent atomic He, and less than 1 percent heavier elements (Ref. 2). Densities and energies of the quiet sun emissions or solar wind are variously given as falling between 10 and 100 particles/cm^3 at energies of from 5 to 0.5 kev (Refs. 2, 3, 12, and 14). In terms of flux rate, the range varies from $4 \times 10^8/cm^2/sec$ at 500 ev (Ref. 12) to $5 \times 10^9/cm^2/sec$ at about 1 kev (Ref. 15). Direction is presumed to be generally radial from the sun (Ref. 2) but could be random. The necessary electrons to neutralize the positive particles may be present in a flux as high as a few times 10^{10} $e/cm^2/sec$ at $E < 2$ ev (Ref. 2).

Solar flare radiations occur about once a month at the maximum of the 11-year solar period and perhaps 1 or 2 per year at the solar minimum. The proton flux near the earth associated with a major flare is typically 10^4 proton/cm^2/sec at energies above 20 Mev, extending up to 10^2 p /cm^2/sec above 100 Mev and 10^0 p/ cm^2/sec above 500 Mev.

Record flares, occurring perhaps twice each solar maximum have had proton fluxes 10 times as great. The proton flux

accompanying a solar storm usually lasts about a day. One measurement after a flare of moderate size showed 10^6 to 10^7 electron/cm^2/sec at roughly 50 kev (Refs. 2, 3 and 15). There are also low-energy flare protons at 0.5 to 20 kev; the flux of these is not well known. It may be lower than 10^8 proton/cm^2/sec (Ref. 2), or as high as 10^{12} proton/cm^2/sec (Refs. 2 and 15). Low-energy electrons at 0.25 to 10 ev presumably accompany the low-energy protons; their flux may be 1 to 40 times the proton flux. These low-energy particles are effectively shielded by the geomagnetic field and exist primarily in regions outside the magnetosphere.

2.1.7.3 Trapped Radiations - Magnetosphere

The earth's geomagnetic field is effective in shielding the earth from solar cosmic rays and, to some extent, galactic cosmic rays, by bending or deflecting these primary, charged particle radiations away from the earth. The higher energy cosmic particles can penetrate the field even at the geomagnetic equator where the field strength is a maximum. However, the lower energy solar particles are much more readily deflected (see Sections 2.1.6, 2.1.7.1, 2.1.7.2). The geomagnetic field also has the property of trapping and holding, for long periods of time, charged particles that are generated within the magnetosphere or penetrate it from without. This trapping ability comes about as the result of the Lorentz force acting on a charged particle moving in a magnetic field. The effect of this motion in the earth's dipole field is to cause the particle to mirror between the poles and remain trapped within the force lines. Particles originating too low in altitude will not mirror before encountering the earth's atmosphere where they are absorbed. Close to the earth the field strength is higher than at greater altitudes. This causes longitudinal drift of the protons westward and the electrons eastward.

Various models of the trapping region have been proposed. These models and the intensity levels and spatial

distributions are changing almost daily as new data become available from orbiting satellites and space probes. To this date the intensity of the trapped radiation, its composition, and the energy spectrum of each component as a function of position in space, direction, and time have not been established conclusively. Until recently, most space radiation measurements have been made with detectors that excluded the softer, lower energy components of the trapped radiations. The resultant effect was to find favored regions within the magnetosphere for high-energy protons and electrons which constitute the better known inner and outer Van Allen belts.

The spatial distribution of the trapped radiations of the magnetosphere may be visualized as a toroidal configuration encircling the earth about the geomagnetic equator. The Van Allen belt radiation is often described in terms of two main belts; an inner zone centering at about 1.5 R_e (earth radii), or 9500 km geocentric radius, distinguished primarily by the existence of high-energy protons of $E_e \geq 30$ Mev; and an outer, more diffuse, belt of electrons with $E_e \geq 1.6$ Mev centering at about 3.5 R_e. The distribution of these energetic particles is given in Fig. 2-14 (Refs. 16 and 17).

Later articles cite new evidence of high-flux levels of low energy protons and electrons existing broadly within the magnetosphere (Refs. 18, 19, 20, 21, and 22). An approximation by Van Allen (Ref. 18) of the structure of these low-energy radiations is given in Fig. 2-15. More quantitative data on these electron and proton intensities are given in Table 2-4 (Ref. 22). This appeared in the literature in March 1963 authored by Frank, Van Allen, Whelpley, and Craven. In May 1962, Davis and Williamson reported (Ref. 23) on the low-energy trapped protons measured by Explorer 12. In May 1962, Freeman reported the presence of an intense flux of low energy protons or ions trapped in the inner radiation zone (Ref. 24). Gringauz, et al. (Ref.25) reported measurements of very low energy, E_e from 200 ev to

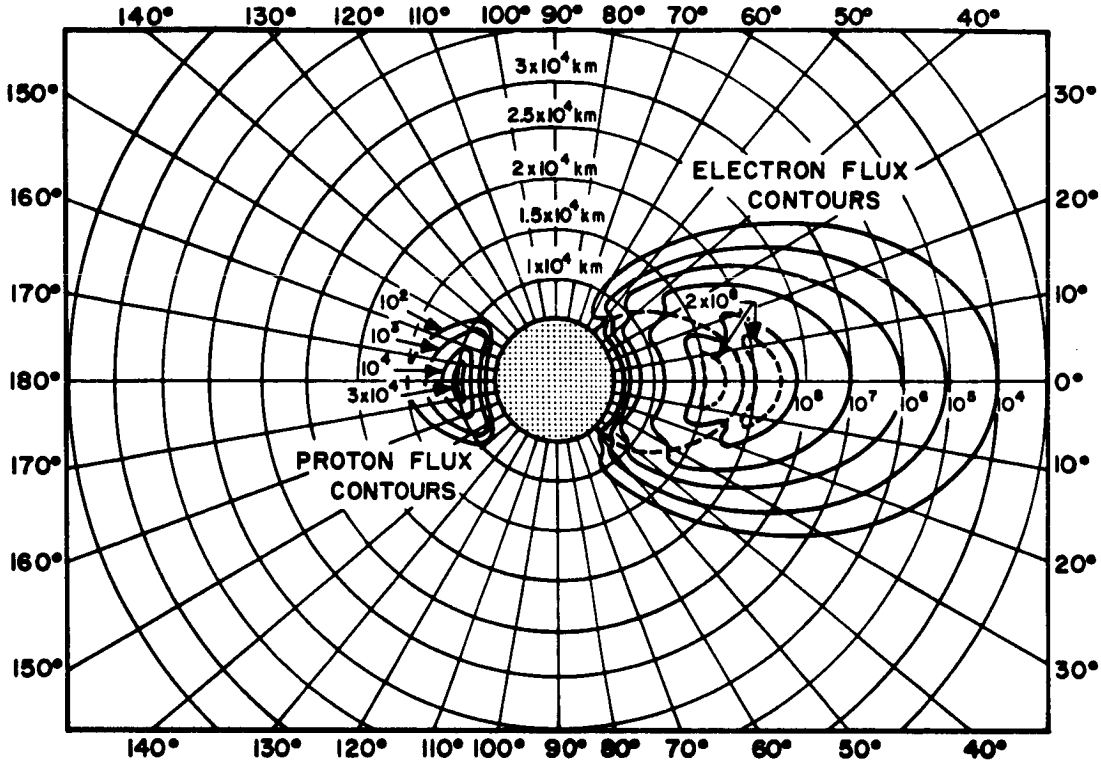

FIG. 2-14 QUIET DAY FLUX (electrons/cm^2/sec) CONTOURS OF ELECTRONS WITH ENERGIES GREATER THAN 20 kev WHICH FORM THE ELECTRON BELT OF THE VAN ALLEN RADIATION BELT. THE HIGH ENERGY PROTON FLUX CONTOURS OF E ≥ 30 Mev ARE ALSO SHOWN FOR REFERENCE (Refs. 16,17)

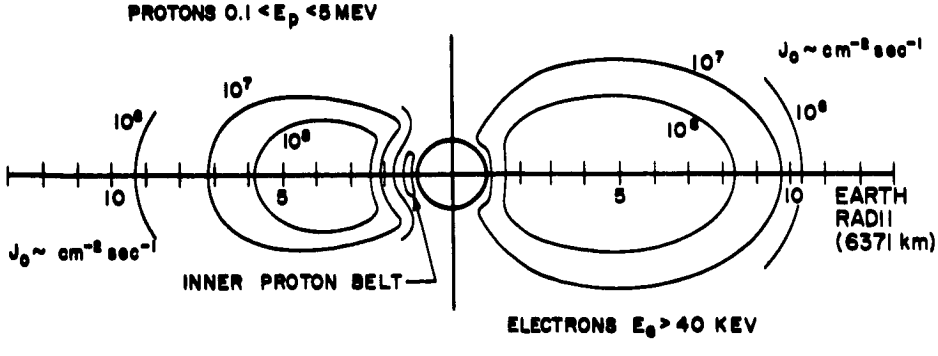

FIG. 2-15 QUIET DAY LOW ENERGY ELECTRON AND PROTON FLUX CONTOURS AS APPROXIMATED BY VAN ALLEN (Ref. 18)

TABLE 2-4

ELECTRON AND PROTON FLUXES MEASURED BY EXPLORER 14 NEAR THE EQUATORIAL PLANE (REF. 22)

R_e, (Radial) Geocentric Dist.		Energy Range	J_o, Particles/cm^2/sec
39,000 km	electrons	≥ 40 kev	1.5×10^8
39,000 km	electrons	≥ 230 kev	1.5×10^6
39,000 km	electrons	≥ 1.6 Mev	2×10^5
20,000 km	protons	≥ 500 kev	$4\ (\pm 2) \times 10^6$
20,000 km	electrons	≥ 230 kev	4×10^4
20,000 km	protons	≥ 4.5 Mev	1.5×10^4
31,000 km	electrons	≥ 40 kev	1×10^8
31,000	electrons	≥ 230 kev	5×10^6
31,000	electrons	≥ 1.6 Mev	1×10^6
55,000	electrons	≥ 40 kev	2×10^7
55,000	protons	≥ 500 kev	5×10^4
55,000	electrons	≥ 230 kev	3×10^4
55,000	electrons	≥ 1.6 Mev	1.5×10^3
65,000	electrons	≥ 40 kev	1×10^6
65,000	protons	≥ 500 kev	1.5×10^4
65,000	electrons	≥ 230 kev	6×10^3
65,000	electrons	≥ 1.6 Mev	2×10^2
75,000 to 103,000	protons	≥ 500 kev	500
"	electrons	≥ 40 kev	500

20 kev, electrons existing in the outer regions of the magnetosphere. Electrons trapped in the inner zone following as a result of Star Fish fission electrons form an artificial belt of a fairly durable type below the lower level of the inner radiation zone. The combined results of these various data are summarized in Fig. 2-16 for electrons and Fig. 2-17 for protons. The energy distributions of electrons and protons vary with altitude and latitude. There is also a time variation introduced by magnetic storms. The electron and proton energy distributions for the steady state or quiet sun are given in Fig. 2-18 for the geomagnetic equator and at selected altitudes. From Fig. 2-17 there is a broad peak of intensity occurring at between 3 and 4 R_e. At this same geocentric radius on the geomagnetic equator the electron flux is below the peak level noted at about 6.5 R_e, but only about a factor of three lower. In the inner regions the flux levels are less susceptible to magnetic storms and disturbances which cause temporal variations in radiation intensities within the magnetosphere and cause major changes in the magnetosphere boundary, as noted in Fig. 2-19 (Ref. 26). In the region of the 1.5 to 20 R_e reliable data are lacking to certain of the electron and proton intensities. For these reasons it is concluded that the intensities given for the trapped radiation levels in the region of 3 to 4 R_e are the most reliable and also most stable as to time variations. For maximum exposure of a surface in the radiation zone a circular orbit in the equatorial plane with a radius of 3 R_e would be ideal. Eccentric orbits of between 3 and 4 R_e between latitudes of $\pm 20^\circ$ would still expose the surface to a substantial fraction of the total possible exposure.

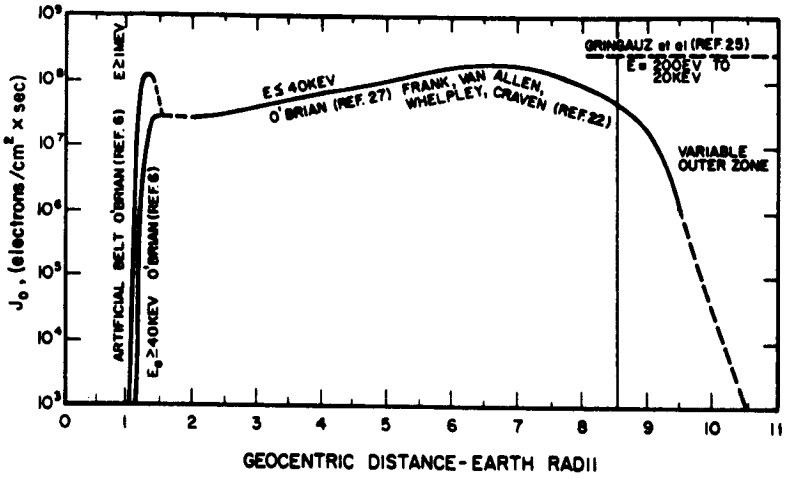

FIG. 2-16

ELECTRON FLUX DISTRIBUTION OF THE MAGNETOSPHERE AS A FUNCTION OF GEOCENTRIC RADIAL DISTANCE ON THE GEOMAGNETIC EQUATOR

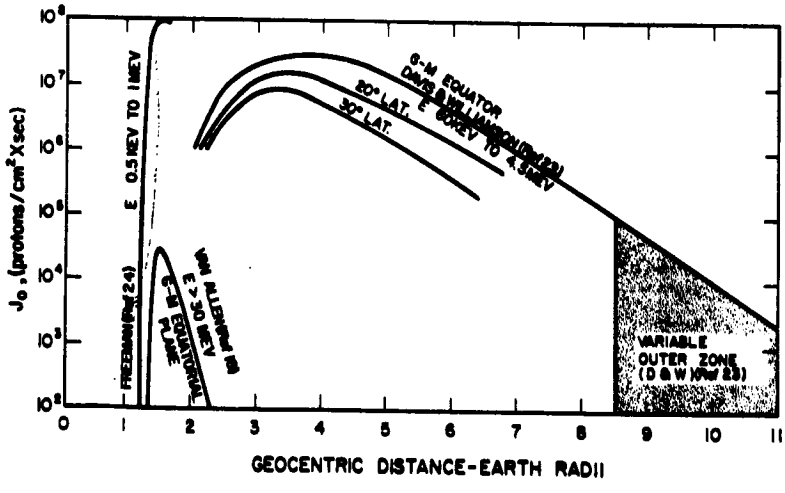

FIG. 2-17

PROTON FLUX DISTRIBUTION OF THE MAGNETOSPHERE AS A FUNCTION OF GEOCENTRIC RADIAL DISTANCE

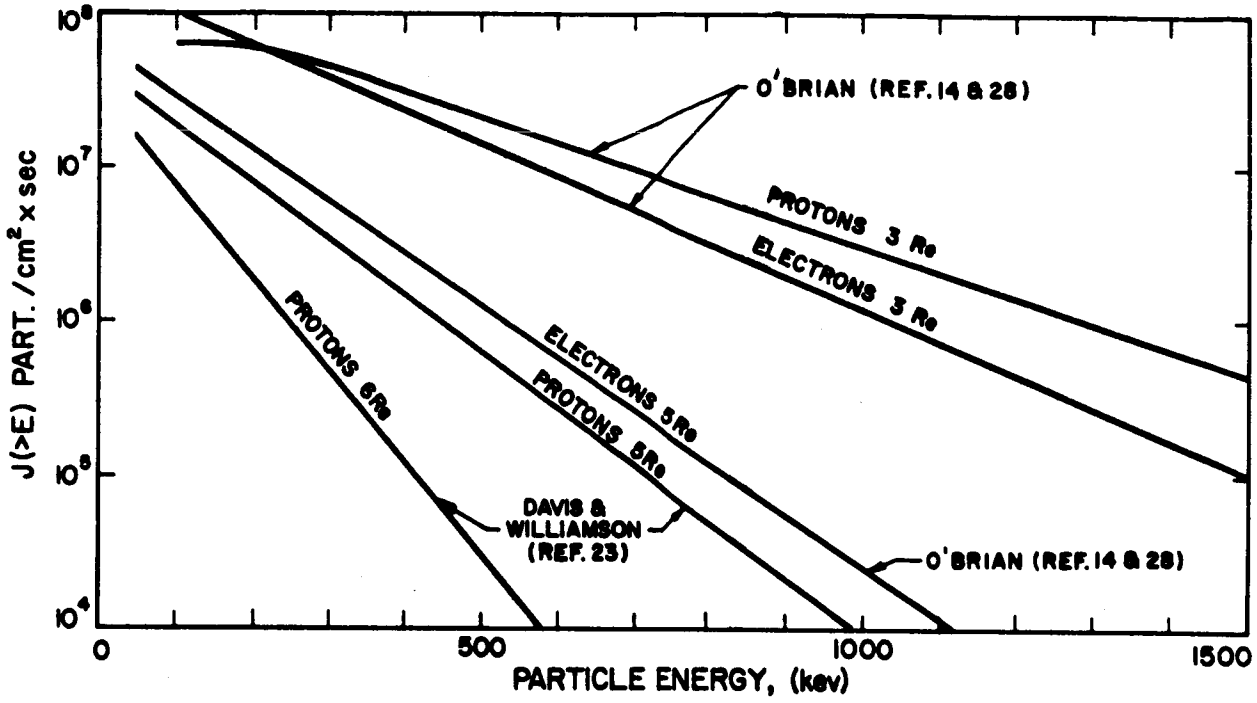

FIG. 2-18 INTEGRAL ELECTRON AND PROTON SPECTRA ON THE GEOMAGNETIC EQUATOR AT VARIOUS GEOCENTRIC RADIAL DISTANCES

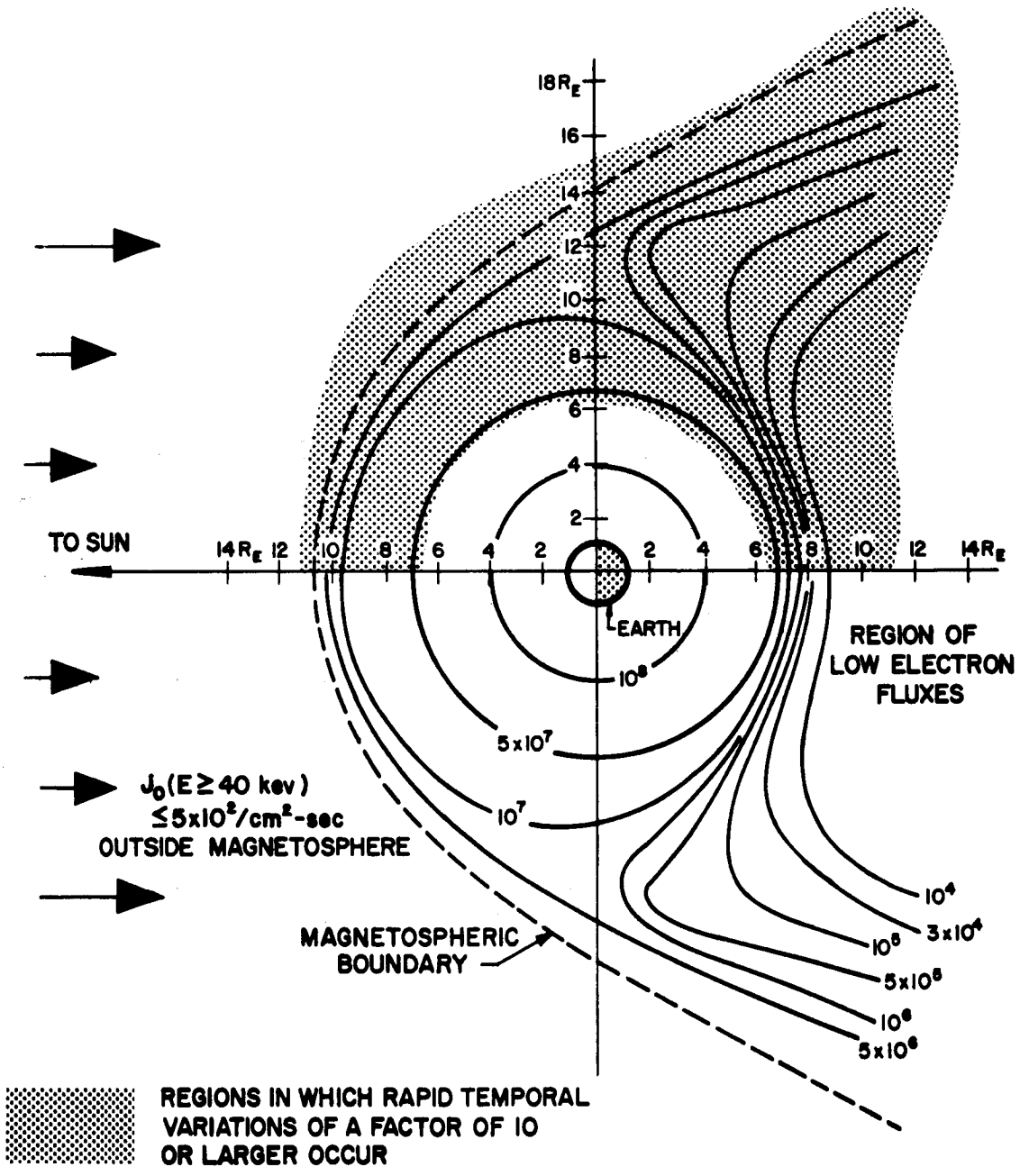

FIG. 2-19 SUMMARY OF OBSERVED OMNIDIRECTIONAL INTENSITIES OF ELECTRONS ($E \geq 40$ kev) IN THE MAGNETIC EQUATORIAL PLANE OBTAINED FROM APPROXIMATELY TWENTY COMPLETE ORBITS OF EXPLORER 14 DURING OCTOBER-DECEMBER 1962 AND FROM EXPLORER 12 DURING AUGUST-DECEMBER 1961 (Ref. 26)

2.2 Sample Selection

A judicious selection of surface samples to be tested in the flight experiment is of greatest importance in assuring the success and usefulness of the experiment. A large number of substrate and coating combinations are of potential interest. The samples selected for testing must be chosen to provide engineering data of value for all current concentrator development programs, as well as sufficient understanding of space environmental effects and degradation mechanisms to form a basis for predicting the behavior of new material combinations to be developed in the future.

2.2.1 Possible Surface Sample Materials

For the purposes of this program, a surface sample consists of the following components:

1. Substrate (plus backup structure)
2. Undercoating
3. Reflective layer
4. Overcoating

Table 2-5 summarizes the samples that are considered to be of interest for space testing. A justification for the selection of these materials is given next.

2.2.1.1 Substrate

The substrate includes both the layer upon which the final coatings are deposited and the backup structure that supports this surface layer. However, the actual surface samples will include only that portion of the backup structure that actually affects the geometry and reflectance of the surface layer. The foam rigidized inflatable concentrator concept provides a useful example. The actual surface layer is a thin sheet of Mylar film. This film is rigidized by a thick layer plastic foam. It would not be satisfactory to test a sample consisting only of a film of Mylar (plus the reflective layer) because the foam has an important effect on the optical properties of the Mylar film. Therefore the sample must consist of the Mylar plus a

layer of foam. However, the foam thickness need not be as great as that used in an actual mirror, since only the last 1/8 or 1/4 inch thickness of foam actually affects the characteristics of the Mylar surface layer. The materials of greatest interest for concentrator substrates are described next.

Nickel. Electroformed nickel is of great interest as a concentrator structural material. This material is formed by electrodeposition on a highly polished glass, metal, or plastic master and has (after parting from the master) a glass-like finish and accuracy. Ordinarily, electroformed nickel concentrators are shell or membrane structures supported at their peripheries. They are generally not provided with any sort of overall backup structure such as plastic foam or honeycomb. Therefore, a typical sample for the flight experiment would be a disc of electroformed nickel having a thickness between 10 and 20 mils.

Copper. Electroformed copper is formed in a manner similar to nickel. Its physical properties are inferior to those of nickel. It would probably be used only for special applications, where the magnetic characteristics of nickel would be detrimental to the mission.

Aluminum. Aluminum is being developed, in several forms, as a solar concentrator material. Ultimately some deposition technique such as electroforming may be developed for aluminum. A program to develop electroformed aluminum solar concentrators is under way at General Electric (sponsored by NASA-Langley). More immediate applications of aluminum for solar concentrators emphasize conventional fabrication techniques such as stretchforming or explosive forming. In this case the aluminum would be highly polished either before or after forming by mechanical or electropolishing techniques. Alcoa "Alzak" Specular Lighting Sheet is an example of a polished aluminum sheet that has been evaluated for solar concentrators. In some cases it may be necessary to coat the aluminum with a layer of vacuum deposited aluminum to cover stains or discoloration caused during the forming operation.

The aluminum might be used in a shell structure without additional backup support or it might be locally rigidized by honeycomb. These various approaches have been investigated by Thompson Ramo-Wooldridge (TRW), Ryan, Boeing, and Fairchild. Typically, substrate samples of aluminum might be of the following types:

1. Disc (20 to 40 mils thick)
2. Skin (5 to 10 mils thick) supported by epoxy bonded aluminum honeycomb.

Aluminum/Epoxy. Because of the difficulty of obtaining a high polish on an aluminum sheet, at least one company (TRW) has experimented with a final dip coating of epoxy that considerably improves the specularity of the aluminum. Although no definite information is available, it is believed that this final epoxy coating is only a few mils thick. This type of substrate could be used in either a shell structure or a honeycomb rigidized structure.

Epoxy. One use of epoxy in substrates has already been mentioned. It is also possible to make a solar concentrator using various layers of unfilled and filled epoxy perhaps further rigidized by honeycomb materials. Many combinations have been investigated by various companies. An approach used by Boeing is perhaps typical. The substrate consists (working down from the surface) of the following materials:

Unfilled epoxy
Filled epoxy
Fiberglass cloth
Honeycomb (aluminum or fiberglass)
Fiberglass cloth

Foam/Mylar. Considerable development is under way on inflatable concentrators rigidized by plastic foam. Goodyear is developing an approach in which the foam is mixed in a central mechanism and allowed to disperse over the surface of the inflated Mylar balloon.

National Cash Register is developing a predistributed foam concept. In either case, a typical sample would consist of a layer of Mylar supported by a layer of plastic foam perhaps 1/4 to 1/2 inch in thickness. (The foam thickness for an actual mirror would be much greater). The Mylar would be 1/2 to 1 mil in thickness.

Mylar (other rigidizing techniques). Other methods of rigidizing an inflatable Mylar collector have been suggested. One technique is to coat the Mylar with a plastic material that hardens in space. A related approach, under development by Viron, involves a two-layer Mylar balloon, with the layers being connected by a large number of threads. The threads are coated with a plastic material that solidifies in space. After inflation the threads stiffen causing the mirror to maintain its shape permanently. A sample of this material would consist of the two layers of Mylar separated by the stiffened threads. Problems would probably be encountered in obtaining a sample of sufficient local flatness for accurate reflectance measurements.

Mylar (pure inflatable). Very lightweight concentrators consisting of partially reflecting balloons have been often suggested. Problems include meteor puncture and darkening of the transparent front skin by ultraviolet radiation. A sample, which would simulate at least the latter effect, could be made using two layers of Mylar mounted in a supporting frame and separated by a fraction of an inch. The rear film would simulate the reflecting surface and would be coated with a reflecting layer. The front film would be transparent. In this way the light from the reflectance instrument would pass through the front layer, reflect from the rear layer, and pass through the front layer again, thus simulating the path of sunlight in an actual inflated concentrator. Inflatable concentrator concepts have been developed by EOS, Schjeldahl, and Viron. Because of the problems with inflatable concentrators, this approach is considered to have a lower priority than some of the above techniques.

Other Materials. Many other materials including steel and beryllium have been suggested as solar concentrator materials. However, because of developmental problems, they have not yet been carried to the point to warrant space tests of surface materials.

2.2.1.2 Undercoatings

In some cases it may be necessary to use a coating between the substrate and the reflective layer for one of the following reasons:

1. To improve adhesion of the reflective layer
2. To prevent diffusion of the reflective layer into the substrate or vice versa.

Depending on the substrate and reflective layer, one or both of these functions often can be satisfied by a vacuum deposited layer of a dielectric such as silicon monoxide or cerium dioxide. In Table 2-5, undercoatings are indicated wherever they are considered necessary or appropriate.

2.2.1.3 Reflective Layers

Only two pure metals, aluminum and silver, have reflectances high enough for solar concentrators. It is also possible to obtain high reflectance using multilayer interference filters of alternating and metallic and dielectric materials. However, the art of applying these coatings to large area curved surfaces has not been developed. Therefore, they will not be considered further.

Aluminum. Vacuum deposited aluminum on an optically smooth substrate has a reflectance of approximately 89 percent for the total solar spectrum. Aluminum is a chemically durable material. Immediately after exposure to the atmosphere a thin, transparent layer of aluminum oxide forms on the surface that prevents further oxidation. Aluminum is rather soft and easily abraded and may require some protective overcoating (see Section 2.2.1.4) if extensive ground handling or cleaning is anticipated.

Silver. Silver can be deposited either by vacuum deposition or by chemical reduction. The latter approach is used as an integral part of the process of fabricating electroformed nickel concentrators. Either type of silver has an average reflectance of 93 percent or more for the total solar spectrum. Silver tarnishes when exposed to certain chemical contaminants such as sulfides and must be protected during ground storage. However, if adequately protected, the reflectance of silver can be maintained at a high level indefinitely, thus offering a worthwhile performance advantage over aluminum for solar concentrator applications. This protection is relatively simple and can take one of the following forms:

1. Storage in a clean atmosphere (clean air, nitrogen, argon, etc.) in a plastic bag or box
2. Coating with a plastic surface layer that would be removed prior to launch
3. Coating with a sublimating plastic layer that would evaporate in space after deployment

Although chemically-deposited silver is much more durable than vacuum-deposited silver, it would be of interest to test both in space. However, chemically-deposited silver must be given first priority. In this case neither undercoatings nor overcoatings would be used. It has been found that vacuum-deposited overcoatings do not satisfactorily protect silver against corrosion. Furthermore, they lower the reflectance to the extent that the advantages of silver are lost.

2.2.1.4 Overcoatings

In many cases it may be desirable to protect aluminum reflecting layers with a transparent overcoating of a dielectric such as silicon oxide. Several oxides of silicon have been investigated. Si_2O_3 appears to give the best optical properties. The primary purpose of such a coating is to prevent damage of the reflective layer prior to launch by providing a hard, durable surface that can be easily cleaned. Some chemical protection will also be obtained from the

overcoating. The real necessity for such a coating is problematical, since a reasonable degree of care in handling the mirror should obviate the necessity for cleaning between fabrication and launch. Protection afforded by a silicon-oxide overcoating in space has not been determined. However, it is conceivable that such a coating might provide some protection against degrading effects. At this stage in concentrator development, it is certainly advisable to test samples both with and without overcoatings. As mentioned previously, it has not been found that vacuum-deposited overcoatings offer substantial protection to silver reflecting surfaces.

A second type of dielectric overcoating is obtained by anodizing the aluminum reflecting layer to form a thicker aluminum-oxide coating. This technique was developed by the group under Dr. Hass at Fort Belvoir and has been further developed at Boeing. When properly formed, such a layer can provide protection and optical properties comparable to those of the silicon-oxide coatings. Goodyear is experimenting with a proprietary coating that can be put on aluminized Mylar to increase the infrared emittance for temperature control purposes. The composition of this coating is not known.

2.2.1.5 Summary of Sample Combinations

If all the permutations of the above substrates, undercoatings, reflective layers, and overcoatings were to be tested, the number would be large indeed. Fortunately, this is not necessary since only a relatively few combinations have any real practical interest. The samples listed in Table 2-5 represent those that are now believed to be sufficiently interesting to be considered for testing. This table is made up primarily of the materials that have been considered in one or more of the concentrator development programs, plus a few additional samples that offer potential performance advantages or will provide comparative data on the necessity for using undercoatings or overcoatings.

2.2.2 Suggested Surface Sample Selection for Flight Experiment

Table 4-1 summarizes the suggested surface sample selection for the Flight Experiment on Solar Concentrator Reflective Surfaces. This selection is based on the best available data, assumptions, and design constraint. However, it is to be expected that the sample selection may be revised somewhat prior to final design and construction of the experiment because of new data or results from solar concentrator development programs, space environmental measurements, or ground simulation tests. The sample selection shown in Table 4-1 represents a condensation of that given in Table 2-5 and is based on the following general assumptions:

1. The selection should contain examples of each important coating presently being developed in a major solar concentrator program in the U.S.
2. No coating combinations are included that are definitely suspected to fail rapidly because of known environmental conditions.
3. The list should contain examples of each type of substrate, undercoating, reflective layer, and overcoating.
4. The primary objective of the experiment is to obtain engineering data that can be used for solar power system design. These data must be in a form that will allow direct prediction of solar concentrator reflectance as a function of time in orbit.
5. A secondary objective is to obtain scientific data that will provide a better understanding of the space environment or the mechanisms of surface degradation, through separation of the effects of various space environmental conditions. However, this information will be obtained only if it does not jeopardize or conflict with the primary experiment objective.

TABLE 2-5

POSSIBLE SURFACE SAMPLE MATERIALS

SUBSTRATE	SAMPLE DESCRIPTION: UNDERCOATING	REFLECTIVE LAYER	OVERCOATING	DEVELOPERS*	NOTES
Electroformed nickel		Silver (chem. dep.)			
Electroformed nickel		Silver (chem. dep.)	Subliming film	EOS	
Electroformed nickel		Silver (vac. dep.)			
Electroformed nickel	SiO	Silver (vac. dep.)			
Electroformed nickel	SiO	Aluminum			
Electroformed nickel	SiO	Aluminum	SiO	Allison, EOS, GE, TRW	
Electroformed nickel	SiO	Aluminum	Si_2O_3		
Electroformed copper		Silver (chem. dep.)			
Electroformed copper	SiO	Aluminum		EOS	
Electroformed copper	SiO	Aluminum	Si_2O_3		
Polished aluminum (e.g. Alzak)				Fairchild, GE, Ryan, TRW	May be rigidized by honeycomb
Polished aluminum (e.g. Alzak)		Aluminum			
Electroformed aluminum				GE	Development pending
Aluminum/epoxy		Aluminum			
Aluminum/epoxy	SiO	Aluminum		TRW	May be rigidized by honeycomb
Aluminum/epoxy		Aluminum	Si_2O_3		
Aluminum/epoxy	SiO	Aluminum	Si_2O_3		
Honeycomb/epoxy	SiO	Aluminum			
Honeycomb/epoxy	SiO	Aluminum	Si_2O_3	Boeing	
Honeycomb/epoxy	SiO	Aluminum	Al_2O_3		
Foam (Goodyear)/Mylar		Aluminum			
Foam (Goodyear)/Mylar		Aluminum	"High emittance"	Goodyear	
Foam (NCR)/Mylar		Aluminum		NCR	
Rigidized Mylar		Aluminum		Viron	
Mylar		Aluminum	Transparent Mylar	EOS, Schjeldahl, Viron	Transparent Mylar separated from aluminized Mylar to simulate inflatable collector

*EOS - Electro-Optical Systems
GE - General Electric
TRW - Thompson-Ramo-Wooldridge
NCR - National Cash Register

2.3 Analysis and Prediction of the Effects of the Space Environment on Reflective Surfaces

Based on the current state of information on the space environment (Section 2.1) this section is concerned with predicting the probable effects of this environment on the reflective surface samples (Section 2.2) with respect to the degradation of reflectivity. Where possible, first order quantitative predictions of the expected degradation are developed to provide a guide for the design of the ground simulation and flight experiments. This is done with the realization that lack of precise environmental data and uncertainties in the degradation mechanisms make these predictions rough approximations. Definitive results can be expected only by performing the experiments.

Those aspects of the environment that are expected to have significant effects on the reflective surfaces are treated in detail here. These are:

1. Temperature, i.e., the thermal balance of the surfaces with solar and earth electromagnetic radiation
2. Micrometeoroids
3. Charged particles, particularly with regard to sputtering
4. Nonthermal effects of the solar ultraviolet radiation

Other environmental conditions, which appear to have only minor effects, are discussed at the end of this section.

2.3.1 Thermal Behavior of Mirrors in Space

It is important that the temperatures assumed by mirrors in earth orbit be known, and if possible controlled, in order to avoid degradation of their performance. Some of the possible undesirable thermal effects are: (1) excessively high or low temperatures leading to changes in material properties, (2) thermal gradients between the front and back of the mirror causing changes in optical figure and mechanical damage, and (3) increase in the damaging effects of the space environment due to extremes of temperature in the mirror. Therefore, it is felt to be useful at this time to make estimates of mirror temperatures in several earth orbits of interest.

2.3.1.1 Heat Balance

The mathematical model used for the mirrors is as follows: a semi-infinite plane area of finite thickness, L, in which heat is received and emitted only from the two surfaces--the mirror surface (indicated by subscript "m") and the back surface (indicated by subscript "b"). The maximum temperatures will occur when the mirror is directly between the earth and sun, receiving solar radiation on the mirror, and earth emission and earth albedo radiation on the back. The minimum temperatures will occur when the mirror is in the umbra of the earth's shadow, receiving only earth emission radiation on the mirror surface. The heat outputs from the mirror are by radiation from the two surfaces. In cases where a temperature gradient exists between the two surfaces heat conducted from one surface to the other must also be considered in the heat balance equations. The two equations given below describe the heat balance at the mirror and back surfaces, respectively, and may be solved for T_m and T_b, the two surface temperatures.

$$\sigma\epsilon_m T_m^4 + \frac{k}{L}(T_m - T_b) = \alpha_s H_s \qquad (2\text{-}1)$$

$$\sigma\epsilon_b T_b^4 - \frac{k}{L}(T_m - T_b) = \epsilon_b H_e F_e + A\alpha_b H_s F_a \qquad (2\text{-}2)$$

where:

- σ = Stefan-Boltzmann constant = 5.67×10^{-5} erg $cm^{-2}sec^{-1}deg^{-4}$
- H_s = solar irradiance constant = 1.40×10^6 erg $cm^{-2}sec^{-1}$
- H_e = earth emission at its surface = 2.20×10^5 erg $cm^{-2}sec^{-1}$
- A = average earth albedo = 0.35
- ϵ_m = emissivity of mirror surface
- ϵ_b = emissivity of back surface
- α_s = absorptivity of mirror surface for solar radiation
- α_b = absorptivity of back surface for earth albedo radiation
- F_e = view factor for earth emission
- F_a = view factor for earth albedo
- k = thermal conductivity of mirror material (erg $cm^{-1}sec^{-1}deg^{-1}$)
- L = thickness of mirror (cm)

Inspection of the pair of simultaneous equations 2-1 and 2-2 will indicate that a great deal of computational labor is required to solve for T_m and T_b. A Fortran program based on Newton's method was written and the computations were performed on the IBM 1620 at Electro-Optical Systems, Inc. The program, which is given in Table 2-6 proved to be quite efficient; average time for solution of the equations was four seconds.

2.3.1.2 Mirror Structures Considered

Four basic types of mirror substrates are under consideration for space applications: (1) thin electroformed metal (Ni or Cu 0.010 to 0.015 inch thick), (2) Mylar-polyurethane foam-Mylar (0.001 inch Mylar sheets spaced with 3 inches of foam), (3) epoxy-fiberglass laminate sheets (0.005 to 0.010 inch) spaced with 1/4 inch thick honeycomb structure of epoxy or aluminum, and (4) aluminum sheets (0.005 inch) spaced with 1/4 inch thick aluminum honeycomb. The dimensions given are only approximate. To these substrates various mirror and back surface coatings may be applied.

The data on the mirror properties required to calculate the surface temperatures are the emissivities and absorptivities of the two surfaces and the effective thermal conductivity between the surfaces. Some data on emissivities and absorptivities are available, and the thermal conductivities of metals and various types of polyurethane foam are known. However, effective conductivities for the two types of honeycomb structures have not been found in the literature, and cannot be readily estimated. At this time, therefore, no thermal behavior estimates on these types will be made. The two types, metal and foam, on which results are given below provide an excellent comparison of the thermal behavior of thin, high k structures with thick, low k structures.

Before listing the results on the metal and foam mirror structures it must be emphasized that the temperatures given depend strongly on the α and ϵ assumptions. Although what are believed to

TABLE 2-6

FORTRAN PROGRAM FOR MIRROR TEMPERATURE CALCULATION

The Fortran program written to solve the simultaneous equations, 2-1 and 2-2, for mirror surface temperatures is reproduced below. In order to make the program of more use for future computations, one additional heat input to each surface, called HM and HB, was incorporated in the program. In the calculations discussed in the text, however, HM and HB were always set equal to zero.

The computer symbols equivalent to the symbols of Eqs. 2-1 and 2-2 are as follows.

SIGMA = σ	A = A	ALPHA-S = α_s	K/L = k/L
HS = H_s	EPS-M = ϵ_m	ALPHA-B = α_b	TM = T_m
HE = H_e	EPS-B = ϵ_b	FE = F_e	TB = T_b
		FR = F_a	

```
C       MIRROR TEMP CALCULATION WA4100
      1 FORMAT(8E10.5)
      2 FORMAT(I3,6F5.1,E8.3,4F5.1)
     11 FORMAT(1H116X31HMIRROR TEMPERATURE CALCULATIONS/7H0SIGMA=E9.3,2X3H
       1HS=E9.3,2X3HHE=E9.3,2X2HA=F6.3,2X9HACCURACY=E9.3/5H0CASE2X5HEPS-M4
       2X5HEPS-B3X7HALPHA-S2X7HALPHA-B5X2HFE7X2HFR7X3HK/L7X2HHM/1H23X2HHB9
       3X2HTM9X2HTB)
     12 FORMAT(1XI3,6(3XF6.4),2(1XE10.4)/1H21XE10.4,2(2XF8.2))
    100 READ 1,SIG,HS,HE,A,EROR
        PUNCH 11,SIG,HS,HE,A,EROR
    200 READ 2,ICASE,EPSM,EPSB,ALFS,ALFB,FE,FR,C2,HM,HB,TM,TB
    300 C1=SIG*EPSM
        C3=ALFS*HS+HM
        C4=SIG*EPSB
        C5=EPSB*HE*FE+A*ALFB*HS*FR+HB
    400 TM2=TM*TM
        TB2=TB*TB
        TERM1=C1*TM2*TM2
        TERM2=C2*(TM-TB)
        F1=TERM1+TERM2-C3
        TERM1=C4*TB2*TB2
        F2=TERM1-TERM2-C5
        F1TM=4.*C1*TM2*TM+C2
        F2TB=4.*C4*TB2*TB+C2
        DET=F1TM*F2TB-C2*C2
        DTM=(-F2TB*F1-C2*F2)/DET
        DTB=(-C2*F1-F1TM*F2)/DET
        TMNEW=TM    +DTM
        TBNEW=TB    +DTB
    700 IF(ABSF(DTM/TMNEW)-EROR)750,750,800
    750 IF(ABSF(DTB/TBNEW)-EROR)900,900,800
    800 TM=TMNEW
        TB=TBNEW
        GO TO 400
    900 PUNCH 12,ICASE,EPSM,EPSB,ALFS,ALFB,FE,FR,C2,HM,HB,TMNEW,TBNEW
        IF(SENSE SWITCH 1)100,200
        END
```

be reasonable assumptions have been made, it is realized that α and ϵ may be changed and controlled over a considerable range of values by special surface coating. In fact, some of the results indicate such control may be necessary to prevent excessively high temperatures in the foam mirrors.

2.3.1.3 Results

Values of the view factors F_e and F_a, which depend on orbital altitude, were calculated as indicated in Ref. 30, and are given in Table 2-7.

TABLE 2-7

EARTH EMISSION AND ALBEDO VIEW FACTOR

Orbital Altitude (nautical miles)	F_e	F_a
300	.85	.84
1000	.60	.58
20000	.021	.019

Values for the k/L ratios are: for 0.010-inch nickel $k/L = 3.3 \times 10^8$ erg cm^{-2} sec^{-1} deg^{-1}; for 3-inch polyurethane foam $k/L = 3.8 \times 10^3$.

In Table 2-8 maximum and minimum temperatures of the surfaces are listed for various α and ϵ assumptions.

2.3.1.4 Discussion of Results

The results given in Table 2-8 are listed in pairs of cases so that the behavior of the Mylar-foam and the nickel mirrors under identical conditions can be readily compared. Cases 1

TABLE 2-8 MIRROR TEMPERATURES UNDER VARIOUS CONDITIONS

Case No.	Mirror Type	Orbital Altitude (Nautical miles)	ϵ_m	ϵ_b	α_s	α_b	Maximum T_m(°C)	Maximum T_b(°C)	Minimum T_m(°C)	Minimum T_b(°C)
1	Ni	300	0.05	0.90	0.15	0.90	70	70	-157	-157
2	Foam	300	0.05	0.90	0.15	0.90	107	68	-155	-157
3	Ni	1,000	0.05	0.90	0.15	0.90	50	50	-166	-166
4	Foam	1,000	0.05	0.90	0.15	0.90	89	47	-165	-166
5	Ni	20,000	0.05	0.90	0.15	0.90	-19	-19	-202	-202
6	Foam	20,000	0.05	0.90	0.15	0.90	26	-23	-201	-202
7	Ni	300	0.05	0.90	0.10	0.90	62	62	--	--
8	Foam	300	0.05	0.90	0.10	0.90	85	60	--	--
9	Ni	300	0.05	0.90	0.20	0.90	78	78	--	--
10	Foam	300	0.05	0.90	0.20	0.90	129	74	--	--
11	Ni	300	0.10	0.90	0.10	0.90	58	58	--	--
12	Foam	300	0.10	0.90	0.10	0.90	72	56	--	--
13	Ni	300	0.05	0.05	0.15	0.15	198	198	--	--
14	Foam	300	0.05	0.05	0.15	0.15	207	191	--	--
15	Ni	300	0.05	0.05	0.10	0.10	155	155	--	--
16	Foam	300	0.05	0.05	0.10	0.10	160	150	--	--
17	Ni	300	0.07	0.90	0.21	0.90	78	78	--	--
18	Foam	300	0.07	0.90	0.21	0.90	124	73	--	--

through 6 give results for three orbital altitudes. It is seen that the maximum temperatures in these six cases stay within a reasonable range so that no adverse effects on material properties would be expected. However, the temperature difference between the mirror and back surfaces in the foam mirror, near 40°C in each case, might give rise to problems of the optical figure changing and mechanical damage to the structure. The differential thermal expansion, using an expansion coefficient of $30 \times 10^{-6}/^{\circ}C$ (Ref. 31), would be 0.12% for the 40°C gradient. Possible methods for minimizing this effect are discussed later in this section.

The minimum temperatures given in Cases 1-6 might cause degradation of both types of mirror. The coatings on the nickel mirrors (e.g., SiO and Al) might craze or peel at these low temperatures. With respect to the Mylar-foam mirrors, the temperatures in each case are well below the recommended operating temperature for both plastic materials; the minimum for Mylar is -60°C (Ref. 32) and for polyurethane foam is -70°C (Ref. 31). The Mylar becomes brittle at low temperatures; while the low temperature degradation mechanism for the foam is not known at this time. The above considerations indicate the need for appropriate temperature cycling of mirror samples during ground simulation tests.

The remainder of the cases in Table 2-8 (7-18) show the results of changes in α and ϵ . It should be noted that such changes might be intentional, to improve thermal behavior, or might result from other prelaunch and space environmental effects, in which case thermal behavior might improve or degrade. Minimum temperatures are not included in this part of the table since they are not particularly sensitive to α and ϵ changes.

Cases 7-12 and 1-2 show the effects of changes in the α_m/ϵ_m ratio while holding $\alpha_b = \epsilon_b = .90$. The nickel mirror is relatively insensitive to these changes; but the foam mirror temperatures are strongly dependent on this ratio. It is seen that the most favorable among these cases (Case 12) is that of $\alpha_m/\epsilon_m = 1$; here both the magnitudes

of the temperatures and the thermal gradient are the smallest. The question arises as to whether these values of α and ϵ can be achieved initially and retained in the space environment. It is known (Ref. 33) that aluminized Mylar typically has $\alpha/\epsilon = 3$, similar to Case 1. Therefore, other coatings would be needed to adjust the ratio and at the same time keep the absolute values of α and ϵ low.

The other approach to control of thermal behavior, that of lowering α_b and ϵ_b, is illustrated in Cases 13-16. The nickel mirror cases (13 and 15) are included for reference only, since there is no advantage in operating this type of mirror with a reflective back coating. The foam mirror shows a lower thermal gradient, but at the expense of considerably higher temperatures (compare Case 14 with Case 2 and compare Case 16 with Case 8). This method of minimizing thermal gradients in the foam mirror might present fewer practical problems than the method discussed in the preceding paragraph. However, the temperatures indicated in Cases 14 and 16 are near the upper limits for the plastic materials used; one type of "high-temperature polyurethane foam" is specified for continuous use only up to 205°C (Ref. 31); while Mylar is said to "remain flexible and stable in a temperature range of -60°C to 150°C" (Ref. 32) and has a melting point of 250°C (Ref. 32).

Cases 17 and 18 are included to show by comparison with Cases 1 and 2 that the magnitudes of α and ϵ as well as the α/ϵ ratio must be known for accurate thermal predictions and control.

2.3.1.5 Conclusion

The most important conclusion which must be drawn from the above discussion, with regard to the reflective surfaces flight experiment, is that detailed measurements of α, ϵ, and effective thermal conductivity must be made on the mirror structures involved in this experiment. In this way realistic predictions of their thermal behavior in space can be made, and the information needed for effective ground simulation tests will be available. The measurement of α and ϵ

after the various ground simulation tests will also allow prediction of possible changes in thermal behavior caused by the space environment.

2.3.2 Degradation of Reflecting Surfaces by Micrometeoroids

In this section equations are developed to predict the effect of micrometeoroid bombardment on reflecting surfaces in earth orbit. Numerical results, which are given for several sets of assumptions, indicate degradation of reflectivity from this source is not too severe. However, since detailed data on the micrometeoroid flux are not yet available and since the theory of hypervelocity impact is not fully developed, these numerical results must be considered as only a first approximation.

2.3.2.1 General Approach

A micrometeoroid striking the reflecting surface of a thick target is assumed to create a hemispherical pit in the surface, as is indicated by hypervelocity projectile experiments (Ref. 34). It is further assumed that the circular area defining the top of the pit has zero reflectivity, which is the worst case. In the following treatment normal incidence is assumed for the entire micrometeoroid flux, although it realized that this, in general, will not be the case. When further inputs on orbits and orientations of the reflection experiment are available the following equations can be corrected for proper angle of incidence distributions.

It has been shown (Refs. 34 and 35) that the volume of material displaced to form the pit is directly proportional to the kinetic energy of the impinging particle. The constant of proportionality, K_T, involves only physical properties of the target material.

Since there are at least three different theories (Refs. 36, 37 and 38) on the calculation of this constant (as discussed later), we will leave K_T as unknown for the moment, and formulate the above statement as:

$$V = 1/2\ mv^2/K_T \qquad (2\text{-}3)$$

where,

V = volume of hemispherical pit (cm^3)

m = mass of micrometeoroid (grams)

v = velocity of micrometeoroid (cm/sec)

K_T = target constant ($ergs/cm^3$)

The area removed from the reflecting surface (i.e., target) is calculated from the formulas for the volume of a hemisphere and the area of a circle to be:

$$A = \left(\frac{3\pi^{1/2}V}{2}\right)^{2/3} \qquad (2\text{-}4)$$

where A = area removed from surface (cm^2).

Combining equation 2-3 and equation 2-4 yields:

$$A = \left(\frac{3\pi^{1/2}\ mv^2}{4K_T}\right)^{2/3} \qquad (2\text{-}5)$$

This expression gives the area of reflecting surface removed for any micrometeoroid of mass m and velocity v.

In order to calculate the integrated effect of the micrometeoroid flux we need a distribution function relating the number and mass of these particles. This function is provided by the work of Whipple (Ref. 36) as:

$$N = K_w/m \qquad (2\text{-}6)$$

where N = number of particles per unit area per unit time ($cm^{-2}\ sec^{-1}$)

K_W = Whipple's constant = $5.3 \times 10^{-16}\ g/cm^2/sec$.

The differential form of equation 2-6,

$$dN = -K_w\ dm/m^2 \qquad (2\text{-}7)$$

may be combined with equation 2-5 to yield:

$$AdN = -\left(\frac{3\pi^{1/2} v^2}{4 K_T}\right)^{2/3} . K_w . m^{-4/3} dm \quad . \tag{2-8}$$

If we assume a constant velocity for all particles, as is generally accepted (Ref. 34 and 36), equation 2-8 may be integrated to give:

$$\int AdN = 1/3 \left(\frac{3\pi^{1/2} v^2}{4K_T}\right)^{2/3} . K_w . m^{-1/3} \Bigg|_{m*}^{\infty} \tag{2-9}$$

The desired quantity, $\int AdN$, which is the fractional area loss per unit time due to the entire flux, can now be found, given the required constants and the lower limit of mass, m*, are known. This lower limit of mass can be calculated based on Whipple's consideration (Ref. 36) that when the solar radiation pressure on a particle exceeds the solar gravitational force, the particle will be forced out of the solar system. The governing equation is:

$$m* = \frac{5.76 \times 10^{-11}}{\rho_m^2} \tag{2-10}$$

where ρ_m = assumed micrometeoroid density (g/cm^3).

We now return to consideration of the target constant, K_T, which is the energy required per unit volume in the formation of the pits. As mentioned above at least three approaches have been proposed for calculating K_T. The first, suggested by Whipple, (Ref. 36), involves the thermal energy required to melt the target material. This is formulated as:

$$K_{T1} = \rho_T (C\Delta T + \Delta H) \tag{2-11}$$

where ρ_T = density of target material (g/cm^3)

C = specific heat of target material (ergs/g/^{o}C)

ΔT = difference between target temperature and melting point of target material (^{o}C)

ΔH = latent heat of fusion of target material (ergs/g).

The second approach, proposed by Barnes (Ref. 37), is based on an empirical fit of data from hyper-velocity impact experiments. Barnes' equation is:

$$K_{T2} = 3.94 \times 10^{-2} \rho_T v_s^2 \qquad (2\text{-}12)$$

where v_s = velocity of sound in the target material (cm/sec).

The third approach, put forth by Eichelberger and Gehring (Ref. 38) is also based on hyper-velocity impact experiments. Their form of the equation is:

$$K_{T3} = 2.5 \times 10^{8} B \qquad (2\text{-}13)$$

where B = Brinell hardness number of the target material.

Considering the wide variety of material properties used in these three approaches the calculated results for area loss agree remarkably well, as is shown in the following section.

2.3.2.2 Calculated Results

Three of the five materials of interest as mirror substrates are aluminum, copper and nickel. In the case of copper or nickel a thin film of silver or aluminum would typically be deposited on the surface to enhance reflectivity; however, these films are so thin (200 to 1000 Å) that we will assume the substrate properties control the pit formation. Physical properties of these substrate materials used in calculating the targets constants (K_{T1}, K_{T2}, and K_{T3}) are given in Table 2-9.

TABLE 2-9 PHYSICAL PROPERTIES OF MIRROR SUBSTRATE MATERIALS

Material	ρ (g/cm^3)	C(erg/g/$^\circ$C)	ΔH(erg/g)	M.P.($^\circ$C)	v_s(cm/sec)	B
Al	2.7	10.4×10^6 (300°C)	3.2×10^9	660.	5.10×10^5	16
Cu	8.93	4.4×10^6 (550°C)	2.0×10^9	1083.	3.56×10^5	140
Ni	8.90	5.4×10^6 (700°C)	3.0×10^9	1453.	4.97×10^5	200

The quantities in Table 2-9 are used to calculate the three different K_T's shown in Table 2-10. For ΔT in the K_{T1} equation (Eq. 2-11) the melting point is used, i.e., the substrate temperature is assumed to be 0°C. It is seen, however, that even if a temperature several hundred degrees above or below 0°C were used K_{T1} would change very little

TABLE 2-10 TARGET CONSTANTS FOR MIRROR SUBSTRATE MATERIALS

Material	K_{T1}(Eq. 2-11)	K_{T2}(Eq. 2-12)	K_{T3}(Eq. 2-13)
Al	2.70×10^{10}	2.68×10^{10}	0.4×10^{10}
Cu	6.07×10^{10}	4.72×10^{10}	3.5×10^{10}
Ni	9.70×10^{10}	7.87×10^{10}	5.0×10^{10}

The other two quantities which must be specified in order to make use of Eq. 2-9 are the average micrometeoroid velocity, v, and the density, ρ_m, of these particles (from which is calculated the lower mass limit, m*, by Eq. 2-10). For velocity we have chosen two cases: 4×10^6 cm/sec, which is believed to be typical (Refs. 34, 39, and 40), and 7.2×10^6 cm/sec, which is believed to be the maximum possible velocity (Ref. 39). For density we have also chosen two cases: 8.9 g/cm^3, which represents a pure nickel micrometeoroid, and 1.0 g/cm^3, which is believed to be more typical of micrometeoroids (Ref. 41). The lower mass limits, m*, calculated from these densities using Eq. 2-11 are, respectively, 7.35×10^{-13}g and 5.76×10^{-11} g.

The fractional surface area loss per year for all combinations of the three materials, the three target constants, the two assumed velocities and the two assumed densities, calculated from Eq. 2-9, are given in Table 2-11. It is seen from Table 2-11 that even with the most pessimistic set of assumptions the surface area losses per year are relatively small: 3.5% for Al, 0.97% for Cu, and 0.76% for Ni.

TABLE 2-11

FRACTIONAL SURFACE AREA LOSS PER YEAR FOR MIRROR SUBSTRATE MATERIALS

Material	Using K_{T_1}	Using K_{T_2}	Using K_{T_3}	Other Assumptions
Al	1.2×10^{-3}	1.2×10^{-3}	4.4×10^{-3}	$v = 4.0 \times 10^{6}$; $\rho = 1.0$
Cu	7.2×10^{-4}	8.5×10^{-4}	1.0×10^{-3}	$v = 4.0 \times 10^{6}$; $\rho = 1.0$
Ni	5.3×10^{-4}	6.0×10^{-4}	8.2×10^{-4}	$v = 4.0 \times 10^{6}$; $\rho = 1.0$
Al	5.3×10^{-3}	5.3×10^{-3}	1.9×10^{-2}	$v = 4.0 \times 10^{6}$; $\rho = 8.9$
Cu	3.1×10^{-3}	3.6×10^{-3}	4.4×10^{-3}	$v = 4.0 \times 10^{6}$; $\rho = 8.9$
Ni	2.3×10^{-3}	2.6×10^{-3}	3.5×10^{-3}	$v = 4.0 \times 10^{6}$; $\rho = 8.9$
Al	2.7×10^{-3}	2.7×10^{-3}	1.5×10^{-2}	$v = 7.2 \times 10^{6}$; $\rho = 1.0$
Cu	1.6×10^{-3}	1.8×10^{-3}	2.3×10^{-3}	$v = 7.2 \times 10^{6}$; $\rho = 1.0$
Ni	1.2×10^{-3}	1.3×10^{-3}	1.8×10^{-3}	$v = 7.2 \times 10^{6}$; $\rho = 1.0$
Al	1.2×10^{-2}	1.2×10^{-2}	3.5×10^{-2}	$v = 7.2 \times 10^{6}$; $\rho = 8.9$
Cu	6.7×10^{-3}	7.9×10^{-3}	9.7×10^{-3}	$v = 7.2 \times 10^{6}$; $\rho = 8.9$
Ni	4.9×10^{-3}	5.6×10^{-3}	7.6×10^{-3}	$v = 7.2 \times 10^{6}$; $\rho = 8.9$

2.3.2.3 Results Based on Whipple's 1963 Estimate of Micrometeoroid Environment

Very recently a new estimate by Whipple of the micrometeoroid environment has become available (Ref. 42). Using this new estimate, the predicted effects on the metal-substrate mirrors are somewhat smaller than those given above.

Based on recent experimental data, Whipple estimates that the micrometeoroids have a mean velocity of 2.2×10^6 cm/sec, a mean density of 0.44 g/cm^3, and a distribution given by:

$$N = 3.31 \times 10^{-19} m^{-1.34} \tag{2-14}$$

where N = number per cm^2 per second

and m = mass in grams

The new density estimate yields a lower limit of mass, $m^* = 2.9 \times 10^{-10}$ g. (See Eq. 2-10).

The revised form of Eq. 2-9, resulting from the above changes, is:

$$\int A dN = 2.98 \times 10^{-19} \left(\frac{3\pi^{1/2} v^2}{4 K_t} \right)^{2/3} m^{-0.67} \Bigg|_{m^*}^{\infty} \tag{2-15}$$

Using Eq. 2-15 the calculated values of the fractional area loss per year for the three materials and three target constants discussed above are given in Table 2-12.

TABLE 2-12

FRACTIONAL SURFACE AREA LOSS PER YEAR FOR MIRROR SUBSTRATE MATERIALS BASED ON NEW WHIPPLE ESTIMATE

Material	Using K_{T_1}	Using K_{T_2}	Using K_{T_3}	Other Assumptions
Al	8.8×10^{-4}	8.8×10^{-4}	3.1×10^{-3}	$V = 2.2 \times 10^6$; $\rho = 0.44$
Cu	5.1×10^{-4}	6.0×10^{-4}	7.4×10^{-4}	$V = 2.2 \times 10^6$; $\rho = 0.44$
Ni	3.7×10^{-4}	4.3×10^{-4}	5.8×10^{-4}	$V = 2.2 \times 10^6$; $\rho = 0.44$

2.3.2.4 Micrometeorite Damage to Reflectors other than the Bulk Metal Type

Several types of reflectors, other than the bulk metal type discussed above, are of interest for use in space. Examples of these are the foam backed aluminized Mylar type, the plastic substrate type and the thin nickel (.007 inch) unbacked type. Also, a variation of the bulk metal type, in which a diffusion barrier layer, e.g., silicon monoxide, is interposed between the nickel substrate and the aluminum film has been considered. Although specific micrometeoroid damage calculations have not yet been made on these types of reflectors, some considerations on damage mechanisms are given below.

The Mylar type of reflector may have less reflecting surface removed by an impinging micrometeoroid than the bulk metal types because only a small portion of the particle's kinetic energy would be dissipated near the surface. This may also be true, to a lesser extent, of the thin nickel type of reflector.

Plastic substrate type reflectors may be quite severely damaged by micrometeoroids, as indicated by the experiments of Kinard and Collins (Ref. 43) on high-velocity impact cratering on plastic targets. They found that relatively large quantities of surface material were broken from the plastic targets by high velocity-projectiles.

The diffusion barrier type reflectors may present some special problems with respect to surface erosion. The mechanical and thermal discontinuities presented at the interfaces between the SiO layer and the two metals may promote the peeling off of the reflecting surface film when a micrometeoroid's kinetic energy is dissipated near the surface.

It would seem quite desirable to determine the validity of the above considerations in a simulated or actual space environment. It is felt that significant differences in the durability of the various types of reflectors would be observed.

2.3.3 Effect of Charged Particles on Reflective Surfaces

Although preliminary estimates, made earlier during this study program, indicated charged particles would have a relatively small effect on a reflective surface, recent experimental evidence shows these particles, especially low to medium energy protons, may cause significant reflectivity degradation and an undesirable increase in the thermal control parameter, α/ϵ. The damage mechanism is non-uniform sputtering of the metal surface, which, in the case of aluminum, results in a high density of irregular pits on the surface in size range of 1 to 5 microns.

The evidence of this type of damage was developed in recent experiments by D. L. Anderson (Ref. 44) and D. L. Anderson and G. J. Nothwang (Ref. 45) in which space proton bombardment of polished metal surfaces was simulated with 1 kev hydrogen ions. Their results for polished pure aluminum, which is most generally used for reflective surfaces, are of particular interest. Bombardment with an integrated flux of 10^{21} hydrogen ions per cm^2 increased the solar absorptivity (α) of the surface to 0.23, compared with its initial value of 0.09. Therefore, total solar reflectivity was degraded from 0.91 to 0.77. However, the degradation of specular reflectivity, which is the measure of a solar concentrator's performance, is even more severe. Study of the photomicrographs of the Al surface before and after this treatment (Ref. 44) leads one to a conservative estimate that after sputtering at least 30 percent of the remaining total reflectivity is diffuse; thus the specular reflectivity is estimated as 0.54. It should be noted that even at an integrated flux of 10^{20} hydrogen ion an increase in α from 0.09 to 0.13 was measured by Anderson.

In order to assess the significance of the above results one must relate the laboratory experiment with 1 kev protons (hydrogen ions) to the space environment. With the present sparse and often conflicting data on the charged particle space environment this is quite difficult. In Section 2.1 of this report a peak proton flux

of $10^8/cm^2/sec$ ($3 \times 10^{15}/cm^2/year$) is indicated. This would imply that very little sputtering damage would be experienced. However, Anderson (Ref. 44) using other estimates gets a proton flux of $3 \times 10^{19}/cm^2/year$ during periods of high solar activity. If this is the case observable, sputting damage would occur in 1 to 3 years. Additional complications arise in estimating the relative sputtering efficiency of the wide energy spectrum of space protons compared with 1 kev protons. Also the possible sputtering effects of other charged particles, electrons and heavier ions, must be considered.

Although no definite prediction of the magnitude of this effect can be made at this time, it is recommended that ground simulation tests be made on the chosen reflective surface sample to determine the significance of sputtering degradation.

2.3.4 Nonthermal Effects of Solar Ultraviolet Radiation

Many reflective surfaces being considered for solar concentrator use have dielectric coatings over the metallic reflective materials. These coatings are used both to provide mechanical and chemical protection for the metal layer, and to lower the ratio of solar absorptivity to infrared emissivity in order to limit the temperature extremes experienced by the mirror structure in orbit. However, the dielectric coatings may be subject to degradation in the space environment, resulting in the lowering of reflectivity.

A specific example of this type of degradation was reported recently (Ref. 46). A large number of reflective aluminum samples coated with various types and thicknesses of anodic oxide, and a few samples coated with evaporated dielectric such as SiO, MgF_2 and TiO_2 were irradiated with a good approximation to the solar ultraviolet spectrum while being held under vacuum of 10^{-5} torr. Although a wide variety of results was obtained, most samples showed a significant decrease in reflectivity (typically 3 percent to 10 percent) after an ultraviolet irradiation equivalent to solar irradiation from 300 to 1200 hours. Evidence was developed to show that the reflectivity

degradation was due to increased absorption in the coating, probably caused by photon-created vacancies.

Although it was not investigated in Ref. 46, it seems most probable that the radiation constants of interest for thermal control, i.e., solar absorptivity and infrared emissivity, were also changed to a significant degree. Therefore it appears to be most important to investigate this solar ultraviolet effect in both the ground simulation and flight phases of the reflective surfaces experiment. Since thermal control is necessary for space-borne solar concentrators, particularly for those using plastic substrates, it is recommended that, in addition to reflectivity, the radiation constants of the samples be monitored during the experiment. This latter measurement appears to be relatively simple using the technique reported by Neel (Ref. 47) since it involves only the measurement of sample temperatures just before and just after the samples enter the earth's shadow. The large amount of additional information on the performance of reflective surfaces in space made available by the temperature measurements makes the inclusion of these in the space experiment very desirable.

2.3.5 Other Causes of Mirror Degradation

Evaporation in the high vacuum of space is currently seen as presenting no problem. At 700°C temperature, aluminum will lose about 20 Å per year and silver 100 Å per year. This extreme temperature, which is not expected on solar concentrators, is chosen to illustrate the small magnitude of the evaporation effect.

It has been pointed out, however, that a metallic film is not amorphous but has microscopic graininess, representing growth in different crystalline directions. It is known that evaporation from the different crystal faces is not a constant and also that evaporation from the grain boundaries and any imperfections are much higher than from perfect crystals. It is not unreasonable to expect a factor of 10 increase in evaporation rate from these grain boundaries. This would mean that in some places 1000 Å/Yr of silver would evaporate, i.e., the

metal film would totally disappear. It has been shown recently that when a metallic surface is "rough" the fraction of specular reflection from it that becomes diffused is given by

$$F = 1-\exp(-\pi d^2/\lambda^2) \; \pi \frac{d^2}{\lambda 2}$$

where λ = wavelength of light being used

d = average heights of "hills" and "valleys" on surface average over the total surface

If 1000 Å valleys are introduced into say 10 percent of the metallic surface, then the average height is only 100 Å, giving at 5000 Å a negligible change to diffuse reflection in one year, and a change of 1 percent in five years.

High-energy electrons and protons will produce very slight changes in the electrical properties of metallic films by atomic displacement. These in turn influence the optical properties. However, the effects in metals are so slight that it is expected that the specular reflectivity will degrade less than 1 percent per year.

High-energy photons, x-rays and ultraviolet from the sun, will produce ionization in metals. However, electrostatic principles show that the electrons which are ejected from the metal form a "sheath" near it and produce a surface dipole effect. It is expected that any other material in space such as dust particles will also look like dipoles due to ionization. At distances greater than a centimeter, the dipoles look electrically neutral with no structure. Hence there will be no electrostatic attraction onto the mirror surface.

It appears that all the mechanisms discussed here will produce negligible changes in reflectivity in a year and only minor changes in up to five years. However, much more experimental data should be made available concerning rough surfaces.

2.4 Experiment Requirements

This section is a general treatment of the space flight experiment on solar-concentrator reflective surfaces. The sample exposure to the space environment and the various types of measurements which could be performed on the samples are discussed. Methods of differentiating between the specific causes of reflector degradation in space are included as well as the overall operational philosophy of the flight experiment. Finally, the relation of the ground simulation tests to the flight experiment is discussed.

2.4.1 Experimental Operational Philosophy

As a result of Sections 2.1, 2.2 and 2.3 a general solar-concentrator reflective surface flight experiment operational philosophy can be established. Section 2.1 is a general definition of the space environment as it is known at the present and Section 2.2 describes the various types of samples which should be considered for testing. Section 2.3 has taken the space environment definition and the selected samples and has attempted to predict the reflectivity behavior of the samples in space. Based on the above it appears that the most predominant causes of reflectivity degradation are sputtering due to low energy protons, ultraviolet radiation which produces photochemical changes especially in dielectric and anodic coatings and micrometeoroids. Some of the predictions are based upon analysis and others on ground simulation data. The predictions on reflectivity degradation vary widely because of the lack of empirical data on the space environment. Also there have been very few ground simulation tests for this specific purpose (although this situation is presently changing). Therefore, predictions of reflectivity degradation vary from less than 1 percent per year to values up to 40 percent per year.

As a result of this uncertainty in performance prediction it is recommended that the overall flights experiment operational philosophy be such that the samples be exposed to the worst possible space environment. This recommendation is part of the experiment requirements and affects the overall satellite system design. With respect to low-energy protons (sputtering) the optimum orbit altitude (most severe exposure) is in the region of 10,000 n. mi. Solar ultraviolet radiation is independent of altitude (for earth orbits) but requires the samples be oriented to the sun. Also, from the analysis and prediction it appears that the duration of the flight experiment should be not less than one year. It is felt that this test duration should provide sufficient data for extrapolation purposes.

The above experiment requirements are from the experiment point of view and may have to be compromised because of practical systems problems and cost. For comparison purposes Table 2-13 shows the above experiment requirements for the experiment point of view, (optimum) and the expected performance of the preferred and minimum experiment.

TABLE 2-13 COMPARISON OF PREFERRED AND MINIMUM EXPERIMENTS TO OPTIMUM

	OPTIMUM	PREFERRED	MINIMUM
Orbit Altitude (n. mi.)	10,000	4,000-5,500 apogee 300 perigee	3000 apogee 200 perigee
Solar Orientation	Yes	Yes	Partial
Experiment Duration	1 Year	1 Year	0.5 Year

For the preferred experiment all requirements are met except the orbital altitude. This is a compromise due to economics, i.e., the cost of the launch vehicle to put a meaningful payload into a 10,000 n. mi. altitude orbit is felt to be out of the scope of the experiment. However, at the 4,000 to 5,500 n. mi. altitude apogee the number of low-energy protons

per unit area per unit time is only down by a factor of ten. For the minimum experiment the orbit altitude is even lower due to the launch vehicle. No active solar orientation is provided for the minimum experiment. However, the spin axis of the minimum experiment is properly aligned for maximum passive solar orientation during its lifetime (6 mos.). The lifetime of the minimum experiment is determined chiefly by the vehicle (P-11).

2.4.2 Sample Exposure

The purpose of the flight experiment is to determine the degradation of solar-concentrator reflective surfaces as a function of exposure to the space environment. This section discusses briefly the aspects of the exposure to the space environment. In accordance with the overall experiment philosophy of maximum sample exposure to the space environment an obvious requirement is that the samples be mounted to the exterior skin of the satellite. Considering sample exposure, the space environment can be divided into roughly two categories with respect to a satellite - directional and omnidirectional. The solar radiation is, of course, directional whereas (for purposes of sample exposure) particle radiation may be considered as omnidirectional. Electromagnetic radiation from the earth's albedo and self-emission is somewhat directional depending on the altitude of the satellite. Thus, the considerations of sample exposure should take into account the geometrical aspects of the space environment.

As a part of the overall experiment requirement it is felt that the samples be tested under conditions similar to those of actual solar-concentrator operation. This should include not only the exposure of the actual solar-concentrator to the space environment but also the expected thermal performance of the solar concentrator. The reason for this is that some degradation effects may be temperature-dependent. In actual operation a solar concentrator will be oriented towards the sun at all times (except when in the earth's shadow). Thus,

the reflecting or front face of the solar concentrator will see the sun. The rest of the 2π steradian field of view of the front face will see the omnidirectional aspects of the space environment, the earth at times and possibly some portions of the spacecraft. For many solar-concentrators the rear surface is used for thermal control and is quite important. The rear surface, of course, will never see the sun but will see the omnidirectional aspects of the space environment, the earth at times and some portion of the spacecraft. These then are the solar-concentrator geometrical conditions of operation which should be simulated for sample exposure for the flight experiment.

Various types of sample mountings and satellite configurations were considered and these are shown in Figure 2-20. From an active satellite attitude control and launch vehicle point of view the basic configuration of the satellite is a flat cylinder. In Figure 2-20 the solar radiation is directed on the satellite from the top of the page. Figure 2-20a shows the samples mounted on the flat face of the cylinder facing the sun. Here the reflective face of the sample simulates very well the actual condition of solar-concentrator operation. However, the rear face of the sample sees only the satellite and not space or the earth. Figure 2-20b shows an effort to rectify this problem where again the sample front face simulates the desired conditions very well and the back face sees space and the satellite since the samples are suspended in a flange. However, the view factor of the sample back with respect to the satellite may be quite large for simulation purposes. Figure 2-20c shows a compromise where the sample back face will see more of space and less of the satellite (depending on the distance between the sample and the satellite curved surface and the length of the satellite). However, now the front surface of the sample sees a good portion of the satellite and, in addition, a mis-alignment in attitude may cause the satellite to occlude the sample from solar radiation. Figure 2-20d shows the sample flange at the bottom of the satellite where the back face of the sample sees only

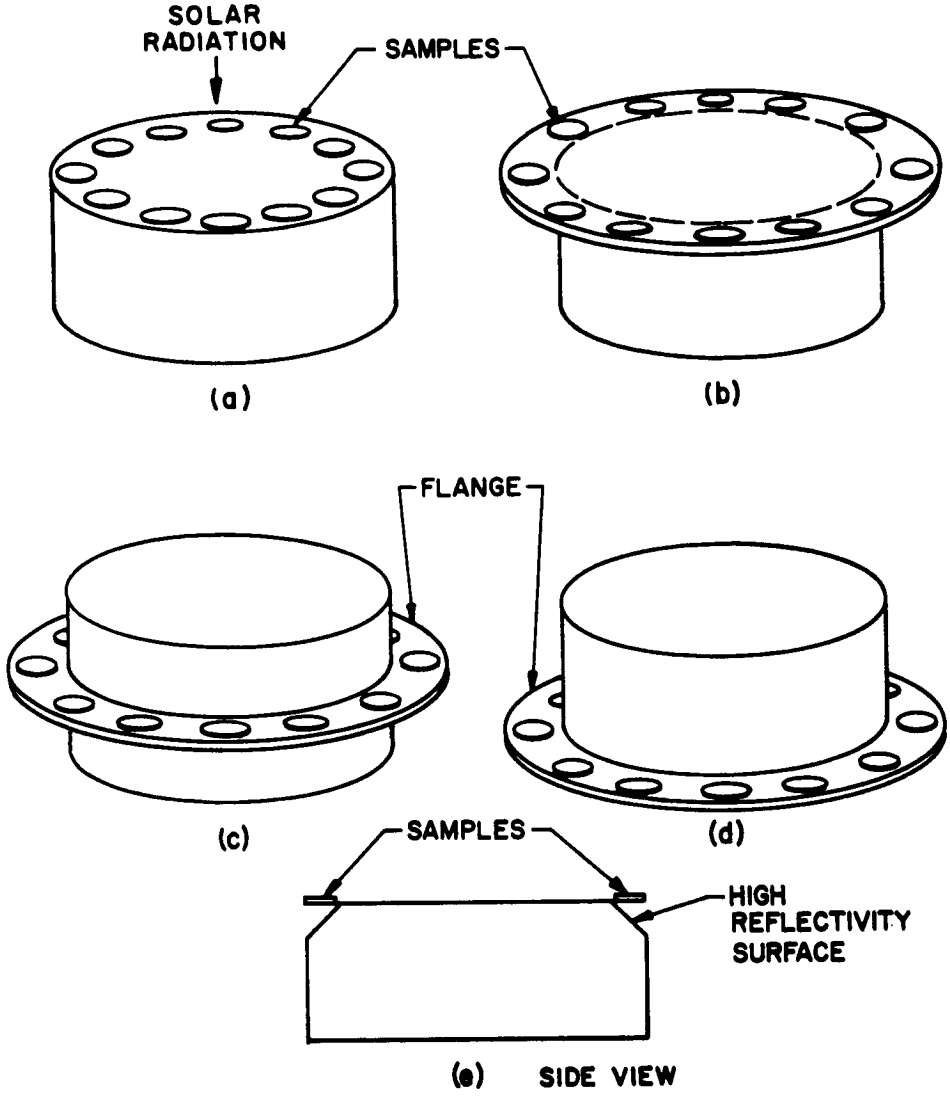

FIG. 2-20 VARIOUS SATELLITE CONFIGURATIONS

space but the same objections for the front face are even worse than those in Figure 2-20c. Figure 2-20e shows a modification of Figure 2-20a where the space environment exposure to the front face of the sample is best and by means of a flange mounted sample and a 45° reflecting surface behind the sample the sample back sees space for thermal control purposes. Even this is not ideal since the sample back face sees space at 90° from the sun whereas a solar-concentrator will see space at 180° from the sun. Finally, the problem of simulating the view factor of a solar-concentrator back face with respect to the satellite is difficult since the view factor will vary with specific solar power system missions and satellites.

The satellite/sample configuration shown in Figure 2-20a was chosen as the optimum for various reasons. These reasons are:

1. It offers a 2π steradian exposure to the space environment for the front face.

2. It offers a minimum problem for solar orientation.

3. Because it was felt desirable to know the α/ϵ and ϵ values of the sample front face via a temperature measurement (see Sections 2.4.3 and 4.1.2) the heat flow from the back face should be kept to a minimum for some samples and flange mounting would be difficult to accomplish this.

4. Means of accomplishing the reflectivity instrumentation appear easier with this configuration.

5. Simplification of overall satellite design and construction is achieved.

The amount of exposure of the samples to solar radiation will depend on the quality of the altitude control and the orbit altitude (earth eclipse). Sample exposure to solar radiation will vary with the cosine of the angle of the attitude control system accuracy and thus it is felt that close tolerances on attitude control are not necessary for sample solar exposure purposes. The fraction of the orbit period that the samples are not exposed to solar radiation (by means of an earth eclipse) is discussed in Section 3.1.

2.4.3 Measurements

The specific parameters which should be measured and how they are to be measured is a very important aspect of the experiment requirement and definition. These measurements will not only be a function of the experiment objectives and mission but also of practical space systems (telemetry, power, etc.) and environmental restrictions. It is recommended that three types of measurements be performed on the flight experiment - reflectivity, temperature, and space environment measurements. These are discussed in the following subsections.

2.4.3.1 Reflectivity

Since the purpose of the flight experiment is to determine the degradation of solar-concentrator reflective surfaces due to the space environment the sample reflectivity becomes a prime measurement. The methods of measuring sample reflectivity and the pros and cons of the various methods are the subject of this subsection.

The reflectance (R) of a surface is the ratio of the amount of electromagnetic radiation reflected from the surface to that incident upon that surface. The factors which influence R are the optical constants of the reflecting surface (which vary with wavelength), the angle of incidence, the angle of polarization of the electromagnetic radiation and the surface roughness. The surface roughness is included because for the solar-concentrator application we are concerned with specular reflections, i.e., diffuse reflection shows up as a reduction in reflectance as far as a converter cavity is concerned. The reflectance of an opaque surface can be expressed as

$$R_p = \frac{(n - \sec \emptyset)^2 + k^2}{(n + \sec \emptyset)^2 + k} \tag{2-16}$$

and

$$R_s = \frac{(n - \cos \emptyset)^2 + k^2}{(n + \cos \emptyset)^2 + k^2}. \tag{2-17}$$

The terms R_p and R_s are the reflectances for incident radiation polarized parallel and perpendicular to the plane of incidence respectively, n and k are the refractive index and extinction coefficient respectively of the reflecting surface (optical constants) and $\emptyset$ is the angle of incidence. If unpolarized radiation is incident on the reflective surface then the reflectance may be expressed as

$$R = R_p/2 + R_s/2. \tag{2-18}$$

For normal incidence the reflectance expression is reduced to

$$R_o = \frac{(n - 1)^2 + k^2}{(n + 1)^2 + k^2} \tag{2-19}$$

The above expressions assume the incident medium to be a vacuum which it is in the case of the flight experiment. Equations 2-16 and 2-17 are shown graphically in Fig. 2-21 which also demonstrates Eq. 2-19.

In defining the reflectivity measurements the question of what to measure must be answered. For example, the engineering community would probably be interested in an overall reflectivity measurement whereas the scientific community might be more interested in a set of reflectivity measurements from which the optical constants could be calculated. The former would, in general, represent less sophisticated equipment than the latter. Of course, the latter would represent more information concerning the performance of solar-concentrator reflective surfaces in space.

For the overall reflectivity measurement the question of angle of incidence from the experiment point of view must be answered. There are many factors in favor of performing reflectivity measurements at near normal incidence. For example, the reflectance at zero incidence is a relatively simple function of the optical constants (Eq. 2-19). As can be seen from Fig. 2-20, working at near normal incidence the measurement is relatively insensitive to

polarization effects. Thus, polarization effects introduced by the optics of the instrumentation will not be serious. Also, the angle of incidence is not critical for near normal incidence. In other words, if the angle of incidence is chosen sufficiently near zero the values of the reflectance coefficients for the two states of polarization, R_p and R_s, will differ from R_o by an amount less than the precision of the measurement.

In actual use, the angle of incidence on solar concentrators is from about 2° to 30° depending upon the configuration of the individual concentrator and its central obscuration.

It would be of interest to know the average angle of incidence on a parabolic solar concentrator. However, this average angle should be calculated with respect to the collected energy. The collector radius at which the average angle (with respect to collected energy) occurs can be approximated by

$$r_3 = \frac{r_1^2 + r_2^2}{2} \qquad (2\text{-}20)$$

where r_1 and r_2 are the collector and obscuration radii respectively.For example, consider a 60-inch radius collector with a 15-inch radius obscuration. The value of r_3 is then 43.7 inches. If we assume the angle of incidence at the 15-inch radius is 2° and at the 60-inch radius is 30° and assume linearity (which it is not) then the average angle of incidence with respect to collected energy is about 27°.

The result of the above discussion is that with respect to the overall reflectivity measurement angles of incidence close to the normal are desireable whereas the average angle of incidence on a solar collector is in the neighborhood of 27°. However, it is felt that simulating the average angle of incidence with the reflectivity measurement is not really necessary since the degradation of the sample due to the space environment should not be a function of the angle of incidence of the measurement in the 0° to 20° range. These considerations seem to

favor performing the reflectivity measurement at near normal incidence. However, one final comment is that using near normal incidence may require fairly long optical paths. This could manifest itself in instrument alignment problems which could result in reflectivity measurement errors.

In addition to angle of incidence the choice of the reflectivity measurement spectral region must be made. Figure 2-22 shows the spectral distribution at a solar concentrator focus. These curves are essentially the solar spectral irradiance as modified by the collector spectral reflectivity. This is what the energy converter "sees" spectrally. Curves are given for silver, aluminum, and aluminum overcoated with two forms of SiO for representative solar concentrator reflective surface spectral distributions. Clearly the spectral range of interest for the reflectivity measurement is from about 0.3 to 3.0 microns.

The question of spectral reflectivity measurements should be considered. First, it is felt that a broad band or "white light" reflectivity measurement be performed which covers most of the significant solar spectrum with respect to solar concentrators. This measurement will give an indication of the overall sample reflectivity. Ideally, the spectral distribution of this measurement (the product of the spectral energy distribution of the instrument light source and the spectral response of the detector) should conform to that of the sun. However, this will be difficult because of the nature of available light sources and detectors.

It is felt that spectral reflectivity measurements will give further information concerning sample reflectivity performance over that of the broadband measurements. This is true not only because there are more data points but also a spectral measurement can give clues as to the mechanism of degradation. For example, the reflectivity degradation of a bare metal sample due to sputtering or micrometeoroids (specular to diffuse degradation) may show up first in

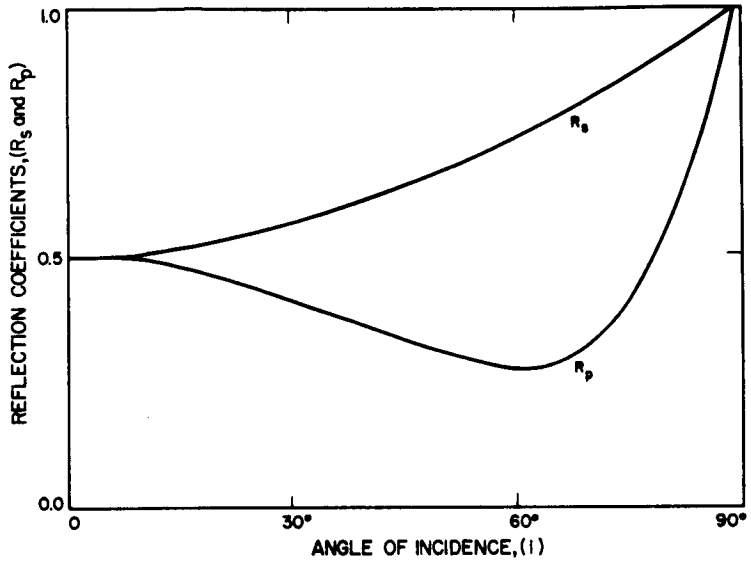

FIG. 2-21 TYPICAL REFLECTANCE COEFFICIENTS R_s AND R_p AS A FUNCTION OF ANGLE OF INCIDENCE

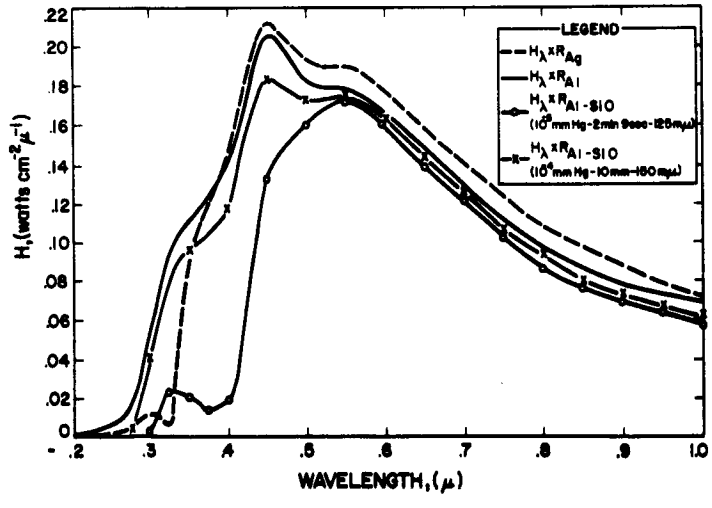

FIG. 2-22 SOLAR IRRADIANCE AS MODIFIED BY REFLECTIVITY CHARACTERISTICS

the low-wavelength region of the spectrum. Also, samples that are coated with dielectric materials may show more degradation in the blue, violet, and ultraviolet region of the spectrum. Thus it is recommended that both broadband and spectral reflectivity measurements be performed on the flight experiment.

It is felt that a specular reflectivity measurement be made since this type of reflection is inherent in the operation of solar collectors. In general, the field of view of the specular reflectivity measurement should not be widely different from that subtended by a cavity at the focus of a parabolic solar concentrator. This is not true, however, of solar-cell type solar concentrators.

Since it is expected that one type of sample degradation will be from specular to diffuse reflection it would be advisable to perform a measurement of this. It should be pointed out that a degradation of specular to diffuse as opposed to some other form (say discoloring) cannot be differentiated by an energy converter cavity. However, the knowledge of the type of degradation is valuable in determining the cause of degradation. Diffuse reflection is best measured by an integrating sphere. The disadvantages of this type of measurement are:

1. The instrumentation is usually bulky.
2. Low light levels are involved thus requiring photomultiplier detectors and their associated difficulties.
3. Calibration is difficult especially for a remote measurement.
4. It does not lend itself easily to the instrument operational philosophy and interferes with other measurements in operation.

Finally, it is not expected that a spectral diffuse reflection measurement would yield significant data in view of other instrumentation and system constraints.

One final measurement which could be performed is a measurement of the optical constants of the reflective sample. This would give another indication of the causes of reflectivity degradation. However, a great number of the samples will have various types of overcoatings and will not be simple surfaces. Thus a measure of the optical constants may yield highly complex data from which little can be deduced. Also, the measurement of the optical constants will increase and complicate the instrumentation (since a normal incidence reflectometer cannot be used) and thus put additional requirements on the satellite system.

2.4.3.2 Temperature

In addition to measuring the reflectivity it will be important to measure the temperature of the reflective sample. This should be done not only while the sample is exposed to solar radiations but also when it is in the earth's shadow to monitor the thermal duty cycle. Sample temperature may be important in the resultant effect of a particular aspect of the space environment on reflectivity. Also, the knowledge of sample temperature is an indication of the α/ε ratio which is vital in space thermal balance considerations. The method of temperature measurement and the mounting of the temperature transducer to the sample is discussed in Sections 4.1.2 and 4.2.2.

2.4.3.3 Space Environment

In addition to measuring sample reflectivity and temperature it would be desirable to measure the magnitude of some aspects of the space environment. This is attractive since both reflectivity degradation and the environment which is causing the degradation will be measured at the same time and place. If this were not done then correlation between reflector performance and space environment would have to rely on environment data taken at a different time

and place and under different circumstances. The philosophy of the space environment measurements should be such that they do not compromise the prime reflectivity measurements. In other words, their power, weight, space, telemetry, and other interface requirements should be a small fraction of those for the prime measurement.

2.4.3.4 Recommendations

As a result of the above discussion it is recommended that the following measurements be performed on the space flight experiment:

1. Specular reflectivity at normal incidence for one broadband and several smaller-band spectral measurements. The exact number and bandwidth of the spectral intervals will be determined from instrumentation and systems considerations. The broadband measurement will give overall reflectivity performance and the spectral will give a clue to the type and cause of degradation.

2. Sample temperature measurements to monitor sample thermal performance and achieve a calculation of α/ε and ε. These data can also be fed back into the reflectivity data for further analysis and correlation.

3. Space environment measurements for correlation with reflectivity measurements. These measurements are also valuable from a scientific point of view.

2.4.4 Separation of Effects

As a part of the experiment requirement and definition it is recommended that the method of measurement and operation of the flight test be performed in such a manner that information can be gained concerning the actual causes of reflectivity degradation. As was mentioned in Section 2.4.3 the spectral reflectivity measurement will give some clue as to the cause of degradation (also with the space environment measurement) but these data will be further strengthened

by a separation of effects of the space environment. If more than one reflective sample of a given type is tested - one being exposed to some aspect of the space environment and the other not, then this technique will offer further proof of the effects of various aspects of the space environment on the samples. It is felt that this technique of separation of effects can be achieved by using the directional/omnidirectional and energy distribution aspects of the space environment.

The separation of effects can best be achieved by differentiating between the electromagnetic and particle radiation aspects of the space environment. For example, the solar radiation can be shielded from a sample because it is directional and the satellite is sun oriented. This shielding can be accomplished so that particle radiation may still impinge on the sample. Shielding can occur by mounting a set of samples on the side of the satellite facing away from the sun. However, this is undesirable since it requires an additional measuring instrument (reflectometer) which will add to the weight, volume, and power consumption of the satellite. Also, the samples facing away from the sun will see the earth's albedo and thus not be truly shielded from electromagnetic radiation. A more satisfactory method is to mount the samples on the side of the satellite facing the sun and place an opaque shield between them and the sun. This is possible since the satellite is sun oriented. If the shield is some distance away from the sample, particle radiation, which is omnidirectional, may impinge on the sample. The occlusion of the particle radiation by the shield should be small compared to the 2π steradian field of view of the sample.

The effects of particle radiation may be separated from electromagnetic radiation by placing an energy shield immediately over the sample. This energy shield should probably be a cover plate or window of fused quartz (the transmission properties of fused quarts are quite stable in the space environment). Fused quartz is transparent to the visible spectrum and a good portion of the ultraviolet and infrared

spectrum. Thus, the sample will be exposed to the electromagnetic radiation while being shielded from the particle radiation (which is intercepted by the quartz). Reflectivity measurements can be made through the quartz window providing its transmission is not affected by the particle radiation (example-sputtering in quartz should be less than in, say, aluminum). If this assumption is not valid then the quartz window can be ejected from the sample after some significant exposure to the space environment and a reflectivity measurement can then be made.

Finally, it is felt that one or more significant samples be shielded completely from the space environment (except the vacuum and thermal environment, of course) as a control. In addition, a good number of the samples should be exposed to all aspects of the space environment which is the prime purpose of the experiment and this will also detect any synergistic effects.

2.4.5 Instrumentation Operational Philosophy

There is probably an infinite number of ways to design and operate a reflectometer for a space flight experiment. However, restrictions due to the experiment mission, the space environment and the launch and satellite vehicles limit the possibilities. The purpose of this section is to give the instrumentation operational philosophy which resulted in the instruments and operations for both the preferred and minimum flight experiments.

A requirement for the measurement of reflectivity is that of calibration. Calibration must be performed if significant data are to be acquired. Reflectometer calibration requires moving parts. These moving parts must be designed with reliability, experiment duration and the space environment in mind. Another requirement is that the samples be mounted on the outside skin of the satellite exposed to the environment. This means that the optical beam of the reflectometer must go outside the satellite (assuming the instrument is inside the

satellite), impinge on the sample and return inside the satellite to the detector. All this must be done with a minimum of shielding the sample from the space environment.

The purpose of the flight experiment is to test more than one sample. This brings up the question of whether to have one reflectometer for each sample or one reflectometer for all samples or some point in between. Having one reflectometer for each sample would prohibitively increase the weight of the satellite due to the redundant number of optical elements, etc. Also, all calibrations would have to be independent thus making comparative data uncertain. As a result, it is recommended that one reflectometer optical system (with a common calibrate) be used on all samples. The best method of accomplishing this is to arrange the samples in a circle and rotate either the samples or a part of the reflectometer. An advantage here is that the moving part can not only be used to measure but it can also be used to calibrate by measuring a calibrate position. Also, when not being measured the sample may be exposed to the space environment.

The next question to resolve is whether to rotate the samples to the reflectometer measuring head or rotate the measuring head to the samples. This question is resolved by the requirement of measuring sample temperature. If the samples were rotated on a disk or wheel the signal from the temperature sensors would have to pass over slip rings for continuous rotary motion. For oscillating motion of the sample wheel the temperature sensor signals could use flexible leads but this type motion is not preferred over the continuous rotary motion. Thus, it is recommended that the samples be mounted in a circle on the outside skin of the satellite and that the reflectometer head rotate and scan the samples (see engineering drawing in Appendix A). The reflectometer optical beam can be scanned over the samples without any electrical slip ring problems simply by rotating a mirror (the rotation is supplied by the rotating reflectometer arm).

For redundancy purposes it is recommended that two sets of light sources and detectors share the common reflectometer optical system. One light source is an incandescent filament and the other is a reflecting specular spherical surface which forms a virtual image of the sun. The spherical surface is irradiated by the sun through a small window in the skin of the satellite. There is one detector for the incandescent source (broadband reflective measurement) and five for the virtual solar image. Four of these five are for spectral measurements (by means of a dispersing prism) and the fifth is for a broad broadband measurement.

2.4.6 Ground simulation

It is recommended that ground simulation tests on solar-concentrator reflective surfaces be performed before, during, and after the flight experiment. The tests which are to be performed before the flight experiment should attempt to accomplish the following:

1. Establish the degradation of reflective surfaces in the space environment.
2. Establish the behavior of the thermal constants (α and ϵ) of reflective surfaces in the space environment.
3. Aid in the selection of samples for the flight experiment.
4. Aid in defining materials for solar-concentrator reflective surfaces which are more efficient and durable in the space environment. This would include materials for the substrate, undercoating, reflective layer, and overcoating.

Ground simulation tests which should be emphasized are those for low energy charged particles (which exhibit surface effects), micrometeoroids and ultraviolet radiation. The tests should be performed with sample thermal simulation. The ground simulation tests which are performed during and after experiment can provide correlation information as well as further tests on items 1, 2, and 4 above.

3. PREFERRED AND MINIMUM FLIGHT EXPERIMENT LAUNCH VEHICLE

3.1 Orbital Analysis

This section describes the work accomplished in investigating the payload weight vs. orbital altitude study. The results of this subtask are an input to the experiment definition subtask and the weight budget of the instrument and system design. An orbital analysis concerning the amount of solar exposure is also included.

3.1.1 Payload/Orbit Altitude Study

Three basic methods for launching a payload into a high-altitude circular orbit about the earth are: (1) a multi-stage chemical rocket, launched from the earth's surface and provided with suitable attitude control; (2) a chemical booster, launched from the earth's surface, which places a low-thrust rocket (i.e., ion engine, arcjet, etc.) in a low-altitude orbit, and the rocket then spirals out (very slowly) to the desired altitude; (3) a chemical booster, launched from the earth's surface, which places a chemical rocket in a low-altitude earth orbit, and after the application of impulse thrust, the rocket moves out along a Hohmann transfer ellipse to the desired altitude. The first method is the quickest and, in principle, the simplest of the three. The second method is able to place the most massive payload into orbit, although the mission times are rather long. The third method is essentially the same as the first, except that the mission times are somewhat longer, but not as long as the mission times in the second method. Determining the relationship between payload mass and orbit altitude by employing the first and/or second launching methods would require the use of a large, digital computer. A digital computer would also be needed to simulate the first part of the third method, i.e., placing the smaller chemical rocket in a low altitude orbit by means of an earth-launched booster. Fortunately, though, the payload masses which various booster combinations (both present and future) can place in a given low-altitude

earth orbit (300 n. mi. circular orbit) are available in the literature. Treating these masses as initial gross weights in the second part of the third method, it is possible to construct the Hohmann transfer ellipse and determine the mass of the payload, without the use of a digital computer. Due to the relative simplicity of this approach, the third method of launch will be employed in this study.

Fig. 3-1 shows the generation of the Hohmann transfer ellipse. Here, r_p and r_a denote the perigee and apogee distances, respectively, of the transfer ellipse, where r_p is also the radius of the initial 300 n. mi. orbit, and r_a the radius of the final orbit. The quantities Δv_1 and Δv_2 represent the changes in orbital velocity resulting from the application of impulsive thrust, where

$$\Delta v_1 = \left(\frac{K}{r_p}\right)^{\frac{1}{2}} \left[\left(\frac{2r_a}{r_a + r_p}\right)^{\frac{1}{2}} - 1\right] \tag{3-1}$$

$$\Delta v_2 = \left(\frac{K}{r_a}\right)^{\frac{1}{2}} \left[1 - \left(\frac{2r_p}{r_a + r_p}\right)^{\frac{1}{2}}\right] \tag{3-2}$$

Here, $K = 14.1 \times 10^{15}$ ft^3/sec^2 and $r_p = 2.272 \times 10^7$ ft. If we assume that the acceleration due to gravity is negligible compared with the acceleration due to thrust (this is a valid assumption), then it is not difficult to show that the payload ratio is given by

$$\frac{M_L}{M_o} = \frac{e^{-\frac{\Delta V}{gI}} - k}{1 - k}, \quad \text{where,} \quad \Delta V = \Delta v_1 + \Delta v_2. \tag{3-3}$$

Here, M_o = mass in 300 n. mi. orbit $= M_p + M_L + M_s$, where, M_p = total propellant, M_L = payload, M_s = structure. Also,

k = structure factor = $M_s/(M_p + M_s)$, and I = specific impulse, of the final rocket stage. For the purpose of this study we shall tentatively take $k = 0.1$ and $I = 400$ sec. Assigning values of orbital altitude, $r_a - R$ (R = radius of earth), in the range $300 \leq r_a - R \leq 19{,}360$ n. mi.,* and employing the different M_o which various booster combinations are able to put into a 300 n. mi. orbit, equations 3-1, 3-2, and 3-3 readily yield the curves shown in Fig. 3-2. Here, the payload in the final circular orbit is plotted against orbit altitude, for several booster combinations. Thus, for example, the Atlas-Centaur booster plus the final rocket stage can put a 7200 lb. payload in a 1000 n. mi. orbit, by means of the Hohmann transfer ellipse.

If the last impulse (Δv_2) were not applied, the final orbit of the payload would simply be the transfer ellipse, having a perigee of r_p = 300 n. mi. + R (R = radius of earth), and an apogee, r_a, related to the first (and only) thrust impulse, Δv_1, according to:

$$\Delta v_1 = \left(\frac{K}{r_p}\right)^{\frac{1}{2}} \left[\left(\frac{2r_a}{r_a + r_p}\right)^{\frac{1}{2}} - 1 \right] \qquad (3\text{-}4)$$

Refer to Fig. 3-1. One advantage of the elliptical orbit over the subsequent circular orbit is the increase in payload, due to the elimination of the second impulse, Δv_2. Thus, the payload fraction M_L/M_o is given by:

$$\frac{M_L}{M_o} = \frac{e^{-\frac{\Delta V}{gI}} - k}{1 - k} \qquad (3\text{-}5)$$

where, now, $\Delta V = \Delta v_1$. Another possible advantage of the elliptical orbit is that the payload (i.e; reflective surfaces) may be subjected to a greater variation in the space environment than would be possible

* Altitude of the synchronous orbit is 19,360 n. mi.

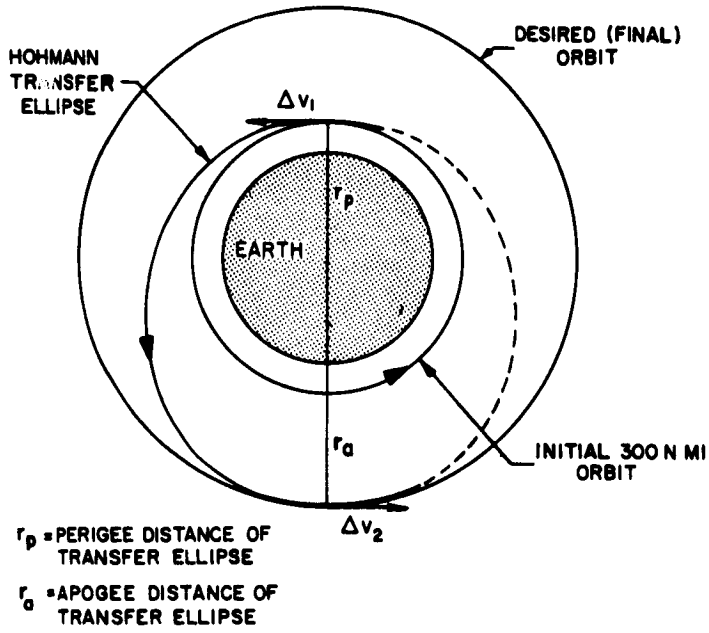

FIG. 3-1

TRANSFER ELLIPSE FROM INITIAL TO FINAL ORBIT

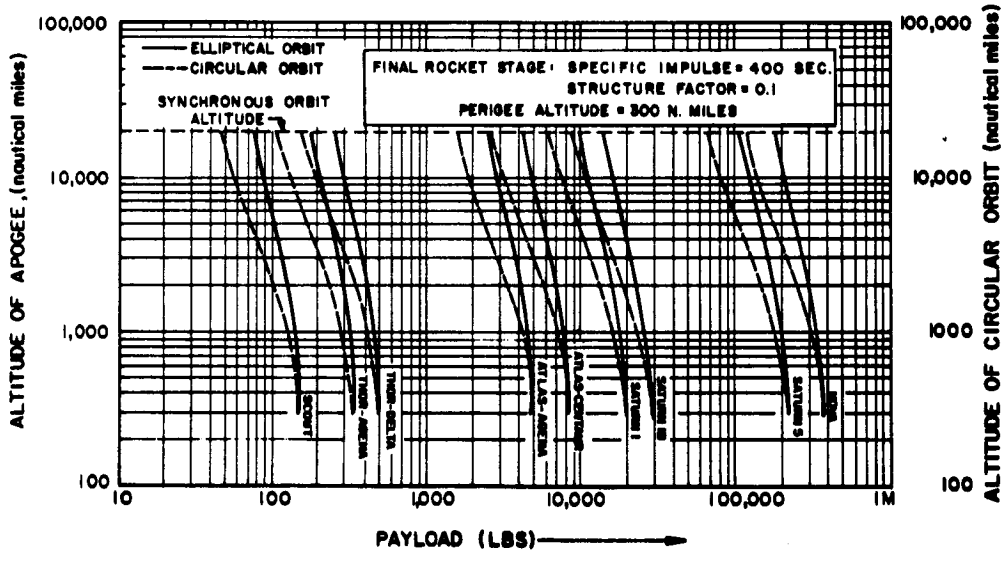

FIG. 3-2 PAYLOAD IN ELLIPTICAL ORBIT VS ALTITUDE OF APOGEE, FOR SEVERAL BOOSTER COMBINATIONS (FIXED PERIGEE ALTITUDE = 300 N. Mi.)

on a circular orbit. Assigning values of apogee altitude, $r_a - R$, in the range $300 \leq r_a - R \leq 19{,}360$ n. mi. (synchronous orbit altitude), and employing the different M_o which various booster combinations are able to put into a 300 n. mi. orbit, equations 3-4 and 3-5 (where $I = 400$ sec, $k = 0.1$) yield the curves (solid lines) shown in Fig. 3-2. For a given booster, note that the increase in payload of the elliptical orbit over that of the subsequent circular orbit becomes greater as the altitude of apogee increases. For a given apogee altitude, the payload difference increases with increasing booster size.

3.1.2 Passage Through Earth's Shadow

Of interest is the fraction of the period spent by the orbiting payload in the earth's shadow. Fig. 3-3, which is not drawn to scale, shows a two-dimensional cross section of the earth's shadow. Here, A is the radius of the sun, a the earth's radius and R the distance between the centers of earth and sun. The umbra, or total eclipse region, extends out into space a distance equal to $Ra/(A-a)$ = 746,000 n. mi., which is 3.6 times the moon's distance from the earth. The angular width, ϵ, of the penumbra, or partial eclipse region, is given by

$$\epsilon = \tan^{-1} \frac{1}{R}(A-a) + \tan^{-1} \frac{1}{R}(A+a)$$

$$= 0.534 \text{ deg.}$$

If the orbital plane of an earth satellite is oriented such that the line connecting the centers of earth and sun lies in this plane (e.g., the plane of the paper in Fig. 3-3), then the satellite will spend maximum time in the penumbra (as well as the umbra) region. As the orbit altitude increases the time spent in the penumbra will also increase, for the following two reasons: a) increase in orbit

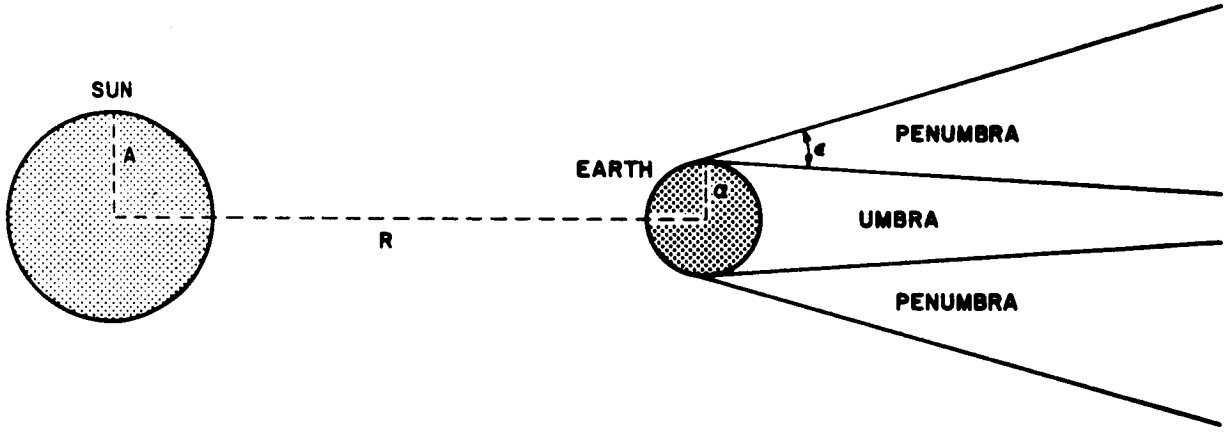

FIG. 3-3 CROSS SECTION OF EARTH'S SHADOW (NOT DRAWN TO SCALE)

altitude, b) lower orbital velocity of satellite. The maximum orbit altitude considered for this study is that of the synchronous orbit, i.e; 19,360 n. mi. Employing the value of ϵ computed above, the maximum time spent in a single penumbra region by a satellite at the synchronous altitude turns out to be 2.14 minutes, which is approximately 0.15 percent of the total period. The time spent in the umbra at this altitude is approximately 70 minutes. In view of the relatively short time spent by the satellite in the penumbra, this region will tentatively be ignored in the study.

The time spent in the earth's shadow by a satellite depends on 1) the altitude of the satellite orbit, 2) the angle between the normal to the orbital plane and the line between the centers of the earth and sun. The latter quantity depends on the time of the year and the orientation of the orbit relative to the fixed stars. It can be shown that the fraction of the orbital period, $\Delta T/T$ (T = period of orbit), spent by the satellite in the earth's shadow is given by

$$\frac{\Delta T}{T} = \frac{u}{\pi}, \qquad [u] = \text{radians} \tag{3-6}$$

where,

$$\cos u = \frac{16.0 + \left[(a + h)^2 - 11.82 \times 10^6\right]^{\frac{1}{2}}}{(a + h) \sin i} \tag{3-7}$$

and

$$\cos i = \cos(\alpha t) \sin \gamma \sin \lambda + (0.3987 \cos \gamma - 0.9170 \sin \gamma \cos \lambda) \sin(\alpha t) \tag{3-8}$$

Here, $a = 3440$ n. mi., h = altitude of circular orbit (n. mi.), i = angle between normal to orbital plane and line connecting earth and sun, $\alpha = 0.9863$ deg./day, t = time of year, measured in days,

where $t = 0$ corresponds to March 21, γ = inclination of satellite orbit to equatorial plane and λ = angle, measured in the equatorial plane, between the ascending node of the satellite orbit and the direction of the vernal equinox. Refer to Fig. 3-4. Here, the directions of the x, y, z axes are fixed in space, where the x axis points to the vernal equinox and the z axis points to geographic north. The normal to the orbit plane is coincident with the orbital angular momentum vector, and the angle λ is measured in the equatorial plane (x y plane). It may be easier to physically measure the angle between the x axis and the ascending node of the orbit in the plane of the ecliptic, rather than in the equatorial plane. If we denote this angle by Ψ, then λ is given by

$$\cos \lambda = \frac{0.3656 \cot \gamma + \cot \Psi \left(\csc^2 \Psi - 0.159 \csc^2 \gamma\right)^{\frac{1}{2}}}{0.84 + \cot^2 \Psi} \tag{3-9}$$

It should be pointed out that if the computed value of $|\cos \mu|$ in eq. 3-7 is greater than unity, then the satellite orbit never enters the earth's shadow. Also, if the computed value of $|\cos i|$ in eq. 3-8 is equal to unity, then the satellite never passes through the shadow. Finally, the values of γ and λ may change over an extended period of time, due to perturbations of the satellite orbit caused by the sun, moon and the earth's oblateness.

3.1.3 Time Spent in Earth's Shadow

The length of time spent in the earth's shadow by the satellite is of interest from the viewpoint of power generation and solar reflective surface deterioration. The time spent in the shadow is a function only of the orbit altitude and the angle, i, between the earth-sun line and the normal to the orbit plane. When this angle is 90°, the shadow time is at a maximum, for any orbit altitude. Employing Eq. 3-7 letting $i = 90^{\circ}$, and taking orbit altitudes, h, in the range $300 \leq h \leq 20{,}000$ n. mi., we obtain the graph shown in Fig. 3-5. Plotted in Fig. 3-5 is the maximum time spent in the earth's shadow by the satellite (in a circular orbit) versus orbit altitude. Included in the graph is the orbital period as a function of orbit altitude. Thus, from a knowledge of shadow time, it is possible to compute the time spent in the sunlight by the satellite.

The time, t_s, spent in the earth's shadow for any angle i is given by

$$t_s = \frac{T}{\pi} \cos^{-1} \left[\cos \left(\pi \frac{t'_s}{T} \right) \frac{1}{\sin i} \right],$$

where t'_s is the maximum time spent in the shadow and T the orbit period, both shown in Fig. 3-5. Clearly, i must satisfy the restriction,

$$\sin i \geqslant \cos \left(\pi \frac{t'_s}{T} \right)$$

which insures that the orbit lies on the border of the shadow or within it, and not outside it.

3.1.4 Direct Ascent Trajectory versus "Parking Orbit"

The payload containing the solar-concentrator reflective surfaces will be launched into orbit in either of two ways: by direct ascent trajectory, or from a booster vehicle already in orbit. In the former, all stages of the launching rocket fire successively

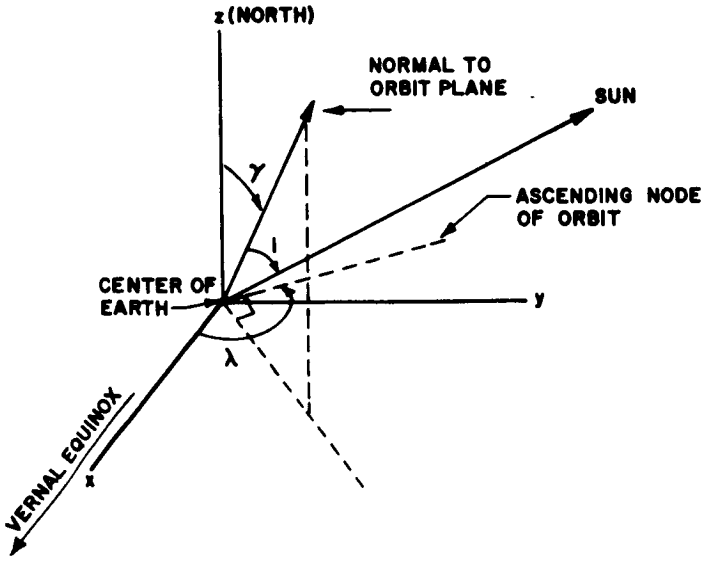

FIG. 3-4 DEFINITION OF γ, λ, i

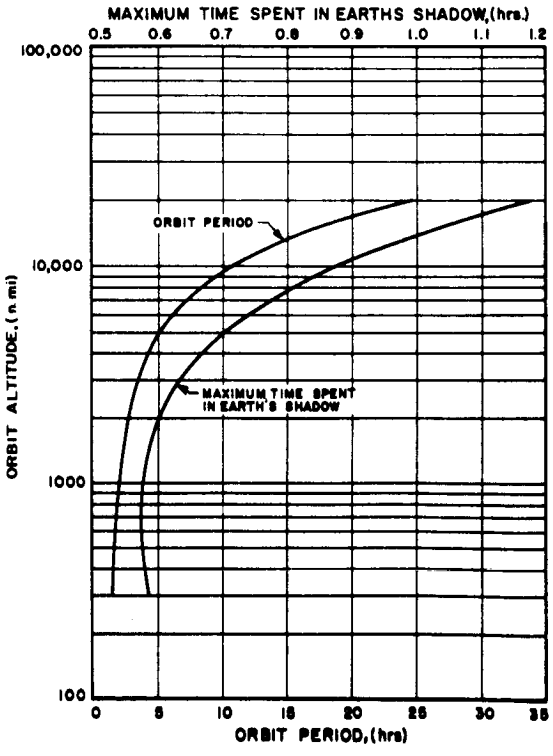

FIG. 3-5

ORBIT PERIOD AND MAXIMUM TIME SPENT IN EARTH'S SHADOW VS ORBIT ALTITUDE (CIRCULAR ORBIT)

(with at most a few seconds delay between stages), and in the latter, the final rocket stage coasts for a prescribed time before firing its motor. An example of a direct ascent launch is the four-stage Scout vehicle. The Atlas-Agena-P-11 combination is an example of a parking orbit launch. Here, the Agena (after thrusting) may coast for several minutes before the P-11 is detached (by spring action) and fires its solid propellant rocket.

The launching trajectory employed for the solar reflective surface experiment will depend on the selected launching vehicle combination. The chief advantage of a 'parking orbit' launch is that it provides a final orbit geometry (such as a particular orbit inclination and/or orientation of line of apsides) that cannot be provided by a direct ascent launch from any one of the limited number of existing launch sites. A disadvantage of this type of launch is a reduction in experimental reliability - for example, the possibility of failure in the firing of the last stage due to a malfunction in the rocket firing mechanism caused by delayed exposure to the space environment. A multistage direct ascent launch, however, is not without its attendant reliability problems. A single stage direct ascent launch (such as an Atlas) is probably the least complicated and most reliable. But the orbit altitudes attained by this type of launch are too low (100-200 n.mi.) for a meaningful solar-concentrator surface experiment.

3.2 Preferred and Minimum Flight Experiment Launch Vehicle Recommendations

One of the tasks of this contract is to give recommendations and estimates concerning a minimum and preferred flight experiment. As set forth in the statement of work these shall be of minimum weight and volume required for a meaningful experiment and the weight and volume for a preferred flight experiment. There is some difficulty in the objective definition of a minimum meaningful and preferred flight experiment. Scientists and engineers may differ somewhat as to the exact definition of these terms. In addition, the definition of minimum and preferred weight and volume should be made with respect to the overall system including the launch vehicle, orbital altitude, etc. In other words, a preferred and minimum experiment instrumentation should be defined in accordance with not only weight and volume but also with compatibility to existing and available launch vehicles, orbit altitude capability, power and telemetry, payload spatial and configuration restrictions, and last but not least, cost of the entire program.

The above method was used to define the preferred and minimum flight experiments. Section 2.4 describes the orbital altitude range which is desired from a meaningful experiment point of view. Section 3.1 describes some of the various launch vehicles capable of orbiting significant payloads in these desired orbits. From the above considerations and in light of launch vehicle cost and availability it is recommended that the preferred experiment be flown prime on the Scout vehicle made by the Chance Vought Corporation and the minimum experiment be flown piggyback on the Agena vehicle via the flight test vehicle P-11 both made by the Lockheed Missiles and Space Company. The payload orbiting capability of both these vehicles is shown in Figure 3-6. The data were obtained from the documents "The Scout", Chance Vought Corp.,

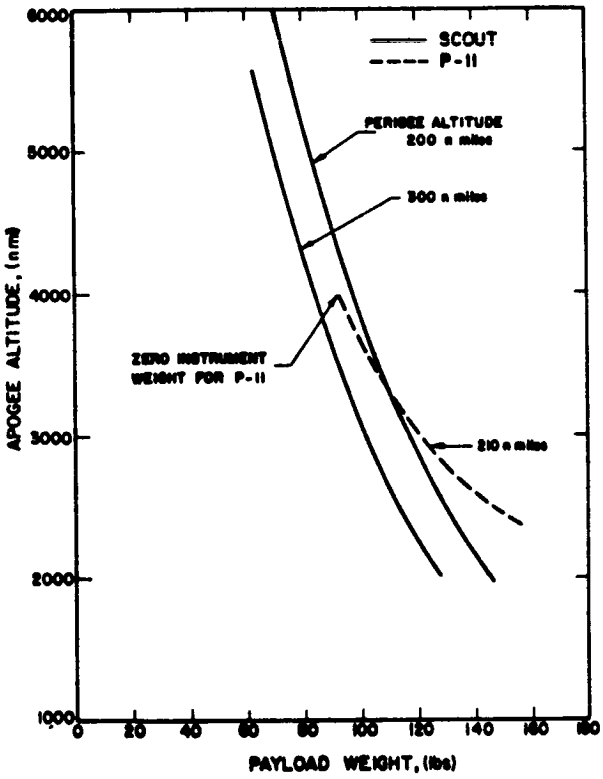

FIG. 3-6

APOGEE VS PAYLOAD WEIGHT FOR SCOUT AND P-11 VEHICLES

revision October 1962 and "Detail Specification Covering Flight Test Vehicle Program 11," report no. LMSC AO 51977A, revised 15 February 1963. The data in Figure 3-6 should be considered as being approximate as they will vary with launch site and azimuth for the Scout and the Agena orbit for the P-11 in addition to other uncertainties.

Larger launch vehicles than the Scout were not considered since it was felt that their costs would be out of proportion with respect to the experiment mission. This is admittedly a subjective conclusion but it appears that the Scout has sufficient orbiting capability for the experiment mission. Other piggyback missions than the P-11 (those which do not separate from the parent vehicle) were not considered because of possible operational and experimental conflicts with the prime experiment and resulting compromises with the present experiment requirements. The following subsections discuss the pros and cons of the Scout and P-11 vehicles with respect to the flight experiment and the expected cost and availability of the vehicles.

3.2.1 The Scout Vehicle

The Scout vehicle appears to be quite suited to the preferred flight experiment for many reasons. Probably the most important advantage and one which has been assumed during this program is that for the preferred experiment the satellite system would be prime on the Scout. The advantages of this method of operation are obvious. The only major interface is with the launch vehicle and this is primarily a mechanical one. The complete satellite vehicle including the subsystems such as power, telemetry, attitude control, etc. can be tailored specifically to the experiment requirements.

A minor disadvantage of the Scout is its inability to place a significant payload into the desired orbit from the experiment point of view. However, the next launch vehicle which has this capability exhibits a large step function in cost. Also, the orbit which can be realized by the Scout (apogee altitude from 4,000-6,000 n.mi.) is a minor compromise from the desired orbit (~10,000 n.mi.) with respect to the

experiment. During the launch phase the Scout does not pose any thermal problems for the experiment instrumentation and with the replacement of the X248 with the X258 fourth stage the launch environmental conditions have been lessened. The fourth-stage spin rate (160-220 rpm) requires satellite despin but this does not appear to be any great problem. The Scout has been reported to be the second most reliable launch vehicle (the first being the Thor-Delta) having had 5 out of 9 (PMR) and 4 out of 6 (Wallops) successful-orbit injections to date. The availability of the Scout has an 8- to 18-month delivery time. The cost of the Scout is quoted at $1,000,000 which includes some engineering services.

3.2.2 The P-11 Vehicle

The P-11 vehicle is stowed inside the aft end of the Agena during the thrusting of the Agena and prior stage. After Agena burnout (and orbit injection) the P-11 is brought out from the Agena through a 90° arc. The P-11 is released, spun up and its own thrustor is initiated thus putting the P-11 into a higher energy orbit. Thus, the orbit parameters of the P-11 are quite dependent on those of the Agena which are a function of the prime (Agena) mission.

One of the greatest difficulties of using the P-11 as a vehicle for the minimum flight experiment is that it exists. Its structure and configuration are fixed, its surface area is assigned (solar cells and thermal control surfaces) and it has its own telemetry and power system. The minimum experiment instrumentation must fit inside the P-11 and, of course, must be designed to accommodate the various P-11 constraints. For example, the instrumentation data system and power requirements must be compatible with the P-11 telemetry and power system respectively. The experiment requires the samples and some of the instrumentation to have access to the surface of the P-11. This means the removal of some of the solar cell panels or thermal control surfaces and possible interface with vehicle structure. Any protrusions (such as a reflectometer head) from the P-11 are quite limited due to the stowage problem in the Agena. The net result of all this is that the

experiment will be compromised by having fewer samples and data points on the samples and lower accuracy. However, it is expected that the results from the minimum flight experiment will be meaningful.

It is recommended that the Model 1207 P-11 be used for the minimum experiment. Its apogee altitude vs payload weight curve is plotted in Figure 3-6. The payload weight for this curve includes the instrument, P-11 structure, power systems and telemetry. The data were plotted in this manner for comparison purposes to the Scout thus the weight of the P-11 thrustor is not included. The curve, of course, is typical. The perigee altitude of the P-11 orbit is shown to be 210 n.mi. and lies fairly close to a Scout curve of comparable perigee. The P-11 curve is not plotted below a payload weight of about 92 lbs since this is the point at which the allowable instrumentation weight reaches zero. With the P-11 the structure, power and telemetry systems are fixed and the only variable is the instrumentation weight whereas with the preferred experiment all are variables. The 210 n.mi. perigee altitude of the P-11 is not ideal from the experimental point of view and it is expected that the apogee altitude will be in the 2500-3000 n.mi. region. Both of these depend upon the initial orbit of the Agena.

The various interface problems with the P-11 can be alleviated by design changes in the P-11. This, of course, will increase the cost of the vehicle. The P-11 is reported to be 100% reliable. However, its operation also depends upon the Agena which is reported to be less reliable than the Scout. Recently, P-11's have been flown at an average rate of one every three months. However, the priority requirement of obtaining a P-11 is another matter which is beyond the scope of this program. Probably more important is the availability of an Agena with the required payload underweight to accommodate a P-11. The cost of an unmodified P-11 is in the neighborhood of $500,000. In conclusion, it is felt that the P-11 is an acceptable minimum flight experiment vehicle. However, care should be taken to insure that modification costs do not get out of hand with respect to the value of the experimental data achieved.

4. PREFERRED FLIGHT EXPERIMENT

This section describes in some detail the recommended preferred flight experiment. In introduction it can be said that the preferred experiment (Figure 4-1) is a self-sufficient, independent satellite launched as a prime experiment by the Scout vehicle. The orbit is elliptical with apogee and perigee altitudes at 4500-5500 and 300 n.mi. respectively with an angle of inclination in the neighborhood of 37°. The minimum duration of the test is one year and the satellite is spin-stabilized. The satellite is solar-oriented by means of pulsed N_2 gas jets. The total payload weight is about 75 lbs (excluding the heat shield) and its overall configuration is a cylinder about two feet in diameter and one foot in length. The flat side of the cylinder which faces the sun contains the reflective samples, the solar cells, some space environment and attitude control sensors and part of the reflectivity measurement instrumentation. The opposite side of the satellite contains the launch vehicle fourth stage adapter, some space environment sensors and the telemetry antennas. The rest of the satellite surface is for thermal control.

A total of 25-28 circular reflective samples, 1.5" diameter can be tested for reflectivity. Provisions are made to attempt to separate the various effects of reflectivity degradation. A distinction will be made between total sample exposure, exposure to electromagnetic radiation, particle radiation, and no radiation (as a control). A tentative sample selection has been made for the preferred flight experiment which is representative of current solar concentrator programs and potential reflective surfaces. Temperature measurements will be made on all samples to evaluate their performance and also to allow the calculation

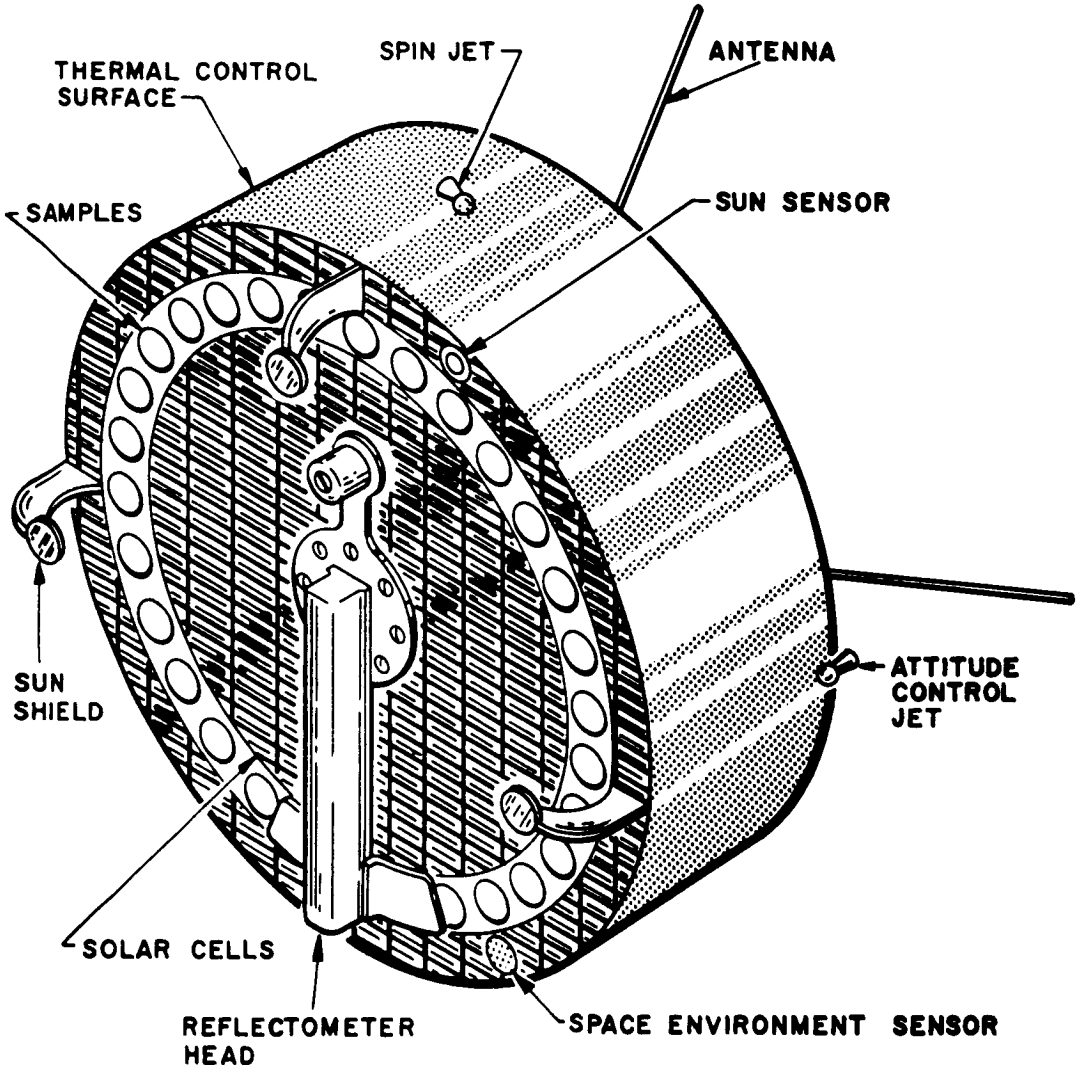

FIG. 4-1 PREFERRED FLIGHT EXPERIMENT

of their absorptivity/emissivity ratios and emissivity. In addition, some aspects of the electromagnetic and particle space environment will be measured. The reflectivity instrumentation uses a single measuring head which is rotated over the sample when a reflectivity measurement is to be made. When not measuring reflectivity the measuring head covers the zero and "100%" reflectivity calibrate positions. The reflectivity instrument has two light sources. One is an incandescent filament and the other is a specularly reflecting sphere which forms a virtual image of the sun as a source. Part of the energy from the solar virtual image is dispersed by a quartz prism giving four spectral reflectivity measurements from 0.3 to 2.8 microns with greater resolution on the low wavelength side. The rest of the energy from the solar virtual image is undispersed and gives a "white light" reflectivity measurement. The energy from the incandescent source also gives a separate "white light" measurement. The overall accuracy of the reflectivity measurements (including the signal conditioning, telemetry, etc.) is from 1 to 2%.

This section discusses in some detail the measurements that are performed on the preferred experiment and the specific instrumentation for performing these measurements. The attitude control is described as well as the satellite power, telemetry and command systems. Also included is a description of the preferred experiment operation. Finally, the ground support equipment and the systems design aspects are discussed.

4.1 Measurements

This section describes the reflectivity, temperature, and space environment measurements as well as a discussion on the preferred experiment samples and aspects of separation of effects.

4.1.1 Reflectivity Measurements

Three basic methods for measuring reflectivity have been considered. These are shown schematically in Figure 4-2. Figure 4-2a shows a reflectometer using a beam splitter. This method of approach has been chosen for the preferred experiment for various reasons which will be discussed. Figure 4-2b shows a system which does not use a beam splitter but where the angle of incidence on the sample is greater than zero. Figure 4-2c is Strong's method where two reference mirrors are used.

The factors which led to the choice of the system shown in Figure 4-2a were calibration and geometry problems. A measurement of reflectivity is of no value unless a calibration is performed. One method of calibration is to compare the sample to a standard. However, the reflectivity of the standard must be known in an absolute sense and must not change with time and exposure to the space environment. Furthermore, the standard must be compatible with the reflectometer optical system. One type of standard would be a front surface aluminized coating on quartz. This standard could be used for the systems shown in Figure 4-2a and 4-2b. The philosophy here is that the standard would be at all times inside the satellite and exposed to the space environment a minimum. However, the problem here is that the standard is of the same material which is to be tested for space degradation and the question of which is changing and how much can be raised. Another type of standard would be to use total internal reflection in, say, quartz.

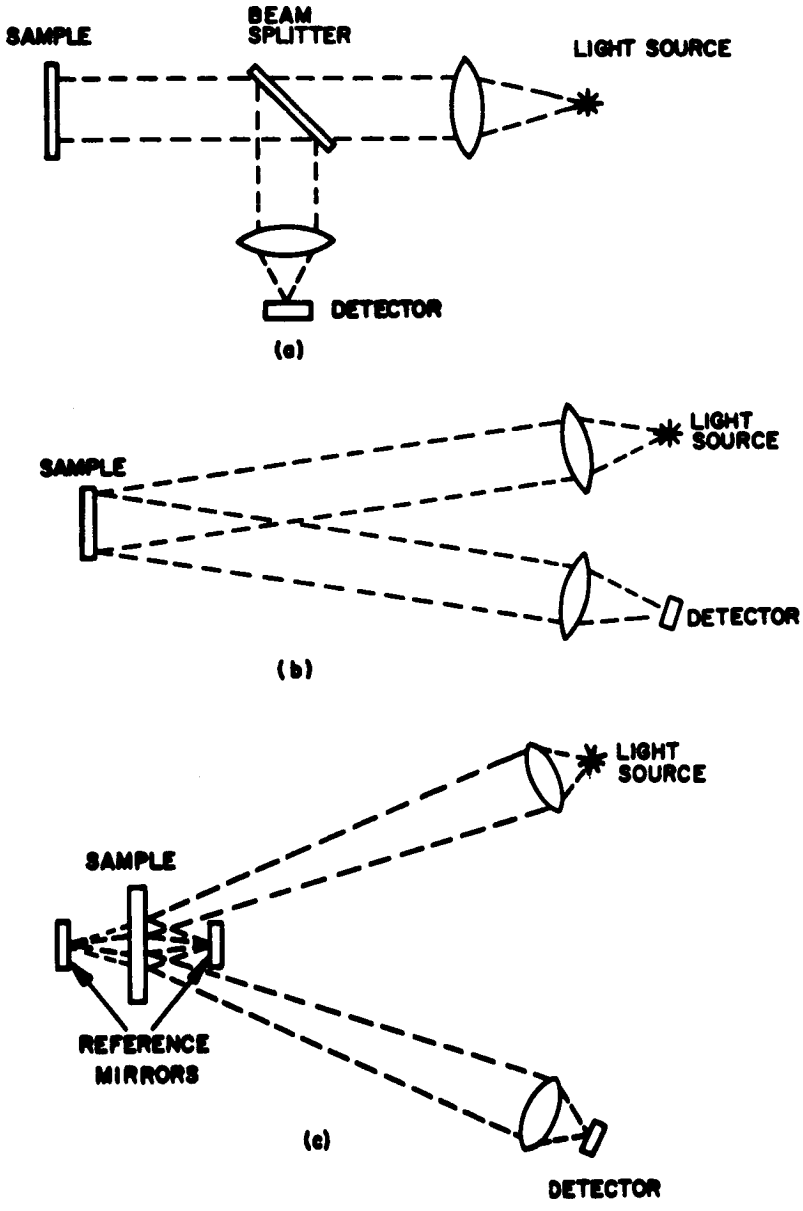

FIG. 4-2 VARIOUS REFLECTOMETER SYSTEMS

The "reflectivity" of this standard is a function of the transmission of quartz (which is least unaffected by the space environment). The condition of total internal reflection is only a function of the refractive index of quartz and space and the angle of incidence on the interface. It is felt that this standard is quite a bit more permanent than the aluminum coating and thus it is recommended as a standard.

In addition to having constant "reflectivity" the standard must satisfy some geometrical requirements. For example, it must reflect the incident light from the instrument in the same manner as a flat sample. Thus, in Figure 4-2a the standard must reflect the beam back on itself and in Figure 4-2b the reflection must occur at some angle. Also, in order to simulate the geometry of sample reflection, the path length in the standard must be a minimum. In the case of the system in Figure 4-2a a standard consisting of a quartz roof prism with the beam incident upon the hypotenuse satisfies all requirements. In the case of the system in Figure 4-2b the requirements are quite difficult to fulfill. The biggest problem is achieving total internal reflection. Quartz has a low refractive index and the critical angle is from about 42° to 44° in the 0.3 to 3.0 micron region. If a standard prism could be designed which was capable of total internal reflection, having the emerging beam at the proper angle and emerging at the same point as the entering beam, it is felt that the path length in the prism would be excessively long resulting in a beam spread problem. Thus, from a calibrate point of view the system shown in Figure 4-2a is favored over that in Figure 4-2b. One final point is that the system in Figure 4-2b is far more efficient than that in Figure 4-2a with respect to energy. However, it will be shown that in spite of the inefficiency of the beam splitter this system will work.

The reflectometer system shown in Figure 4-2c works on a "sample-in" "sample-out" basis. With the sample-in the light beam goes to the sample, to the reference mirror, to the sample and then to the detector. With the sample-out the light goes to the other

reference mirror and then to the detector. The path length in both cases is the same. The advantage of this method of measuring reflectivity can be shown by considering the detector output which can be expressed as

$$i_{si} = S\ K\ R_s^{\ 2}\ R_r \tag{4-1}$$

for the sample-in case and

$$i_{so} = S\ K\ R_r \tag{4-2}$$

for the sample-out case. The terms in these expressions are:

i_{si} = detector current for sample in
i_{so} = detector current for sample out
S = detector sensitivity in amps/watt
K = a constant involving the output wattage of the light source and the geometrical aspects of the optical system
R_s = sample reflectivity
R_r = reference mirror reflectivity

If we divide equation 4-1 by 4-2 we obtain

$$i_{si}/i_{so} = R_s^{\ 2}. \tag{4-3}$$

Thus, this method of reflectivity measurement does not involve any absolute standard. It does require that the differential reflectivity of the two reference mirrors is zero. Also, the term R_s appears as the square in the expression for the current ratio providing a more precise measurement. Equation 4-3 can be compared to the detector outputs of the beam splitter method (Fig. 4-2a) where

$$i_{si} = S\ K\ R_s \tag{4-4}$$

and

$$i_{ci} = S\ K\ R_c \tag{4-5}$$

where K now includes beam splitter losses, i_{ci} is the detector current with the calibrate prism in and R_c is the reflectivity of the calibrate standard. Dividing Equation 4-4 by 4-5 we obtain

$$i_{si}/i_{ii} = R_s/R_c. \tag{4-6}$$

Here the reflectivity of the sample requires the knowledge of the absolute value of the standard reflectivity.

In spite of the apparent advantages of the system shown in Figure 4-2c the system employing the beam splitter was favored for the preferred flight experiment for various reasons. The main reason is that the beam splitter approach lends itself more easily to the experiment requirements and overall satellite conceptual design. For the experiment requirements it was felt that the best approach was to have many samples and one reflectometer. The problem of bringing the sample to the reflectometer or the reflectometer to the sample was resolved by the requirement of measuring sample temperature. Bringing the sample temperature sensor output signal over slip rings is undesirable so the samples are affixed to the vehicle. This means that the optical system of the reflectometer must be brought to the sample. In addition, there is the requirement that the sample be exposed to the space environment and must face away from the vehicle which contains the reflectometer instrumentation. Thus, the optical system must come through a rotating joint, come outside the satellite and come to the sample. Comparing Figures 4-2a and 4-2c it can be seen that the beam splitter approach is

better adapted to perform the above contortions primarily because it is more compact and the required light beam bending can occur in the leg between the beam splitter and sample. Also, sample misalignment problems are fewer with the beam splitter since only one reflection off the sample occurs whereas with the system in Figure 4-2c two sample reflections occur. As a result of the above discussion it is recommended that a reflectometer using the beam splitter approach be used for the preferred flight experiment.

4.1.2 Temperature Measurements

Measurements of the temperature behavior of all reflective surface samples during the flight experiment are strongly recommended for the following reasons: (1) they will provide the data to check the designed temperature behavior of the samples, and, (2) they will provide a measure of the samples' solar absorptivity and thermal emissivity (α and ε) as a function of time in the space environment. These aspects of the temperature measurements are discussed below.

4.1.2.1 Temperature Control of Reflective Samples

The temperature extremes experienced by a solar concentrator in orbit may have considerable influence on degradation of its reflective properties, as indicated in Section 2.3 (Analysis and Prediction). Therefore, the control of the sample temperatures in this experiment so as to approximate the extremes expected on a large concentrator will yield more valid results.

Other requirements of the experiment make it inconvenient to have the backs of the samples viewing the earth or space as would large concentrators; therefore, temperature control must be effected by controlling the radiant and conductive heat interchange between the samples and the vehicle surface. This will be done by employing a sample mounting cup similar to that used by C. B. Neel of NASA Ames Research Center (Ref. 48) in the measurement of thermal

radiation characteristics of surfaces in space. The sample is attached to the cup by three Kel-F posts and is positioned flush with the top of the cup, which is slightly larger than the sample. Several radiation shields, also attached to the posts, are interposed between the back of the sample and the bottom of the cup. With this arrangement, Neel experimentally determined the heat loss from the sample back to be $0.11\,\sigma\,(T^4 - T_c^4)$, T and T_c being the sample and cup temperatures respectively, and σ being the Stefan-Boltzmann constant. Recently Neel (Ref. 49) indicated that improved radiation shields have reduced this loss to about $0.05\,\sigma\,(T^4 - T_c^4)$.

By adjusting the number and types of radiation shields in the sample mounting cup the maximum temperature of the sample can be controlled over a large range. For example, with an aluminum front surface sample ($\alpha = 0.15$, $\epsilon = 0.05$) under full solar irradiation, mounted in the lowest loss cup (emissivity factor = 0.05), and an assumed cup temperature of 77°C, the thermal balance equation indicates the sample temperature would rise to 186°C. Under these same conditions, if a maximum sample temperature of 100°C were required, the radiation shields would be adjusted to provide an emissivity factor of 0.62.

It is reasonable to assume that solar concentrators in general will be thermally designed to avoid temperatures as high as 186°C in orbit, particularly in those cases where plastics are used (see discussion in Section 2.3). It appears the method discussed above would be entirely satisfactory to reproduce the predicted maximum operating temperatures of solar concentrators in the reflectivity experiment samples.

The minimum temperatures experienced by large reflectors are not reproduced with this method. The body of the vehicle (and therefore the mounting cups which are thermally connected to the vehicle) is designed to reach a minimum temperature of about 0°C while in the earth's shadow. The samples, with the earth infrared emission input to their fronts and the 0°C vehicle emission input (through

low loss radiation shields) to their backs, will reach a temperature minimum of about -16°C. As indicated in Section 2.3, large reflectors radiate to cold space from their backs while in the shadow, and may reach temperatures below -150°C. At this time no method can be found to achieve such low temperatures in the samples, consistent with other experimental requirements. However, since high rather than low temperatures appear to be the more important in influencing reflective surface degradation, it is believed the lack of very low temperatures will not significantly lessen the validity of the experiment. This assumption should be thoroughly explored in the ground simulation program.

Temperature measurements on the samples would be very useful in checking on the functioning of the thermal control method recommended here. In addition, the data would be available to make correlations between reflectivity degradation and sample temperatures.

4.1.2.2 Measurement of Thermal Radiation Constants

Metals used to produce the reflective surfaces on solar concentrators, such as aluminum and silver, have a relatively large ratio of solar absorptivity (α) to infrared emissivity (ϵ); typically α/ϵ is greater than 2. This would cause concentrators with bare metal surfaces to operate at undesirably high temperatures. In general this problem is overcome by coating the metal surface with a dielectric, such as SiO or Al_2O_3, which greatly increases ϵ without changing α significantly. Therefore, the temperature control of the solar concentrators depends on the stability of the dielectric coating in the space environment.

There has been some evidence that the α/ϵ ratio of dielectric-coated metal surfaces increases with exposure to solar ultraviolet radiation, thus degrading thermal control (see Section 2.3). It would therefore be useful to monitor the α and ϵ of the reflective surface samples during the flight experiment. This is

possible, as described below, using Neel's method (Ref. 48) which requires only sample-temperature data.

Neel's method uses a series of temperature measurements just before and just after the sample enters the earth's shadow. It is shown by thermal balance equations that α/ϵ can be calculated from the temperature and its derivative with respect to time just before eclipse, and ϵ can be calculated from these same quantities measured just after eclipse. Thus α and ϵ can be determined once during each orbit, although much less frequent determination is anticipated--perhaps once per week.

In using this method it is necessary to use the lowest loss mounting cups (described in Section 4.1.2.1) in order to achieve fairly precise α and ϵ values. Therefore, for some samples there may exist a conflict between limiting the maximum temperature and measuring α and ϵ. In these cases separate samples would be used for the α and ϵ determination, with the understanding that somewhat accelerated degradation in reflective properties might result from the higher temperatures.

4.1.3 Space Environment

The preferred flight experiment requires quantitative measurement of all environmental factors contributing to degradation of the sample surfaces to be studied, together with accurate measurement of the extent and type of damage. This information will enable a complete analysis of cause and effect. The data will also allow correlation with pre-flight and post-flight ground simulation experiments. A successful, quantitative flight experiment at this time would reduce or eliminate the need for additional flight studies.

In addition to the measurement of reflectivity and temperature, as discussed in Sections 4.1.1 and 4.1.2, a complete experiment should include measurement of electromagnetic and charged particle radiations and micrometeoroid flux levels. In these cases, our minimum interest requires evaluation of the total time integrated fluxes and energies of particles and radiations to which the samples have been exposed. For more complete analysis and correlation of cause and effect, measurement of flux rates is desirable.

Motion of the satellite through the planned orbit will expose the surfaces to wide variations in charged particles, intensities, and energies. Additional temporal variations due to sudden solar events can cause extreme changes in intensities of charged particles and in the electromagnetic radiations below 3000 Å lasting for periods of many hours. The damaging effect of these transients can be best evaluated if their energies and rates can be isolated and measured.

In the case of micrometeoroids it would be desirable to known of the times of encounters with dust clouds to determine if sensitivity of the samples to the other factors of the environment or damage rate, such as protons or electrons, is increased measurably following meteoric hits.

Quantitative measurements of electron and proton intensities and spectra of the space environment are difficult because of a wide distribution of energies of both electrons and protons and

the inherent sensitivities of detectors to all of these ionizing radiations. Approximations of the energy spectra may be made by differential measurements with various thicknesses of absorbers and shields. This must be done in the presence of high background levels introduced in the detectors by high fluxes of charged particles, which penetrate the shields, and induced Bremmstrahlung radiations that are even more penetrating than the charged particles. Data reduction time may be reduced appreciably by the use of more sophisticated payload instrumentation such as electron and proton pulse height analysis, magnetic or electrostatic spectrometers. Although these instruments may not involve appreciably greater payload weight or power consumption, there is an increased probability for malfunction.

Another measurement of possible value would be to determine whether the satellite gains a static charge as a result of launching into orbit. It would be useful to know its polarity and whether or not there is a gradual change or leakage of this charge with time. This static charge may arise from ionization of rocket gases used to launch the satellite into orbit. These charges would be effective in altering the velocities of charged particles encountered by the satellite and may be a generally disturbing influence in space physics measurements of the natural space environment.

The addition of a magnetometer to the experiment would enable correlation of environmental measurements made during this flight experiment with data from other experiments.

For the preferred experiment, which might be more appropriately called the "optimum" experiment, instrumentation for environmental measurement have been chosen as objectively as possible with utility and reliability being the major considerations. The selected equipment is based on instruments that have been flown successfully.

4.1.4 Samples and Separation of Effects

There are a total of thirty measurement positions on the preferred experiment. By measurement position is meant a position of the reflectometer rotating arm in which a reflectivity measurement may be made. Two of the thirty measurement positions are taken up by the "100%" and zero calibrate measurement consisting of a total internal reflecting retrodirective prism and a black cavity (light trap). Three of the measurement positions are taken up with the space environment measurements. These consist of three reflective samples each with their own "cover glass". The transmission of the "cover glasses" is sensitive to varying degrees to some aspects of the space environment. Thus, by performing a reflectivity measurement the transmission of the "cover glasses" may be measured. The remaining measurement positions number 25 and these are used for the reflectivity measurements.

As was discussed in Section 2.4 it is felt desirable to not only measure reflective surface degradation but also to understand the causes of degradation. In order to do this some method for separation of effects must be provided. The basic division of separation of effects is between electromagnetic and particle (charged and neutral) radiation. Thus, if an opaque shield is placed between a sample and the sun (assuming the vehicle is solar oriented) and is located at some distance from the sample the electromagnetic radiation is prevented from impinging on the sample whereas particle radiation which is largely omnidirectional can still be incident on the sample. Of course, the sun shield will occlude a small solid angle of particle radiation on the sample. If a quartz cover plate is placed immediately over another sample, the sample will "see" only the solar electromagnetic radiation including a good portion of the ultraviolet (down to the cutoff of the quartz) and the cover plate will take the brunt of the particle radiation. Assuming the particle radiation does not affect the transmission properties of the quartz then the sample reflectivity may be measured through the cover plate. If this assumption is not valid then the cover

plate may be blown off the sample after some significant period of time has elapsed and the reflectivity measurement may then be made. Finally, it is felt desirable to have at least one sample which is exposed to neither electromagnetic or particle radiation as a control. This sample would have an opaque (to both types of radiations) shield immediately over it at all times during the experiment.

The recommended list of samples for the preferred flight experiment is shown in Table 4-1 . At the outset it should be stated that the choice of samples to be flight tested is not easy because of the large number of variables involved. In some cases the samples chosen were quite arbitrary. Also, it should be stated that this list is not firm and could and should be changed with other inputs, late developments and with the results of further ground simulation tests. In chosing the recommended samples an attempt was made to represent a major portion of present solar concentrator programs. The structural aspects of the substrate (such as Al honeycomb) are not included in the substrate heading since this affects the geometry of a solar concentrator more than its reflectivity. The exception to this is the foam-backed mylar where the mylar itself would not have sufficient rigidity for a sample. The two basic reflective coatings are aluminum and silver. The overcoatings of SiO and Si_2O_3 are somewhat questionable as to their differentiation since this varies with the conditions of coating. The Si_2O_3 is more attractive for solar concentrator reflectivity. The final SiO/Si_2O_3 differentiation and choice should be deferred until more ground simulation tests have been made. The type of high emissivity (ε) mylar overcoat is not known probably because of its proprietary nature and has been designated only as "high ε". The barrier layer overcoating is of anodic form. The separation of effects column shows which samples are exposed to total radiation and which are shielded from electromagnetic, particle and both. The samples are circular and 1.5" in diameter.

TABLE 4-1 PREFERRED EXPERIMENT SAMPLE SELECTION AND SEPARATION OF EFFECTS

NO.	SUBSTRATE	UNDERCOAT	REFLECTIVE COATING	OVERCOAT	SEPARATION OF EFFECTS
1	Ni	SiO	Al		Surface mounted, no shield
2	Ni	SiO	Al		Partially recessed
3	Ni	SiO	Al		Fully recessed
4	Ni	SiO	Al	Si_2O_3	No shield
5	Ni	SiO	Al	Si_2O_3	Sun shield
6	Ni	SiO	Al	Si_2O_3	Particle shield
7	Ni		Ag		No shield
8	Ni		Ag		Sun shield
9	Ni		Ag		Particle shield
10	Ni		Ag		Total shield (control)
11	Foam/Mylar		Al		No shield
12	Foam/Mylar		Al		Sun shield
13	Foam/Mylar		Al		Particle shield
14	Foam/Mylar		Al	High ϵ	No shield
15	Foam/Mylar		Al	High ϵ	Sun shield
16	Foam/Mylar		Al	High ϵ	Particle shield
17	Al/Epoxy	SiO	Al	SiO	No shield
18	Al/Epoxy	SiO	Al	SiO	Sun shield
19	Al/Epoxy	SiO	Al	SiO	Particle shield
20	Epoxy	SiO	Al	Barrier layer	No shield
21	Epoxy	SiO	Al	Barrier layer	Sun shield
22	Epoxy	SiO	Al	Barrier layer	Particle shield
23	Epoxy		Al		No shield
24	Epoxy		Al		Sun shield
25	Epoxy		Al		Particle shield

At one time during the program it was felt that more than one of the same type of sample should be exposed to the same environment for statistical purposes. The philosophy here was that if two or more samples (of the same type and exposed to the same environment) behaved in the same manner then the level of confidence in the results would be higher. However, because of the large number of variables which affect the experiment it is felt that this luxury of redundant samples cannot be realized.

4.2 Instrumentation

This section describes in some detail the specific instrumentation that would be used to perform the measurements defined in the experiment requirements (Section 2.4). This instrumentation provides for the reflectivity, temperature and space environment measurements for the preferred flight experiment.

4.2.1 Reflectivity

4.2.1.1 Requirements of Reflectometer

The reflectometer designed for measuring reflectivity of the samples in this experiment must meet several requirements. First it must be capable of measuring several samples representing the different test surfaces of the experiment. Second, it should be able to perform reliably over a long period of time. This requirement indicates simplicity of design. Third, it must provide both broad spectrum measurements and a few narrower spectral band measurements. Fourth, the method of calibration should be accurate, reliable, and unchanging with time or exposure to experimental environment. Finally, since the instrument is to be satellite-borne, it must be as lightweight as possible and consume as little power as possible.

4.2.1.2 General Description of the Reflectometer

The engineering drawing shown in Appendix A depicts the reflectometer that has been designed to meet the requirements listed above. The optical features of the instrument are best understood by viewing Fig. 4-3, which shows schematically the principal optical parts, and the method by which the reflectometer works. After careful consideration of various trade off parameters, it was decided to provide a single instrument capable of measuring all samples. This method has a very great advantage because the measuring apparatus is common to all measurements allowing for intercomparison of data taken from all samples. If, for example, each sample were provided with its own reflectometer there would always be uncertainties as to the calibration relationships between reflectometers and consequently less value could be placed on intercomparisons of sample reflectance data.

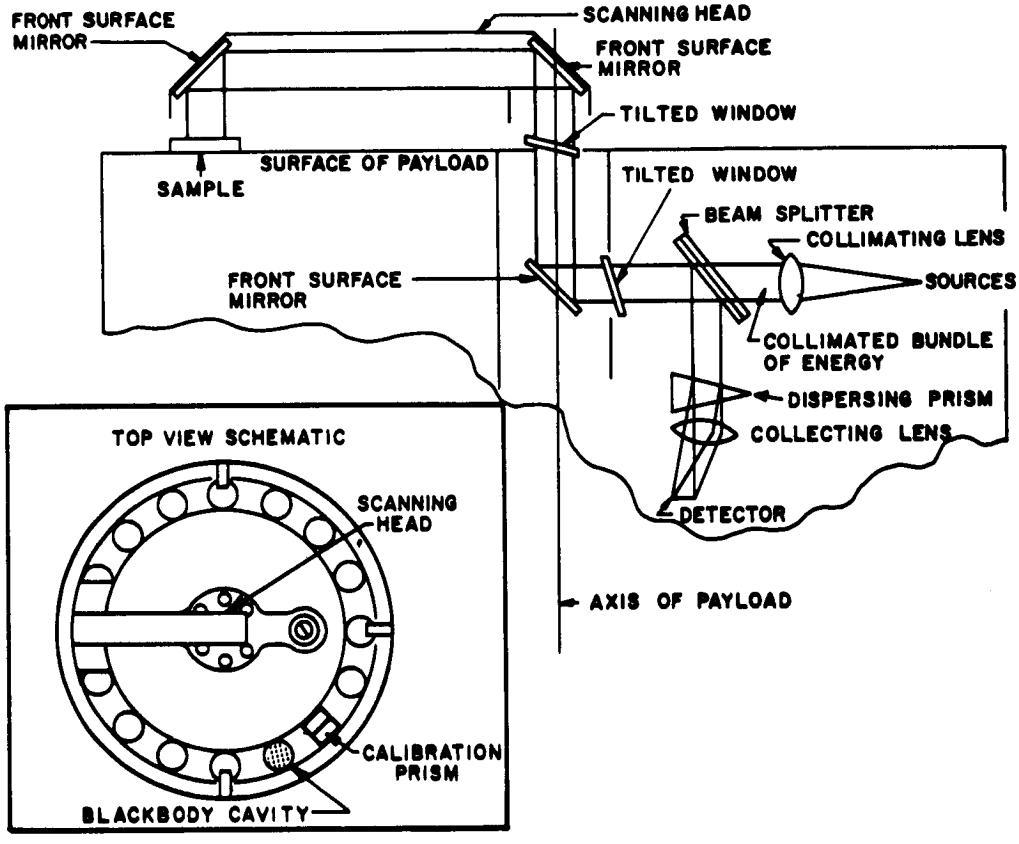

FIG. 4-3 REFLECTOMETER OPTICAL SCHEMATIC

An additional advantage lies in the reduced size, weight, and cost of a single instrument over that of a multiple array of instruments. The one sacrifice that is made is that a scanning mechanism is required. Figure 4-3 shows that the upper part of the reflectometer (the scanning head) rotates about the axis of the payload. This scanning head requires the use of bearings and a drive motor which are discussed elsewhere in this report. Instead of rotating a member of the reflectometer, it would have been possible to rotate the circular array of samples under the reading head. Under these conditions it would have been more difficult to monitor sample temperature with thermocouples as the electrical outputs from the thermocouples would have had to be taken out over slip rings. Thus it was decided to fix the samples in a circular array and rotate a portion of the reflectometer.

A possible disadvantage of one instrument system is the chance that either the light source, detector, electrical system, etc. may fail. This, of course, would destroy the value of the experiment. Thus it has appeared mandatory to include a certain amount of redundancy in the system. To this end two sources of energy and two sets of detectors are to be used. One source is a small ribbon filament tungsten lamp that operates at low power. The second source is a virtual image of the sun formed by a segment small metallic sphere. The energy from the tungsten source is received by one detector whereas the solar energy is directed by the optics to a dispersing prism and a detector array. Since the payload vehicle is to be oriented with the samples directed toward the sun, there should be little problem with the virtual image solar source. If the vehicle orientation system were to fail or experience wide drifts so that the solar source were cut off, or if the metallic sphere surface would be degraded in reflectance by environmental conditions, the tungsten source system would be available to continue measurements. If, on the other hand, the tungsten bulb were to burn out or its power supply were to fail, the solar source system would be available to continue measurements. Similar arguments can be given for the use of two detector arrays. It is unlikely that both arrays would fail at the same time. This gives some assurance that at least limited data would always be taken on all the samples.

Events that would be catastrophic to this experiment have been reduced to complete power failure (in which case any satellite system is doomed) or failure of the motor that drives the scanning head.

The general design of the reflectometer has been kept as simple as possible to further aid in achieving reliability. The most durable optical materials have been selected to assure resistance to damage from environment such as ultraviolet radiation, micrometeorites, or other sources of damage. Refracting components will be made from fused quartz, a material that has proven durability under adverse conditions. The number of reflecting components will be kept to a minimum; the mirrors and beam splitter used will be made of durable coatings on quartz substrates. Furthermore, all optics in the reflectometer will be protected from external sources of damage. A majority of the optical parts are protected by their location inside the satellite payload (see the engineering drawing in Appendix A).

Probably the most important feature of the reflectometer is the method of calibration. It has been decided to calibrate the system by placing a roof prism in one sample position and a blackbody cavity in an adjacent sample position. Thus as the reflectometer head scans the samples, it will see a zero calibration point (the blackbody cavity) and a 100 percent reflectance level (the corner prism). This allows calibration for full-scale deflection. Since this calibration occurs once each cycle the certainty with which quantitative reflectivity measurements can be regarded is greatly enhanced.

The 90° roof prism has been used because of its retro-directive characteristics. Energy entering at an angle α will leave the prism at the same angle α. Furthermore, the surfaces of the quartz prism are extremely durable and unchanging. Thus the requirements for an accurate, reliable, and durable calibration method have been met. It should be noted that by calibrating for full scale detector drifts, amplifier drift, light source drift, or other drifts are rendered unimportant.

4.2.1.3 Detailed Description of Reflectometer Spectral Regions and Resolution

The spectral region in which reflectivity will be measured extends roughly from 0.3 microns to 3 microns. A broad spectral measurement (referred to as white light measurement) covering this entire region will be made in both channels of the reflectometer. Energy from the sun will be dispersed into four spectral bands distributed throughout this range. The spectral resolution of these measurements is affected by the source size, optical aberrations, detector size and spacing, and the spectral resolution of the quartz dispersing prism. The spectral ranges will cover roughly the following regions:

1. 0.30μ to 0.54μ
2. 0.54μ to 0.74μ
3. 0.74μ to 1.05μ
4. 1.05μ to $2.6\ \mu$

Figure 4-4 shows the scheme that is used to disperse the solar energy. A small 23° prism is placed in front of the collecting lens. This prism covers only a portion of the aperture of this lens. In fact not all of the energy from the solar source passes through the prism, and none of the energy from the tungsten source. Thus a portion of the solar energy (approximately 80 percent) is dispersed into the spectrum and the remaining 20 percent is imaged by the lens into a white light image. Reference to the same figure (front and top views) shows that all light from the tungsten source is imaged in a white light image. This arrangement is possible because of the divergence of the two beams. Figure 4-5 shows schematically how the tungsten and solar beams diverge through the reflectometer. Two sources A and B are located in the focal plane of the collimating lens. The spacing between the sources is 1/8 inch, which represents an angular separation of slightly more than one degree for a six-inch focal length lens. The aperture stop (3/4-inch diameter) is placed at this lens. Thus, the beams from the two sources are each 0.75 inch diameter

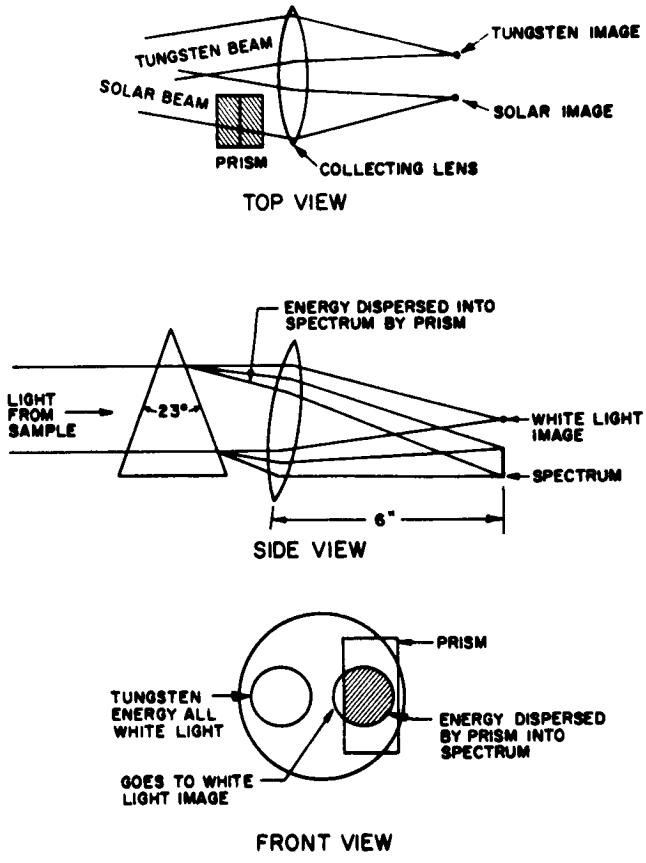

FIG. 4-4

DISPERSING SYSTEM SCHEMATIC

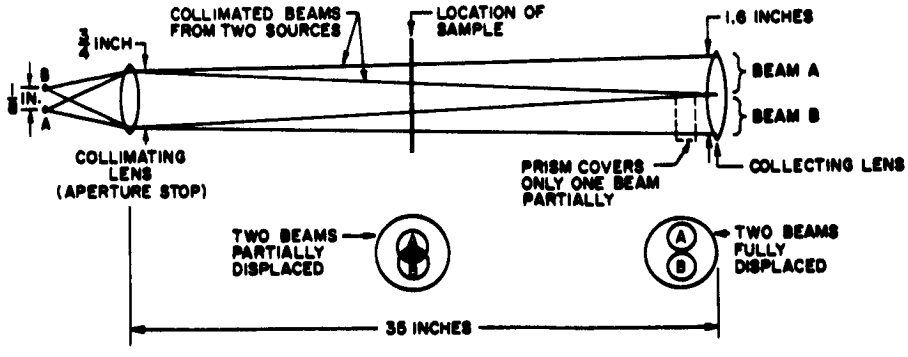

FIG. 4-5

BEAM DIVERGENCE SCHEMATIC

and are superimposed at the collimating lens as shown. As these two beams progress through the reflectometer they diverge. By the time they reach the sample their centers are separated by approximately 0.4 inch as shown. By the time they reach the prism and collecting lens, they are entirely separate. Thus, the prism can be placed in one beam without affecting the other.

Light Source

The requirements for the light source to be used in the reflectivity instrument can be stated in fairly broad and obvious terms. The source must have relatively uniform output in the spectral region of interest. sufficient output to allow the use of simple detectors and amplifiers, long life, good efficiency, simple operating procedures, and stable output in all respects.

There are few sources that satisfy the above requirements. Even fewer are suitable for prolonged, unattended operation in a hostile environment.

It would require many pages to list the characteristics of the many varieties of available sources. Most may be rejected in a categorical manner. The various arc type sources such as mercury and xenon are not suitable, in spite of their sometimes high intrinsic brightness. In general, the starting procedure is somewhat complicated, the arc is unstable in both position and output; the average operating life is, at best, a few hundred hours. In addition, except for high pressure arcs operating at about 300 atmospheres, the spectral output is very non uniform.

The fluorescent and luminescent sources, while long-lived, have very low intrinsic brightness.

Considering all factors, the incandescent tungsten filament lamp is the most suitable source. It has reasonable efficiency, brightness, and is easily operated. With proper design and application, the tungsten lamp has a lifetime measured in tens of thousands of hours. The operating time for a particular lamp can be

markedly increased by operating at a reduced voltage with little decrease in output. The life of a tungsten lamp is proportional to the inverse of the 12th power of the voltage while the light output is proportional to the 3.6 power of the voltage. The major disadvantage to a tungsten source is its relatively low output in the spectral regions at 0.4 and at 3 microns. Figure 4-6 illustrates this point. Also to be noted from the figure is that tungsten does not radiate as a blackbody. The output is relatively high in the visible portion of the spectrum due to increasing emissivity at the shorter wavelengths.

The consequence of low output around 0.4 and 3 microns is not especially great since approximately 85 percent of the solar energy falls between these wavelengths. The integrated distribution of solar energy is illustrated in Fig. 4-7.

A suitable lamp for this application would be like a GE # 1819 operating at 28 volts and 0.04 amperes. This unit has a rated average life of 1000 hours. While this is insufficient for one to two years continuous operation (8800 to 17,600 hours) the lamp need operate at full voltage only during the brief measuring period. To avoid turn-on failure, the lamp would be operated at approximately 30 percent voltage between measurement periods. Just prior to the reflectivity measurement, the voltage would be slowly increased to full value. In this manner, thermal shock failures associated with rapid application of full voltage are prevented.

It would be advantageous to provide a special lamp with a quartz bulb for better efficiency and an indexing base to simplify alignment.

A second, and in some respects, more desirable light source for the reflectometer would be the sun itself. The spectral distribution as shown in Fig. 4-8 is that which is desired and the flux density is high and constantly available. Some method is, of course, required to collect and direct the sunlight. An active system

FIG. 4-6

RELATIVE OUTPUT OF TUNGSTEN AT 2800°K AS A FUNCTION OF WAVELENGTH

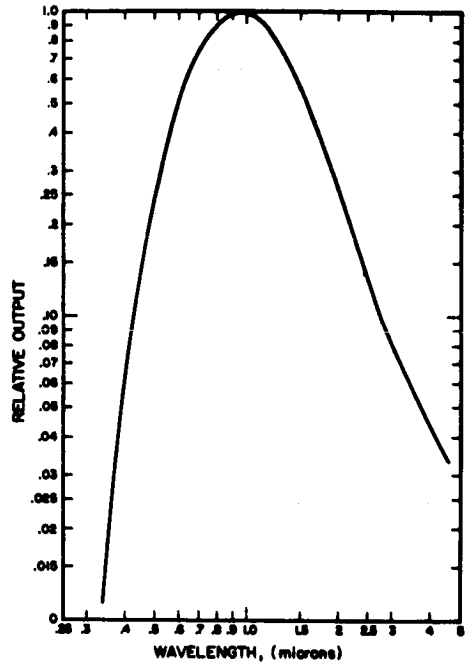

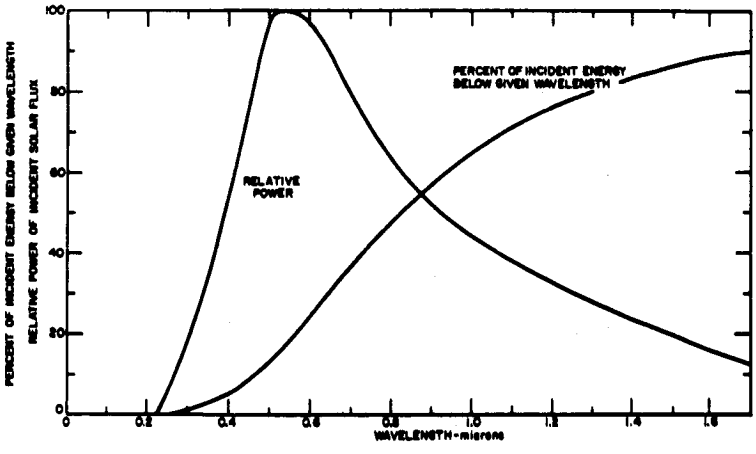

FIG. 4-7 SOLAR SPECTRUM

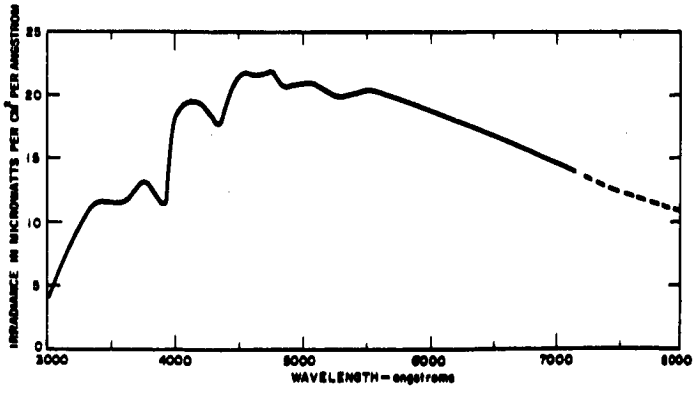

FIG. 4-8
SOLAR SPECTRAL IRRADIANCE OUTSIDE THE EARTH'S ATMOSPHERE AFTER STAIR AND JOHNSON, AND DUNKELMAN AND SCOLNIK

consisting of small collecting optics, sun tracker and drive system is clearly unsuitable because of the attendant weight and power penalty and reduced system reliability. A simple, passive collection method is possible through the use of a spherical specular reflector. Such a reflector is indicated in Fig. 4-9.

While the image varies somewhat in quality and location, the spherical reflector is, nonetheless , a free source that is useful over a wide range of view angles.

Note that (Fig. 4-9) as the angle ϕ becomes larger, the location of the (virtual) focal point moves toward the surface of the sphere. The change in ϕ will be limited to fairly small values by the satellite orientation system. The motion of the focal point implies that the optical system must be "slow" enough to provide the necessary depth of field.

Detectors

Certainly there is a large variety of devices available for the detection of radiant energy.

These devices can be separated into three general groups which are photoelectric, photothermal, and photochemical. It is difficult to imagine how photochemical types might be applicable to the problem at hand. Efficiencies in general are low and most processes are essentially irreversible. Photothermal devices as a class have lower detectivities and longer time constants than the photoelectric devices. Thus, although the power requirements and weight are low, they are not considered further. The photoelectric detector as a class is the more desirable. A detailed examination of the photoelectric detector is shown in Table 4-2.

Here several photoelectric detectors are compared in terms of spectral response, detectivity, time constant, temperature stability, approximate weight, approximate power requirements, and responsivity. A few devices, such as the photoelectromagnetic detector are listed for information only. It should be mentioned that this table is only a partial listing of the detectors

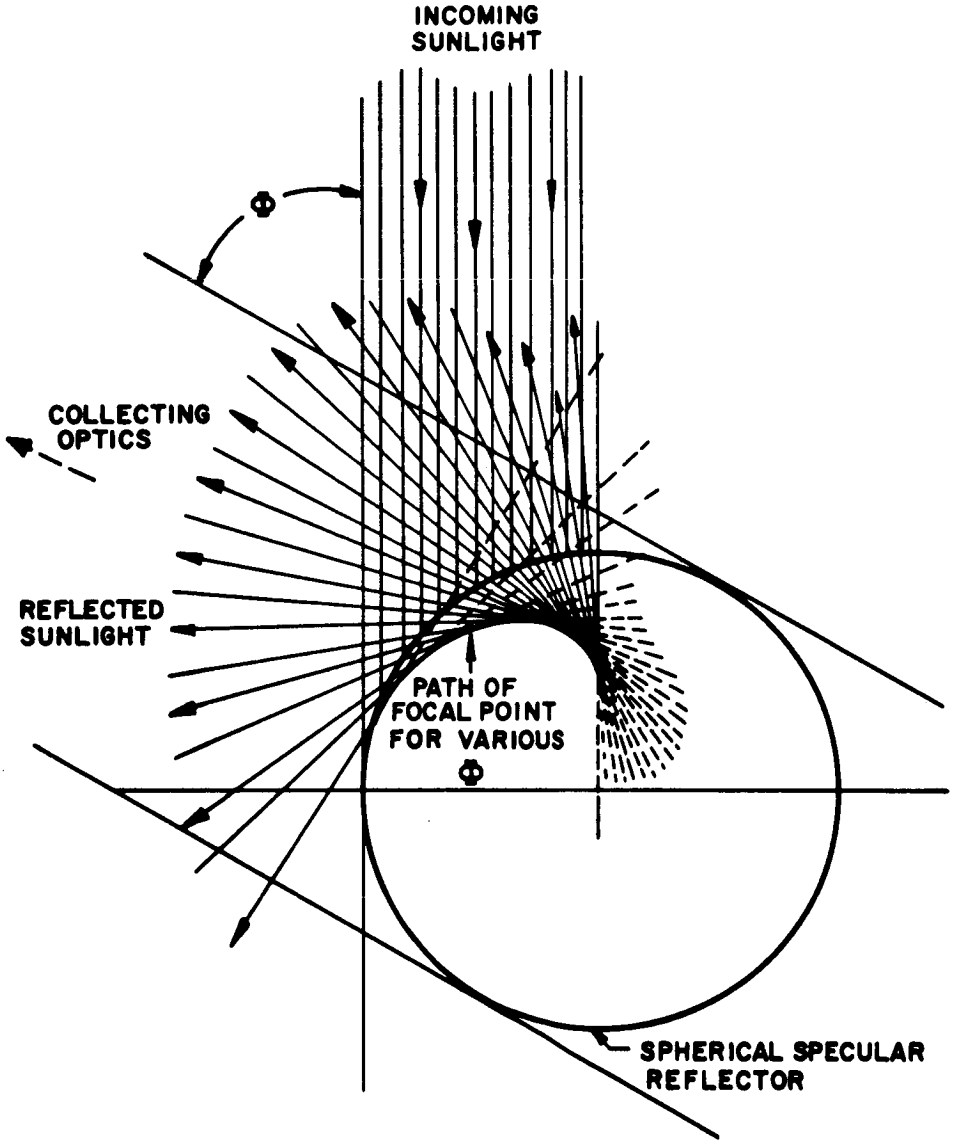

FIG. 4-9 GEOMETRY OF SPHERICAL REFLECTOR

TABLE 4-2 CHARACTERISTICS OF PHOTOELECTRIC DETECTORS

Detector Type	Manufacturers Type	Material	Spectral Response Microns	Detectivity in Reciprocal Watts at Maximum Response 1 cps Bandwidth	Time Constant in Micro. Sec.* or Rise Time	Decay Time	Temperature Stability	Approx. Item Weight	Approx. Item Power Requirements in Watts	Responsivity in ua/uw (unless noted)
Photoemissive	RCA 7265 Multiplier Phototube	Cs-K-Na-Sb Semitransparent Photocathode	.3 to .75	10^{15}	.003	.003	Good	8 oz.	2.5	Cathode: .064 Anode: 6×10^5
Photoemissive	RCA 6810A Multiplier Phototube	Cs-Sb Semitransparent Photocathode	.32 to .65	1.2×10^{14}	.003	.003	Good	8 oz.	2.5	Cathode: .048 Anode: 6×10^5
Photoemissive	RCA 7029 Multiplier Phototube	Cs-Sb Photo-cathode on reflecting sub-strate	.3 to .65	5×10^{13}	.01		Good	5 oz.	2	Cathode: .085 Anode: 2.7×10^4
Photoconductive	RCA 6957	Cadmium Sulfide	.34 to .74		About 10^6		Fair	1 oz.	.5	300
Photoconductive	RCA 7467	Germanium p-n Junction	.35 to 1.8	10^{10}	6	30	Fair	.03 oz.	.03	.5
Photoconductive	Typical	Lead Sulfide	.35 to 3	10^{12}	100 to 1000		Fair	0.1 oz.	.05	About 100 μv/μw
Photoconductive	Typical	Lead Selenide	.7 to 4.5	4×10^9	About 10		Fair	1 oz.	.05	About 12 μv/μw
Photoconductive	T1 1NZ175	Silicon	.3 to 1.2	10^{13}	30		Fair	.003 oz.	.2	7
Photovoltaic	Typical	Silicon	.5 to 1.0	About 10^{12}	About 20		Fair	1 oz.	None	About .2
Photovoltaic	Philco ESC-301	Indium Antimonide	.6 to 5.5	2×10^{10} (AT-195°c)	1		Fair	2 oz.	None	
Photo-Electro-Magnetic	Honeywell 5A	Indium Antimonide	.6 to 7.5	10^9	.4		Fair	3 oz.		

*To 10 per cent or 90 per cent of final value.
All data at 25°C unless noted.

investigated. Many others such as the lead telluride photocell and many vacuum and gas phototubes and photomultiplers were considered and found lacking in many respects. Image amplifier or image converter tubes are other photoemissive devices that may be considered. However, their photocathodes are the same material as used for multiplier phototubes. Thus, image tube detectivities could be no better than multiplier phototube detectivities. Detectivity is the most important consideration while temperature stability and weight are the least important, although they certainly must not be ignored. The power requirements and weight listed are exclusive of any required accessory equipment such as power supplies, amplifiers and environmental control devices. The approximate spectral response is listed in the first column. Spectral response is the second most important consideration since it is highly undesirable to use a multiplicity of detector types. The temperature stability comments are rather loosely derived from considerations of maximum and minimum operating temperatures and possible instabilities within these ranges.

Detectivity is simply the reciprocal of noise equivalent power and is equal to responsivity in, say, amperes/watt divided by the noise or rms fluctuation in the detector output in, say, amperes. Since the responsivity of a detector is usually dependent upon temperature, detector area and wavelength and modulation frequency of the radiation, detectivity must be dependent upon these quantities, plus the frequency bandwidth of the noise. One should, therefore, specify completely the measurement conditions. In an actual measurement of detectivity the input power is adjusted until the output signal is just equal to the noise.

All the detectivity data were referred to a one-cycle bandpass and modulation frequencies and cell areas were such that the response of the particular detector was maximized. These data were obtained from manufacturer's literature and the detector evaluation reports published by the Naval Ordnance Laboratory, Corona, California.

An examination of temperature stability, approximate item weight, and approximate item power requirements shows that most of the photoconductive and photovoltaic devices are nearly the same in this regard. The time constants with the exception of the cadmium sulfide cell are sufficiently short to meet the requirements. In comparing the photoemissive devices with the photoconductive devices, we see that the photoemissive detectors are characterized by higher detectivity, shorter time constants, better temperature stability, and higher weight and power requirements than the photoconductive cells. The higher weight and power requirements combined with the very limited spectral response eliminate the photoemissive types.

The lead sulfide cell provides the best combination of detectivity and spectral response and is the detector chosen for this application. A plot of lead sulfide detectivity as a function of wavelength is shown in Fig. 4-10. It is noted that the response curve is extrapolated toward the shorter wavelengths. Discussions with cell suppliers have confirmed that the response does extend to the blue region in this manner. The published data do not show this since the usual application of lead sulfide is in the infrared region.

In general, a lead sulfide cell has a resistance of several hundred thousand ohms. In order to provide the required high-load impedance for the detector and a low-source impedance for the subsequent data handling circuits, the circuit of Fig. 4-11 is utilized. The use of high-gain planar transistors with leakage currents on the order of 4×10^{-10} amperes results in a reduction in "1/f" noise. An input impedance of the order of 500 K ohms is easily realizable with this circuit. Since positive feedback is not required to obtain the high-input impedance, the amplifier is quite stable. The emitter-follower output stage provides an output impedance of a few thousand ohms.

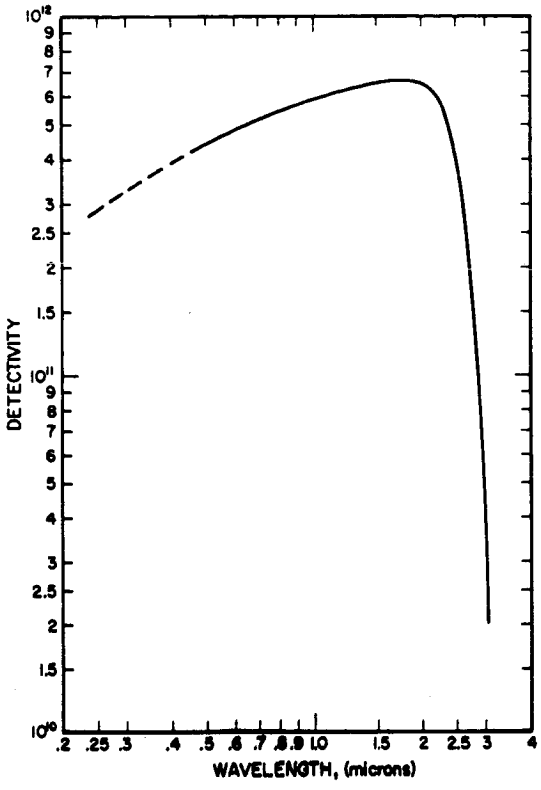

FIG. 4-10

DETECTIVITY AS A FUNCTION OF WAVELENGTH FOR LEAD SULFIDE WITH A CUTOFF OF 2.5 MICRONS AT 25°C

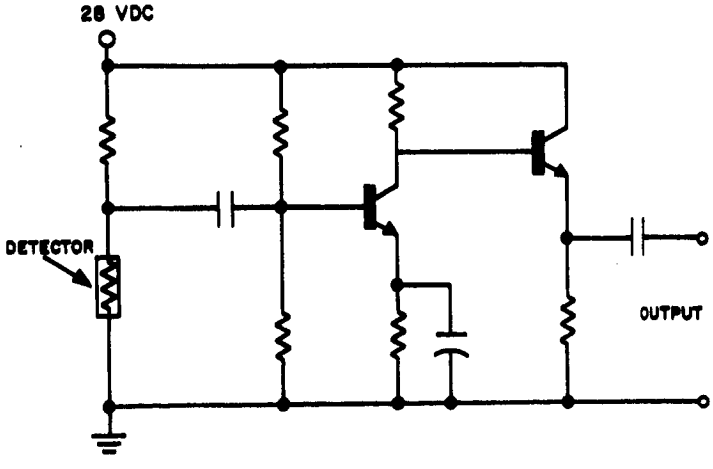

FIG. 4-11

DETECTOR AND HIGH INPUT IMPEDANCE AMPLIFIER

Optical Components

A simple fused quartz lens of focal length six inches and aperture diameter 0.75 inches will be used as a collimating lens. At this speed (f/8 approximately) the spherical aberration, coma, and chromatic aberrations of the lens will be small so as not to degrade the collimation of the beams of energy. The low index of refraction of quartz (approximately 1.46) causes the surface reflection losses to be low. From Fresnel's equations for normal incidence of light the reflection loss per surface is given by

$$\text{Loss} = \left(\frac{n - 1}{n + 1}\right)^2$$

$$= \left(\frac{1.46 - 1}{1.46 + 1}\right)^2 = \left(\frac{0.46}{2.46}\right)^2 = 0.035 = 3.5 \text{ percent}$$

Thus the total reflection loss for two surfaces is 7 percent. The average transmission of quartz from 0.3 to 3 microns should exceed 97 percent ignoring reflection losses. Thus, the overall efficiency of this lens is estimated to be 90 percent. As mentioned elsewhere in this report this lens serves as the aperture stop for the reflectometer optical system.

Beam Splitter

The beam splitter is placed in the system to assist in achieving a desirable reflectometer configuration. Without a beam splitter the incident and reflected beams would have to use entirely different light paths. This would increase the number of optical parts required which in turn would increase the space and weight used by the system. Furthermore the reflectance measurements could not be made at normal incidence. The beam splitter will be constructed of two fused quartz plates with the metallic (nichrome) coating coated on the interface between the plates. Thus the coating is protected from external environmental conditions which could degrade its performance. Mounting the beam splitter inside the payload structure also helps to protect it. The dimensions of the beam splitter are

estimated as 1.0 inch wide by 2.5 inches long. The beam splitter will be approximately 30 percent efficient for transmitted as well as for reflected light. It is estimated that of 100 percent of light incident on the beam splitter coating, 30 percent is reflected, 30 percent is transmitted and 40 percent absorbed. This of course varies with wavelength and depends upon the type and quality of coating. Nichrome coatings will be fairly neutral over the spectral range 0.3 to 3 microns. In addition there will be surface reflection losses of 3.5 percent per surface for each quartz plate.

Tilted Fused Quartz Windows

The fused quartz windows serve no optical purpose. They must be included to allow the region in which the bearing is located to be pressurized. Since the light path must travel along the rotational axis of the bearing as shown in the optical schematic, Fig. 4-3, windows must be supplied to allow the beams to pass in and out of this pressurized chamber. These windows are tilted to cause the 3.5 percent reflected light per surface to return along a different path than the light reflected from the sample. If this were not done, the reflected stray light would be confused by the system with reflected light from the sample thus creating a signal-to-noise problem. By tilting these surfaces this inaccuracy is removed.

Front Surface Mirrors

Three front surface mirrors are used, one in the stationary portion of the reflectometer and two in the rotating scanning head. Some 45°-90°-95° prisms had been considered for this function instead of mirrors but the reflected light from each flat face of the prisms posed a problem similar to the one discussed above concerning the tilted fused quartz windows. Since all of these mirrors are located inside of a protective structure, it is felt that any deterioration of coatings or surfaces will be small if indeed deterioration is experienced at all. It is estimated that these mirrors will be about 80 percent efficient in the ultraviolet, 88 percent in the visible, and 95 percent in the infrared.

Calibration Prism

A 90° roof prism will be used to provide the 100 percent reflectivity calibration. The phenomena known as total internal reflection is used to provide a very efficient reflectivity standard. If energy strikes an optical interface from the high refractive index side, it will be totally reflected provided the angle of incidence is greater than the critical angle. The critical angle is defined by this equation:

$$\theta_c = \sin^{-1} \frac{n'}{n}$$

where θ_c = critical angle

n' = index of refraction - low index media

n = index of refraction - high index media

Tabulated below are some representative critical angles for fused quartz. It is assumed that the low index medium is vacuum for which $n' = 1.0$.

λ	n	θ_c
0.35 microns	1.475	$42^{\circ}46'$
1.00 microns	1.450	$43^{\circ}38'$
2.00 microns	1.438	$44^{\circ}\ 6'$
3.00 microns	1.419	$44^{\circ}55'$

Since the angle of incidence between the incident beams and the faces of the calibration prism will be 45°, total internal reflection is obtained in each case. However, for 3.0 micron energy the alignment problem becomes more critical because the critical angle for fused quartz is $44^{\circ}55'$ for this wavelength. This would require overall system alignment accuracies of 3 to 4 minutes of arc. It is possible to alleviate this condition by either reducing the

long wavelength measurement limit or by using a higher index glass thus reducing the critical angle values. The latter appears to be desirable if a glass which is radiation resistant can be found. The reason for preferring fused quartz is its high resistance to discoloration or other optical deterioration under high radiation exposure. However, since the calibration prism is shielded from this exposure, other higher index glasses may be perfectly suitable. The calibration prism will have a 1.5 inch square hypotenuse face.

Dispersing Prism

A fused quartz prism will be used to disperse the solar energy into a spectrum such that a few spectral measurements can be made. The prism will be oriented at such an angle with respect to incoming energy to achieve minimum deviation of the dispersed energy. For example a prism with a 23° apex angle oriented for minimum deviation will disperse the spectral region 0.3 to 3 microns into a 1.9 degree angular subtense. The 3 micron energy will be deviated about 10° from the incoming direction. Thus, the 0.3 micron energy will be deviated by 11.9 degrees. If a six inch focal length lens is used to form an image of the spectrum the length of 0.3 to 3 micron spectrum will be 0.2 inch or 5 millimeters. Since this lens is used to form both the spectral and white light images, the smaller the deviation the smaller the field of view required of the lens and hence the better the resolution. Thus minimum deviation orientation of the prism appears to be very desirable.

The dimensions of the prism are as follows:

apex angle	23° approximately
face width	1 inch
face height	1 inch

Collecting Lens

The collecting lens is used as stated above to form an image of the sources on the respective detectors. One lens of six inch focal length will be used as shown in Fig. 4-4. By making this lens 1.6 inches in diameter it can collect all energy from both the tungsten lamp and the solar source. Whereas the field of view of the collimating lens was one degree or a little more, the field of view of this lens is approximately 12 degrees because of the deviation and dispersion of the spectrum with respect to the white light image.

Stray Light Controls

The long path length and relatively small apertures and small field help reduce the effects of stray light which may enter the system. As further insurance, all internal surfaces will be blackened with flat black paint to absorb stray radiation. In addition light traps will be provided to absorb and dissipate energy which is rejected by the beam splitter from the measurement beam. The tilt of the quartz windows described above is a further effort to minimize troubles from stray light. The gap between the reflectometer and the samples will be kept small to reduce the amount of stray light which can leak in around the scanning aperture. A system of black baffles will be distributed along the optical paths to collect oblique stray light bundles.

Vignetting

Vignetting is avoided in the reflectometer by making the optical components large with respect to the beam sizes. Each of the two beams is 0.75 inch in diameter nominally. Aberrations and light source size will cause each beam to grow above this dimension. The dimensions of the beam splitter, mirrors, windows, samples, calibration optics, dispersing prism, and collecting lens are all 1.5 inches or larger. Of course, as the measuring beams scan across the test samples, the calibration prism, or the black body cavity vignetting occurs as the beam moves on and off. This effect is avoided by making measurements only when the entire beam is incident on the sample area.

System Alignment

One of the most important factors affecting the performance of the reflectometer will be the alignment of the optical components. Since there are several optical components and 9 or 10 changes of direction in the optical path, alignment is critical. The alignment of the beam directions with the samples or calibration prism is extremely important. The alignment of the beam splitter with respect to the detection system will be critical. It is estimated that only a few minutes misalignment of these key parts can be tolerated without producing noticeable vignetting.

The low thermal expansion of the quartz optics used throughout the reflectometer will be an aid in retaining high quality optical performance. Rigid tubes and support structure will be provided to avoid misalignment through deflections, etc. The light weight and location of the key parts of the reflectometer make this task simpler.

System Weight

The weight of the reflectometer including all optics, mounts, tubes, detectors should not exceed 10 pounds. The combined weight of the optical components is estimated to be less than 0.5 pounds. The weight of the detector assembly is also less than 0.5 pounds. Therefore, allowing a liberal weight of 9 pounds for tubes, mounts, baffles, and other strucutre directly associated with the reflectometer the overall weight does not exceed 10 pounds.

Reflectometer Signal Calculation

Below are presented calculations on the reflectometer system efficiency and the signal output resulting.

Light passing through the reflectometer from source to detector undergoes several reflections and traverses several dielectric interfaces. For the spectral measurements, the band from 0.30 to 2.6 microns is divided into four regions containing nearly equal amounts of solar energy. These plus other related losses are given below.

Reflection loss occurs at each mirror. Approximate values of reflectance (R) for the wavelength regions chosen are noted. The number of reflections (N) is seven.

1. 0.30μ to 0.54μ R_1 = 80 percent
2. 0.54μ to 0.74μ R_2 = 90 percent
3. 0.74μ to 1.05μ R_3 = 90 percent
4. 1.05μ to 2.6μ R_4 = 95 percent

Thus the total reflectance; $R_T = R^N$ and;

$R_{T1} = 0.20$
$R_{T2} = 0.48$
$R_{T3} = 0.48$
$R_{T4} = 0.69$

For the white light measurements, R_{TW} is 0.48.

Loss occurs at each dielectric interface, of which there are effectively 14 in the reflectometer. For quartz elements the loss is about 3 percent at each face. Thus:

interface efficiency, $E = 0.97^{14} = 0.65$

Two losses occur in the beam splitter. One is absorption and the other simply results from the beam being divided. About 1/3 of the light entering the beam splitter is recovered. Since the light passes the beam splitter twice the resulting beam splitter efficiency B is 0.10.

Additional losses (L) of a miscellaneous nature, such as absorption is the quartz elements, misalignment, etc., are pessimistically established at 0.5.

Thus the power P_R incident on the detector is simply the power transmitted P_T diminished by the various losses, or;

$$P_R = P_T \times R_T \times E \times B \times L$$

Now the power transmitted is not all that is available since collection is not 100 percent efficient.

In the case of the tungsten source the source power is radiated into (nearly) a full sphere while the collecting lens collects only that portion represented by the solid angle subtended by the lens.

The solid angle ω subtended by a 3/4 inch diameter lens with a six inch focal length is given as follows

$$\omega = 4\pi \frac{\text{lens area}}{\text{sphere area}} = \frac{\pi\ (0.375)^2}{(6)^2} = 0.012 \text{ steradian}$$

A one watt lamp radiating into a full sphere, 4π steradians, provides 0.08 watts per steradian. Thus:

$$P_T = P\omega = 0.08 \times 0.012 \approx 10^{-4} \text{ watts}$$

In the case of the spherical sunlight collector it is desirable to provide a power level approximately five times that of the tungsten source. This is because the spectral measurements made with the sun source will divide the power over five detectors (four spectral and one total or "white").

Tousey (Ref. 50) has shown that the total flux P reflected from a specular sphere of radius x is given by:

$$P = \frac{E\ x^2}{4}$$

where E = intensity of sunlight = 0.14 watt per centimeter squared. Thus, requiring P to be five times greater than the tungsten case above and solving for x, we have:

$$x^2 = \frac{4P}{E} = \frac{4 \times 0.4}{0.14}$$

$$x \approx 3.4 \text{ centimeters}$$

While this results in a fairly large sphere it is recognized that the geometry of the collecting optics is fixed so that only a small segment of the sphere is required.

It is now possible to calculate the power incident upon the detectors for the several cases

For tungsten:

$$P_{RW} = P_T \times R_{TW} \times E \times B \times L$$
$$P_{RW} = 10^{-4} \times 0.48 \times 0.65 \times 0.1 \times 0.5 = 1.6 \times 10^{-6} \text{ watts}$$

For sunlight:

$$P_{R1} \approx 0.6 \times 10^{-6} \text{ watts}$$
$$P_{R2} \approx 1.6 \times 10^{-6} \text{ watts}$$
$$P_{R3} \approx 1.6 \times 10^{-6} \text{ watts}$$
$$P_{R4} \approx 2.2 \times 10^{-6} \text{ watts}$$
$$P_{RW} \approx 1.6 \times 10^{-6} \text{ watts}$$

Utilizing the lead sulfide detector design data provided by several manufacturers it is now possible to calculate the expected signal level and signal-to-noise ratios. Since the incident power is similar in all cases only the tungsten case will be presented.

Detector parameters:

temperature	25° C
bias	20 volts dc
time constant	1 millivolts
resistance	0.2 megohms
area	0.062 centimeters squared
power input	1 microvolt (3000°K black body)

Under these conditions a typical detector will have an output of 0.017 volts. This is well within the 0 to 20 millivolt range required by the telemetry system. Variations in output due to slightly different conditions may be compensated by a gain adjustment on the amplifier following the detector.

Power requirements for the light source detectors and amplifiers will be about 2 watts.

4.2.2 Instrumentation for Temperature Measurements on Samples

Temperature measurements on each reflective sample are required, as indicated previously, to provide the thermal history of the samples in orbit, and to provide data for calculation of changes in the solar absorptivity (α) and thermal emissivity (ϵ) of the reflective surfaces as a function of time in the space environment. These measurements must be made without significantly changing the thermal balance of the samples, and must be compatible with the available power system and telemetry. In addition the instrumentation is required to produce data of meaningful precision over a wide temperature range.

A survey of temperature-measuring elements indicates that the Temp-Sensor, supplied by Micro-Systems, Inc., Pasadena, California, is quite suitable for these measurements. This device, made of single-crystal silicon, exhibits a relatively linear positive resistance change with temperature of about 0.9 percent/$^{\circ}$C over the temperature range of interest in this experiment (-75°C to + 200°C). It has the added advantage of small size (0.040 inch x 0.030 inch x 0.0005 inch) and is supplied with gold wire leads of 0.003 inch diameter. The devices are available with nominal resistance at 25°C of 1000, 2000, and 5000 ohms.

The instrumentation required for using the Temp-Sensor is extremely simple. The device is used as one part of a two resistor voltage divider supplied with the available regulated 28 v power. For example, the 1000 ohm unit has resistance values of 300 ohms at -75°C and 2700 ohms at 200°C. Its use in the 28 v divider circuit with a 12,400 ohm resistor as the other element would give a 5.0 v output at 200°C and a 0.66 v output at -75°C. Therefore, 87 percent of the 0 to 5 v dynamic range is used. The power dissipation in the sensor, approximately 0.002 watt, has negligible influence on the thermal balance of the sample to which it is affixed. The power consumption during the

measurement, assuming 30 sensors are used, is about 1.7 watts. Since the longest temperature measurement cycle occurs at the end of the sun-lit portion of the orbit (see Section 4.1.2) this drain on the fully charged batteries should not cause a problem. If power consumption is approblem a higher resistance Temp-Sensor can be used, which would result in a higher impedance output to the sub-commutator.

The 0 to 5 v output range of the temperature would be transmitted as 256 discrete steps in the PCM telemetry system. Therefore, each step would represent approximately 1.25°C with the system described. This would be sufficient precision for the proposed experiments.

4.2.3 Space Environment

4.2.3.1 Charged Particle Detection - Rate

A list of charged particle radiation detectors is given in Table 4-3. The sensitivity of these detectors to proton and electron energies is also given in the table. The primary function of the three Geiger-Mueller tubes is to determine the electron flux rate and provide integral energy points at three representative energy thresholds. Unfortunately these detectors will also be directional for the low energy protons and omnidirectional for high energy particles and cosmic rays as well as Brehmsstrahlung radiation. Corrections will have to be made to the data after a determination of the proton spectrum. This determination is made by means of a proton spectrometer. The proton spectrometer is based on the instrument flown on Explorers 12 and 14 and described by Davis and Williamson for their measurements of proton down to 60 kev. It consists of a thin layer of ZnS(Ag) deposited on the face of a photomultiplier tube. A set of thin absorbers of varying thickness mounted on a wheel are periodically rotated into position to serve as windows for the detector in order to obtain energy spectra. The dc and pulse outputs of the photomultiplier tube are both monitored. Suitable choice of phosphor thickness and discriminator settings enable measurement of protons in the rangeoof 100 kev to 4.5 Mev.

TABLE 4-3

FLIGHT EXPERIMENT - RADIATION DETECTION INSTRUMENT

CH. NO.	DETECTOR	ORIENTATION	PROTON (E) RANGE	ELECTRON (E) RANGE	EST. POWER
1	302 G-M Tube	OMNI.	≥ 20 Mev.	≥ 1.5 Mev.	140
2	213 G-M Tube	$\theta = 180^{\circ}$	≥ 0.5 Mev.	≥ 40 kev.	140
3	213 G-M Tube	$\theta = 180^{\circ}$	≥ 0.4 Mev.	≥ 250 kev.	140
4	Scint. (DC)	$\theta = 180^{\circ}$			
	Direct		10 kev. to 0.1 Mev.	5 kev. to 100 kev.	
	Scatter			10 kev. to 80 kev.	140
5	Scint. (Pulse)	$\theta = 180^{\circ}$	100 kev. to 4.5 Mev.		
6	CdS (crystal) w/broom magnet	$\theta = 180^{\circ}$	0.1 kev. to 10 Mev.	≥ 500 kev.	60

H. V. SUPPLY		300
STEPPING MOTOR	40 milliwatts average power	
PEAK POWER		1020

TOTAL WT. APPROXIMATELY 4 POUNDS

Use of a position on the absorber wheel which allows only scattered electrons to hit the phosphor enables selective measurement of low energy electrons in the range of 10 kev to 80 kev.

A modification to this experiment involves the addition of a CdS crystal counter with broom magnet. This assembly is mounted behind the absorber wheel which also includes a thin transparent window and an opaque window of equal stopping power to differentiate between response of the detector to charged particles vs light. Use of aluminum oxide coated and uncoated clear Mylar films as absorber windows serve to extend the proton low energy cutoff down to 20 kev.

4.2.3.2 Charged Particles - Integrate

The previously described detectors give quantitative information of electron and proton spectra. This information is of analytical value in the evaluation and correlation of radiation damage of the sample surfaces under test. Time integration of these fluxes and energies is another necessary calculation in the analysis. A simplified method of accomplishing this integration, and serving as a check on the calculated values, is obtained by the use of dosimetric devices in the payload. This is accomplished by the use of silver activated glass as a dosimeter having the property of discoloring or darkening upon exposure to radiations. These devices are made in the form of back-surfaced mirrors. They are situated on the circle of samples where they are fully exposed to the environment. Analysis of coloration is made by the reflectance analyzer by measuring the loss in reflectance occuring when the light beam traverses the glass to the reflecting surface and back out of the glass. Accurate calibration of change in reflectance as a function of proton and electron exposures for identical samples of the glass disks will enable interpetation of the integrated dose up to the time of the measurement. Each disk will be of different thickness to give a measure of integrated doses of low energy, medium energy, and high energy radiations.

In addition to these dosimeters further data on integrated dose can be obtained from calibration of the solar cells for their degradation following exposure to electrons and protons. Housekeeping readings of solar power supply output under full sun conditions can be interpeted in terms of total integrated dose. Preflight studies would include damage sensitivity of the solar cells to ultraviolet, x-ray, and charged particle radiations and calibration of these effects.

4.3 Orientation System

Any object in free fall in the vicinity of the earth will be subject to a variety of forces, which, although weak, are persistent. The motion of the object over long periods of time can therefore be strongly affected. Since the satellite must always point toward the sun, some form of orientation control must be provided to correct the perturbing effects of the force field. This section will discuss the perturbations and the effect of the correcting torques on the dynamics of the satellite.

4.3.1 Perturbing Torques

If the satellite had a spin initially directed toward the sun and there were no disturbing torques, it would preserve its orientation indefinitely. Since, in the vicinity of the earth, there does not exist any force-free environment it will be necessary to provide the satellite with a means of applying occasional corrective torques. For a cold gas torquing system, the total stored impulse must be at least equal to the total perturbing impulse during the useful life of the satellite. In mathematical form, $J \geq \int_0^T L dt$, where J is the stored (angular) impulse, L is the disturbing torque, and T is the lifetime.

In order to compute J, and from it the mass and volume of stored gas, it is necessary to know the magnitude of L as a function of time. The following paragraphs will establish some orders of magnitude; accurate values must await a detailed design.

4.3.1.1 Earth's Orbital Motion

If the satellite were subjected to no external forces, it would point in a fixed direction in inertial space. Consequently, as the earth moves around the sun, the spin axis will drift to the west, relative to the sun, at a rate of 0.986 deg/day, which must be compensated by an average easterly precession of the same amount. The velocity of precession is given by

$$\omega_p = \frac{L}{C\Omega}$$

where

ω_p = precession vel.

L = torque

C = moment of inertia about spin axis

Ω = spin vel.

from Eq. 4-7,

$$L = C\omega_p\Omega \tag{4-8}$$

From Eq. 4-8 it is clear that the required torque is proportional to the spin velocity, which should therefore be kept as small as other requirements permit.

If the satellite is assumed to be in the form of a short cylinder weighing 40 kg and having a radius of 30 cm, $C \approx 2 \times 10^7$ gm cm^2. Expressed in radians per second, $\omega_p = 2 \times 10^{-7}$, and assuming $\Omega = 1$ radian/sec, L = 4 d cm sec. For a one year life, therefore, the total stored impulse required would be $4 \times 3 \times 10^7 = 12 \times 10^7$ d cm sec.

4.3.1.2 Gravity Gradient

A body in free fall in a nonuniform gravitational field will experience a torque about its center of mass. Assuming a cylindrical body having an axial moment of inertia C and a perpendicular moment A, the torque is (Ref. 51)

$$L = \frac{3}{2}\gamma\frac{M}{R^3}(C-A) \sin 2\alpha \tag{4-9}$$

where

γ = gravitational constant

M = mass of primary (earth)

R = primary-satellite distance

α = angle between C-axis and local vertical

The greatest torque will exist for the lowest orbit and for $\alpha = \pi/4$. Taking R = 6970 km (600 km altitude), $A = \frac{2}{3}C$, and inserting values of γ and M the result is $L \approx 12$ d cm sec.

This torque will not exist at all times, but will vary as the satellite traverses its orbit. The average torque will be smaller and may even be zero for the circular orbits shown in Figs. 4-12 or 4-13. In Fig. 4-12 the torque is alternately clockwise and counterclockwise averaging to zero every half-orbital period. In Fig. 4-13 it is identically zero at all times. The worst case is shown in Fig. 4-14. The component of torque about an axis normal to the plane of the diagram is always counterclockwise and hence will have a nonzero average. The component about a vertical line in the plane of the diagram will alternate in sign every 90 degrees and can be disregarded.

These results can be generalized to obtain the average torque for any angle, i, between the normal to the orbit plane and the solar vector. The result is that sin 2α in Eq. 4-9 is replaced by

$$\frac{\sin 2i}{2} \tag{4-10}$$

If the orbit normal remained fixed in inertial space throughout the year, the average of sin 2i would be

$$< \sin 2i > \; = \frac{2}{\pi} \left(\cos i_o + \sin^2 i_o \ln \frac{1 + \cos i_o}{\sin i_o}\right) \tag{4-11}$$

where i_o is the minimum value of i, occurring when the normal lies in a plane perpendicular to the ecliptic. The maximum of Eq. 4-11 is at $i_o \approx 35$ degrees, which gives

$$< \sin 2i > \; = \frac{2}{\pi} \times 1.21 \tag{4-12}$$

hence $\frac{< \sin 2i >}{2}$ over one year is $\frac{1}{2} \; \frac{2}{\pi} \times 1.21 = 0.385$ and the average torque is $12 \times 0.385 = 4.6$ d cm sec. The stored impulse must therefore be $4.6 \times 3 \times 10^7 \approx 14 \times 10^7$ d cm sec.

Because of the earth's oblateness, any but a polar orbit or an equatorial orbit will undergo a precession. The line of nodes in the equatorial plane will turn westward if the satellite

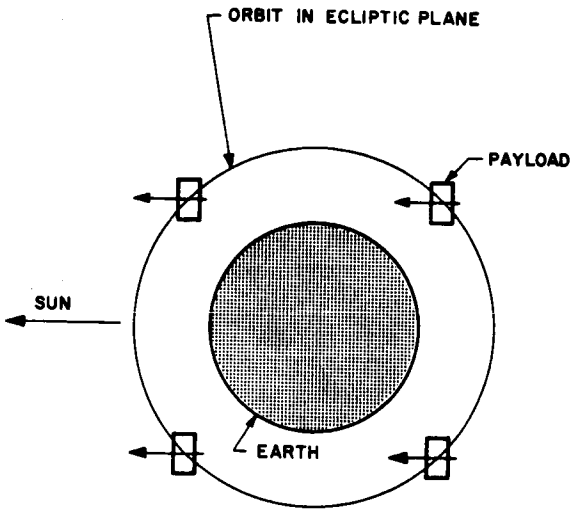

FIG. 4-12
ORBIT IN ECLIPTIC PLANE

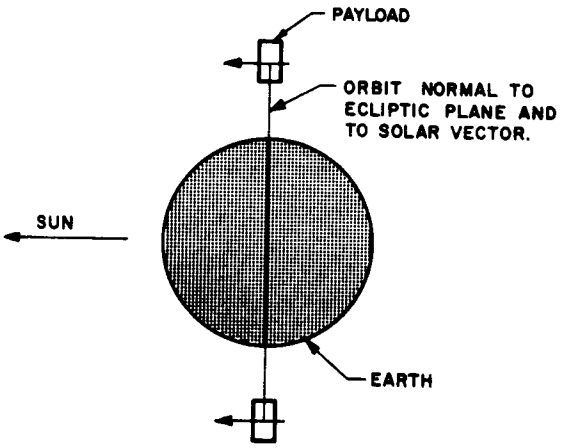

FIG. 4-13
ORBIT NORMAL TO ECLIPTIC PLANE

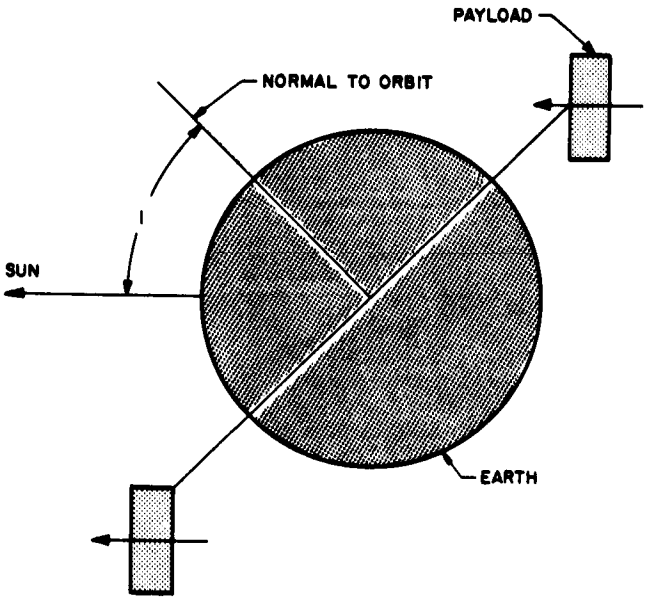

FIG. 4-14
ARBITRARY ORBIT ORIENTATION

motion is direct and eastward if it is retrograde. As a result, the angle i will not vary in the simple manner assumed in the derivation of Eq. 4-11, but will be modulated in a complicated way by functions having the period of the precession. If the satellite motion were retrograde the nodes could precess eastward at a rate sufficient to keep i constant. However, since all boosters are fired with the earth's rotation, this situation will not occur.

A calculation of the effect of orbit precession indicates that the value of $< \sin 2i >$ given by Eq. 4-12 is not materially altered, hence the stored impulse will be taken as 14×10^7 d cm sec.

4.3.1.3 Magnetic Fields

A conductor spinning in a magnetic field will have eddy currents induced in it that will react on the field to produce a torque. In general, the torque will have a component along the spin axis, which will cause spin damping, and a perpendicular component tending to precess the spin axis.

In addition to eddy torques, there may be others caused by permanent magnets in the body or by equivalent dipoles generated by currents flowing in the internal circuits.

In order to estimate the eddy drag the satellite will be treated as a spherical shell. The solution can then be obtained from a modification of Prob. 12, in Ref. 52. The precessional torque is

$$L_p = \frac{1}{3} \frac{\pi B^2 a^4 \omega}{\sigma} \sin 2\alpha \qquad (4\text{-}13)$$

and the spin torque

$$L_s = \frac{1}{3} \frac{\pi B^2 a^4 \omega}{\sigma} (1 - \cos 2\alpha) \qquad (4\text{-}14)$$

where

B = magnetic field (Webers/m^2)

ω = spin

a = sphere radius (meters)

σ = surface resistivity (ohms/square)

α = angle between ω and B

A suitable value for a in terms of the radius of the cylindrical satellite can be chosen on the basis of dimensional reasoning. In Fig. 4-15 the rectangle is a cross-section of the satellite, assumed to have a length equal to its radius, giving $A = \frac{2}{3} C$ as in the discussion of gravity gradient. The circle is a cross section of the equivalent sphere. For any cross section, the EMF around the loop is proportional to its area x $B\omega$. The resulting current is inversely proportional to the resistance, hence to the circumference, and the torque is proportional to current x B x area. Therefore,

$$L_\alpha \frac{\omega B^2 \, (\text{area})^2}{\text{circ.}} \; \alpha \; \frac{(\text{area})^2}{\text{circ.}} \tag{4-15}$$

For the cylinder

$$L_c \alpha \frac{4r^4}{6r} = \frac{2}{3} r_c^3 \tag{4-16}$$

And for the sphere

$$L_s \alpha \frac{\pi^2 r^4}{\pi r} = \frac{\pi}{2} r_s^3 \tag{4-17}$$

Equating L_s and L_c yields

$$r_s = \left(\frac{4}{3\pi}\right) \frac{1}{3} r_c = 0.75 \, r_c \tag{4-18}$$

The value of σ will depend on the thickness and type of metal used for the skin as well as on the arrangement and dimensions of internal stiffeners. An approximate equivalent shall thickness can be obtained from

$$m = At\rho \tag{4-19}$$

where

m = total mass of structure

A = surface area

t = equivalent shell thickness

ρ = sp. gr. of structural material

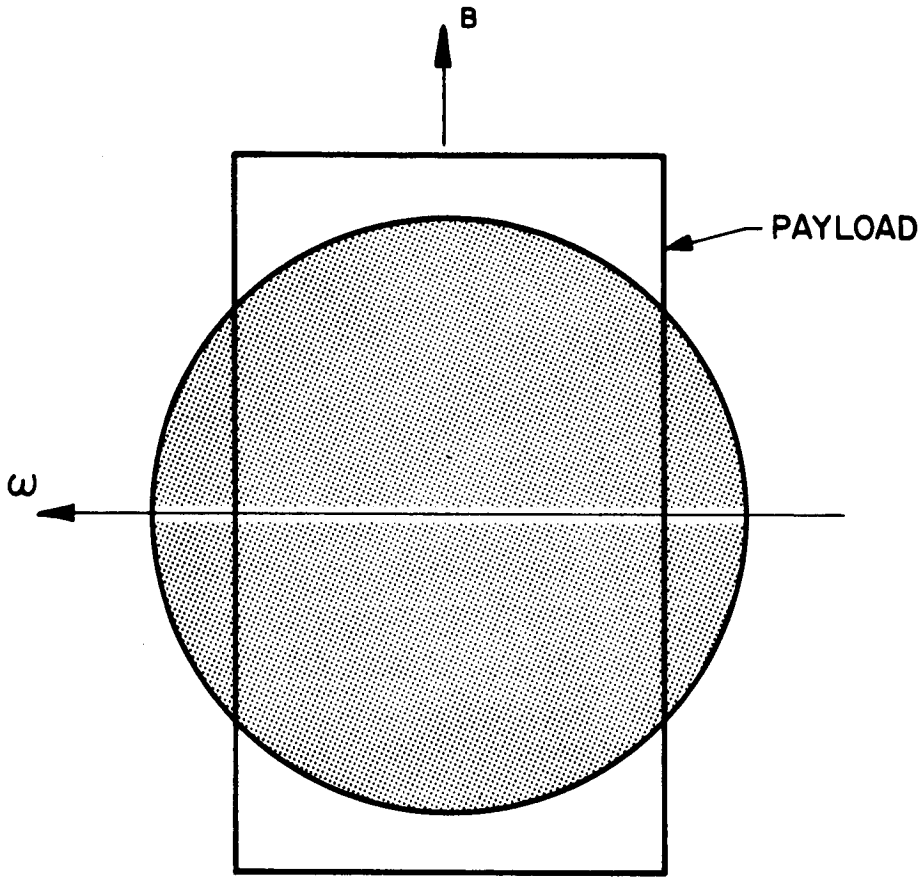

B = MAGNETIC FIELD

ω = ANGULAR VELOCITY

FIG. 4-15 EQUIVALENT SPHERE FOR SATELLITE

Using the estimated weight and dimensions of the structure, and assuming Al alloy as the metal, Eq. 4-19 gives t = 0.066 inch, or 1.67 mm. For this thickness of 2024-T4 alloy, $\sigma = 3.4 \times 10^{-5}$. Taking $B = 2.5 \times 10^{-5}$, $\omega = 1$, a = 0.225 meter and $\alpha = \frac{\pi}{4}$, Eq. 4-13 gives $L_p \approx 5 \times 10^{-8}$ newton meters or 0.5 d cm sec.

It is probably not useful to attempt to find an average torque, but it is certainly safe to use $\frac{1}{2}$ of the value just found. The stored impulse would therefore be $0.25 \times 3 \times 10^7 = 7.5 \times 10^6$ d cm sec.

Permanent magnets contained in the satellite would cause torques also, and these could easily be many times the eddy torque. This disturbance can be theoretically cancelled by using compensating magnets placed anti-parallel to the functional magnets.

The compensators need not be adjacent to the others; they can be anywhere in the satellite provided only that they are anti-parallel.

As an example, assume an Alnico V bar 10 cm long and of 1 cm^2 area, having a flux density just outside the end faces of 2000 gauss. The pole strength is then $2000/4\pi$ and the magnetic moment is $10 \times 2000/4\pi$. Taking the earth's field as 0.25 gauss, the maximum torque would be 400 d cm sec. If this could be 99 percent cancelled the residual torque would be only 4 d cm sec, but if the cancellation were only 90 percent the residual would be 400 d cm sec, about 3 times the next greatest torque, that due to gravitational gradient. It is thus clear that permanent magnets should be avoided wherever possible.

The torque exerted by internal current loops cannot be calculated until a design exists but a rough estimate can be made. During standby the circuits will draw about 5w, and during transmission, about 23w, hence, assuming a 28vdc supply the currents will be 0.18 amp and 0.82 amp, respectively. Assume also that the total loop area of the circuits is 1000 cm^2. The equivalent magnetic shell will have a magnetic moment

$$\mu = iA \tag{4-20}$$

where

i = current in emu

A = loop area

and the torque will be

$$L = iAB \tag{4-21}$$

where B is the ambient field. The torque during standby will therefore be

$$0.018 \times 10^3 \times 0.25 = 4.5 \text{ d cm sec}$$

and during transmission, $0.082 \times 10^3 \times 0.25 = 40$ d cm sec. These numbers could easily be reduced by a factor of 100 by using twisted pair or coaxial cable for all dc cabling, by facing similar circuit boards in opposite directions and, if necessary, by inserting small bucking loops in series with the various loads. The standby torque would then be negligible compared to the gravity gradient torque. The torque during transmission would be 0.4 d cm, but it would act only 1 minute out of each day, giving an average value of 0.4/1440, which can certainly be ignored.

Such residual torques as may exist will in any case not be unidirectional because of the changing attitude of the satellite in the earth's magnetic field, so it seems safe to take an average of no more than 1 d cm, which leads to a stored impulse of 3×10^7 d cm sec.

4.3.1.4 Aerodynamic Torque

At an altitude of 600 km the mean free path of the atmospheric molecules is so large compared to the satellite dimensions that aerodynamic flow does not exist; however, order of magnitude pressures can be estimated by considering the flow of momentum.

If the velocity of the satellite is v and the atmospheric density is ρ, the flow of momentum per square centimeter per second is ρv^2, and if the satellite is regarded as a sink of momentum

this is also equal to the pressure. Taking $v = 7.5 \times 10^5$ cm/sec and $\rho = 1.6 \times 10^{-15}$ gm/cc, this pressure is $\sim 10^{-3}$ d/cm^2. Because of the cylindrical symmetry, if the satellite flies face forward or side forward there will be no torque, whereas for some intermediate angle the torque should be a maximum.

However, on the basis of these simple assumptions it turns out that a smooth, right circular cylinder would experience no torque for any angle of attack. The same result is obtained if the cylinder is assumed to be a perfect specular reflector instead of a sink.

If some parts of the surface are specular and others are "black" a torque will exist. The reason lies in the different directions of the forces in the two cases. The force on a "black" surface is in the direction of the incident particles, whereas the force on a specular surface is along the surface normal, regardless of particle direction.

As an unrealistically extreme case, establishing an upper bound for the torque, assume that the face of the cylinder is specular and the side is black. The torque for a 45 degree angle of attack is then ~ 20 d cm. The torque will, in general, have a nonzero average which obeys the same relations as the gravity gradient. Hence, referring to Section 4.3.1.2, the average value will be $20 \times 0.385 \approx 8$ d cm. The satellite will actually have neither specular nor "black" surfaces, so it seems safe to reduce this figure by at least a factor of 2, which gives an average value of 4 d cm and a stored impulse of 12×10^7 d cm sec. If the surface were made spherical this torque would be essentially zero. If propellant weight becomes a problem, this geometry may become necessary.

The satellite will not be perfectly smooth but will have projections in the form of nozzles, reflectometer housings, and possibly antennas. Even these will tend to form a balanced structure, but if one assumes an unbalanced area of 10 cm^2 having a lever arm

of 20 cm, the torque will be $10 \times 20 \times 10^{-3} = 0.2$ d cm. Assuming an average value of 1/2 of this, the stored impulse must be $0.1 \times 3 \times 10^7 = 3 \times 10^6$ d cm sec. Whip antennas would be especially serious sources of torque and should be avoided if possible by the use of slot antennas.

4.3.1.5 Radiation Pressure

Sunlight exerts a pressure of $\sim 10^{-4}$ d/cm^2 and can therefore produce a torque in the same way as a molecular flow of gas. However, it is an order magnitude less than the gas pressure, and in any case the satellite will always face the sun in a zero torque attitude, so that radiation pressure can be ignored. If the satellite does not face the sun, it will be due to failure of the control system, and questions of perturbation become academic.

4.3.2 Spin Damping

There will be three sources of spin damping: magnetic eddy drag, aerodynamic drag and an effective drag caused by the transfer of propellant from the interior of the satellite to the rim.

4.3.2.1 Magnetic Damping

The equation for the magnetic drag has already been given, Eq. 4-14. Using the numbers of Section 4.3.1.3, the drag torque is 0.5 d cm when the spin axis is normal to the field. The average value will be assumed to be half of that, or 0.25 d cm leading to a stored impulse of $0.25 \times 3 \times 10^7 = 7.5 \times 10^6$ d cm sec. The decay time constant can be found from the relation

$$L = K\omega = C\dot{\omega} \tag{4-22}$$

where K is the coefficient of ω in Eq. 4-14 and C is the moment of inertia about the spin axis. The solution to this differential equation is

$$\omega = Ae^{-Kt/C} \tag{4-23}$$

hence the time constant T, is C/K. Using values given previously, the result is $T = 8 \times 10^7$ sec or about 2 2/3 years.

4.3.2.2 Aerodynamic Damping

Atmospheric spin damping can be estimated by considering the momentum imparted to incident molecules by the spin motion of the satellite. From the density, temperature, and mean molecular weight one can calculate the number of molecules incident on 1 cm^2 in one second. Assuming that each molecule incident on the cylindrical surface acquires the tangential velocity of the surface, it is possible to derive an expression for the momentum carried away by the gas per unit time. The resulting torque is

$$L = \frac{\pi a^4 \omega \rho}{3} \left(\frac{3RT}{\mu}\right)^{1/2} \tag{4-24}$$

where

ρ = gas density

a = radius of cylinder

R = universal gas constant

μ = mean molecular wt

Taking $\rho = 1.6 \times 10^{-15}$, $T = 1500$, $\mu = 15.6$, $a = 30$ and $\omega = 1$, Eq. 4-24 gives a torque of $\sim 2 \times 10^{-4}$ d cm, which is completely negligible compared to the magnetic torque.

4.3.2.3 Propellant Transfer

The transfer of propellant from the interior to the nozzles will cause a braking torque if the nozzles are at a larger radius than the storage tank.

A unit mass of gas stored at radius b will have an angular momentum ωb^2. After transfer to radius a the angular momentum will be ωa^2, which is then lost in the exhaust. Thus, every gram of propellant consumed will remove $\omega(a^2-b^2)$ units of momentum which must be made up by an accelerating impulse of equal amount.

As an extreme case, assume that the propellant is stored in a spherical tank at the center of mass, so that $b \approx o$. Then the loss of momentum per gram is $\omega a^2 = 1 \times 900$ gm cm^2/sec or d cm sec.

Assuming that a year's supply of propellant is about 2 kg, the total impulse would be 900 x 2000 = 1.8×10^6 d cm sec. This is only about 1/2 percent of the storage required for precession and gravity gradient.

4.3.3 Impulse Budget

The results of Sections 4.3.1 and 4.3.2 are summarized in Table 4-4. The important satellite parameters are:

diameter	60 cm
length	30 cm
mass	40 kg
Axial mom of inertia	2×10^7 gm cm^2
Transverse mom of inertia	1.3×10^7 gm cm^2
Spin	1 rad/sec
Velocity	7.5 km/sec
Altitude	600 km
Orbit	Circular
Mag. Field	0.25 gauss
Gas density	1.6×10^{-15} gm/cc
Mol. wt	15.6
Gas temperature	1500 K

4.3.4 Orientation Control

The disturbing torques discussed in Section 4.3.1 will be balanced by control torques applied whenever the pointing error exceeds some preset limit. The proposed control system is shown in Fig. 4-16. The satellite spins normally about its axis of figure. A lens forms an image of the sun, which sweeps across the strip detector once each revolution, whenever the solar vector $\bar{S}$ lies outside some preassigned tolerance angle. The detector then actuates the nozzles, which produce a torque $\bar{L}$ lasting for about 0.1 sec. The vector $\bar{\omega}$ then precesses about axis P toward the sun. This action is repeated every revolution until the sun's image again lies within the central tolerance zone.

TABLE 4-4 IMPULSE BUDGET FOR ONE YEAR

TORQUE

SOURCE	VALUE d cm	IMPULSE d cm sec
Precession	4	12×10^7
Gravity	4.6	14×10^7
Mag. field		
Eddy	0.25	7.5×10^6
Circuits	1.0	3×10^7
Aerodynamic		
Body	4.0	12×10^7
Projections	0.1	3×10^6
Spin damping	--	--
Magnetic	0.25	7.5×10^6
Aero.	0.0	0
Prop. Trans.	--	2×10^6
TOTAL	14.2	42.6×10^7

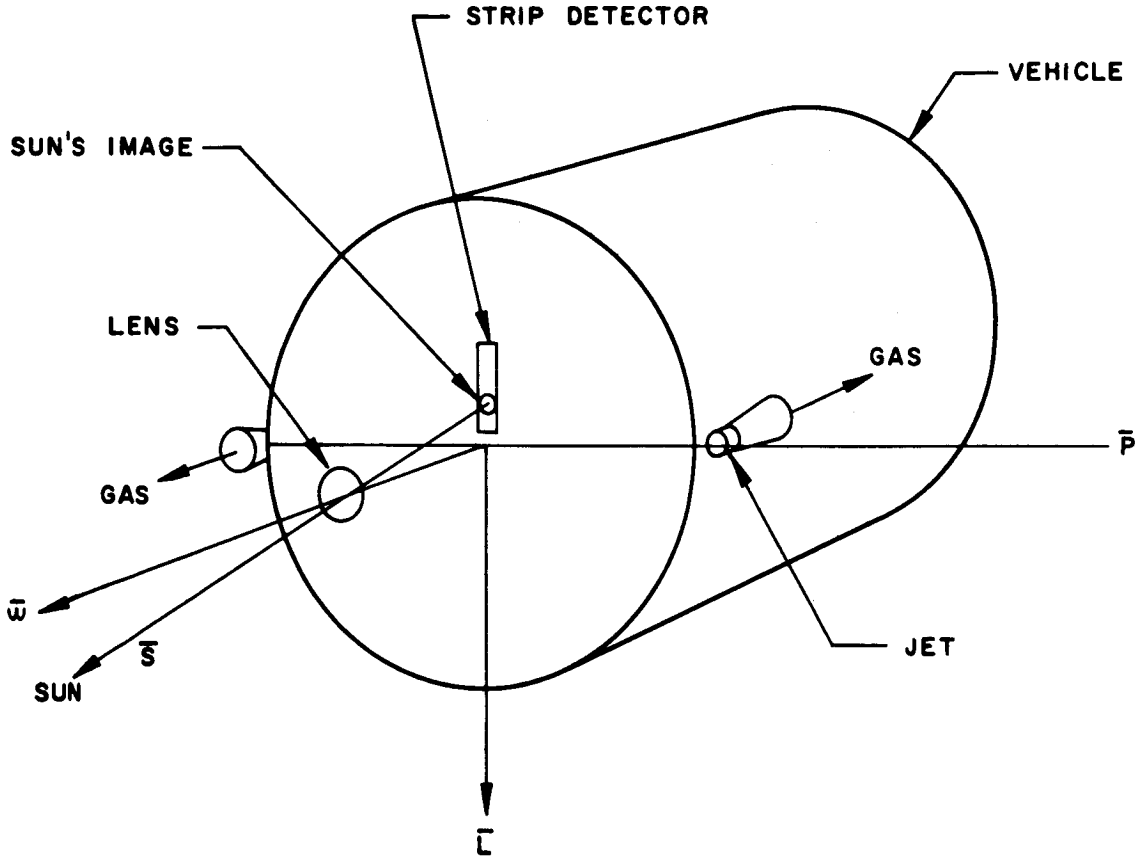

FIG. 4-16 SATELLITE ATTITUDE CONTROL SYSTEM

The foregoing description is much simplified, giving only the net effect of the control impulses. Actually, it is the total angular momentum vector of the body, $\bar{H}$, that moves directly toward the sun at each impulse. The $\bar{\omega}$ vector moves perpendicularly, in the direction it would go if the body had no spin, with the result that a precessional motion is induced in which $\bar{\omega}$ follows a conical locus about $\bar{H}$. Repeated torquing will, in general, increase the amplitude of the precession so that instability would result if the motion were not damped.

A more realistic picture of the sun sensor is shown in Fig. 4-17. A filter attenuates the energy to prevent detector burnout and the lens forms an image of the sun on the mask. A silicon solar cell placed behind the mask generates a control signal whenever it can see the image. Figure 4-18 shows the construction of the mask. As long as the sun's image is within the central dotted region no signals will be generated, but when the error increases enough to place the image outside of the tolerance zone the image will fall on the detector each time it crosses the slit, and corrective action will occur.

In addition to the orientation control nozzles shown in Fig. 4-16, a spin-up set will be needed to overcome spin drag. A spin-braking set may also be required because a fraction of the precessional energy is not dissipated in the damper, but is converted into increased spin. The effect is very small, but over a long mission an excessive spin could accumulate, especially in a high orbit where opposing atmospheric and magnetic spin drags become negligible. A simple centrigugal switch would be sufficient to control both sets of nozzles.

4.3.4.1 Acquisition

Initial acquisition of the sun presents no theoretical problems. It would occur automatically if the sun were in the sensor's field of view at the time the satellite achieved orbital speed, and if the satellite were then spinning with its designed angular velocity. However, it is important to minimize the initial angle between the optical axis and the sun in order to avoid excessive consumption

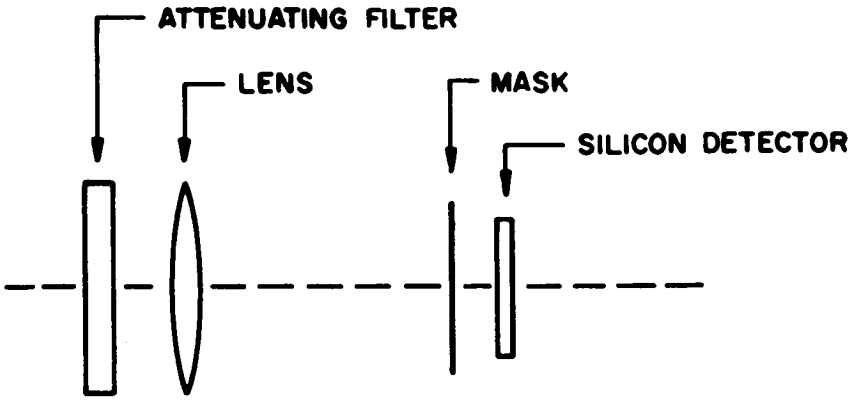

FIG. 4-17 SUN SENSOR

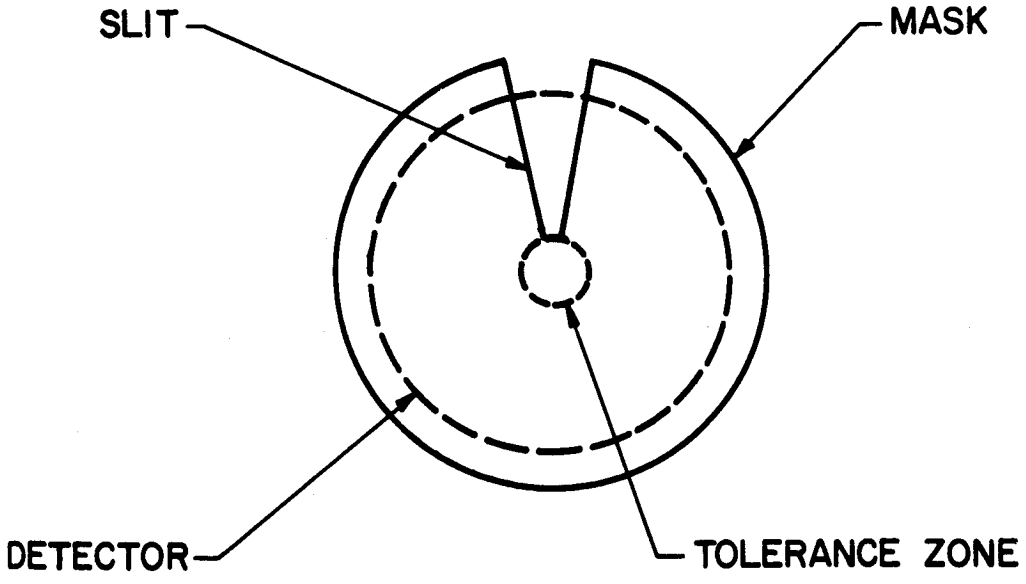

FIG. 4-18 SUN SENSOR MASK

of propellant. Acquisition from an initial angle of 90 degrees, for example, would expend as much gas as 3 months of the forced easterly precession required by the earth's orbital motion.

If no particular orbital inclination were desired, and if the launch azimuth were unrestricted, it would always be possible to choose an azimuth and a launching time at any latitude that would place the sun on the optical axis at the instant of last-stage burnout. Any specification of the azimuth is at the same time a specification of the inclination, since they are related by sin 2 = $\frac{\cos i}{\cos L}$, and a limitation on the minimum angle between the sun and the optical axis, because only one variable (the time) can then be adjusted. All U.S. launching sites have a limited range of permitted launch azimuths and therefore of possible inclinations. A further geometrical restriction is that the minimum inclination is equal to the latitude of the site, so that the lowest inclination obtainable in the U.S. is 28 degrees, the latitude of Cape Canaveral. The minimum for the Pacific stations is ~ 35 degrees, and for Wallops Island, ~ 37 degrees. Except for near-polar orbits, the East Coast stations are preferable because the firings can be made to the east, with the earth's rotation.

The equation cited in the last paragraph does not uniquely determine Z for a given choice of i, but rather, two possible supplementary values, and consequently two "best" launching times. One would choose the value giving the lesser angle, φ, between the optical axis and the sun assuming, of course, that both balues of Z are permitted at the site. As a typical example, assume an inclination of 35 degrees and a firing from Cape Canaveral (latitude 28 degrees) at winter solstice. The possible values of Z are 68 degrees or 112 degrees, which give "best" values of the sun's easterly hour angle of 100.7 degrees and 79.3 degrees, respectively. The first value gives φ = 43 degrees, and the second, φ = 5 degrees. Therefore the booster should be fired at an azimuth of 112 degrees when the hour angle is 79.3 degrees, or $5^h\ 17^m$, corresponding to 6:43 A.M. local apparent time. At summer solstice the conditions are

exactly reversed, that is, the firing should be at 68 degrees azimuth and hour angle 100.7 degrees, or 5:17 A.M. local apparent time. The angle φ would be the same in both cases, i.e., 5 degrees. The general rule is: choose the greater value of Z when the sun's declination is south, and the lesser value when it is north. The firing times for equal but opposite declinations are complements with respect to 12^h.

Owing to the low latitude of the Pacific sites, acquisition from a solar orbit will require the expenditure of much greater quantities of propellant than for easterly firings from Cape Canaveral or Wallops Island. For a true polar orbit ($i = 90^o$) there is only one favorable firing time regardless of the sun's declination, namely, local apparent noon. The value of φ is then 90-(L-d), where d is the declination. At summer solstice φ = 78.5 degrees. Comparing this with the previous example it can be seen that the polar launching will require 78.5/5 = 15.7 times as much propellant for acquisition, or roughly as much as is needed for 2 1/2 months of easterly precession. The total propellant mass and storage volume would have to be increased by about 5 percent over the values given in Table 4-5.

TABLE 4-5

ATTITUDE CONTROL PROPELLANT MASS AND STORAGE VOLUME

GAS	MASS - GMS	VOLUME - CC
H_2	56.4	3360
He	94.4	2780
N_2	212.	903
O_2	224.	834
Ne	149.	1775
Ar	202.	1340

Both of these examples have neglected the distance of the satellite from the launching site at last stage burnout. The error is small for easterly firings, but can be appreciable for the polar orbit. A typical distance for the Scout launch vehicle is 1200 n mi,

or 20 great circle degrees. Thus, φ, in the last example would be increased to 98.5 degrees. For polar orbits, therefore, it will be necessary to have a wide angle sun sensor in addition to the fine control sensor already described.

Much less propellant would be needed for acquisition if the satellite were not spinning during this phase of the operation. The apparent advantage disappears, however, when weighed against the additional complications it introduces. First, a different type of control system would have to be used, since the normal system will work only if the satellite is spinning. This brings with it a weight penalty and a reduction of reliability. Second, after acquisition the auxiliary control system would have to be permanently disabled and the satellite would have to be spun up to its rated angular velocity. The disabling function adds still more circuitry, and in general, the spin-up will require as much propellant as acquisition in the spinning condition.

It is a serious disadvantage for the present purpose, that the last stage of the Scout is spin stabilized at 160 rpm, far in excess of the one radian/sec desirable for the satellite. Before the satellite can become operational it will be necessary to remove essentially all of its original spin. Three methods of doing this appear to be possible. The obvious solution is to use the spin control system of the satellite to produce the necessary braking, but this would require a supply of propellant 8 times as great as that needed by all other control operations for one year.

A better solution would be to provide solid propellant spin motors, which are commercially available. There is a practical difficulty in this approach, caused by the spin tolerance of the Scout, which allows spins between 160 and 220 rpm. If the motors were designed to remove 190 rpm, the satellite could be left with 30 rpm of spin in either direction, which the gas system would then have to

remove, again at the expense of a considerable fraction of the total supply. It may be possible to use spin motors designed for the highest spin rate, which would be jettisoned, still burning, when the spin had been reduced to the prescribed value.

Probably the simplest method is that of dumping angular momentum by means of weights and cables. It has the advantage of extreme simplicity, and, if the final angular velocity is to be zero, of complete independence of the initial spin. The spin tolerance of the launch vehicle would therefore cease to be a problem. It would be necessary, however, to expend some gas in order to bring the satellite up to rated speed from the zero spin condition after release of the weights. This would necessitate an increase of about 4 percent in the stored gas, which is quite acceptable. The weight penalty is small; two 200 gm masses an cables 195 cm. long would stop the spin completely if release occurred when the cables were radial.

The basic operations after third stage separation would then be:

1. Fourth stage spin-up
2. Fourth stage ignition
3. Fourth stage separation
4. Satellite despin to zero ω
5. Satellite spin-up to 1 rad/sec
6. Sun acquisition

4.3.4.2 Attitude and Spin Control Circuits

The amplifier and valve control circuit for the attitude system is shown in Fig. 4-19. It is a very straight forward, conventional circuit, consisting of the sun sensor, a one-stage amplifier, and a one-shot pulse generator. The amplifier is biased to cut-off and conducts only when a pulse is received from the sun sensor. The abrupt change in amplifier output then triggers the one-shot, which forms a 0.1 sec pulse. The pulse is amplified by transistor power amplifier which operates the valve solenoid. The steady drain of the circuit, when no pulses are occurring will be 5 or 10 ma.

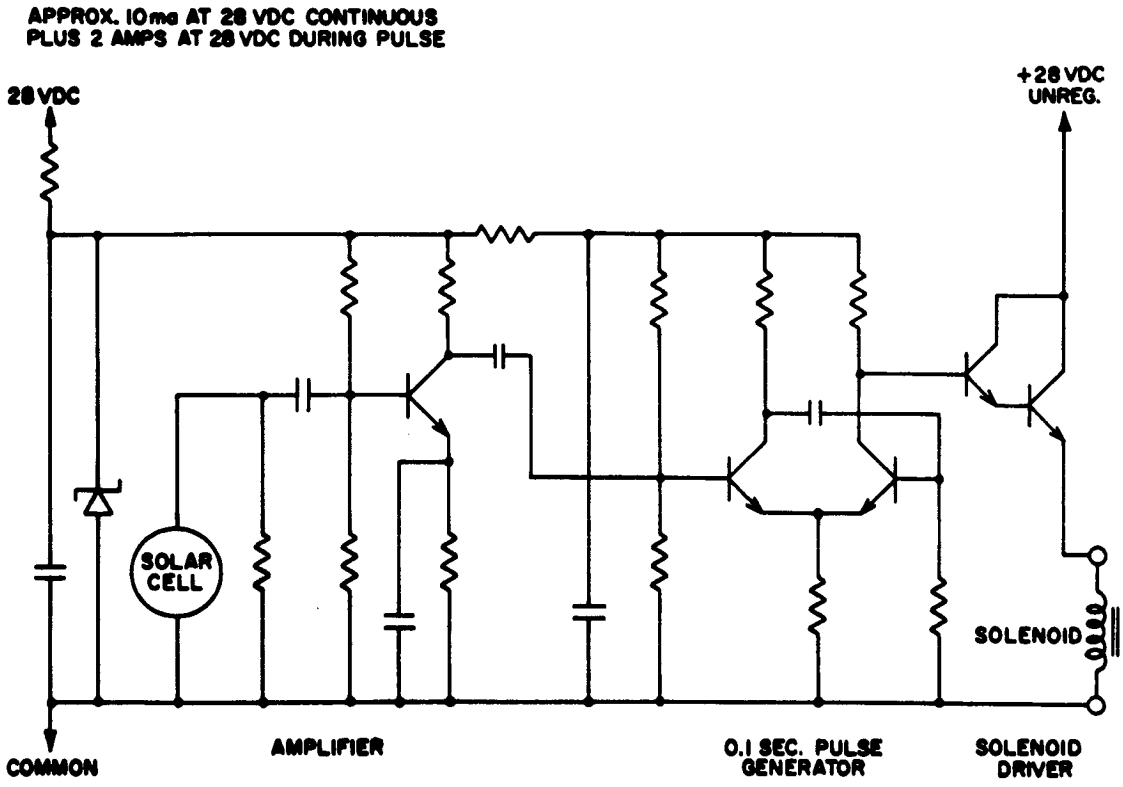

FIG. 4-19 SCHEMATIC OF ATTITUDE CORRECTION ELECTRONICS

The spin control system will require no amplifiers and no standby current. The basic control element will be a centrifugal switch having an inner and an outer contact. If the spin is too high, the outer contact will close and operate the appropriate valve solenoid, either through a relay or a power transistor. Similarly, if the spin is too low, the inner contact will cause operation of the spin-up nozzle.

4.3.4.3 Nonspinning Satellite

Although the feasibility of spin stabilization has been demonstrated, it is worth while considering the possibility of stabilizing and orienting nonspinning bodies. The expected gains would be greater simplicity of control mechanisms (because of the simpler dynamics) and greater design freedom (owing to the removal of restrictions on the moments of inertia).

In the absence of spin, a passive control system depending on solar radiation pressure becomes an attractive possibility, although it will be shown that it is not feasible at low altitudes. Among the active systems gyros, reaction wheels, gas reaction systems, or electric propulsion can be used.

Gyros and reaction wheels will not be considered, since they must run continuously and would therefore consume a considerable amount of power, and would be subject to mechanical failure in a long mission. In addition, a reaction wheel system will eventually saturate and must therefore be supported by a gas system. Electric propulsion is also rejected because of its power demand and the likelihood of failure.

4.3.4.4 Gas Control Systems

Two basic types of control system have been considered: (1) proportional impulse and (2) constant impulse. Both systems include a two coordinate damper consisting of two free-floating wheels in a viscous fluid.

The proportional system will always seek a stable null, that is, the sun's image will be brought to rest on the optical axis of the control sensor. Functionally, this type of control is completely satisfactory, but it carries the penalty of increased mechanical and electrical complexity, and therefore of diminished reliability.

The single impulse system can correct the vehicle attitude with no more than two successive opposing impulses, but unfortunately, only if the vehicle never acquires any angular momentum other than that generated by the control system. Thus a very slow drift would be corrected, but an impulse caused by a meteoroid would not, and the vehicle would continue to rotate indefinitely. It is doubtful that the system could even acquire the sun to begin with, since an initial angular momentum would be an unavoidable consequence of the search motion.

In view of the added complexity of a proportional system, and the short comings of a constant impulse system, it appears that gas control is not favorable for a nonspinning vehicle intended for a long mission.

4.3.4.5 Radiation Pressure Orientation

If the vehicle were provided with a light, shiny tail-fin and if the perturbing torques could be sufficiently reduced, solar radiation pressure would keep it pointed at the sun. The minimum altitude at which such a control system can work is set by the ratio of direct solar radiation pressure to the pressure of the sunlight reflected from the earth. Assuming that the earth's surface is uniformly bright, with an Albedo of 0.35, this altitude is around 5000 km for a pressure ratio of 10:1. Because of this minimum altitude limitation, a radiation-oriented satellite is not practical for the present program and will not be considered further.

4.3.5 Orientation Control Analysis

4.3.5.1 Orientation Control Coordinate System

Two coordinate systems are needed to define the behaviour of the satellite under the influence of applied torques; body-fixed and inertial. The coordinate frames are defined in Figs. 4-20 and 4-21. The vector $\vec{\omega}$ is the instantaneous angular velocity, which in general is not constant in either system, although scalar ω will be constant if there are no torques.

4.3.5.2 Motion of $\vec{\omega}$ in Body-Fixed Coordinates

The principle moments of inertia of the satellite are: A and B normal to the axis of figure; and C along the axis of figure. Also, the satellite is dynamically cylindrical, so that A = B. It is then possible to solve Euler's equations for an impulsive torque applied about a transverse axis. The solution can be extended to any number of impulses occurring at arbitrary intervals. The result is that the trace of the tip of the $\vec{\omega}$ vector on the XY plane (Fig. 4-20) is a series of circular arcs as shown in Fig. 4-22. Whenever the torque is acting, the path will be a circular arc centered on the point $(0, \frac{L}{AP})$, where L is the amplitude of the torque, and p is equal to $\frac{C-A}{A}\omega_z$. The parameter ω_z is the Z-component of $\vec{\omega}$. It is a constant of the motion, independent of applied torques. When the torque is zero, the path is a circular arc centered at the origin. The figure is drawn for the case $C > A$, ω_z positive. All arcs are traversed in the same direction, counterclockwise, and at the same angular rate, P.

4.3.5.3 Damping of Eulerian Motion

Each time a control torque is applied to the satellite the vector $\vec{\omega}$ will be shifted to a new conical locus about the Z-axis. In general, one must expect that $\vec{\omega}$ will drift farther from Z with repeated torquing, so that some means of damping must be provided to remove the components ω_x and ω_y from $\vec{\omega}$. It is important to note that,

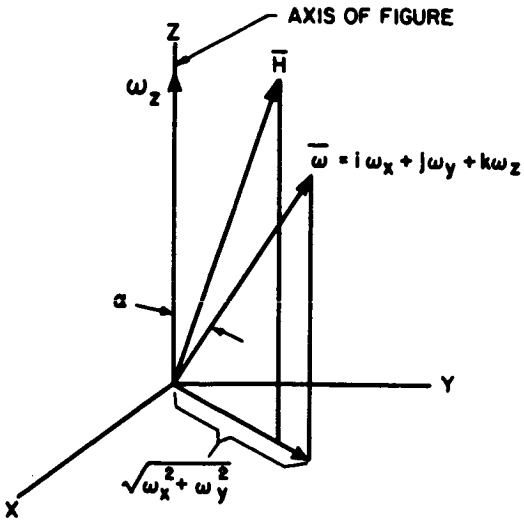

FIG. 4-20

BODY-FIXED COORDINATE SYSTEM

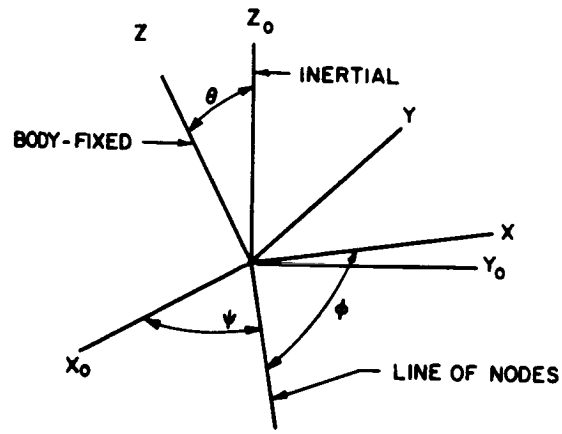

FIG. 4-21

RELATION OF BODY-FIXED TO INERTIAL SYSTEM

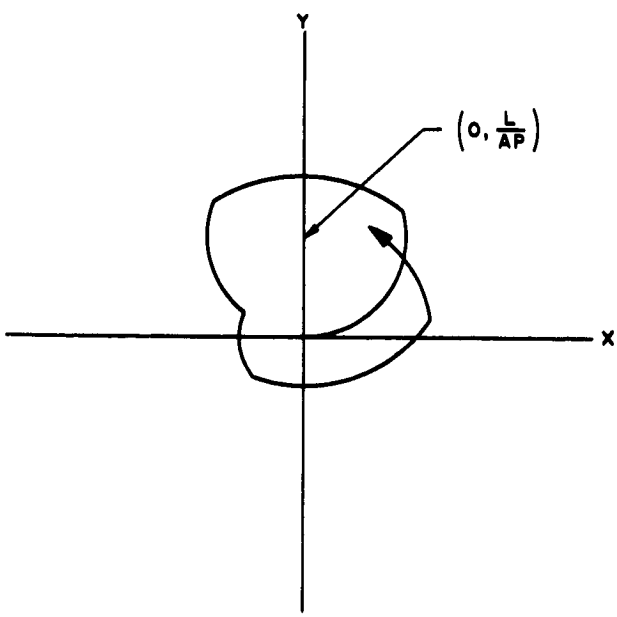

FIG. 4-22

PATH OF $\bar{\omega}$ IN BODY-FIXED COORDINATES

in a rigid body, there is no natural tendency for this to occur; once the conical, or precessional motion of $\vec{\omega}$ is excited, it will persist indefinitely in a torque-free body.

By considering the energy and angular momentum of the body it is possible to demonstrate that if $C > A$ the effect of a damper is to drive $\vec{\omega}$ to coincidence with Z, whereas if $C < A$, the effect is reversed, so that eventually all of the angular velocity will be about a line in the xy plane and none about the axis of figure (Z-axis). It is thus imperative that C be greater than A.

Another consequence of damping is that a part of the energy extracted from the precession is transferred to rotation about Z, the balance being dissipated as heat. The angular velocity of the satellite will therefore slowly increase under repeated torquing and damping. Opposed to this effect is the spin drag due to the forces discussed in Section 4.3.2.

The principle of the damping system is illustrated in Fig. 4-23. The tubes conform to a circular arc centered at the center of mass, and contain loose-fitting balls and some viscous fluid. The balls will tend to lie on a line perpendicular to $\bar{\omega}$, so that as $\bar{\omega}$ precesses about z they will move back and forth along the tubes against the fluid resistance. The motion will cease only when $\alpha = 0$, hence the Eulerian motion is selectively damped out.

If R is the resistance (force/velocity) and m the mass of one ball, the damping will be a maximum when $R/m = \frac{C}{A}\,\frac{2 - C/A}{C/A - 1}\,\omega_z$, where C and A are the polar and transverse moments of inertia, respectively. The time constant, T, can then be shown to be

$$T = \frac{4A\,(2-C/A)}{n\,m\,r^2\,\omega_z}$$

where n is the number of dampers. It appears that T can be made arbitrarily small by making nm very large, but there is a limit imposed by

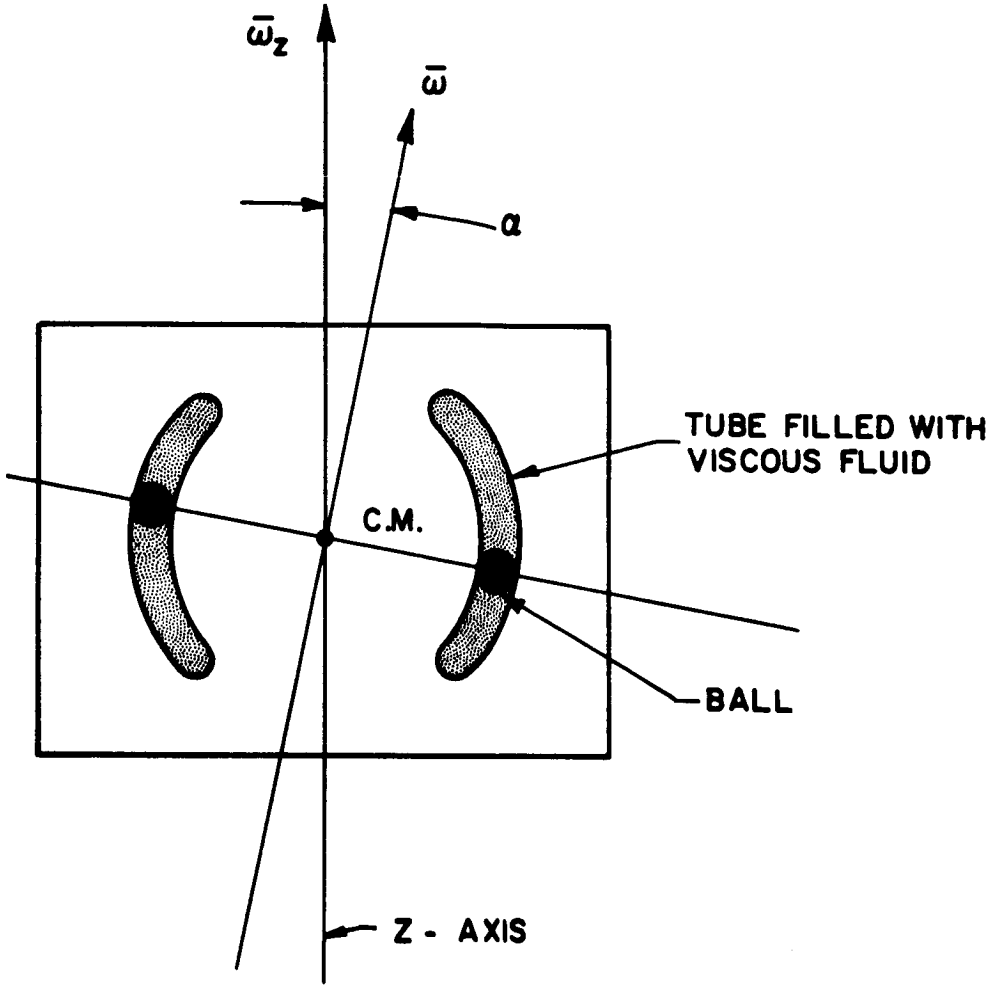

FIG. 4-23 DAMPERS

the necessity for preserving the symmetry of the body. As the balls move along the tubes they will introduce cross products of inertia proportional to αnm, which, if allowed to become too large, will disturb the motion. Assuming that α does not exceed 0.1 radian, four 50 gm balls would create a cross product less than 0.1 percent of the polar moment in inertia, which would be tolerable.

Taking $C/A = 3/2$, $C = 2 \times 10^7$, $r = 30$, $m = 50$, $n = 4$, and $\omega_z = 1$, the time constant is 148 seconds. R can be adjusted by varying the fluid viscosity and the clearance between the tube and the ball.

4.3.5.4 Motion in Inertial Coordinates

The attitude motion of the satellite in inertial coordinates is described in terms of the coordinate system shown in Fig. 4-24. The coordinates $(x\ y\ z)_o$ are the inertial, and x y z the body-fixed axes. Since the orientation torque will be small, δ and ψ will be also, and Euler's equations can be solved in closed form.

Initially, let z lie along z_o and x along x_o, so that $\psi = \delta = 0$. Also, let $\bar{\omega}$ coincide with z (no precession). The application of a unit function torque L along the x axis, will, if maintained indefinitely, produce the motion of z shown in solid line in Fig. 4-25. The torque will also induce precession so that the angular momentum vector, $\bar{H}$, will not follow z, but will describe the dotted path. The curves are drawn for $C/A = 3/2$ and $\omega_z = 1$ (where C is the moment of inertia about the spin axis, A the moment normal to the spin axis, and ω_z is the Z-component of the instantaneous angular velocity). The numbered points are seconds from $t = 0$. The numbers along the coordinate axes are relative values only, the actual values of δ and ψ being only a few tenths of a degree at most. Figure 4-26 is an enlargement of the region near the origin of Fig. 4-25. Up to about 0.2 second, the effect of the torque is, practically speaking, to shift $\bar{H}$ to the right and z vertically downward. If the torque is then removed, $\bar{H}$ must remain fixed

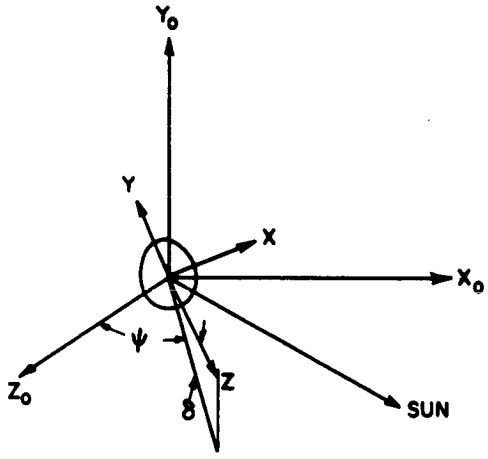

FIG. 4-24 COORDINATE SYSTEM

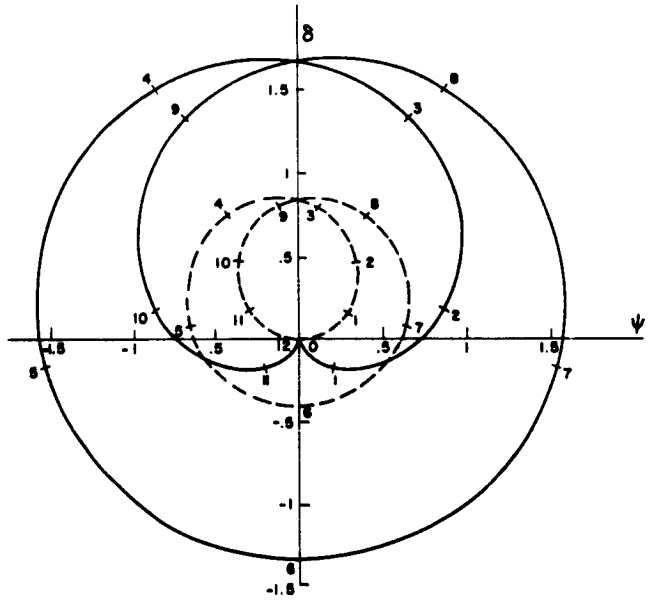

FIG. 4-25

MOTION OF Z AND H IN INERTIAL COORDINATES

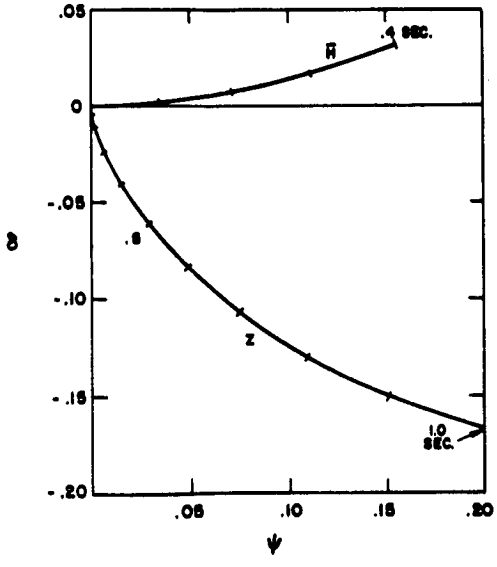

FIG. 4-26

INITIAL MOTION OF Z AND H

and z will move around it in a circular path, with angular velocity $\omega_p = \frac{C}{A}\omega_z$, as shown in Fig. 4-27. If no further torque impulses occur, z will spiral in until it coincides with H.

The solar image detector is placed along the negative x axis of the body, and therefore at t = 0 it also lies along $-x_o$. Let the sun lie in the $x_o z_o$ plane (Fig. 4-24). The sun's image will therefore fall on the detector, actuating the nozzles and applying a torque impulse about x. $\bar{H}$ will therefore shift toward the sun and z will circle around it as in Fig. 4-27. When the body has turned once about its own axis (not one turn of z about $\bar{H}$) the detector will again lie in the $-x_o$ direction, and another impulse will occur. The z axis will then be at some point P on the circle, determined by the ratio C/A. Since, in the small-angle approximation the differential equations are linear, the successive solutions can be added to obtain the motion after n impulses. A typical path for the case of zero damping is shown in Fig. 4-28. Only the net motion of z is shown by the arcs; actually z will make one turn around $\bar{H}$ plus the segment shown. $\bar{H}$ moves toward the sun in equal increments, z swinging about it at various radii.

Since high pointing accuracy is not required, the detector will have a central dead zone, within which the sun's image will cause no pulses. Points such as P (Fig. 4-27) will therefore eventually fall within the dead zone, so that finally the only situation in which a pulse can occur will be one in which z lies to the left of $\bar{H}$, on the x_o-axis, and the detector is in the $-x_o$ direction. The motion thereafter is shown in Fig. 4-29, in which all pulses occur at P, just outside the dead zone. $\bar{H}$ continues to move toward the sun, and even beyond, while z gyrates at ever-increasing angles from $\bar{H}$. The motion therefore becomes inherently unstable. When damping is included, however, stability is restored. The motion of Fig. 4-30 then occurs. After every impulse, z begins spiralling in toward $\bar{H}$, so the point P of Fig. 4-29 is no longer fixed, but moves into the dead zone. No further impulses will then occur and z will spiral in until it coincides with $\bar{H}$.

FIG. 4-27

PRECESSION OF Z-AXIS FOLLOWING IMPULSE

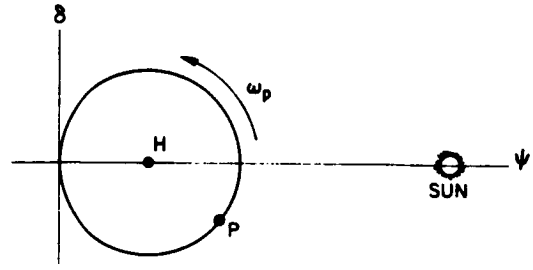

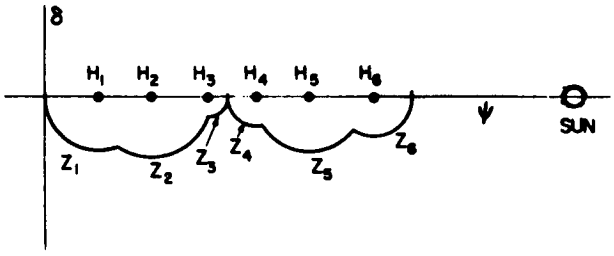

FIG. 4-28

MOTION OF Z AND H WITH REPEATED TORQUING

FIG. 4-29 MOTION IN DEAD ZONE

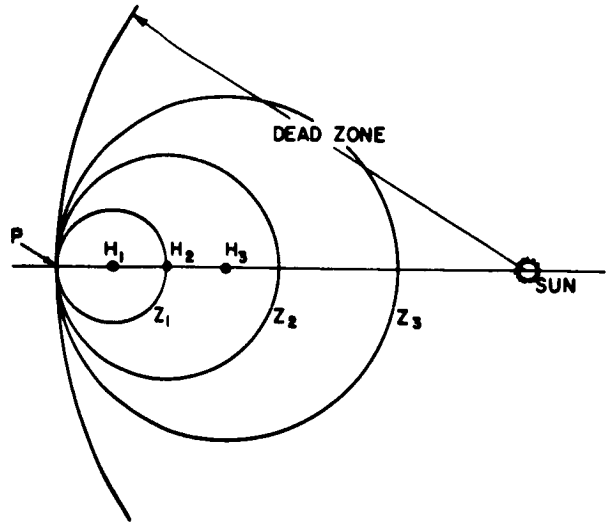

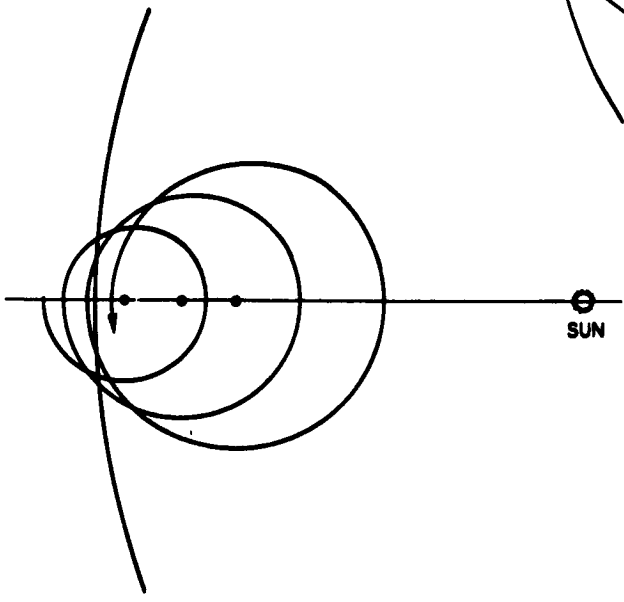

FIG. 4-30

EFFECT OF DAMPING ON MOTION IN DEAD ZONE

4.3.6 Propellant Requirement

The total angular impulse for a one year satellite has been given in Section 4.3.3 as 42.6×10^7 d cm sec. Allowing for errors, call it 50×10^7 d cm sec.

Knowing the lever arm of the nozzles, the angular impulse can be converted to a linear impulse, which, divided by the specific impulse of the propellant gives the propellant mass. Table 4-5 gives the mass and volume requirements for several different gases, assuming a storage pressure of 3000 psi, a reservoir temperature of $300^{\circ}K$, and a nozzle lever arm of 30 cm.

Since the required masses are so modest, it will be best to choose the gas requiring the least storage volume, i.e., O_2. However, oxygen is chemically active, so the next best, N_2, is the logical choice.

These estimates do not include any allowance for inefficiencies in the valves or nozzles, nor for leakage.

4.3.7 Propellant System

A study of the nozzle design has shown that it will not be practical to apply the full 3000 psi storage pressure directly to the nozzles, because the resulting mass flow would develop far too much thrust for any reasonable throat diameter. It will be necessary to have an auxiliary low pressure reservoir connected to the primary storage tank through a pressure reducer. Since the rate of gas consumption is very low, the transfer from the high to the low pressure will be isothermal and there will be no loss of specific impulse.

For a reduced pressure of 30 psi, an impulse duration of 0.1 second, and a displacement of $\bar{H}$ of 0.1 degree per impulse, the required throat diameter of a single, unbalanced nozzle will be 0.026 inch. If a balanced pair is used the diameter will be 0.018 inch. Although these diameters are small by rocket standards, shaping the nozzles presents no really difficult problems for an expert instrument maker.

The nozzle expansion ratio is found from

$$\frac{A_t}{A_e} = K \frac{T_e}{T_o}^{\frac{1}{\gamma-1}} \quad 1 - \frac{T_e}{T_o}$$

where: A_e = exhaust area

A_t = throat area

T_e = exhaust temperature

T_o = reservoir temperature

K = a function of γ

T_o is assumed to be 300°K, and ideally, T_e would be 0°, but N_2 is not an ideal gas and cannot be cooled to absolute zero without change of state. However, comparing published enthalpy data (Ref. 53) with calculated enthalpies, it appears that in an isentropic expansion from 30 psi, 300 to 60 degrees or even lower, the agreement is as close as the curves can be read. Using these temperatures, the expansion equation gives $A_e/A_t = 16$, or a diameter ratio of 4. The single nozzle exit would thus be 0.112 inch and the double nozzle exit would be 0.072 inch.

The original estimate of propellant mass was obtained using the approximation $T_e = 0$. Using the more realistic value 60°K, the mass for one year is raised from 212 to 240 gms. The mass of propellant consumed per impulse will be about 0.02 gms, so in one year there will be about 12,000 impulses, or an average of one every 42 minutes. Actually, the impulses will occur in short groups at a rate of one every six seconds, separated by long intervals of inactivity.

4.3.8 Balanced vs Unbalanced Torquing

A critical study of the concept of balanced torquing reveals that its merits are largely academic. A single nozzle would require only one valve and less piping, thus giving a more reliable system.

A single force acting on a free body at a point other than the center of mass is equivalent to the same force acting at the center of mass plus a couple $\bar{r} \times \bar{F}$. $\bar{F}$ is the vector force and $\bar{r}$ is the vector radius from the center of mass to the point of application of $\bar{F}$. The body will thus experience a torque and a translational acceleration $\bar{F}/m$. It is this acceleration that will produce orbital perturbation in unbalanced systems.

The semi-major axis of any elliptical orbit is given by

$$a = \frac{GM}{-W} = \frac{k}{-W} \tag{4-25}$$

where:

G = gravitational constant

M = mass of primary

W = total energy of satellite/gm

Also, $W = 1/2\ v^2 - \frac{k}{r}$ which is intrinsically negative for a closed orbit. If the body receives an impulse, r will not change and all of the energy change will appear in -v. Differentiating Eq. 4-25,

$$\frac{da}{a} = \frac{dW}{-W} = \frac{vdv}{-W} \tag{4-26}$$

Assume that the orbit is initially circular, then

$$W = -\frac{1}{2}\frac{k}{r} = -\frac{1}{2}v^2$$

Equation 4-26 is then

$$\frac{da}{a} = \frac{2dv}{v} \tag{4-27}$$

The greatest change in v will occur when the impulse, J, is either parallel or antiparallel to v. In this case dv is J/m and

$$\frac{da}{a} = \frac{2J}{mv} \tag{4-28}$$

As an extreme, but actually impossible case, assume that the whole propellant supply is expelled in one brief impulse. The stored angular impulse has been estimated as 50×10^7 d cm sec for a nozzle radius of 30 cm. The linear impulse is thus 1.6×10^7 d sec. Taking $m = 4 \times 10^4$ gm and $v = 7.5 \times 10^5$ cm/sec, Eq. 4-28 gives $da/a = 10.6 \times 10^{-4}$. Therefore if the term a is initially 6970 km (600 km altitude), it will increase by 7.4 km. If the impulse increases v, the new orbit will have a perigee of 6970 km and an apogee of 6984.8 km, whereas if v is decreased, the new orbit's apogee will be 6970 km and the perigee will be 6955.2 km.

It is apparent that unbalanced operation will have no adverse practical effect, especially when it is remembered that the propellant is discharged in minute quantities, at random times and in random directions.

4.4 Satellite Power System Design

The basic design approach employs solar panels in conjunction with rechargeable secondary batteries. Three voltages will be provided: (1) +28 regulated at 2 amperes, (2) +28 volts unregulated, and (3) +13 volts regulated. The unregulated 28 volts is supplied directly from the battery and will be used to provide power for solenoids. The output of the battery will be conditioned with a series regulator to provide up to 2 amperes of current. This line will provide power for the telemetry system, and the experiments carried on the vehicle. The regulated 13 volts is tapped from the regulated 28 volt line and is used for the telemetry system. The battery will be recharged by a constant current series regulator having an automatic shut-off when the battery is charged to the recommended potential. The output of the solar panel is clamped by Zener diodes to prevent excess voltages from being developed when the vehicle is emerging from the earth's shadow and the panel is still cold.

4.4.1 Selection of Storage Battery Type

Of paramount importance in the selection of the type of battery to be used is its cycle life and operating life. For a 1 - 2 year mission, not only must the battery be operational for this period, but it must be able to withstand thousands of charge-discharge cycles as well. A comparison of 30 types of storage cells made by 18 different manufacturers indicates that (for long cycle life and operational life) only three types qualify. These are: lead-acid, nickel-cadmium, and silver-cadmium cells. Of these, silver cadmium offers the highest power density. Silver-zinc cells have an even higher power density but a very low cycle life. Yardney Electric, a leading manufacturer of silver-cadmium cells, quotes that their silcad cells have undergone over 10,000 cycles of charge and discharge in still-continuing tests. These discharges are made to a depth of 35 percent of total capacity. Yardney further quotes an operating life of 3 years. Thus, for this application, silver-cadmium cells are well suited.

4.4.2 Probable Orbit and Solar Panel Power Output

For analysis purposes two orbits are considered:

1. A circular orbit of 625 n. mi. altitude.
2. An elliptical orbit with a perigee of 300 n. mi. and an apogee of 3,000 n. mi.

The period of the circular orbit is 1.81 hours with a maximum time in the earth's shadow of 0.575 hours. The period of the elliptical orbit is 2.53 hours with a maximum eclipsed time of 0.775 hours. The ratio of the maximum time spent in the earth's shadow to the orbital period is very nearly the same for both orbits. Using n on p solar cells, little or no degradation can be expected for the circular orbit while, for 10 ohm-cm cells with 60-mil quartz windows, the elliptical orbit will result in a reduction of efficiency during the two year mission to about 78 percent. The initial efficiency of this type of cell is about 9.5 percent. Thus, the efficiency at the end of the two year mission can be expected to drop to about 7.4 percent.

The solar irradiance in free space is about 140 mw/cm^2. The power available from the solar panel at the end of two years will be about 10.4 m $watts/cm^2$ of array. There will be approximately 2 square feet of exposed surface available. Thus, the available solar panel power will be:

$$(2.54)^2 \times 144 \times 2 \times 10.4 = 19.3 \text{ watts}$$

The time in the sunlight per day for the elliptical orbit is 16.6 hours. Therefore, the solar panels can provide:

$$16.6 \times 19.3 = 320 \text{ watt-hours of energy}$$

4.4.3 The +13-Volt Regulator

The telemetry system requires 13 v at 8 ma during standby and a momentary current of 100 ma at the beginning of an interrogation command. The regulation required is about ± 2 v.

Because of the relatively low current level under steady state operation and the rather loose regulation requirements,

the 13 v regulation will employ a simple Zener diode. The diode will be shunted by a capacitor to provide for the 100 ma pulse. The regulator will be fed from the output of the 28-volt regulator and will draw an average current of about 30 ma.

4.4.4 The +28-Volt Regulator

This consists of a series control transistor capable of passing a 2 a current. A Zener diode reference and a differential feedback amplifier will be used to control the series transistor. The 28-volt regulator is driven from the battery and will draw about 100 ma plus 110 percent of the current it is delivering to the various loads. The regulator will be capable of handling input voltages from 30 to 45 volts and output currents from 0 to 2 a. The output voltage of the regulator will be held at +28 ± 0.2 v.

4.4.5 The Storage Battery and Constant Current Charger

The battery to be used will be made of 28 silver-cadmium cells in series. These cells will provide about 1.1 volts after a 35 percent discharge and should be recharged to 1.5 volts for long cycle life. The battery voltage will thus vary from 30.8 volts to 42 volts.

The battery will be charged from the solar panel through a constant current circuit. This will deliver a constant current until the back voltage of the battery is 3 v below the input voltage and then the current falls off rapidly. In this manner, the battery is prevented from overcharging. When the battery is charged to the recommended level of 1.5 volts per cell, the back emf will be 42 v. The input to the constant current charging circuit is 45 v nominally. That is, the output of the solar panel is 45 volts under steady state conditions. The solar panel is clamped with Zener diodes at 50 v. The output of the panel when it first emerges from the earth's shadow is thus held to 50 v. Since the nominal output of the solar panel is 19.3 watts, the current available at 45 v will be

430 ma for 16.6 hours per day. The constant current circuitry will consume about 30 ma of this, leaving about 400 ma to charge the battery. If the battery is discharged by 35 percent or less the energy required to recharge is approximately 110 percent of the energy removed. The energy that can be supplied by the solar panel and constant current charger circuit is:

$$0.4 \times 16.6 = 6.6 \text{ amp-hours per day}$$

Thus, the energy that can be removed from the battery is:

$$\frac{6.6}{1.1} = 6 \text{ amp-hours per day}$$

The energy required by solenoids, which are driven directly from the battery, is about 2.5 ma-hours per day. Thus, while these solenoids require heavy currents when energized, their duty cycle is so low that their energy requirements are almost negligible compared to the demands of the overall system.

The current required from the 28-volt regulator is about 95 ma continuously and 850 ma during operation of the experiment. Referred to the input of the regulator the current levels are 205 ma during standby and 1.03 amps maximum during transmissions. The continuous energy required per day is therefore:

$$205 \times 24 = 4920 \text{ ma hours} = 4.92 \text{ amp-hours}$$

This leaves approximately 1.1 amp-hours to run the experiment. The additional current required during transmission is:

$$1.03 - 0.205 = 825 \text{ ma}$$

Thus, the total transmission time available per day is

$$\frac{1.1}{0.825} = 1.33 \text{ hours}$$

If the time required to extract data is taken as 30 sec, roughly 160 interrogations can be made per day.

If full use is made of the available 6 amp-hours per day and the period of the orbit is taken as 2.5 hours, the average battery drain for the mission is:

$$\frac{2.5}{24} \times 6 = 0.625 \text{ amp-hours per cycle}$$

It is expected that the discharge for some orbits will be greater than for others. As a safety factor the peak energy drain per orbit will be taken as 1.5 amp-hours. To ensure that the battery is not discharged more than 35 percent, the ampere-hour capacity rating will be made 4.5 amp-hours.

4.4.6 Power Supply Housekeeping

Temperature sensors will be mounted to the battery case and to the solar panel. The output of these sensors will be used to provide voltages to telemetry. The solar panel output voltage, the battery output voltage, the 28-volt regulator output, and the 13-volt regulator output voltage will each be divided down to provide four additional telemetry signals. Thus, six telemetry channels will be utilized to provide power system housekeeping measurements.

4.4.7 Summary

Figure 4-31 shows a block diagram of the power system. The system is designed to operate for a two-year mission in the radiation environment of the Van Allen Belt. The system will provide power continuously throughout the mission. Three voltage levels are provided, 28 volts unregulated, 28 volts regulated to less than ± 1 percent from zero to 2 a, and 13 v ± 1 v at low current levels. Power system temperature and voltage levels are monitored for housekeeping purposes. The system is designed to adequately provide the necessary voltage and current levels for the preferred experiment.

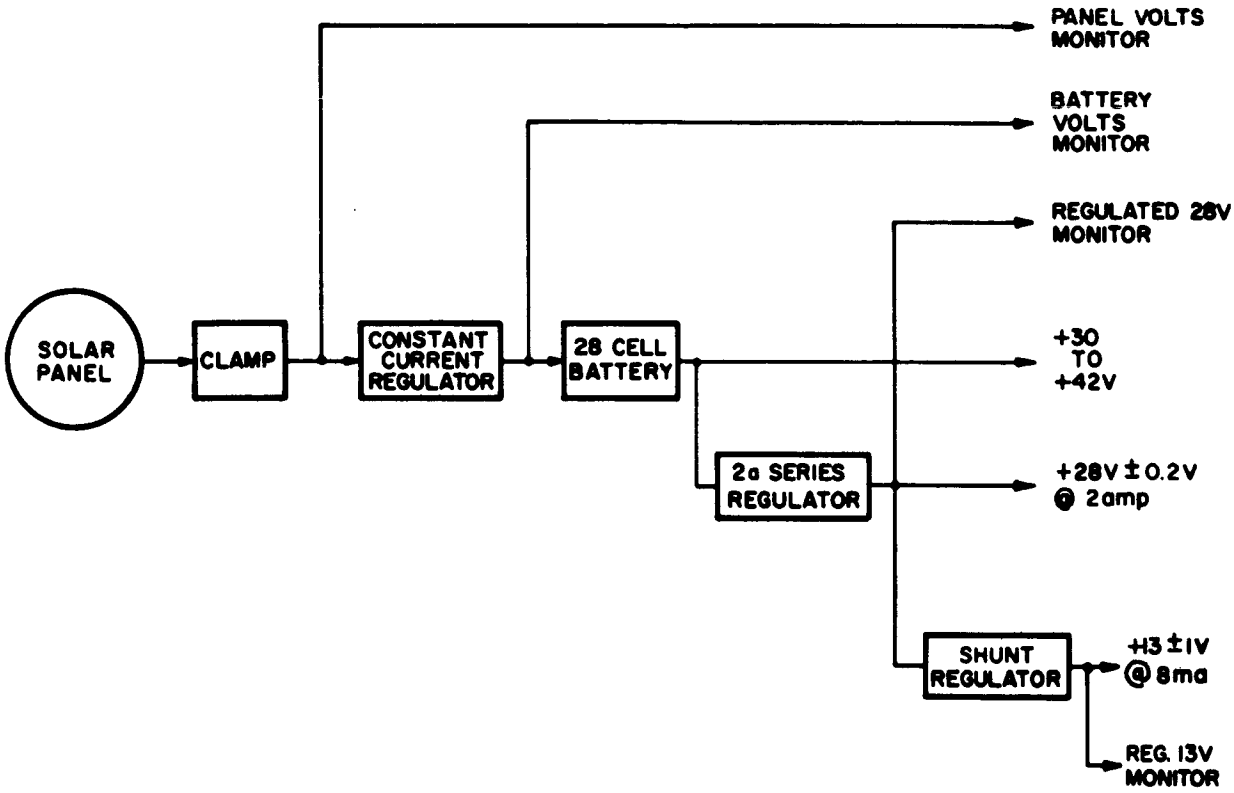

FIG. 4-31 BLOCK DIAGRAM, POWER SUBSYSTEM

4.5 Telemetry and Command System

The paramount constraints affecting the configurations and design of the preferred experiment telemetry and command system are data requirements, accuracy of measurements required, orbit selected, and capabilities of the ground support facilities used. Once these constraints are imposed by the operational aspects of the experiment further limitations are imposed by such factors as flight subsystems interrelationships, weight, power requirements, etc., which result in many compromises in the design of each of the subsystems. The items are discussed in further detail in this section.

4.5.1 Functions of Telemetry and Command Subsystem

As the subtask nomenclature indicates,this subsystem provides the telemetry and command functions of the flight system. These two functions are subdivided as follows.

4.5.1.1 Telemetering Function

This consists of the multiplexing, processing, and transforming the several instrumentation and transducer signals into a form suitable for transmission to the ground receiving station.

4.5.1.2 Command Function

Under this function are two distinct modes of operation to be controlled. First is the experiment mode whereby all subsystems directly involved in the reflectivity and space environmental measurements are energized by a command signal from the ground receiving station. The satellite requires automatic timing to turn off (or deenergize) the system at the completion of the experiment measurement cycle. Provision for turning off the system by command from the ground is also necessary in event the automatic timing device and malfunctions.

The remaining mode of operation is the tracking mode for determination of the satellite's orbit. Here it is necessary to energize only the TM transmitter for one or two orbits and provide for turn-off by command from a ground station.

4.5.1.3 Relation to Other Subsystems

Although the other subsystems of the satellite will not affect the basic functioning of either the TM or command subsystems they will affect the design and capabilities. For instance, the capabilities of the satellite power system determines the power at which the transmitter can operate and also affect, to some extent, the multiplixing methods chosen.

4.5.2 Constraints on Experiment Telemetry

Below are listed those factors and items affecting the requirements and design of the telemetry subsystem.

4.5.2.1 Satellite Instrumentation

Space Measurements

Six channels for space environmental measurements are required. The signals are slowly varying, low level (0-20 mv) dc voltages.

Reflectivity Specimen Temperatures

Twenty-five channels are required for this data at slowly varying, high level dc voltages.

Housekeeping Measurements

Seven channels of low level dc voltages and two high level temperature measurements.

Reflectometer

The nature of this instrument is such that six data channels are required for the measurements on each sample. The form of these signals is shown in Fig. 4-32. This signal results as the reflectometer head passes over each sample. Since the head rotates at two-thirds rps over 30 positions the rate of this signal is 20 pulses per second. The full scale variation between the dark level and 100 percent reflectance reference level will be 20 mv. The flat top portion of the pulse occurs while the reflectometer beam is fully on each specimen. Due to the sample size, beam size, and rotation rate this period is approximately 20 ms. Two reflectivity readings will be taken on each specimen during this period.

Accuracies Required

The accuracies required for the space environmental measurements and housekeeping measurements are very lax. A maximum error of ± 5% is adequate. The voltages resulting from the reflectivity specimen temperature transducers must be measured to an accuracy of ± ½%.

4.5.2.2 Ground Station Capabilities

As the NASA-Goddard minitrack network services are provided as part of the Scout system it will be used for tracking and data acquisition purposes. The telemetry and command system design is compatible with the minitrack system. The pertinent constraining characteristics and capabilities of this ground receiving network are listed and discussed below.

Receiving System Capability

The telemetry and tracking operating frequency is in the 136 to 137 Mc band. The receiving system noise figure is 3 db. Use will be made of those receiving stations having the 85-foot paraboloid antennas above an altitude range of 900 nautical miles to conserve transmitter power. Below 900 miles 40-foot paraboloid antennas may be used. Bandwidth capabilities are 10, 30, 100, 300 Kc and 1 Mc. Demodulation capabilities are for amplitude frequency, and phase modulation.

Tracking Capabilities

Interferometric at 136 to 137 Mc at an accuracy of 150 to 200 seconds of arc.

Data Processing Capability

Non-return-to-zero pulse code modulation (PCM) capabilities to 64,000 bits/sec; 7 channel magnetic tape recording of frequency translated, undemodulated and demodulated telemetry signal; processing of recorded FM/PDM/AM and PCM data available at Goddard Space Flight Center.

Command Capabilities

Tunable 108 to 152 Mc 122 and 148 Mc used. Amplitude modulation at 200 watts. Antenna gain = 12 db.

4.5.2.3 Orbit Selected

Eliptical with 300 nautical mile altitude at perigee and 4,500 - 5,500 nautical miles at apogee.

4.5.2.4 Flight Power System Capabilities

From the orbit selected and area available for solar cells under worst conditions of operation a total of 112 watt hours of energy are available per day at 28 volts.

4.5.3 Design of Telemetry

4.5.3.1 Multiplexing and Data Processing Technique

The multiplixing method used will depend, to a great extent upon the data accuracy required and the transmission bandwidth available. The TM system accuracy requirements will be determined by the more important data requirements. These are the reflectivity measurements and the reflectivity sample temperature measurements. An error of ± ½% contributed by the TM system will satisfy the reflectivity and temperature measurement requirements. This required minimum error of ± ½% is well below the capabilities of any type of FM/FM system. To achieve this kind of accuracy and achieve the maximum transmission of information using the minimum bandwidth (also minimum transmitter power) a pulse code modulation (PCM) system will be used.

A PCM telemetry system will require time multiplexing of the data channels. Due to the sequential reflectivity measurements, subcommutation of much of the remaining data will reduce much useless repetition of these measurements. Many possible combinations of submultiplexers using standard multiplexers are shown in Fig. 4-33. The weight and power requirements for these combinations using multiplexers now available are shown in Table 4-6.

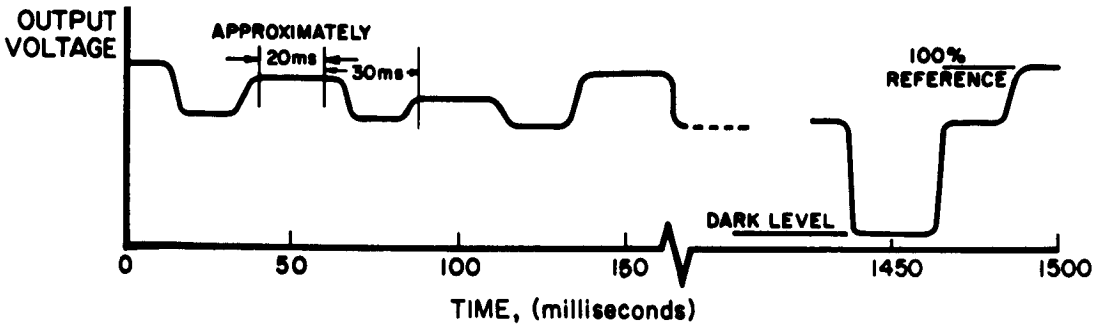

FIG. 4-32 REFLECTOMETER DETECTOR OUTPUT WAVE FORM

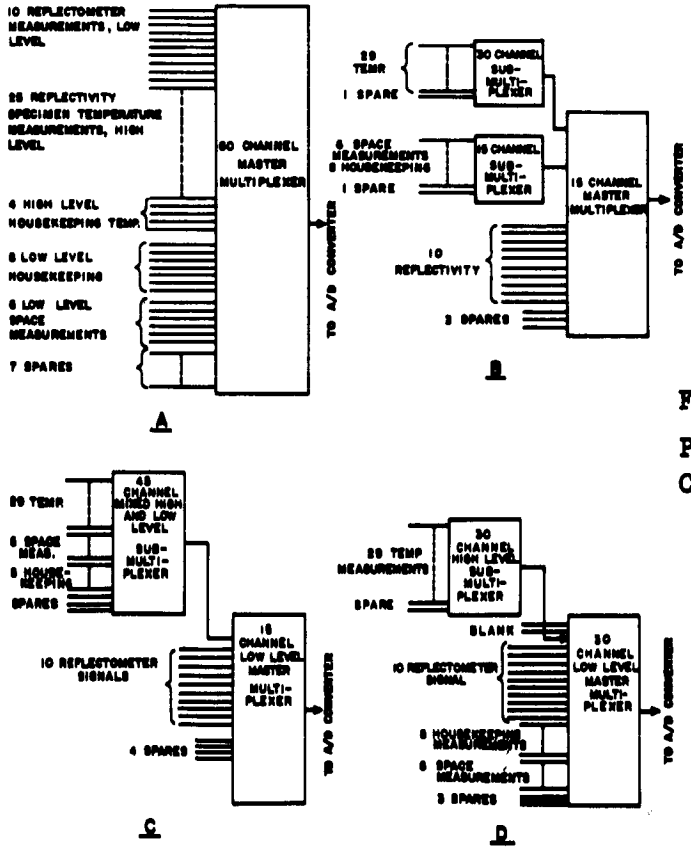

FIG. 4-33

POSSIBLE SUBCOMMUTATOR COMBINATIONS

TABLE 4-6

TYPICAL WEIGHT AND POWER REQUIRED OF VARIOUS SUBMULTIPLEXER COMBINATIONS

Case	A	B	C	D
Power watts	4.2	5.9	5.1	5.0
Weight lbs.	3.5	5.4	4.5	4.0

Case A, (Table 4-6) appears most desirable as it requires minimum power and weight. The required sampling rate shows that the use of this combination of multiplexers is impossible while Cases B and C do not send data over the entire measurement cycle and are, thereby, extremely inefficient.

The required sampling rate is established as follows: The 10 reflectometer detector signals must be sequentially sampled once during the 20 millisecond period during which the reflectometer beam is fully on the reflectivity sample. This fixes the sampling rate to a minimum of 10 samples/20 x 10^{-3} sec = 500 samples per second. With a period of 30 milliseconds before the next successive reflectivity specimen there is only sufficient time for fifteen more samples. This makes the use of Case A impossible as it has 50 remaining channels (including spares). In either Case B or Case C there are only five remaining channels to be sampled in this 30 millisecond period which has room for twenty samples. This would leave approximately 22 milliseconds during which measurements are not being made which is extremely inefficient.

Case D provides twenty channels to fill in this 30 millisecond period. By adjusting the sampling rate to 667 samples per second the twenty remaining samples of Case D can be sampled in this period. The required bit rate is the number of binary digits required per work (or sample) times the sampling rate.

In order to sample the reflectivity signals only while the beam is entirely on the specimen requires that the multiplexers be closely synchronized to the motion of the reflectometer optical head. This is easily provided by use of a microswitch and cam or a code wheel geared to the optical head. To further assure that all of the reflectometer measurements occur only while the beam is fully on the specimen, the sampling rate was increased slightly (to 667 samples/sec) to allow +10 to +15% variation in the angular speed of the optical head. Since the sampling rate is fixed by electronic control there need be no lower limit to the head speed.

In order to acheive an accuracy of $\pm \frac{1}{2}\%$, a PCM encoder (analog to digital converter) must be able to distinguish at least 200 levels of the full scale data voltage. The closest value to be acheived in a binary coding system is 256 levels requiring eight binary digits per measurement period. Allowing one synchronization and one parity bit (binary digit) per work (one measurement) gives a requirement of 10 bits per word. The required bit rate is then 10 x 667 = 6670 bits per second.

The resulting PCM format for this combination of multiplexers is shown in Fig. 4-34. From this format the digital programming requirements can be determined. From this diagram it can be seen that the reflectometer head sync pulse initiates the sampling and measurements sequence at the beginning of each reflectivity specimen measurement period (one frame on master multiplexer). To do this the reflectometer head sync pulse gates the free running 667 PPS clock signal to the multiplexing system. The multiplexers are then stepped in synchronism with this constant rate clock signal. A frame sync work and a sample number work (to identify the reflectivity sample being measured) are inserted into the serial binary signal prior to the measurement. At the completion of the measurements a 3335 pps square wave is inserted into the resulting serial PCM signal until the beginning of the next frame. This represents alternate ones and

zeros at the required bit rate. This provides an uninterrupted serial binary signal on which the receiving PCM equipment can synchronize. In a similar manner this same signal is inserted before sample # 1 to allow the ground equipment time to synchronize before the first measurements start.

Since all of the data signals (except temperature) are in the 20 millivolt range a low level electronic master multiplexer will be used. This requires amplification of the multiplexer PAM output signal to drive the analog to digital converter. The high level temperature measurements make a high level submultiplexer necessary. This will require attenuation of the submultiplexer output signal to meet the input requirements of the master multiplexer. A few spare channels are left on both multiplexers for any additional measurements.

A functional block diagram of the multiplexers, the analog to digital converter, signal amplifier and a detailed breakdown the digital programming unit is shown in Fig. 4-35. The digital programmer provides the necessary pulses to step an analog multiplexer and a submultiplexer and to start an analog to digital converter to convert the analog signals to digital form. Additionally, the digitized data signals must be combined with certain synchronization and identification digital words and the resulting composite digital information produced in serial form in order to be transmitted over a telemetry link to the ground. Some of the analog information being handled by this pulse code modulation system comes from a mechanically rotating reflectometer. This reflectometer will rotate above a number of samples mounted on the front surface of the satellite. Therefore, the first problem encountered in the system is that of synchronizing the PCM system with the rotation of the mechanical wheel. This is done by the block labelled "sync logic". Out of this block will come clock pulses required for the operation of the rest of the PCM control system, these pulses occur at the proper times to synchronize the system with the mechanical wheel.

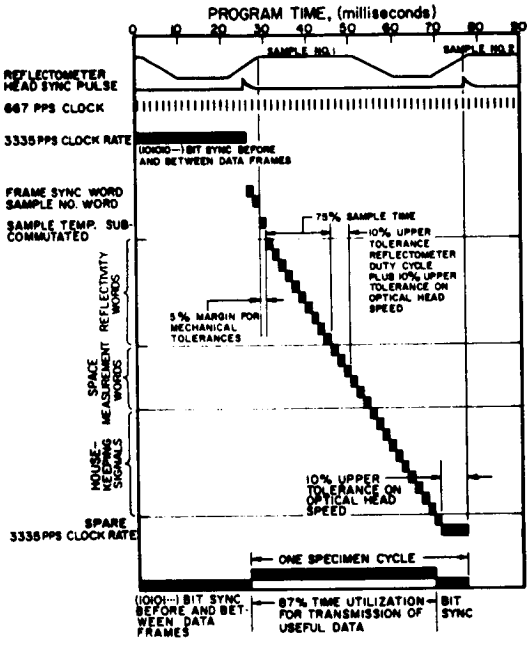

FIG. 4-34

PULSE CODE MODULATION DATA PROCESSING FORMAT

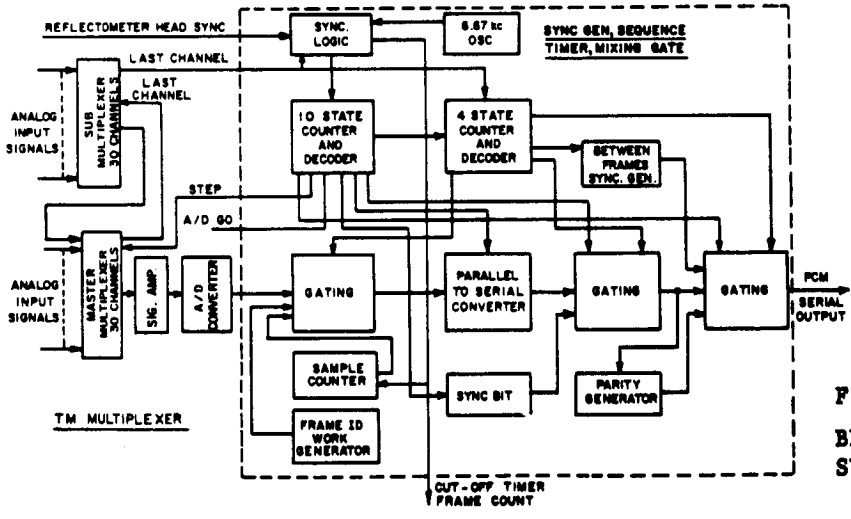

FIG. 4-35

BLOCK DIAGRAM OF TELEMETRY SYSTEM DATA PROCESSOR

The output of this sync logic is used, among other things, to step two counters. These consist of a 10 state counter which is stepped directly by the synchronized clock, and with the output of this counter being used to step a 4 state counter. The purpose of the 10 state counter is to count out the 10 bit-time increments which ultimately will be required for gating out the 10 serial bits required for telemetry. The 4 state counter being stepped by the 10 state counter will then be stepped at the rate that analog data words are being digitized. The purpose of this 4 state counter is to mark the first two word times in a data frame. It is necessary to mark these words in order that certain identification and synchronization information may be inserted at this time.

This counter will be in one state during the first word of a frame, a second state during a second word of a frame, and a third state during all the remaining words of the actual data-gathering frame. It will then be in its fourth state during the time between data frames.

An output from the 10 state counter is also used to step the master multiplexer and to give a start signal to the analog to digital converter. The multiplexer will in turn have an output signal indicating when it has reached its last channel. This signal is used to step the submultiplexer. The submultiplexer also will have an output signal indicating when it is on its last channel. The signal indicating the last channel position of the submultiplexer will then be used to indicate when a frame of data has been completed and when the system is entering into its "rest" time.

The output of the analog to digital converter is gated with the output of a sample counter which is used to indicate which sample within the revolution of the reflectometer head is currently being digitized and it is also gated with the output of a frame identification word generator. This gating is controlled by the output of the 4 state counter. The first state of this counter which indicates

the first word in a frame will be used to initiate the frame identification word; the second state indicates that the second word in the frame will be used to gate out the contents of the sample counter; and the third state indicates all the rest of the words in the frame will be used to gate out data from the analog to digital converter.

The output of this gate is in the parallel form and goes to a holding register which also functions as a parallel to serial converter to produce the serial data train required by telemetry. The output of this parallel to serial converter is gated along with a sync bit.

Pulses from the 10 state counter will gate 8 bits from the parallel to serial converter comprising the data words of the system and then will gate 1 sync bit after each 8 data bits. The output of the gate performing this operation goes two places. First, to a parity generator which will function to generate a parity bit on the 9 bits in each work comprising the data and the sync. The output of this parity generator is then combined in another gating unit. In this unit 9 bits comprising the data and sync bit will be gated from the previous gating circuitry and then the tenth bit will be gated from the parity generator. The output of this final gating unit will then go directly to the transmitter for transmission to ground.

This final stage of gating also has the additional function of gating a pattern of synchronization bits which are transmitted between frames of actual data. It will then gate out data during the frame comprising the 8 bits of digitized analog information, a sync bit, and a parity bit for each output word and then between frames will gate a fixed sync bit pattern.

4.5.3.2 Transmitter Requirements

For simplicity of the telemetry and command system, the same transmitter will be used for tracking and data transmission purposes. The minitrack tracking and telemetry frequency

band of 136 to 137 megacycles will be used. The required power will be determined by the PCM bit rate, ground receiving system sensitivity, and the maximum range over which it is desired to transmit. With these factors and the antenna gains and the antenna polarization factors and the antenna gains and the antenna polarization factor, the required equation

$$P_t = \frac{(4\pi R)^2 \; P_r \; (\text{Polarization factor}) \; (\text{Safety factors})}{\lambda^2 \; G_T \; G_R}$$

where

P_t = transmitted power in watts
R = range in feet
P_r = received power in watts
λ = wavelength in feet
G_R = receiving antenna gain

As per the IRIG Standards on PCM telemetry, the required receiver bandwidth is equal to 1-1/2 times the bit rate. This results in a bandwidth of 1.5 x 6670 ≅ 10,000 cycles per second. The receiving system sensitivity (P_R) is dependent upon the receiver noise figure (3 db), the ground antenna equivalent noise temperatures, and the signal to noise ratio required for satisfactory operation of the ground PCM data receiving equipment.

From the IRIG Standards on PCM a signal to noise ratio of 17 db will result in a bit error probability of about one bit in 10^7 bits. For example, if data were gathered at the rate of about one minute per day for the two year period, the total information gathered will be, at a data rate of 6670 bits per second.

I = information = No. of years x 365 x bit rate x 60
I = 2 x 365 x 6670 x 60 = 29.0×10^7 bits in two years.

This error rate, then, will result in about 29 bit errors for the entire program which is quite acceptable. Since the transmitting range will usually be much less than that (2000 nautical miles) to be used in the transmitter power computations, the signal to noise ratio will be considerably higher than 17 db. This will result in a lower average bit error rate.

The ground antenna equivalent noise temperature is determined from Fig. 4-36. This is a plot of antenna temperature as a function of frequency which is due mainly to cosmic background noise. As can be seen from this figure, there are two curves: one for cosmic noise in quiet parts of the sky, and one for cosmic noise from hot, or noisy, parts of the sky. Since the noisy parts of the sky are due usually to a relatively few point sources and the Galactic plane of the Milky Way the probability of transmission taking place in one of these areas of the sky is remote. In the event this does occur, the measurement can be repeated in a short time when the satellite is no longer in a noisy region of the sky. The transmitter power requirements will then be based upon the curve for the quiet part of the sky. At 136 Mc the antenna noise temp (T_A) is 380° Kelvin. The entire receiving system equivalent noise temperature is the sum of the antenna temperature and the receiver temperature. The receiver noise temperature is

$$T_r = 290 \text{ (receiver noise factor - 1)}$$

where noise factor = antilog of noise figure in db
= antilog 3-2

Then

$$T_R = 290 \ (2 - 1) = 290^\circ K$$

and the receiving system equivalent noise temperature is

$$T_E = T_A + T_R = 380 + 290$$

$$T_E = 670^{\circ} K$$

The required receiver signal power can now be determined from the required signal to noise ratio (17 db) and the noise power appearing at the receiver input due to external cosmic noise and internal noise. This noise power is equal to $K\ T_E\ B$. K is Boltzman's constant equal to 1.38×10^{-23} joules/$^{\circ}$Kelvin and B is the receiver bandwidth. The required received power is

$$S = P_R = K\ T_E\ B \times \text{(signal to noise ratio)}$$

$$P_R = 1.38 \times 10^{-23} \times 670 \times 10{,}000 \times 50$$

$$P_R = 4.6 \times 10^{-15} \text{ watts}$$

The maximum range over which it is necessary to transmit is determined by the orbit. An approximate plot of the orbit is shown in Fig. 4-37. The choice of range is somewhat arbitrary. It is certainly not necessary to retrieve data from the satellite in all parts of its orbit but neither should it be limited to the minimum range of 300 nautical miles. If the orbit and tracking station lie in the same plane, a distance of 2,000 nautical miles (Radii of arcs about points A, B, C, D, E, F of Fig. 4-37) will give horizon to horizon coverage at position A. From the figure if is seen that the coverage angle decreases from point A but is still adequate to point E. Beyond E to F, it quickly decreases to one point of contact at E beyond which satisfactory reception would probably not occur. Since the orbit and the tracking stations usually won't lie in the same plane, the coverage will be considerably less for most cases.

The satellite antenna will be of the turnstyle type. This will give a near omnidirection antenna pattern which

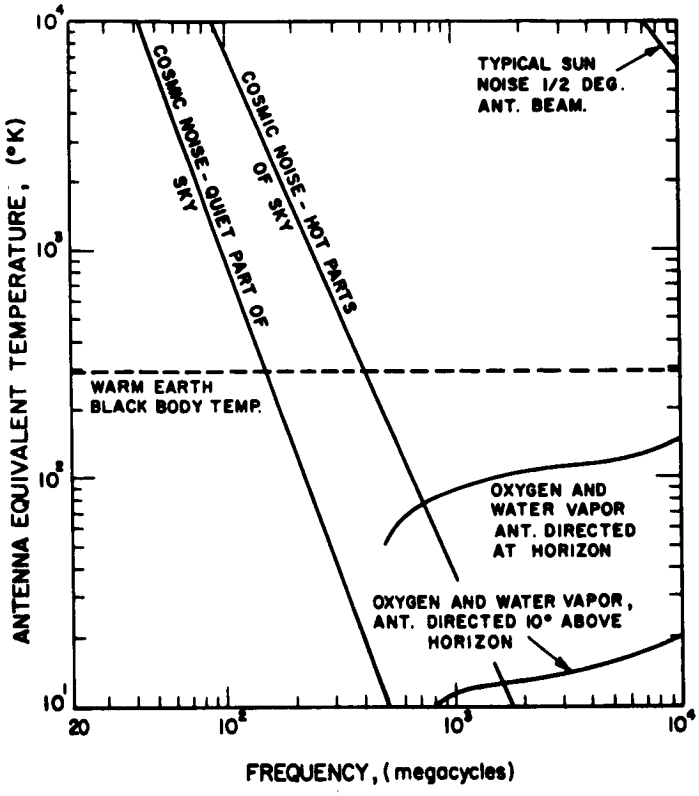

FIG. 4-36

ANTENNA EQUIVALENT NOISE TEMPERATURE AS A FUNCTION OF FREQUENCY

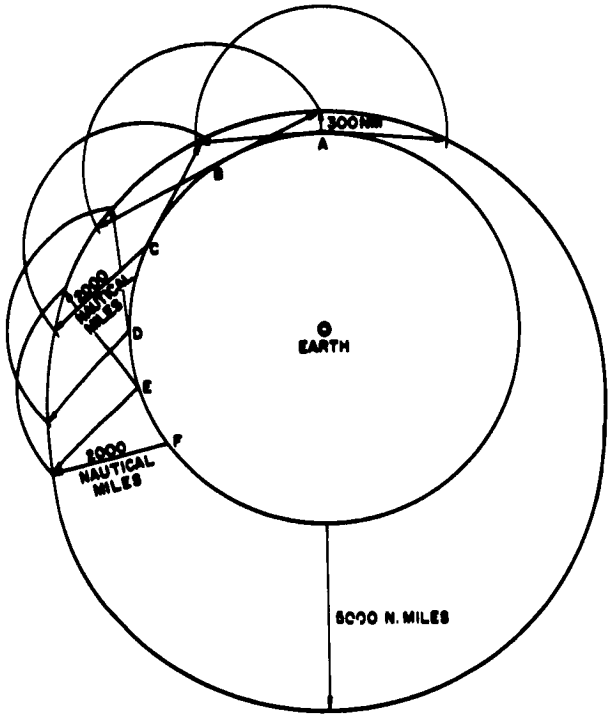

FIG. 4-37

APPROXIMATE ORBIT OF SATELLITE

is desired since the satellite orientation with respect to a ground receiving station will be continually changing. The minimum gain to be expected from this type antenna is approximately -3 db. A factor of about -6 db will be allowed for polarization changes due to orientation changes of the satellite.

The gain of the 85-foot paraboloid receiving antenna is approximately 29 db at 136 Mc. The wavelength λ, at this frequency is 7.2-foot. The 40-foot antenna gain is 22 db.

With this information, the transmission equation may be used to determine the transmitter power. The necessary data are

R = range in ft. = 12.16×10^6 ft. (2000 nautical mile)
P_R = received power = 4.6×10^{-15}
λ = wavelength = 7.2-ft.
G_T = transmitter antenna gain - 1/2
G_R = receiving antenna gain = 790
PF = polarization factor = 1/4

$$P_T = \frac{(4\pi \times 12.16 \times 10^6)^2 \times 4.6 \times 10^{-15} \times 4}{7.2^2 \times 1/2 \times 790}$$

P_T = 21 milliwatts

To allow for any unknown transmission conditions and because 50 milliwatts is a standard size transmitter readily available, this value of power will be used. Transmitter power will be monitored as part of the house keeping measurements.

4.5.3.3 Telemetering system Functional Block Diagram

The basic telemetry system that follows from the investigation in Section 4.5.3 is shown in Fig. 4-38.

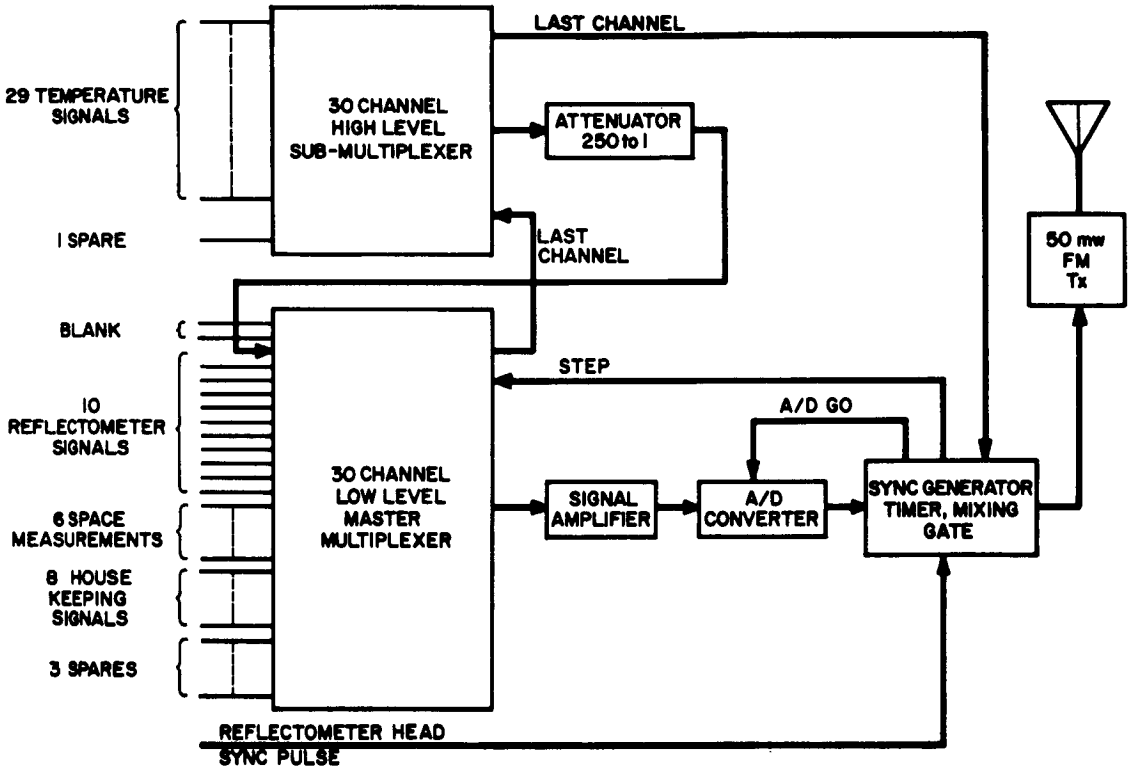

FIG. 4-38 TELEMETRY SUBSYSTEM FUNCTIONAL BLOCK DIAGRAM

4.5.4 Synthesis and Design of Command Sub-System

The function of the command sub-system was briefly deliniated in subsection 4.5.2. This will be covered in detail in the section to follow on Power Programming Requirements. Before a power programmer can function, a receiving system is required to receive the coded command signal from the ground station and transform and decode this rf command signal into a form suitable to operate the programming circuit.

The required components of the command subsystem are command receiver and antenna, a command decoder, and a programming unit. A detailed discussion of each follows.

4.5.4.1 Command Receiver

This unit will operate at one of the satellite command frequencies: 122 or 150 Mc. To be compatible with the Minitrack ground station, it will be an AM type receiver. Since there are several satisfactory units available, no design work here is necessary. The only electrical requirements are low power drain, high receiver sensitivity. All that is required is to see that the 200 watt ground station transmitter capability is sufficient to operate the command system at the maximum range to be encountered from Fig. 4-37. This is about 5300 nautical miles (from point F to the Apogee).

Since the telemetering (TM) and command frequencies are very close, the same antenna will be used in both. A narrow band pass filter may be placed between the command receiver and the antenna feed system to protect the receiver from the comparitively high transmitter power.

The required transmitter power (P_T) can be found by use of the basic transmission equation. This is

$$P_T = \frac{(4\pi R)^2 \, P_R}{\lambda^2 \, G_T G_R \, PF}$$

The quantities for use in the transmission equation are:

P_R receiver sensitivity = 4.5×10^{-14} watts

G_R = receiving antenna gain = 1/2

PF = polarization factor - 6 db = 1/4

G_T = transmitting antenna gain - 16

R = range = 32×10^6 ft

λ = wavelength = 6.55 ft. (f = 150 Mc for worst case condition)

The value is then

$$P_T = \frac{16 \times 9.9 \times 32^2 \times 10^{12} \times 4.5 \times 10^{-14} \times 4}{6.55^2 \times 16 \times 1/2}$$

$$P_T = 85 \text{ watts}$$

This is well within the capability of the command transmitter. Since the normal operating range will be considerably less than the maximum, a receiver with this sensitivity is quite adequate.

4.5.4.2 Decoder Requirements

Decoders are commercially available that operate in conjunction with a compatible command receiver. The o only electrical requirements here are low power consumption and the necessary number of command channels to handle the power programming function.

4.5.4.3 Power Programming Requirements

The command functions of the satellite are:

1. Experiment Mode: Reflectivity Experiment command Turn on, automatic turn-off at completion of experiment, and command turn off capability.

2. Tracking Mode: Transmitter command turn-on and turn-off.

As with the receiving and decoding functions no design work is necessary for the power programming section. The only necessity is to determine the type of components that will accomplish the task. Rather than use a timing device to turn off the experiment it was decided to use the frame synchronization pulse from the telemetry system Sync Gen. Timer and Mixer gate as a time reference. All that is necessary is to count these pulses using an appropriate counting device and turn the experiment off when it has gone through the sufficient number of cycles.

A very efficient programming system was devised using commercially available components. A detailed functional block diagram is shown in Figure 4-39. The operation of this subsystem is very simple. The individual power programming units are sealed latching relays that consume power only during the switching operation. It is switched by the signal from the appropriate channel from the command decoder. In doing this the programmer feeds a set pulse to the cut-off timer pulse counter. This initiates the counting sequence of the timer which counts the number of frames of the main multiplexer. This can be accomplished by counting frame synchronization pulses or the last channel pulse of either multiplexer. The counter can count up to 2048 pulses. For a one minute experiment 1200 pulses must be counted. At the completion of the counting cycle the timer feeds a reset pulse to the instrument and telemetry power programmer and itself. This resets the counter and switches the programmer off. This occurs in the experiment mode. In the Tracking Mode the command turn-on signal is applied to the transmitter power programmer. To utilize only one command channel to turn off either mode of operation, this signal is applied directly to the transmitter power programmer and through the turn-off steering diode. The polarity of this diode is such that it will pass the turn-off command signal to all three units through the

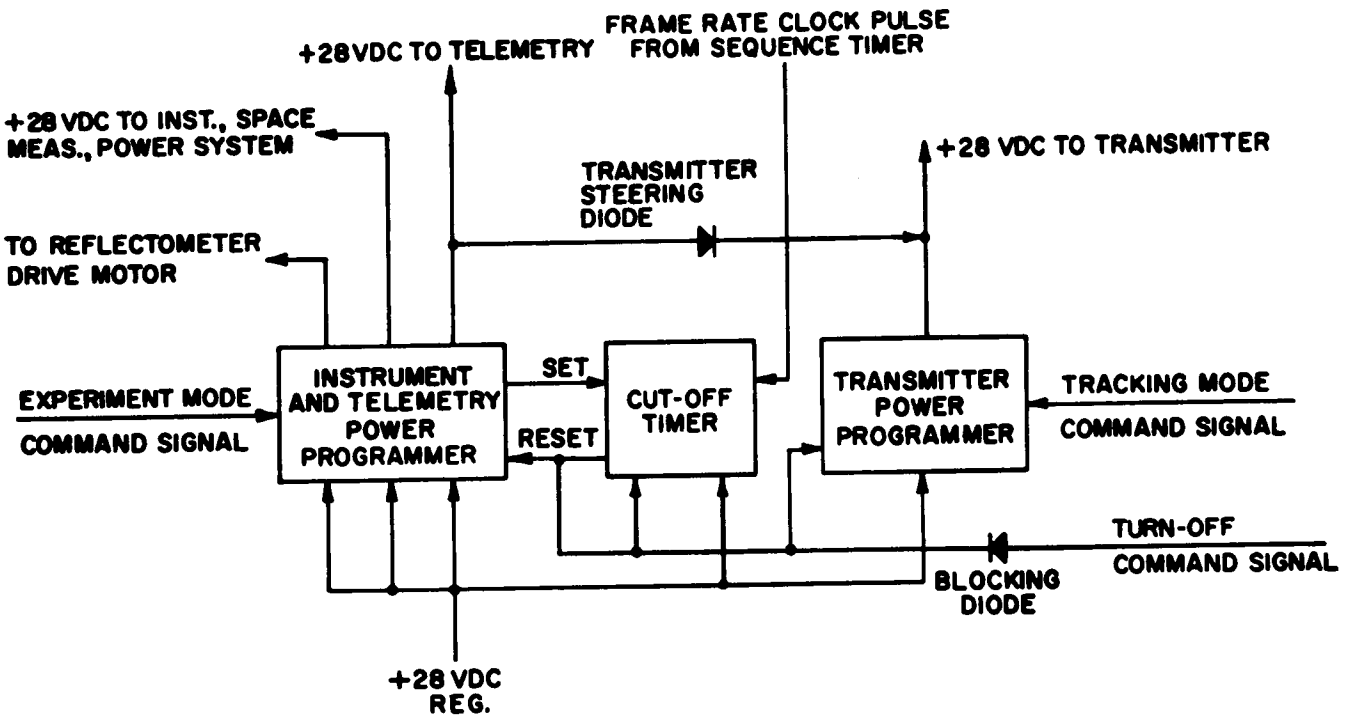

FIG. 4-39 SYSTEM POWER PROGRAMMER AND CUTOFF TIMER

turn off steering diode. It will block the cut off timer reset pulse from entering the output of the command decoder. In the Experiment Mode, when the transmitter power programmer is in the OFF position power is applied through the transmitter steering diode. When operating in Tracking mode only this diode blocks the transmitter B+ voltage from the rest of the telemetry system. A 3-pole unit is used for the instrument and telemetry power programmer to reduce the current through the relay contacts.

4.5.5 Selection of Components for a Functional Telemetry and Command System

Selection of hardware components was made after a survey of commercial off-the-shelf-items. Suitable items were found for most of the components. Only a few specialized or non-standard units will require a special order or design. The items selected and their pertiment characteristics with remarks are tabulated in Table 4-7. The attempt was made to select the items by the following criteria:

1. Necessary electrical characteristics to perform the task
2. Minimum power consumption
3. Minimum weight
4. Sufficient environmental characteristics
5. Reliability

Of course, it was not always possible to satisfy all criteria. Some may have to be sacrificed or comprimised in order to obtain acceptability in another aspect of performance. It should be pointed out that the components selected in no way indicate that these items are the only ones available that will perform the task. They only represent currently available items that, at present, best satisfy the requirements. It is obvious that the design of a system as this is extremely flexible.

TABLE 4-7

TELEMETRY AND COMMAND SUBSYSTEM COMPONENT PARTS LIST

Component	Manufacturer	Type or Model No.	Weight, oz.	Size and Configuration	Power Consumption, Watts	Power Requirements	Number Used in System	Approximate Current Price	Remarks	Temperature Characteristics: Operate	Temperature Characteristics: Storage
Master multiplexer	United Electro-Dynamics	CE-22	32.0	4.7 x 2.9 x 2.5 in^3 Parallelepiped	2.5	+28 vdc ±15% @ 90 ma	1	$ 4,800	30 channels, low level 0-10 mv	-35°C to +125°C	-60°C to +150°C
Sub-multiplexer	United Electro-Dynamics	CE-21	27	4.1 x 2.9 x 2.5 in^3 Parallelepiped	1.7	+28 vdc ±15% @ 60 ma	1	4,000	30 channels, high level 0-5 v	-35°C to +125°C	-60°C to +150°C
Signal amp	United Electro-Dynamics	DA-22	5	1.58 x 2.1 x 1.7 in^3	1.1	28 vdc ±10% @ 40 ma	1	890	Wideband dc amplifier	-20°C to +85°C	-65°C to +125°C
Analog-to-digital converter	United Electro-Dynamics	AD-8	43		3.8	+28 vdc ±10% @ 135 ma	1	7,000	8 digit A/D converter	40°C to +100°C	
Sync Generator, timer, mixing gate	Electro-Optical Systems, Inc.		5	3.0 x 3.0 x 1.0 in^3 Parallelepiped	2.8	+28 vdc ±10% @ 100 ma	1		Special requirements	-55°C to +100°C	-60°C to +150°C
Telemetry transmitter	Microdot, Inc.		16	20 in^3	2.5	+28 vdc ±10% @ 90 ma max	1	800 to 1,300	50 mw, 136-137 Mc FM transmitter	-40°C to 85°C	
Bandpass Filter	Electro-Optical Systems, Inc.		2	1.0 x 1.0 x 1.0 in^3			1		122 or 150 Mc narrow bandpass filter	-55°C to +100°C	
Command Receiver	AVCO Corp.	184003	16	3.5 x 5.0 x 1.0 in^3 Parallelepiped	0.084 standby 0.17 operate	+13 vdc @ 3 ma +13 vdc @ 6 ma		8,500	122 or 150 Mc AM	-35°C to +80°C	
Command Decoder	AVCO Corp.	184046	24	3.5 x 5.0 x 1.0 in^3 Parallelepiped	0.005 standby 1.0 operate	+13 vdc @ 0.2 ma +13 vdc @ 36 ma	1	8,500	Decoder: up to 21 individual command output signals available	-35°C to +75°C	
Transmitter Power Programmer	Data Science Corp.	150	1.5	1.6 x 1.2 x 0.8 in^3 Parallelepiped			1	128	Single pole double pole relay-2 amps. Power: a few milli-watts during switch-ing	-55°C to +100°C	
Inst. and telemetry programmer	Data Science Corp.	150	2.5	2.0 x 1.2 x 0.8 in^3 Parallelepiped			1	200	3 pole double pole relay. Power: a few milliwatts during switching	-55°C to +100°C	
Transmitter power measure	Electro-Optical Systems, Inc.		1.0	1.0 x 1.0 x 1.0 in^3			1	50	Consists of an attenuator network and a diode detector	-55°C to +100°C	
Cutoff timer	Data Science Corp.	MC-11	3.0	3.2 x 1.2 x 0.8 in^3 Parallelepiped	0 standby 30 mw operate	+28 vdc ±30% @ 1 ma	1	585	Magnetic core counter: Resets on any number of pulses up to 2,048	-55°C to +100°C	

4.5.5.1 Thermal Aspects of Telemetry and Control System

The only thermal constraint imposed by the Telemetry and Command subsystems upon the rest of the satellite is that each item be mounted in the satellite structure with sufficient heat sink area to keep each component within its operating temperature limits. These are included in Table 4-7.

4.5.5.2 Packaging or Component Mounting Requirements

The mounting arrangements of the telemetry and command components are governed only by the balancing requirements of the entire satellite package and the need to keep the low level signal leads from the transducer elements to the low level master multiplexer as short as possible to minimize noise pickup. It is also desireable in the entire system to keep all interconnecting wiring as short as possible to keep weight down.

4.6 Preferred Experiment System Operation

This section presents a brief qualitative discussion and summary of the operational sequence of the flight experiment. Detailed descriptions are, of course, contained in the various sections on specific topics.

The preferred launch direction is to the east in order to obtain maximum exposure to the radiation belts. This launch direction is available at Wallops Island. Launch time should be in the early morning hours so that the payload is injected into orbit in a nearly sun oriented attitude. This condition will minimize the maneuvers required for solar acquisition. In addition, the field of view requirements for the acquisition sensor are minimized.

Subsequent to separation, the payload is despun to zero and then respun to the proper spin rate. When the correct spin rate is established, solar acquisition occurs and the payload is oriented in the sun directed attitude.

During launch and the first few (1-2) orbits the satellite transmitter operates continuously in the "tracking" mode in order to establish the ephemeris for the vehicle. Subsequent corrections to the ephemeris are made by operating continuously in the tracking mode for one or two orbits once every two weeks.

For the first 3 to 4 weeks of the flight the satellite would be commanded to operate in the "experiment" mode several times each day. A relatively high interrogation rate is required to establish any rapid trends in the experimental data and determine vehicle status through analysis of the engineering or "housekeeping" measurements. The actual frequency of interrogation would be established by the trends as they develop. An upper limit is established by the state of battery charge, which is one of the telemetered housekeeping measurements.

After the first few weeks of flight it is expected that the interrogation rate would decrease to a few times per week. Once again the exact rate being dictated by the data trends and the requirements of the experimenter.

The quartz cover plates are removed from the samples so covered at about six months after launch. This technique permits a measurement of the relative separate effects of ultraviolet and particle radiation.

The termination of the flight experiment may be determined by either of two factors. One is simply the exhaustion of the orientation system gas supply and the other is the cessation of interest on the part of the experimenter. In either case range requirements may require a command or timed cut-off of the satellite power system in order to preclude unwanted radio transmissions.

4.7 Ground Support Program

The ground support requirements to support the successful launching of an instrumented satellite and acquire data from it after launch can be divided into three distinct and separate categories: (1) prelaunch check of satellite, (2) countdown checks, and (3) post launch data acquisition and tracking. These items are discussed in the next few subsections.

4.7.1 Prelaunch Check

This phase consists of visual inspection and functional check of the satellite after shipment to the launch site. This will be followed by complete electrical testing of the satellite and final rocket stage combination. These operations will be supported by the required test and checkout equipment. This equipment will check the performance of the entire space vehicle system as well as indicate malfunctions and their sources should they occur. The link between this ground support equipment and the satellite will be through the telemetry and command rf links and the vehicle umbilical connections.

4.7.2 Countdown Check

This operation will consist of a turn-on and functional check of the entire flight vehicle during the countdown activities and just prior to launch. A ground checkout and control system identical to the equipment used in the prelaunch checks will be used in the

operation. It will also be used to switch from satellite external to internal power just prior to launch. The medium connecting the ground support equipment and the satellite will be as before: The telemetry and command rf links and the umbilical connections. A functional block diagram of a tentative testing system that will fulfill the objective of both the prelaunch and countdown checks is shown in Fig. 4-40. This system is by no means the only configuration that could be used and, at this time, is only being offered as one approach to the problem. The design of such a system could not take place until the detailed design of the satellite was firm. It would, however, be useful for the environmental testing portion of the program.

4.7.3 Post Launch Data Acquisition and Tracking Ground Support Program

This portion of the space measurements program will be a service performed by the NASA-Goddard Minitrack network. Since the satellite will be completely compatible with this network no discussion will be made here on the electronic parameter requirements. Instead, this section deals with certain operational aspects of the flight test program that will put some constraints or limitations in the ground stations that may be used.

4.7.3.1 Tracking Requirements

At the time of launch, the telemetry satellite transmitter will be turned on so that the satellite may be tracked for 1 or 2 circuits of its orbit. This will establish the orbit of the spacecraft. Once the orbit is known the transmitter can then be turned off by command from the ground. This can be done in any part of the orbit as the ground network command transmitters have more than sufficient power to activate the command system at the greatest distance expected.

4.7.3.2 Receiving System Constraint

In an effort to keep the required transmitter power to a minimum the use of the receiving stations must be limited to those with the 85-foot parabolic antenna when data acquisition is required

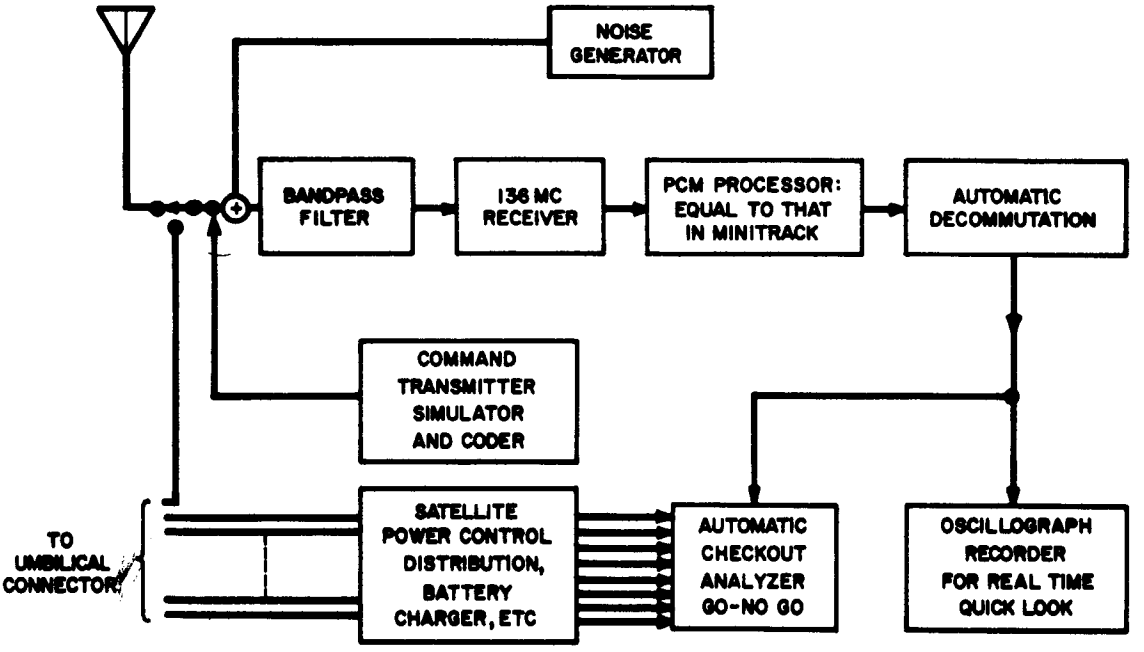

FIG. 4-40 SATELLITE AUTOMATIC TEST SYSTEM

at satellite ranges between 900 and 2000 n. mi. At distances less than 900 n. mi., the sites with the 40-foot parabolic antenna may be utilized. Those stations having only the self-tracking yagi array with gains of 18 to 22 db may be utilized at ranges less than 550 n. mi.

4.7.3.3 Compatibility of Minitrack Station Locations with the Satellite Orbit

It is expected that the satellite will be given an eastward launching from the Wallops Island Station such that the inclination of the orbit is about 37 degrees. Under these initial conditions a detailed analysis of the orbit relationship to the Minitrack station locations has been made with the following conclusions: If apogee (apogee altitude = 5000 n. mi.) of the orbit is located in the northern hemisphere at the maximum possible latitude, i.e., the orbit inclination (relative to the equatorial plane) angle i (= 37 degrees), the satellite will be observed at least once a day by one of the following tracking stations: Rosman, North Carolina; College, Alaska; St. Johns, Newfoundland; and Quito, Equador. It is possible that all four of these stations may (with appropriate initial conditions) aquire the satellite simultaneously.

If the apogee is at zero latitude, i.e., lies in the equatorial plane of the earth, then the satellite will be observed at least once a day from one or several of the following tracking stations: Rosman, North Carolina; Woomera, Australia; Johannesburg, South Africa; St. Johns, Newfoundland; Santiago, Chile; and Quito, Equador. It is possible that all these stations, except Woomera, Austrailia, may aquire the satellite simultaneously.

If the apogee of the orbit is located in the southern hemisphere, i.e., 37 degrees, the satellite will be observed at least once a day from one or several of the following tracking stations: Johannesburg, South Africa; Santiago, Chile; Quito, Equador. It is possible that all three of these stations aquire the satellite simultaneously.

Since the apogee will (more than likely) lie some where between these two extreme latitudes the satellite will be observed by some other combination of tracking stations. In view of the relative ease with the tracking stations can aquire the satellite for the extreme locations of apogee, (it can safely be said that) no matter what the location of apogee the satellite will be observed at least once every day by at least one of the seven tracking stations.

4.7.3.4 Command Requirements

The coding requirements of the space vehicle command system will be in complete accordance to the Minitrack Network requirements.

4.7.3.5 Data Handling Requirements

The specific processing requirements following recording of the received and regenerated serial PCM signal are undefined at this time. However, it is recognized that the following general requirements would exist.

In order to establish that the satellite is functioning properly, a cursory real time readout would be desirable at the tracking station. This quick look capability might prevent excessive interrogation of the satellite in the case of premature power system degradation or marginal temperature condition. The latest available reports on Minitrack station capabilities indicate the feasibility of such a function.

Secondly it would be desirable to write and record a computer program that could be provided with the recorded PCM tape for rapid computer conversion to an easy-to-read type written format. The technique of discreet measuring PCM that is utilized in the satellite data processing facilitates this type of conversion.

For detailed analysis and study of the data, the original tape should be kept available in the event of misleading data bit errors or inconsistancies in the data.

4.7.3.6 Special or Nonstandard Requirements

As every effort has been made to make the satellite telemetry and command subsystem completely compatible with the existing Minitrack network no special or nonstandard ground station requirements are foreseen at this time.

4.8 Systems Design

4.8.1 Systems Performance Requirements

Any payload systems design must be worked out to satisfy the intents and purposes of the program in which it is being used. The payload must be physically capable and suited for the performance of a specific function, it must be reliable in its working environment, it must have rf and data handling compatability with the ground support stations to be used, and it must be capable of complying with the program time table. In the paragraphs to follow, the suggested systems design will be discussed in terms of these various categories of required compatability.

4.8.1.1 System Description

In order to expose the mirror samples under test to as severe a representative environment as possible, an elliptical orbit was selected that should carry the satellite through the more destructive regions of near space. The calculated payload weight is such that the Scout missile should be adequate for providing the desired orbit. A selection of samples has been picked to best represent the existing available solar reflector techniques. The reflectivity measuring instrument has been designed to provide a relatively high order of precision as might be desired for subsequent detailed analysis. A measurement is made of the temperature of each individual reflector sample in order to monitor any changes which might occur in the α/e ratio for a given specimen, and to recognize when reflectivity degradation might be a function of high temperature. Additional instrumentation is included for the detailed measurement of the space environment to which the solar specimens are exposed. Telemetry techniques and information rates have been selected so as never to become the "weakest link" in the experimental data accuracy. An orientation system that keeps the satellites experimental surface directed towards the sun brings about a truer simulation of the circumstances than would be experienced by an actual solar collector in orbit. Power supply parameters have

been based upon a conservative two-year flight program.

These various considerations are described at greater length in the respective subsystem design studies found elsewhere in this report.

4.8.1.2 Environmental Constraints on the System

All components have been selected to function properly and reliably in space environment. A thermal analysis has been performed as a part of systems engineering to define the anticipated systems constraints regarding all aspects of temperature in the payload (see section 4.8.2.3). An equivalent mechanical and packaging analysis has also been performed that not only reassures reliable operation of the payload in space but also precludes probability of damage during launch (see section 4.8.2.2). Shock and vibration considerations have been based upon the data available in NASA Report R-97 on the Scout Vehicle.

4.8.1.3 Compatibility with Ground Support Facilities

A typical 136 Mc FM telemetry transmitter has been selected for the payload. A command channel in the payload is provided for activating this transmitter with the rest of the instrumentation turned off. This narrow band transmission will facilitate long range tracking by such facilities as the Minitrack network. Once the satellite ephemeris has been determined, another command channel is available for turning off the transmitter. This mode of operation, requires a 6.67 kc bandwidth, however, which would consequently impress additional constraints on the telemetry range of those ground stations with the smaller receiving antennas. At the conclusion of a measurement cycle, the satellite automatically turns itself off until further interrogated, thereby precluding the necessity of additional command channels. Calculations show that by using the 85 foot dish antennas available at certain facilities, the experiment data transmission range might be extended out to the vicinity of the satellite's apogee.

The command receiver will respond to either 122 Mc or 148 Mc whichever frequency is chosen at the time of the actual payload design. This frequency is sufficiently close to the telemetry transmitter frequency that a common telemetry antenna may be used on the payload with bandpass filter to prevent receiver damage by the telemetry transmitter. The command channel will be on at all times from before launch till the conclusion of the flight test program, such that its schedule of interrogation may be altered on the ground with no constraints other than the range limitations of the rf link.

The data processing techniques to be used on the payload will include standard NRZ binary format. The bit rate is well within the data handling capability of the Minitrack ground station PCM equipment. The nature of the programming is such as a computer program can easily be written to convert the serial code to a typewritten chart that present the information in an easy-to-read format. these tabulated data along with the magnetic tape recording of the received data can be preserved for the final data evaluation at the end of the flight experiment. It is understood that existing ground station PCM equipment capabilities make it possible to have at least a cursory real time read-out for the purpose of quick-look evaluation of the operational status of the satellite.

A quantitative elaboration of these relationships is presented in some detail in the telemetry subsystem design and the ground support system portions of this report.

4.8.1.4 Compliance with Program Plan

During the execution of the discussed experiment probe a detailed flight program plan should be devised, which could depict all of the sequential aspects of the program starting with pre-launch checkout of the satellite and extending through the data evaluation phase at the end of the flight program.

The pre-launch satellite checkout could be effectively performed using manually programmed test equipment. This operation would be primarily intended to check the operability of the

various satellite functions rather than to give a complete quantitative test. An umbilical connector will be provided on the satellite for this testing. The Bendix "twist/pull" quick disconnect type would be used to permit use of existing tower cables that utilize this type of connector with certain modifications for reliable lanyard uncouple. The connections provided will also allow for last minute battery charging. With the exception of the orientation control circuitry, the instrumentation in the satellite will be turned on prior to launch and be ready to operate. The missile telemetry equipment will satisfy all telemetry requirements until the payload has been placed in orbit. At the time of the disconnect of the fourth stage the despin system will go into operation reducing the spin rate to zero and then up to the required spin rate. At this time the attitude control circuitry will be turned on so that the payload will be able to orient its experimental surface towards the sun. Once the orbit has been established, it would be possible to interrogate the satellite thereby instigating the first experiment program. The transmitter is automatically turned off at the end of a measurement. If for some reason it is desirable to turn on the transmitter without the instigation of the test, a separate command channel has been provided.

The remainder of the program will consist of successive interrogations and the compilation and evaluation of test data. The frequency of interrogation could be arranged according to the measured rate of reflectivity degradation of the samples under test. The final evaluation of the flight test experimental data could begin and continue throughout the duration of the flight experiment. The ground simulation test study would also yield certain test data which would be fed into the data evaluation program.

4.8.2 Interface Parameters

As well as having to satisfy external requirements to the payload system the payload subsystems must be compatible. The primary areas of required compatibility are electrical (data and power), mechanical, and thermal. Of particular importance is the possible accumulation of optical, mechanical, and electrical tolerances and the resulting effect of the quality of the final data. Studies have been performed in each of these areas of concern; the results are given in the following paragraphs.

4.8.2.1 Electrical Analysis

The payload system electrical analysis has evolved into a comparison and matching of input and output characteristics between subsystems. These relationships can further be categorized into the areas of power compatibility and signal compatibility. A block diagram of the satellite electrical system is shown in Fig. 4-41. A chart of electrical interconnections between subsystems only has been prepared which demonstrates power delivery requirements and signal characteristics such as voltage amplitude and loading characteristics (see Appendix B). A power profile is provided in Fig. 4-42, which demonstrates graphically the energy required of the power supply portion of the satellite. On the basis of a twenty scan test, the total test time would be approximately 30 seconds. With an amplitude of about 24 watts throughout the tests, approximately 1/5 of a watt hour would be consumed per interrogation. If the power supply is capable of providing on the order of 200 watt hours per day, this represents around a thousand tests per day capability, which is certainly far in excess of what would be required. This margin is desirable, however, because of component degradation throughout the rather long flight program, the desirability of having the telemetry transmitter on for some periods of time for tracking purposes, and because of the additional large power pulse drain by the solenoids in the satellite orientation subsystem. It should be noted that the orientation pulses are not significant regarding energy consumption, but must be considered from the

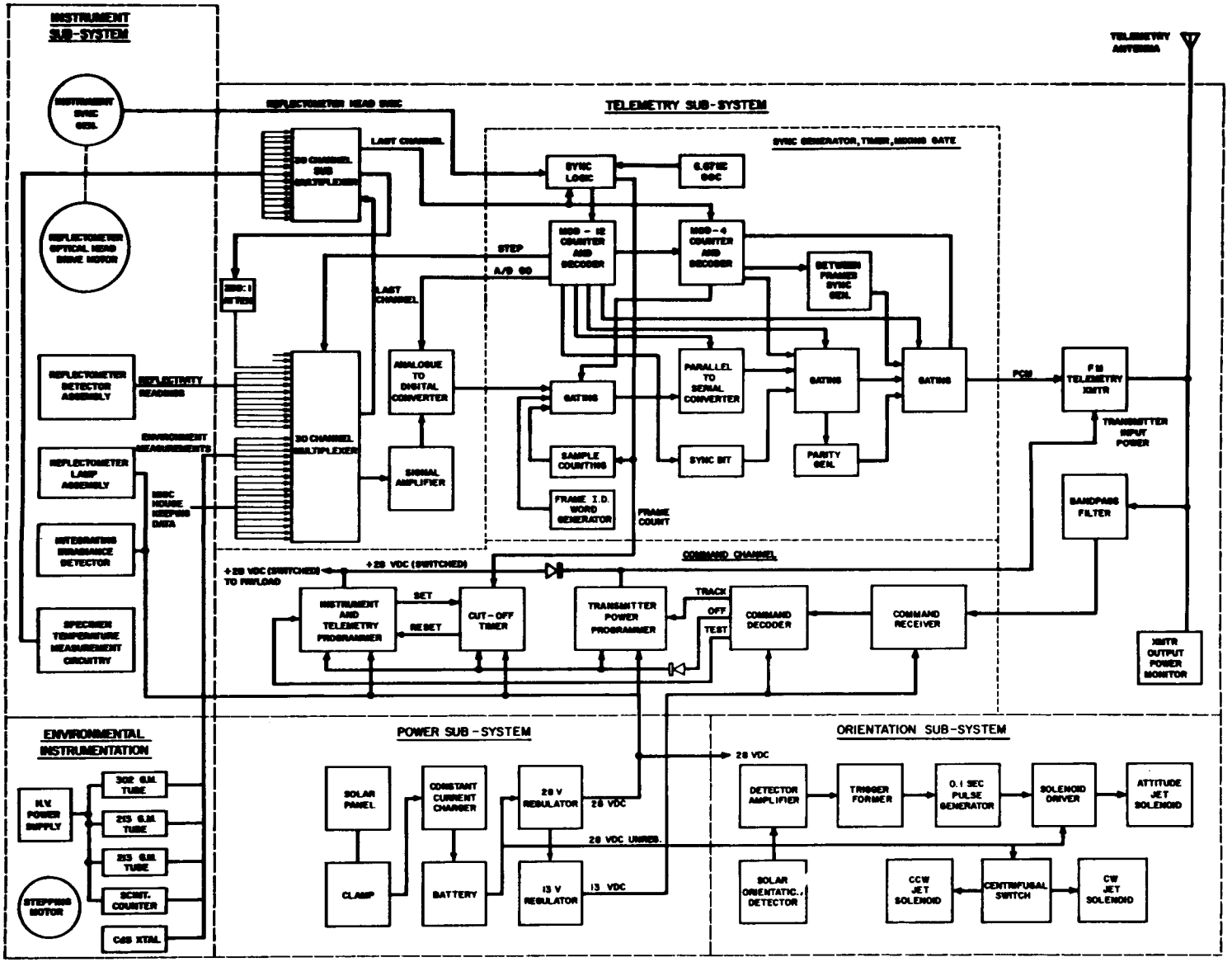

FIG. 4-41 ELECTRICAL BLOCK DIAGRAM OF THE SOLAR COLLECTOR TEST SATELLITE

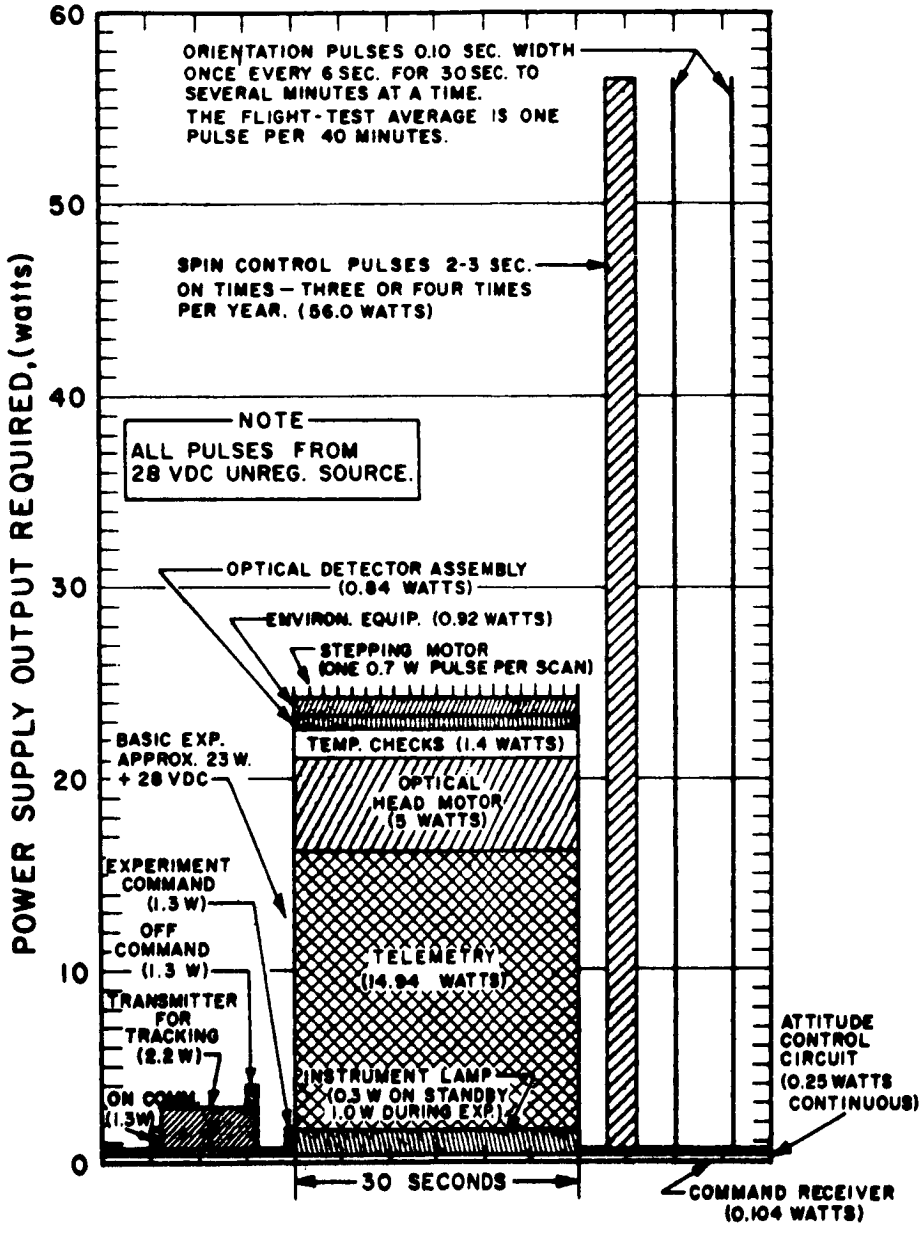

FIG. 4-42 POWER PROFILE

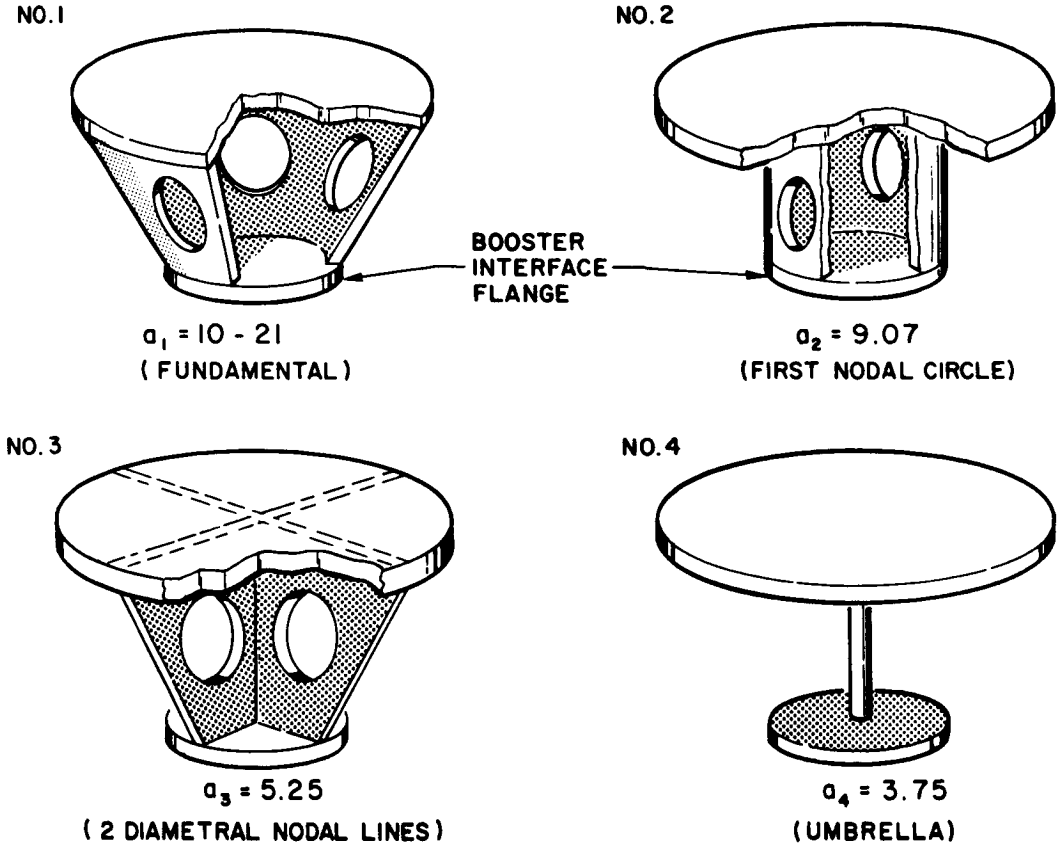

FIG. 4-43 PAYLOAD SUPPORT SYSTEM

standpoint of instantaneous power. According to calculations, it is unlikely (but conceivable) that total instantaneous power drain could be as great as 135 watts. This would occur in the event that both orientation and spin rate correction is required during an experiment test. Extensive detail on the capabilities and requirements of the power subsystem are given in Section 4.4.

4.8.2.2 Mechanical Design Considerations

The mechanical design analysis is intended to evolve a structural configuration of static and dynamic support that will provide the best possible functional performance of the various subsystems with the smallest weight penalty. The satellite is envisioned as being arbitrarily divided into five subsystems each of which is discussed indicating how its functional requirements influence component arrangements and structural geometry. The five subsystems are: (1) basic structure, (2) instrumentation, (3) electronics and telemetry, (4) orientation or attitude control, and (5) power supply and regulation.

Basic Structure

Since there are no clear cut functional boundaries separating the subsystems, a basic structure is assumed as a starting point. A number of rudimentary supporting basic structural schemes can be conceived. However, one that lends itself both to becoming a practical solution to the overall design problem and at the same time admirably demonstrates the design analysis procedures, is a single flat elastic plate suitably attached to the booster rocket interface flange.

Starting with a simple flat plate it is clear that the weight of the support structure will be a function of the plate radius, its thickness, and of the method of connection to the booster. The design constraints that exist are the dynamic and static load factors that the booster creates during launch, and the total satellite payload weight desired. The problem then becomes a process of determining a support system that will give the minimum thickness of the plate for a given diameter.

Letting, for the moment, the plate diameter to be the maximum allowable that will fit within booster shroud, thus obtaining the maximum solar cell area, a clear cut relation exists between the method of attachment of the plate to the boost and the plate thickness. It can be numerically shown that the technique of connecting the basic plate, which will create an overall supporting structure having the highest fundamental frequency, will result in the thinnest plate to satisfy the vibration load factors and thus result in the lightest structure. For small deflections of elastic flat plates (Ref. 54), the fundamental frequencies for a variety of vibrational modes is given. Figure 4-42 illustrates the application to practical support system.

Let ω = fundamental resonant frequency, rad/sec

a = non-dimensional constant pertaining to the vibrational mode of the plate

E = the tensile elastic modulus for the structural material, psi

t = plate thickness, in.

g_o = graviational constant, in/sec^2

W_T = total weight of the satellite, pounds

D = the overall diameter of the plate

ν = Poisson's ratio

$$\omega^2 = a^2\, 4\pi \frac{E g_o t^3}{12(1 - \nu^2) W_T D^2} \tag{4-29}$$

The geometry that constrains the plate to the first nodal circle response mode thus not only gives nearly the lightest structure, but it all adapts itself well to the general geometry needed by the overall satellite system.

The next question is to examine the effect of dividing the single plate into a deck of thinner plates, each plate carrying an equal portion of the total weight.

Let n = number of plates used

t_n = thickness of any plate, in.

W_t/n = distributed load per plate, pounds

t_0 = thickness of a single plate to carry the load, inches (i.e., for n = 1.0)

σ_m = maximum stress in the plate, psi

G = maximum booster acceleration, g-units

k = non-dimensional constant depending upon the plate support geometry and the load distribution

$$t_n = \left[\frac{kGW_t}{n\sigma_m}\right]^{1/2} \qquad \text{(Ref. 55)} \qquad (4\text{-}30)$$

Thus, for the same boost acceleration, structural geometry, and material, the relation between the structure weight of a multi-plate structure and a single plate can be shown.

$$\frac{nt_n}{t_0} = \frac{\text{multi-plate system}}{\text{single plate system}} = (n)^{1/2} \qquad (4\text{-}31)$$

The conclusion then is that, under the plate concept, a single plate will give the lightest structure.

The process for determining the effect of the plate diameter on the structure weight is shown by rearranging Eq. 4-29 in terms of plate weight instead of thickness.

Let W_s = weight of the structure, pounds

ρ_s = density of the structural material, lbs/in^3

$\lambda = (W_s/W_t)$, weight of structure weight to total weight

$$W_s = \left[\frac{\omega^2\pi^2(1-\nu^2)\rho_s^3}{21.33\, a^2\lambda E g_o}\right]^{1/2} D^4 \qquad (4\text{-}32)$$

Keeping all load and geometrical constraints fixed with the exception of the plate diameter, Eq. 4-32 can be rearranged to give the relationship

between decreasing the plate area and decreasing the structure weight.

Let $W_{s,o}$ = original plate weight

A_o = original plate area

$W_s = fW_{s,o}$ = reduced plate weight

f = plate weight reduction ratio

A_s = reduced plate area

$$W_s = fW_{s,o}$$
$$A_s = (f)^{1/2}A_o \tag{4-33}$$

Applying the principles to a plate configuration optimized by Eq. 4-29 that are contained in Eqs. 4-31 and 4-33, a single aluminum plate (2.0 feet in diameter) connected to the booster by a hollow column would have to be 0.33 inch thick to support a 75 pound total load during a 60 G booster acceleration. It would then weigh 16 pounds and should resonate at about 28 cps. If two plates were used, the structure weight would increase to 23 pounds; other characteristics being the same. The weight of these two plate arrangements could be reduced to about 12 pounds by reducing the area by 28 percent.

The general component arrangement has been to locate as much of the subsystems as possible on the base plate so as to minimize the multi-plate weight penalty. This is advantageous in keeping bending moments reduced in response to transverse load factors. The single plate geometry is inadequate in providing sufficient heat transfer radiation area, so the structure resolves into the cylindrical form shown in the engineering drawing (Appendix A). Around the circumference of the structural cylinder is an aluminum skin 0.020 inch thick. The purpose of this skin is to provide radiation area, damping to the top and bottom plate vibrational responses, and to carry the despin cable through. The implications of gaining lightness by reducing

plate area becomes a trade-off between apogee for the satellite against the solar cell area needed to power the satellite. A weight breakdown for all five subsystems is tabulated at the end of this section. Other support geometries besides the flat plate are possible. One of the most common used is the truss as is exemplified by Ranger series of spacecraft. It is possible that this system would provide a lighter structure when analyzed according to principles governing the plate. However, the plate evolves into a workable answer which would probably be the most economical to produce.

Instrumentation

The static support of the instrumentation is first considered from the need to locate the collimated light path of the spectrometer along the polar axis of the satellite. The basic structural configurations accommodate this as well as locating the drive motor. The spectrometer analyzer is entirely contained in an independent module box which is assembled apart from the basic structure and accurately located in position by bracketry. A central column inside the primary structural support column is incorporated to provide support and location for the vacuum housing of the drive motor so that only one rotating seal is required. This column also stiffens the central portion of the overall structure to keep dynamic structural motion that might result in misalignment of the optical elements. The data conditioning and coding portion of the instrumentation is included in the electronic and telemetry portion of the system.

An additional instrumentation support and location function is provided for the space environment sensors. The static portions of this equipment are three detector tubes positioned so that the face of one is exposed to the direct external radiation. This particular set of tubes is positioned on the bottom support to permit maximum solar cell space on the solar cell support plate.

The dynamic considerations for the instrumentation involves providing an intermittent, short duty, rotation to the

spectrometer scanning arm. The best solution to dynamic functions is to eliminate them, but in this case sufficiently redundant optical calibrating equipment would be excessively weighty and complicated to the point of questionable reliability. The main consideration pertaining to the reliability of this proposed long duration motor is to completely seal it. According to Jaffe and Rittenhouse (Ref. 56), there are other schemes which will provide lubrication and sealing, but their performance lack long duration proof. Motors have been run for a number of months (Ref. 57), by incorporating very low vapor pressure oils impregnated into porous packing glands which provide lubricating atmosphere by very slow outgassing. However, the problem of this bleed vapor collecting elsewhere makes this process questionable. It seems that the best guarantee for performance is to completely seal the motor and gear reduction unit to insure the small amount of vapor required to prevent seizing at the gear surface, and reliable motor functioning, particularly over the long duration proposed for these experiments. The controlling factor in determining the motor size is the friction of the rotating seal. With the geometry shown in the drawing, only one sealing flexible ring is needed. The motor was sized against a conventional O-ring. It is felt that there are lower friction seals available, but this requires further investigation. It is felt that this is the primary engineering problem to be solved. The seal will degrade with heat, hard vacuum, and radiation and will eventually tend to seize and corrode. Redundant seals may be an answer if lower friction seals can be incorporated.

The scanning arm itself has a spring detent in it to insure accurate location of the arm for the beginning of each duty cycle. This might also be accomplished by a solenoid. This will also be used to hold the arm in position during the launch.

All of the rotating machining is selected so that each rotating unit has a counter rotating unit so that the angular momentum of the entire rotating system is contained within

movable internal components. This prevents the satellite body itself from obtaining rotational kinetic energy that would have to be eventually removed by expending attitude control gas.

The space environment system also has a stepping motor which rotates the filter wheel. This system has been used successfully before (Ref. 57), and it is contemplated to incorporate this system exactly to maximize reliability.

Electronics and Telemetry

The static function required here is mainly to locate the various "black boxes" in such a way as to keep the center of gravity located on the polar axis of the overall spacecraft and generally to provide as uniform a mass distribution as possible in keeping with minimizing cabling weight and accessibility. For mass symmetry, it would seem advisable to support half the weight on each of the two plates, however, a thermal constraint of the space environment sensing equipment is that the electronics operate as cool as possible to keep the signal-to-noise ratio as high as possible. The major portion of the absorbed heat is involved in the solar cell surface, hence the desirability of locating the electronic packages as far removed from this surface as is practical. Again, by locating these units, which constitute the bulk of the subsystem mass, on the lower plate, the rigidity of the satellite as a cantilever when mounted on the booster and experiencing transverse load factors will be increased. For these reasons, all of the electronics is packaged on the bottom plate which is made 0.250 inch thick, not because of static or dynamic load factors, but because sufficient material is necessary to attach the cells, bracketry, etc.

The single dynamic function needed by the telemetry system is the erection of the antennas. Four quarter-wave length whip-type antennas, 24 inches long, are hinged only to the periphery of the bottom base plate, and spring loaded to erect themselves when the shroud is removed. Atmospheric effects and structural damping of these whip wires will probably gradually degrade the kinetic energy of the

system, decreasing its spinning stabilization. However, the electronic distribution is such that the ratio of the polar to transverse moments of inertia is about 1.35, providing a lower dynamic energy configuration of the satellite in the desired orientation. Gas is available to maintain the attitude in any event.

Attitude Control

As the drawing shows, three gas nozzles are located to provide thrust to either spin up or spin down the satellite, and to control it in attitude. The 2.0 cubic feet of gas is contained in four gas bottles which are manifolded to insure equal drainage from each bottle during gas depletion. The bottles are incorporated within the basic support column since their geometry is structurally sound, and their strength can be used for structural integrity as well as gas containment. Four bottles were chosen so that the plate containing the centers of each of the tanks also contains the center of gravity of the entire satellite. Since the greatest portion of this mass is located within the electronics and the heavier lower portion of the overall structure it is estimated that the center of gravity will be about 2.0 inches above the inside surface of the base plate. The radius of each tank, if four tanks are employed, is 1.92 inches, which will thus locate these bottles near the bottom of the support column. The four base plate stiffening gussets are located under these tanks to add rigidity where the material section is the thinnest.

The dynamic requirements of the attitude control system are that a de-spin cable and weight be built on the exterior surface of the 0.020 inch side wall. It is contempleted to provide a thin channel which will be wrapped around in the plane of the center of gravity and which will contain the despin mechanism. Despin mechanisms have been used successfully in the past, and in keeping with reliability objectives it is desired to emulate these proven systems as much as possible.

The requirement of the attitude control subsystem to keep all of the angular momentum of the drive motors by counter rotating units has been previously discussed. The "black box" components are expected to be mounted on racks that extend radially so that their positions can be at least radially adjustable for the gross adjustments needed to provide centering of the center of gravity experimentally.

Power Supply and Regulation

The power supply system has two major subcomponents, the solar cells and the battery. The attachment of the solar cells to the sun-exposed face of the satellite is accounted for in the usual manner of most solar cell power producing systems. The battery has the further requirement of not wanting to be below 0°F. Hence, it will probably be necessary to locate it near to the top plate itself. The batteries contemplated are small and do not present much of a load problem. Similarly, they contain no moving parts eliminating the solution of problems in this area.

Satellite Weight Budget

Table 4-8 shows the satellite weight breakdown by subsystem and component.

Summary

In summation, it seems that the structure weight needed to provide the required mechanical support will weigh between 22 and 26 pounds when all brackets, mounting pads, housings, etc. are included. Without going to magnesium, it does not seem that the weight can be much reduced below this.

The static and dynamic requirements of all of the subsystems can be resolved with good reliable techniques with the exception of the driving motor and scanning arm. It seems that more investigation into this problem, specifically in the area of seals and their consequent performance in space under intermittent operation, is needed.

TABLE 4-8

SATELLITE WEIGHT BREAKDOWN - TOTAL WEIGHT = 1138 oz (71.1 lb)

SUBSYSTEM	COMPONENT DESCRIPTION	DIMENSIONS AND CONFIGURATION	NUMBER USED	COMPONENT WEIGHT	SUBSYSTEM WEIGHT
Basic structure	Solar cell support plate	2 ft. diameter plate 0.125 inches thick	1	91 oz	
	Base support plate	2 ft. diameter plate 0.250 inches thick	1	166	
	Support cylinder	Hollow cylinder 8 inches long, 0.125 inches thick	1	54	
	Motor seal box	Closed cylinder 5 inch diameter, 0.125 inches thick	1	12	
	Drive shaft	Hollow shaft, 2 inches long, 2 inches I.D.	1	5	
	Mounting flange	Hollow cylinder, 6 inch diameter, 1.5 inches long	1	32	
	Flange gussets	Angle brackets	4	10	
	Radiation skin	Wrap around aluminum sheet 0.020 inches	1	19	
	Scanning arm	Aluminum channel 1 inch x 1 inch x 10	1	12	
	Brackets	Varied to carry equipment	1	32	433 oz
Instrumentation (optical)	Sample plate) Optical Ass'y		1	53 oz	
	Optical head)		1	8	
	Source		1	10	
	Reflectometer detector ass'y.	1.5 inches x 0.75 inches x 3 inches			
	Optical head drive mechanism)		1	30	
	Optical head drive motor)				
	Instrument sync generator		1	8	
(environmental)	Stepping motor		1	53	
	G-M tube assembly		1	30	
	HV power supply		1	25	217 oz
Telemetry	FM transmitter and power amp	5 inches^3	1	5 oz	
	Bandpass filter	1 inch^3	1	2	
	Antenna and cabling	Cabling figured 30 percent electronic wt	4	70	
	Command receiver	3.5 inches x 5.0 inches x 1.5 inches	1	16	
	Command decoder	3.5 inches x 5.0 inches x 1.5 inches	1	24	
	Power programmer	1.6 inches x 1.2 inches x 0.8 inches	2	2	
	Cutoff timer	3.2 inches x 1.2 inches x 0.8 inches	1	3	
	Submultiplexer	4.1 inches x 2.9 inches x 2.5 inches	1	27	
	Master multiplexer	4.7 inches x 2.9 inches x 2.5 inches	1	32	
	Synch. generator)	3.0 inches x 3.0 inches x 1.0 inch	1	5	
	Sequence timer and mixer)				
	Analog/digital converter	2.7 inches x 5.4 inches x 3.0 inches	1	43	
	Signal amplifier	1.58 inches x 2.1 inches x 1.7 inches	1	5	234 oz
Orientation	Gas jets	0.25 inch diameter x 0.30 inches long	3	2 oz	
	Solenoid		3	-	
	Gas tank	3.59 inch diameter spheres	4	100	
	Electronic module		1	3	
	Sun sensor	1 in.^{3}	1	2	
	Centrifugal switch		1	3	
	Integrating irradiance detect		1	5	
	Pressure regulator	2.0 in.^{3}	1	1	
	Low pressure tank		1	2	118 oz
Power supply	Battery Rack		1	88	
	Solar panel		1	32	
	28v and 13v regulator and charger		1	16	136 oz

The thermal requirements seem to indicate that the satellite will run toward the warm limit for most components. This theoretical estimate will probably tend to be even too cold for long duration space experimentation due to changes in the radiant environment. If more radiation is needed it can be added, with the resulting weight penalty, as a skirt extension onto the cylindrical side skin extending below the base plate. In this way the area could be more than doubled.

4.8.2.3 Thermal Analysis

In an orbiting vehicle it is necessary to provide the proper thermal environment for all component parts and systems. In general, it is desirable to keep the average temperature near "room temperature" (25°C) and to minimize the excursions from this average. Specific requirements are discussed later in this section.

Satellite temperature control systems are broadly classified in "active" and "passive" types. Active systems depend on varying some thermal control parameter while the satellite is in orbit; an example of this is Telstar in which movable shutters varied the average emittance of the electronic package (Ref. 58). Passive systems depend only on prelaunch design of the satellite; Vanguard, Explorer and many others are examples of passive control. Where satellite temperature requirements are not extremely critical, the passive system is generally preferred for its simplicity.

In the following subsections we will: (1) consider the specific thermal requirements of the proposed reflective surface experiment satellite, (2) consider the expected heat inputs to the satellite, and (3) give an example of a passive thermal control system that is compatible with the experiment as presently visualized.

Thermal Requirements

The electronic components to be used (see Section 4.5) are well specified as to maximum and minimum temperatures for both operation and storage, since in general these are commercially

available items. The lowest maximum operating temperature is +75°C for the command decoder, and the highest minimum operating temperature is -20°C for several components. The great majority of the electronic components will tolerate operating temperatures from -35°C to +100°C and storage temperatures from -60°C to +125°C.

Temperature sensitive components in the power system are the storage battery (specified for operation between -30°C and +75°C) and the solar cells, have rather flexible limits (depending on what is required of them), but which should be operated at relatively low temperatures for good conversion efficiency. It should also be noted that the storage battery output declines significantly below -10°C. The power system calculations are based on solar panel outputs at an equilibrium temperature of 55°C in the sunlit portion of the orbit. However, somewhat higher temperatures will not greatly lower the power output, as evidenced by Mariner 2 data (Ref. 59), which showed that at 120°C the cell output was 70 percent of that at 45°C.

The temperature requirements for the reflective surface samples are an integral part of the experiment, and are discussed in Section 4.1.2. In the rest of the experimental payload, only the detectors in the reflectometer and the scintillator for environmental measurements are particularly temperature sensitive; in both cases as low a temperature as possible is desired.

The rest of the vehicle components and structure are considerably less temperature sensitive than those listed above. Based on these requirements, a reasonable design objective would appear to be to limit temperature extremes to -10°C and +75°C for the entire package. In the few cases where the 75°C would be undesirable, such as the detectors, these components might be thermally isolated from the main part of the vehicle so that the equilibrium high temperature would not be reached.

Heat Inputs to the Orbital Vehicle

The four significant heat inputs to a satellite in earth orbit are direct solar radiation (H_S), reflected solar radiation from the earth or albedo radiation (H_A), infrared radiation from the earth (H_E), and internal heat dissipation (H_I). The orbit is assumed to be high enough to eliminate atmospheric frictional heating, and heat inputs from micrometeoroid collisions, charged particles, x-rays, etc., are negligible.

Direct solar radiation is the major, and most uniform, heat input. Except for annual variations of ±3.3 percent, which can be ignored in this preliminary analysis, H_S is a constant equal to 1.4×10^6 ergs/cm^2/sec.

The earth's infrared emission, although somewhat variable with latitude, can be well approximated by a 250°K blackbody radiator at the earth's center, emitting 2.2×10^5 ergs/cm^2/sec at the earth's surface. The H_E input is therefore calculated by the inverse square law relating the geocentric orbital distance to the emission at one earth radius.

The albedo radiation input is quite variable and very difficult to calculate precisely. The main problem is that the earth albedo itself is variable, ranging from 0.2 to 0.6, depending on latitude, cloud cover, and season of the year. For most simple analyses the albedo is assigned an average value of 0.35. The other problem concerning the H_A input is one of computational complexity. The portion of the illuminated hemisphere of the earth which is seen from the satellite is a function of the orbital parameters and position in orbit. In the case of an elliptical orbit, both the amount of the albedo source seen and the irradiance produced by the whole albedo source, as a function of distance, are variables. In practice, for detailed final thermal designs, the albedo input equations are solved by an electronic computer, as are the thermal balance equations for the vehicle itself (Refs. 60

and 61). At the stage of satellite design discussed in this report, such detailed computations are not justified. Therefore, simplifying assumptions are made, as indicated in following paragraphs, in this preliminary analysis, since our purpose is to demonstrate a principle of thermal control rather than produce the final control system.

The remaining heat input, internal electrical dissipation, is quite small compared to the other inputs in this particular satellite since the fraction of time for full operation of the electronic systems is quite small. It is estimated that an average of 1 watt (10^7 ergs/sec) will be dissipated during the shadowed part of the orbit, and 5 watts during the sunlit part when the power conditioning circuitry is operating.

Example of Thermal Control System

The model of the reflective surface experiment vehicle for purposes of this analysis is as follows: shape and dimensions -- cylinder 24 inch diameter by 8 inches high; mass -- 3400 g. (75 lbs.); effective specific heat -- 8.37×10^6 ergs/g/$^\circ$C (0.20 cal/g/$^\circ$C), based on a weighted average of aluminum and the other materials used. The vehicle is oriented with one face of the cylinder toward the sun; this face contains 2 ft^2 of solar cells. It is assumed the rest of all surfaces are available for thermal control coatings. (This ignores the area occupied by the reflective surface samples, but this does not significantly change the results). It is also assumed that most components of the vehicle are well connected by thermal conduction paths, so that all parts will rapidly reach the same temperature. The exception here would be a few small components, such as the detectors, which are intentionally thermally isolated.

The orbit assumed is based on a due east launch from Wallops Island, Virginia, with a perigee of 300 nautical miles and an apogee of 3000-5000 nautical miles. The orbital period is 9100 sec, with a maximum earth eclipse of 2800 sec and minimum eclipse of 1700 sec.

Some general remarks on the thermal control of this type of vehicle are useful at this point. It is necessary to prevent overheating in the sunlit portion of the orbit indicating a relatively high ϵ is needed; but also the necessity to prevent too low a temperature being reached in the eclipsed portion of the orbit indicates a relatively low ϵ. The sun oriented solar cells with $\alpha = 0.75$ and $\epsilon = 0.85$ (Ref. 62) provide a large heat input in the sun, and a large heat output in the shadow. Therefore the radiation characteristics of the rest of the vehicle surfaces must compensate as much as possible for the effects of the solar cells.

Thermal balance calculations made for a number of thermal control coating schemes indicate reasonably good results are achieved if the remaining portion of the sun oriented surface is coated with a material with $\alpha/\epsilon = 0.23$, for example Zircon-pigmented K silicate (Ref. 33) with $\alpha = 0.195$ and $\epsilon = 0.830$. The rest of the vehicle surfaces, bottom and side, are given a polished metal surface with $\alpha = 0.10$ and $\epsilon = 0.05$.

The thermal balance equations for the vehicle are:

<u>In Sun</u>

$$mc^{dT}/dt = H_S\,(\alpha_c A_c + \alpha_f A_f) + (H_A F_{Ab}\alpha_b + H_E F_{Eb}\epsilon_b)\,A_b + H_I - \sigma T^4\,(\epsilon_c A_c + \epsilon_f A_f + \epsilon_w A_w + \epsilon_b A_b) \tag{4-34}$$

<u>In Shadow</u>

$$mc^{dT}/dt = H_E F_{Ef}\,(\epsilon_c A_c + \epsilon_f A_f) + H_I\,\sigma T^4\,(\epsilon_c A_c + \epsilon_f A_f + \epsilon_w A_w + \epsilon_b A_b) \tag{4-35}$$

where T = Temperature (^{o}K)

t = time (sec)

H_S, H_A, H_E = solar, albedo, and earth emission heat inputs ($ergs/cm^2/sec$)

H_I = internal heat (ergs/sec)

A = Area (cm^2)

α = solar absorptivity

ϵ = low temperature emissivity

F = view factor

c, f, w, and b are subscripts of A, α, ϵ, and F, which refer to the solar cells, the rest of the front surface, the side surface and the bottom surface, respectively.

m = total vehicle mass (g)

c = effective specific heat ($ergs/g/^{o}C$)

σ = Stefan-Boltzmann constant (c.g.s.)

It is seen from these equations that certain simplifying assumptions have been made concerning the heat inputs. In Eq. 4-34 the H_A and H_E are assumed to radiate only to the bottom surface. This under-estimate is balanced by an over-estimate in F_{Ab} and F_{Eb}, both taken as unity. Similar balancing of assumptions is used in Eq. 4-35. The overall effect of these assumptions is small; the net result is somewhat pessimistic estimates of both high and low temperature.

The first results of interest are the equilibrium high and low temperatures, i.e., assuming the vehicle spends enough time in both sunlit and eclipse portions of the orbit to reach thermal equilibrium. The results, obtained by seeting $dT/dt = 0$ in Eq. 4-34 and 4-35 are $T_{max.} = +80^{o}C$ and $T_{min.} = -41^{o}C$. The maximum temperature is not too much higher than the desired $75^{o}C$ maximum, but the minimum is far below the -10° requirement.

Next we must examine the maximum and minimum eclipse time orbits to determine if these equilibrium temperatures are reached. The results of this calculation, given in Table 4-9, show that T_{max} is reached in about 4500 sec, but T_{min} is not reached. The minimum temperature in the worst case is -6°C, slightly above the required minimum. It is readily seen that the maximum temperature of 80°C is reached in both maximum and minimum eclipse orbits.

It can be concluded from this preliminary analysis that passive thermal control of the vehicle is feasible, with a minimum number of components requiring thermal isolation.

4.8.2.4 Tolerances and Data Accuracies

It is rather difficult to quantitatively predict all errors influencing the reflectance measurement accuracy. This is more properly a subject for detail design when the many subtleties are given careful attention. It is proper, however, to consider the sources of error, and suggest limits.

It is the nature of the reflectometer design that all sources of error, excluding the samples, are common to each measurement. Thus, except for those changes occurring during one reflectometer rotation, variations in source output, detector sensitivity, etc., have little bearing on measurement accuracy. It is unlikely that significant changes will occur during one rotation of the reflectometer. Those changes which do occur are unlikely to be repetitive so that system accuracy is improved by allowing for many rotations (40 to 50) during the interrogation.

The above is possible by calibrating the system at the sample level. This calibration is done by utilizing a shielded retrodirective low-loss roof prism of high purity fused silica. The calibration prism is subject to two possible sources of error; changes in position of the prism and, changes in transmission of the prism.

TABLE 4-9

CALCULATED THERMAL HISTORY OF VEHICLE

Time (seconds)	Temperature (°C)	Remarks
0	80	Enter shadow minimum eclipse orbit
300	61	
600	46	
900	34	
1200	25	
1500	17	
1700	12	End shadow minimum eclipse orbit
2000	26	Sunlit for 300 seconds
2800	48	
3200	62	
3800	70	
4400	74	
5000	77	
5600	79	
6200	80	
9100	80	End sunlit portion of orbit
0	80	Enter shadow maximum eclipse orbit
500	50	
1000	31	
1500	17	
2000	7	
2500	-2	
2800	-6	End shadow maximum eclipse orbit

Additional measurement errors result from changes in sample position such as tilt or curvature. These errors are accounted for, to some extent, by providing several samples of each surface type.

The remaining error results from data handling and transmission. By utilizing pulse code modulation all nonlinear propagation effects are avoided and the fundamental transmission accuracy is limited only by the coding level. In this design, the 8 bit (plus parity and sync bits) data word yields a minimum error of 0.4 percent.

The error allocation and resulting rms error for the entire reflectometer system are noted below.

Data transmission	-	0.4%
Calibrate prism orientation	-	1.5%
Calibrate prism transmission	-	1.0%
Sample flatness and orientation	-	1.5%
Miscellaneous	-	0.5%
System rms error	-	2.4%

4.8.3 Reliability Considerations

Because of the long term nature of the flight experiment a system having high reliability is essential. It is difficult at this time to accurately predict the reliability of the system because detailed design and specifications have not been made. However, some reliability considerations can be given.

Two basic concepts form the basis of numerical reliability predictions for electronic equipment and systems. These are:

1. Failure by performance degradation,
2. Random catastrophic failure of components. Complete reliability analyses should consider both. However, the first can usually be eliminated by conservative design, careful testing, and maintenance practices which replace parts approaching wear-out before failure.

Thus, equipment reliability can be reduced to the determination of the number of catastrophic failures as a function of time.

During the useful portion of equipment life, catastrophic part failures occur randomly and at a fairly constant rate. These are generally caused by thermal stress, electrical stress, mechanical stress such as shock, vibration, etc. The inherent equipment reliability can be determined, in general, by:

1. Determining the failure rate for each part whose independent failure can cause failure of the equipment (under the conditions of use).
2. Summing these failure rates for all such parts used in the equipment.

This can be stated mathematically by:

$$\lambda_T = \sum_{i=1}^{i=N} (\lambda_P + \lambda_M + \lambda_E)_i \ .$$

where,

λ_T = composite failure rate for equipment under specified conditions

λ_P = nominal failure rate of part

λ_M = failure rate term which accounts for change in failure rate because of circuit application

λ_E = term which accounts for change in failure rate because of environment

The survival probability for the complete equipment can now be expressed as:

$$P_s = e^{-t\,\lambda_T}$$

This is valid only under the following conditions:

1. The equipment is debugged.
2. Applies only to true random catastrophic failures.
3. Routine maintenance will replace parts prior to expected wear-out.
4. No overstressed or misapplied components.

Table 4-10 gives in chart form P_s as a function of time for various failure rates.

For convenience, failure rates are given in failure "bits" where,

One failure "bit" = $\frac{1}{1000}$ x (% failure/1000 hours)

m = MTBF (mean time before failure) = $1/\lambda_T$

The problem of determining the individual component values to be used in in these calculations is beyond the scope of this report. It is sufficient to say that basic values are available for most electronic, electrical, and electromechanical parts, which can be applied to any system design and specific application to allow evaluation of the survival probability of the total equipment.

TABLE 4-10

CHART FORM OF THE EXPONENTIAL FAILURE

LAW ($P_s = \frac{-t}{m}$)

Percent Failure per 1000 hrs	Bits	MTBF (hours)	Survival Probability Percentage After Operation For: 5 hr	10 hr	20 hr	50 hr	100 hr	200 hr	500 hr	1000 hr	2000 hr	5000 hr
1	1,000	100,000	-	-	-	-	-	-	-	99.0	98.0	95.1
2	2,000	50,000	-	-	-	-	-	-	99.0	98.0	96.1	90.5
3	3,000	33,333	-	-	-	-	-	-	98.5	97.0	94.2	86.1
4	4,000	25,000	-	-	-	-	-	-	98.0	96.1	92.3	81.9
5	5,000	20,000	-	-	-	-	-	99.0	97.5	95.1	90.5	77.9
6	6,000	16,667	-	-	-	-	-	98.8	97.0	94.2	88.7	74.1
7	7,000	14,286	-	-	-	-	-	98.6	96.6	93.2	86.9	70.5
8	8,000	12,500	-	-	-	-	-	98.4	96.1	92.3	85.2	67.0
9	9,000	11,111	-	-	-	-	-	98.2	95.6	91.4	83.6	63.8
10	10,000	10,000	-	-	-	-	99.0	98.0	95.1	90.5	81.9	60.7
20	20,000	5,000	-	-	-	99.0	98.0	96.1	90.5	81.9	67.0	36.8
30	30,000	3,333	-	-	-	98.5	97.0	94.2	86.1	74.1	54.9	22.3
40	40,000	2,500	-	-	-	98.0	96.1	92.3	81.9	67.0	44.9	13.5
50	50,000	2,000	-	-	99.0	97.5	95.1	90.5	77.9	60.7	36.8	8.2
60	60,000	1,667	-	-	98.8	97.0	94.2	88.7	74.1	54.9	30.1	5.0
70	70,000	1,429	-	-	98.6	96.6	93.2	86.9	70.5	49.7	24.7	3.0
80	80,000	1,250	-	-	98.4	96.1	92.3	85.2	67.0	44.9	20.2	1.8
90	90,000	1,111	-	-	98.2	95.6	91.4	83.6	63.8	40.7	16.5	1.1
100	1×10^5	1,000	-	99.0	98.0	95.1	90.5	81.9	60.7	36.8	13.5	.7
200	2×10^5	500	99.0	98.0	96.1	90.5	81.9	67.0	36.8	13.5	1.8	-
300	3×10^5	333	98.5	97.0	94.2	86.1	74.1	54.9	22.3	5.0	.25	-
400	4×10^5	250	98.0	96.1	92.3	81.9	67.0	44.9	13.5	1.8	.03	-
500	5×10^5	200	97.5	95.1	90.5	77.9	60.7	36.8	8.2	.7	-	-
600	6×10^5	167	97.0	94.2	88.7	74.1	54.9	30.1	5.0	.25	-	-
700	7×10^5	143	96.6	93.2	86.9	70.5	49.7	24.7	3.0	.09	-	-
800	8×10^5	125	96.1	92.3	85.2	67.0	44.9	20.2	1.8	.03	-	-
900	9×10^5	111	95.6	91.4	83.6	63.8	40.7	16.5	1.1	.01	-	-
1,000	1×10^6	100	95.1	90.5	81.9	60.7	36.8	13.5	.7	-	-	-
2,000	2×10^6	50.0	90.5	81.9	67.0	36.8	13.5	1.8	-	-	-	-
3,000	3×10^6	33.3	86.1	74.1	54.9	22.3	5.0	.25	-	-	-	-
4,000	4×10^6	25.0	81.9	67.0	44.9	13.5	1.8	.03	-	-	-	-
5,000	5×10^6	20.0	77.9	60.7	36.8	8.2	.7	-	-	-	-	-
6,000	6×10^6	16.7	74.1	54.9	30.1	5.0	.25	-	-	-	-	-
7,000	7×10^6	14.3	70.5	49.7	24.7	3.0	.09	-	-	-	-	-
8,000	8×10^6	12.5	67.0	44.9	20.2	1.8	.03	-	-	-	-	-
9,000	9×10^6	11.1	63.8	40.7	16.5	1.1	.01	-	-	-	-	-
10,000	10×10^6	10.0	60.7	36.8	13.5	.7	-	-	-	-	-	-

5. MINIMUM FLIGHT EXPERIMENT

The minimum flight experiment is, as defined, that minimum experiment which will provide meaningful data regarding the performance of reflective surfaces in the space environment. Such minimum meaningful data can be supplied by a simplified version of the reflectometer previously described. Spectral measurements, separation of effects, redundant samples and vehicle orientation would not be provided.

The vehicle chosen to support the minimum experiment is the P-11 Flight Test Vehicle provided by Lockheed Missiles and Space Company (LMSC). The P-11 is a piggyback structure carried to initial orbit by the Agena vehicle. The P-11 is then released and a self-contained rocket motor places the P-11 in its own, different orbit. Other piggyback configurations, such as SATAR supplied by General Dynamics/Astronautics, were considered. However, detailed data were not obtained in time for inclusion in this study. Data concerning the P-11 were obtained from LMSC report number A051977A, February 1963 revision, Detail Specification Covering Flight Test Vehicle Program 11, and discussions with LMSC staff members.

Any experiment placed aboard a piggyback vehicle is subject to compromise and limitations in several areas. Among these are: (1) limitations in dimensions, volume, weight, and electrical power, (2) restricted choice of launch times and directions, and (3) increased cost due to the large number of physical and temporal interfaces and extensive liaison. Some of these are discussed in more detail in the following subsections.

5.1 Minimum Reflectivity Experiment

The reflectometer provided for the minimum experiment is of the same basic design as that described in Section 4.2. However, some important changes are made in order to accommodate the P-11 limitations. Firstly the flat surface dimension and location of payload volumes of the P-11 are such that the maximum number of sample positions available is ten. As illustrated in Fig. 5-1 the reflectometer would mount on one of the front-outboard surfaces of the P-11. The thermal control surfaces on the front and back of the vehicle are not available for instrumentation. The reflectometer would displace 5 solar panels from the surface.

The clearance between the P-11 and the Agena shroud is quite limited, being less than one inch maximum. This then requires that no portion of the reflectometer extend past the nominal envelope of the P-11. Considerable structural modification is required in the outboard section since the recessed reflectometer and sample disk would displace several support ribs in the basic structure. Additional structure would be required to carry loads around the reflectance instrument as it would not be a load-bearing element.

The reflectometer itself would accept ten sample surfaces, and provide full scale and dark calibrate positions. The light source would be a tungsten lamp while the detector is a single lead sulfide cell. Lamp and detector characteristics and operation would be the same as previously described. The optical and mechanical design would be similar to that for the preferred experiment, differing only in detail as required by the P-11 configuration. It should be noted that the recessed location of the sample surfaces coupled with the fact that the sample disk does not nominally face the sun, results in a less than maximum exposure to solar radiation.

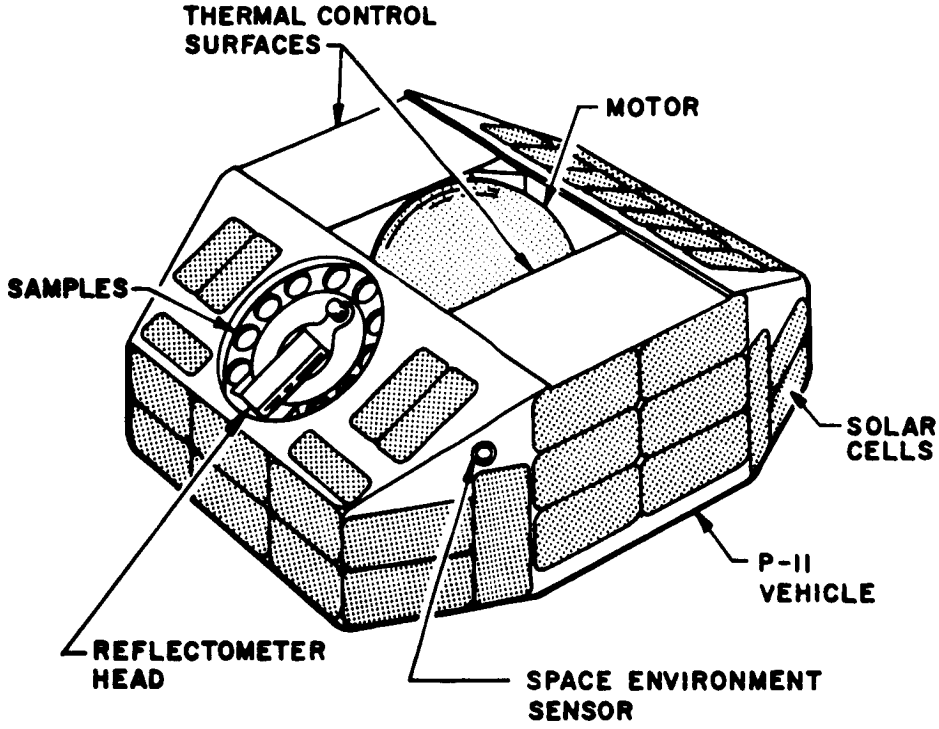

FIG. 5-1 MINIMUM FLIGHT EXPERIMENT

5.2 Orientations and Orbits

It is unlikely that controlled orientation can be applied to the P-11 vehicle without extensive modification. The expense of the orientation system and vehicle modifications are deemed unjustified for a minimum experiment. Since the P-11 is spin-stabilized it would tend to point toward the sun for six months and in the opposite direction for six months. The geometry and dynamics of the vehicle are such that gravity gradient, magnetic and aerodynamic perturbations are high.

Two P-11 models with different telemetry and rocket motors are available. The model 0207 can, typically, put a 50-pound instrument load into an orbit of 224 n. mi. perigee and 250 n. mi. apogee. The drag lifetime is about 8 months. The model 1207 will orbit the same load with a perigee of 210 n. mi. and an apogee of about 2500 n. mi. Drag lifetime in this case is in excess of 20 years. The above orbital calculations are based on an initial (Agena) orbit of 113 n. mi. perigee, 224 n. mi. apogee and 65 to 105 degree inclination.

5.3 Additional Instrumentation

The exact amount of additional instrumentation that could be applied to the minimum experiment is critically dependent upon the extent of structural modifications required to accommodate the sample plate and reflectometer. It is anticipated that sufficient weight and volume would remain available to perform most of the space environment measurements discussed in Section 4.2.

Temperature measurements of the reflective surface samples would be accomplished in the same manner as on the preferred experiment.

Since the P-11 vehicle would not be sun oriented it is necessary to make a measurement of the integrated solar flux incident on the sample plate. While indicating the extent of sample exposure the measurement would offer some insight as to the causes of temporal changes in reflectivity. An integration time of about one day would provide sufficient accuracy and resolution.

5.4 Telemetry and Command

The design efforts for the minimum experiment telemetry and command systems is minimized by the fact that they are included as part of the P-11 flight vehicle package.

Study of these two P-11 vehicle subsystems shows that the standard command system requires no modification to meet the requirements. The only modifications required will be those to meet the telemetry-reflectometer instrument interface requirements. The block diagram of the P-11 telemetry and command systems is shown in Fig. 5-2. Modifications and connections required for this experiment are indicated by dashed lines.

Ten temperature measurements will be fed into Ring No. 2 of the 1 x 60 commutator. This requires no modification of the telemetry system. Since these are dc voltage measurements, the one frame per second rate is suitable.

The detector data rate is determined by the reflectometer head rotation and the number of specimen positions. The head speed is 2/3 revolution per second with twelve sample positions. This provides an output pulse rate of 8 pulses per second. To adequately reproduce this waveform a data transmission bandwidth of approximately 30 cycles per second is needed. Since the sampling rates of the existing commutators are inadequate for transmission of this bandwidth a separate voltage-controlled oscillator (VCO) must be used. IRIG channel 8 will be adequate for this data rate. VCO's suitable for operation with the nominal 20-millivolt output of the lead sulfide detector are available. Additional measurements such as the integrated solar flux detector may be accommodated through the existing "research instrumentation" channel.

The P-11 telemetry system is of the FM/FM type operating in the 215 to 245 megacycle band. Reception at this frequency is apparently not available in the Minitrack network. Thus a transmitter operating in the 136 megacycle band must be substituted for the existing

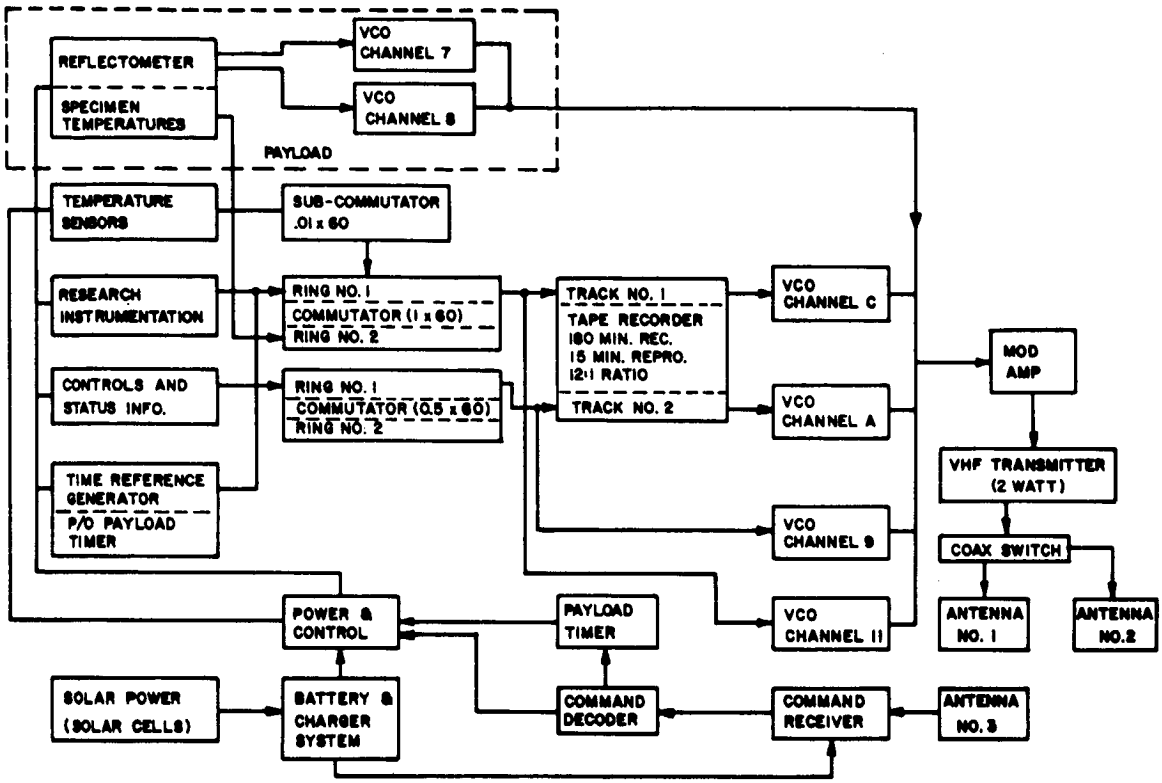

FIG. 5-2 BLOCK DIAGRAM OF P-11 TELEMETRY AND COMMAND SYSTEM

transmitter. If this change in transmitter is made the transmitter antennas must be redesigned for proper operation at the lower frequency. Since the existing tape recorder is not required for the reflectivity experiment nor for vehicle status monitoring, it and its associated VCO's may be removed. The recorder and VCO's weigh approximately ten pounds.

Allowing for the greater and more unpredictable errors associated with FM/FM telemetry, the minimum experiment and transmission error would be about 5 percent.

5.5 Power System

The minimum experiment will employ the P-11 vehicle's existing power system. The system employs filtered solar cells in conjunction with a nickel-cadmium storage battery. The P-11 power system provides an unregulated voltage of 22 to 29.25 volts. The average power output over any one orbit will vary from 8 to 28 watts. The maximum discharge rate is 90 watts or 80 watt-hours per orbit. Minimum battery capacity is 4 ampere-hours while the solar cell output is about one ampere. The removal of the 5 solar panels to accommodate the reflectivity experiment will reduce the power system capability by about 20 percent. The system is designed for a six-month mission.

6. SUBTASK 3.1 - GROUND SIMULATION TEST DEFINITION

6.1 Introduction

The ensuing subtask report reflects the results of efforts expended in Task 3.1, Ground Simulation Test Definition. In the performance of this task, an intensive literature search was conducted, and a number of authorities were contacted in order to amass sufficient data to establish awareness of the state of the art regarding the techniques and circumstances that might affect a suitable ground simulation test program. Those areas where reference data were incomplete (or contradictory) were pursued to a point where either conclusions could safely be drawn, or where a specific problem or type of uncertainty could be defined.

These data were complied and referred to in the description of the resulting testing that is outlined in this report. Due to the extensiveness of the information studied in the performance of this task, it was determined that only pertinent technical abstractions and limited discussions would be presented in this report.

The first step in the development of the required outline was to establish the basic testing approach and philosophy in terms of the information made available by Subtasks 1.1, 1.2, and 1.3, in the light of the fundamental limitations of existing test instruments. This suggested basic test philosophy, and various considerations based on earlier task results, is given in the general discussion to follow. A detailed look into the problems of the suggested tests is then given and specific techniques and procedures are outlined, along with anticipated test durations in Section 6.3.

The outlined test sequence and the conclusions drawn regarding techniques and procedures are given as representative of best knowledge to date.

6.2 General Discussion

6.2.1 Samples to be Tested

Work done as part of Subtask 1.2 has resulted in a list of samples that will warrant further testing for space endurance. This list was divided into three groups by priority. The first group represented the minimum selection of samples required for a meaningful flight test. The second group added several desirable samples, and the third group completed the list. Regardless of which samples are used in the flight test, it would be desirable to include them all in the ground simulation testing program. An obvious advantage of the ground testing program is that additional samples not presently anticipated could be added to the list at the last minute. Those samples that are tested both in space and on the ground should yield correlation data between the two tests and thereby provide a basis for significantly evaluating additional samples that might be tested on the ground only. The specific selection of samples to be tested will not affect the basic approach for the ground testing and therefore will not be shown again.

6.2.2 Space Environment Definition

The compilation of data resulting from Subtask 1.1 is intended to define the types of environment that should be experienced by the samples to be tested. In the space tests, the samples will be exposed to all the variations that will occur due to solar duty cycle, altitude variations resulting from orbital eccentricity, and of course, other unknowns that cannot be anticipated at this time. However, the ground simulation test will establish how these specimens respond to known environments, thereby establishing a form of "yardstick" for better interpreting the results of the space test. Consequently, the testing parameters for the ground simulation tests will be based on worst case conditions. In order to expedite the ground testing program, certain aspects of the testing may be accelerated

where it can be determined that the net effect on the reflectivity of a given sample is the result of the integrated testing and that no misleading side effects would interfere with the ultimate validity of the test. Full elaboration on the actual test procedures and durations will be given later in this report.

6.2.3 Thermal Considerations

Subtask 1.3 (Analysis and Prediction) has established various maximum and minimum temperature limits that can be anticipated in the ultimate space application of the various samples listed. These values must, of course, be classified as tentative until substantiated by actual space testing. However, they can be used advantageously for establishing a temperature range capability required in ground testing. A thermal testing phase is planned in which such characteristics as the ratio of absorptivity to emissivity and thermal conductivity in a vacuum will be determined for each type of specimen under test. The results of this test combined with the calculations performed in Subtask 1.3 will better define the temperature ranges that may be anticiapted in space. The actual temperature extremes to be experienced by the samples in space will be strongly dependent upon factors that cannot now be defined, such as the thermal conductivity in the support structures that might be used. Much of the information of this type must be gained actually from a flight experiment. The ground simulation testing will yield the most useful form of complimentary information by making temperature an independent variable. That is to say, all of the subsequent testing on the various samples on the ground may be performed with their temperatures held at the anticipated extremes, as well as possibly an intermediate value arbitrarily selected for the purpose of continuity.

6.2.4 Pressure Considerations

A simple market survey has established the inability to simulate actual space pressures, such as 10^{-15} torr. However, the lowest pressures available with even the most exotic test

equipment would be on the order of 10^{-10} or 10^{-11} torr. The analysis and predictions subtask work regarding pressure effects shows that it is not justified in the ground testing to attempt to achieve pressures lower than 10^{-5} or 10^{-6}. The ground testing will yield its designated share of the program data quite adequately at this pressure level. The large sums of money that would be required to achieve more extreme pressure levels could be better spent in the perfecting of the flight test portion of the program, which will yield the ultimate answers anyway. The operating capabilities and characteristics of the vacuum system and test chamber will be elaborated upon in a later portion of this report where these devices are discussed.

6.2.5 Micrometeoroid Investigation

Results of the Analysis and Prediction (Subtask 1.3) in this report indicate that micrometeoroid bombardment will not seriously degrade the reflectivity of metal-substrate mirrors. Other types of mirrors, e.g., the Mylar-foam, epoxy-substrate and diffusion-barrier types, may degrade in a significantly different manner from the metal-substrate types. However, very little data are available on which predictions of reflectivity changes of these other types might be based. Therefore, ground simulation tests to detect gross differences among the various types with respect to micrometeoroid bombardment effects would appear to be desirable.

Complete simulation of the space micrometeoroid environment would be extremely difficult. Also, the statistical information available is based on relatively few samplings. These facts tend to strongly support the need for an actual flight experiment in the generation of reliable, meaningful data. Ground simulation testing would be desirable for establishing degradation rates under known, controlled conditions, so that the percentage of the degradation of the flight-test samples directly attributable to micrometeoroids can be determined.

Whipple's most recent estimate (Ref. 42) of this environment gives the mean velocity as 2.2×10^6 cm/sec, the mean density as 0.44 g/cm^3, and the distribution function as $N = 3.31 \times 10^{-19} \times m^{-1.34}$, where N is the number impinging per square cm per second and m is the mass in grams.

The most generally used apparatus for generating hypervelocity particles is the light-gas gun (Ref. 63). With the present state of the art, particles in the mass range of 10^{-3} to 10 g may be accelerated up to velocities near 1.0×10^6 cm/sec with this apparatus. Both the relatively low velocity and the relatively large mass of these particles makes the light-gas gun a poor choice for micrometeoroid simulation. For example, the impingement rate for particles of 10^{-3} g mass or greater, calculated from Whipple's estimate, is approximately one meteoroid per hundred years on an area of ten square meters.

A novel, and much more suitable hypervelocity particle generator, located in the Los Angeles area, has recently come to our attention. This is a facility in which positively charged iron and graphite particles of 10^{-10} g mass and less have been accelerated up to 2.9×10^6 cm/sec by a 2 Mev Van de Graaff accelerator (Refs. 64 and 65). This apparatus apparently has the capability of supplying particles in both the mass and velocity ranges of interest for micrometeoroid simulation. We have been informed (Ref. 65) that this facility is available, on contract, for bombardment of samples.

Due to the specialized nature of the micrometeoroid simulator it would probably be necessary to conduct this part of the ground simulation program as an independent experiment. Samples of the various mirror types could be bombarded with a relatively small number of similar particles and then examined and compared with respect to damage of the surfaces. It is believed this procedure would, as a minimum, yield valuable information on the relative resistance of the different types of mirrors to the space micrometeoroid environment.

6.2.6 Ground Simulation Testing Philosophy

Perhaps the keynote of the ground testing philosophy would be to primarily perform such testing and derive such data as would complement the required flight testing program by the generation of correlation data, and then to augment the flight test data with supporting results on the ground and information on samples that may not be included in the flight test due to various practical limitations. Reaction to individual and cumulative stimuli will be determined, compared, and analyzed for consistency and significance. This approach will facilitate the determination of weakness of certain specimens to specific types of stimuli as well as revealing the "blanket" effect of cumulative space phenomena. This exhaustive ground testing program may be executed according to the following plan:

1. Thermal Tests. These tests would be performed for the purpose of defining pertinent thermal characteristics of the samples under vacuum. This information would be used in the ultimate definition of the temperature extremes to which the various samples would be subjected during all subsequent ground testing. Any other characteristics of the samples affecting their reflectivity as a function of strictly thermal conditions would be studied and classified at this time.

2. Electro-Magnetic Radiation Test. This test would be performed on each sample to determine reflectivity degradation as a function of time at each of three temperature levels, maximum temperature, minimum temperature, and the mean arbitrarily selected temperature. Source radiation would cover the significant spectral ranges between 25,000 angstroms and approximately one angstrom, while vacuum would be maintained at a constant, predetermined level. The test setup should have sufficient versatility to allow subsequent testing

of selected samples within specific portions of the spectrum in the event that the inclusive electro-magnetic tests points up the need for further analysis or study.

3. Charged Particles (Electrons, Protons). This test is for the purpose of revealing any tendency toward degradation of reflectivity resulting from bombardment of charged particles exclusive of the effects of the electromagnetic radiation discussed in paragraph 2 above. Each sample would again be tested at the two extreme anticipated temperatures and a mean temperature, with the pressure being held at a constant level. The intensity of bombardment would be such that the reflective degradation versus the integrated bombardment effect could be established. The result of this testing would be curves that would be useful in extrapolating to determine the effects of this phenomenon on solar concentrator devices for the period of time that they are intended to be used.

4. Combined EMR and Charged Particles. This test could be the culmination of the sequential ground test program, wherein new samples of the same types previously tested would be exposed simultaneously to electromagnetic radiation and bombardment by charged particles. The results of this test would not only substantiate the results achieved by the individual tests preceding, but would also expose any peculiar manifestations that might occur in the presence of both environments but not in the presence of either one individually. It is conceivable that this test could also expose any peculiar effects that might result in the presence of only one test but would be inhibited in the presence of both types of environments. At any rate, this final test should adequately complete the ground simulation test program

leaving few stones unturned, if any, in the rigors of establishing conclusive results. (It is to be re-emphasized at this time that the extensiveness of the ground test program must be optimized in the light of practical considerations to compliment the space test and not to replace it. The actual flight test is recognized to be necessary and inevitable in the ultimate determination of the information required.)

5. Additional Tests. There are additional types of tests which would be desirable to perform on the ground, yet need not appear as part of the testing sequence here outlined. It would be premature to attempt to enumerate the various tests that might fall into this category at this time. However, an example of the type of test that might be desired would be the investigation of various protective coatings, which could be incorporated to protect the surfaces from the earth's atmosphere and during the ascent of the vehicle through the atmosphere, and then sublimate in space leaving the reflective surfaces untarnished. Goodyear Aircraft Company, in Akron, Ohio, manufactures a "photolizable" film that has been used in similar applications, and certainly other materials such as napthalene, might warrant investigation. Another test that could be performed independent of the described testing sequence is the investigation of the effects of micrometeoroids on the reflectivity of various samples. It is felt, however, that in spite of the usefulness of this ground test, the ultimate set of data must be derived by the actual flight experiment. Micrometeoriod simulation has been discussed in Section 6.2.5.

Descriptions and discussions of the various phases of the ground testing sequence will be given in greater detail at a later point in this report.

6.3 Test Program

This section of the report is intended for the detailed discussion of the various tests comprising the suggested ground test sequence.

A tentative schedule is shown in Fig. 6-1, which shows the anticipated time-table for the entire ground simulation testing program. This schedule is based on rough estimates and is suggested in terms of the data known to date in this study program. As new information becomes available that would affect the timing or procedures discussed, the ground test schedule should be revised accordingly. The methods, types of equipments and procedures are presented in some detail, and are based on the results of extensive investigations into the state of the art. The methods of other major space-simulation facilities, and the capabilities of existing test instrumentation are considered, as well as reliability and economic factors in the resolution of the following series of ground simulation tests.

6.3.1 Thermal Study

1. Purpose and Justification

The purpose of this first set of tests is primarily the determination of values of absorptivity, emissivity and thermal conductivity for each of the various mirror samples to be evaluated subsequently for degradation. These experimental results will be used in the thermal balance equations, shown in the Subtask 1.3 portion (Section 2.3) of this report, to arrive at a set of extreme temperatures for each sample. The mirror samples may then be studied for degradation in the presence of various space phenomena while they are held at their respective extreme temperatures, as well as some convenient nominal temperature.

In the process of performing these thermal studies, any unusual reflectivity degradation that might result strictly as a function of temperature and vacuum, will be discovered, analyzed and classified.

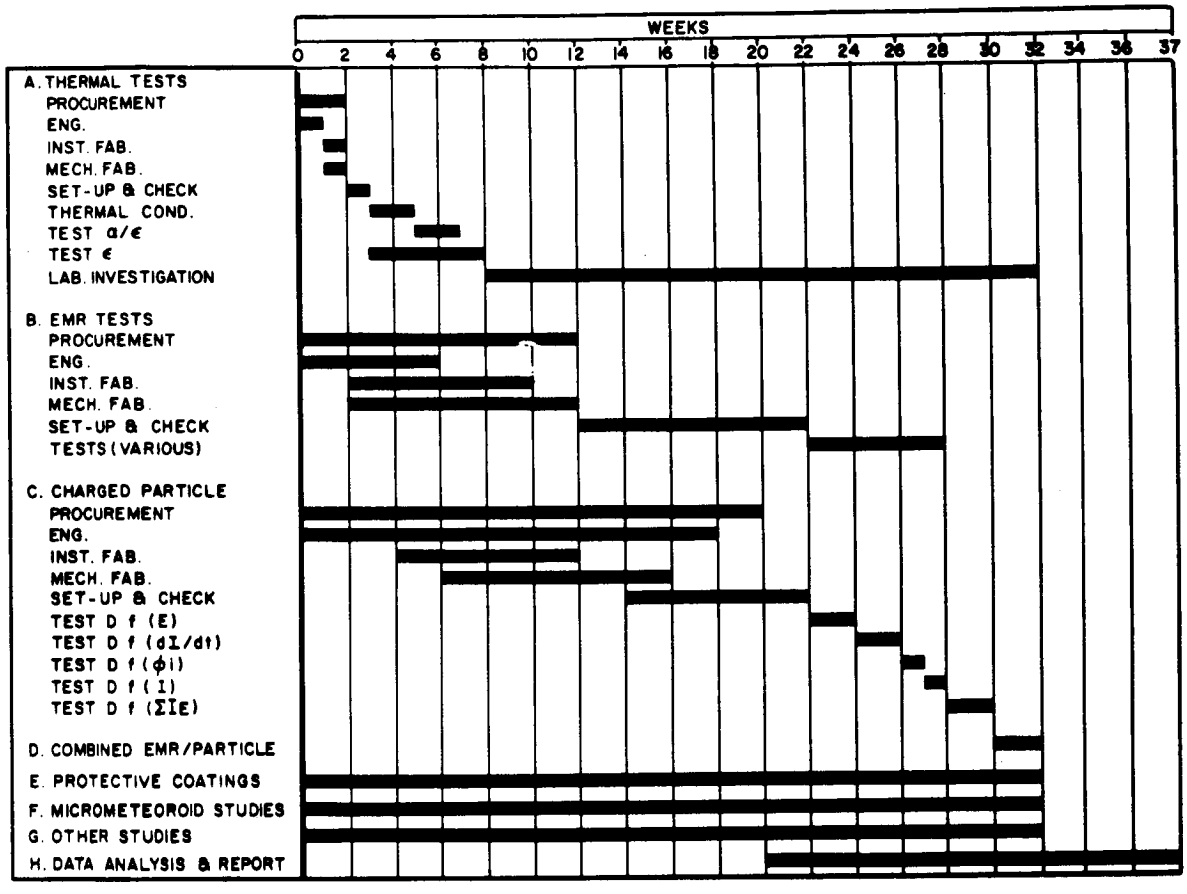

FIG. 6-1 TENTATIVE GROUND SIMULATION TEST SCHEDULE

2. Description of Test Setup

Figure 6-2 is a schematic description of the test setup that will be employed in the determination of thermal conductivity. The sample will be clamped between aluminum plates to be used for thermal integration. One plate will have an electrical heating device attached to it that can be controlled remotely. A suitable heat sink will be attached to the opposite aluminum plate. This entire assembly (except for controls and indicators) will be enclosed in a vacuum chamber. A differential thermocouple will be employed in the measurement of temperature difference through the thickness of the specimen. A conventional thermocouple will be used to monitor the temperature of the heater.

Figure 6-3 is intended to describe the test setup to be used in the measurement of absorptivity/emissivity. The sample is supported by spokes, having low thermal conductivity, to a support ring with a built-in electrical heater. A differential thermocouple is used to determine the temperature difference between the sample and the support ring. The ring is, in turn, supported by a fixture (not shown) having low thermal conductivity. The experiment is enclosed in a liquid nitrogen cooled compartment with a black interior surface to simulate space.

A solar irradiation simulator (a special carbon arc) will be directed at the sample. The temperature of the support ring will be monitored by a conventional thermocouple. The entire experiment will be enclosed in a vacuum chamber with the exception of the control and measurement equipment and the light source.

The test setup for the measurement of effective emissivity is shown in Fig. 6-4. Similar to the previously discussed test setup, this experiment is performed in a vacuum chamber with nitrogen-cooled walls surrounding the samples. The sample configuration must be such as to allow internal electrical heating by the insertion of a disc-shaped heating element. A thermocouple will

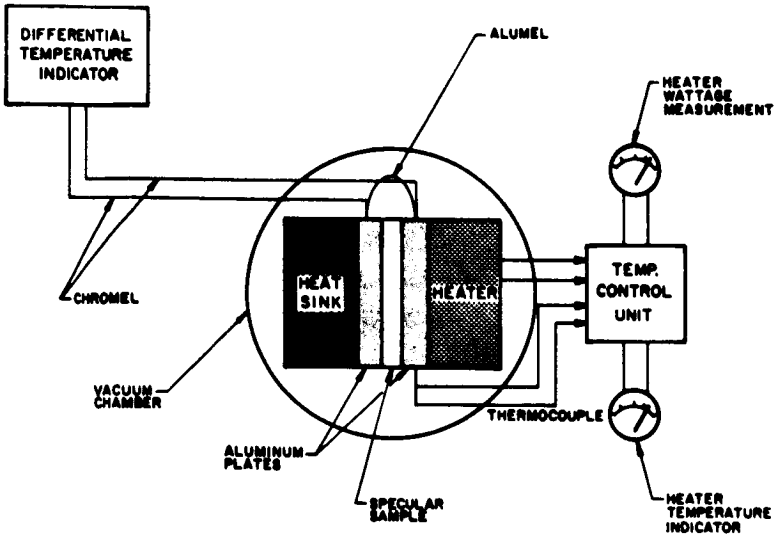

FIG. 6-2

MEASUREMENT OF THERMAL CONDUCTIVITY

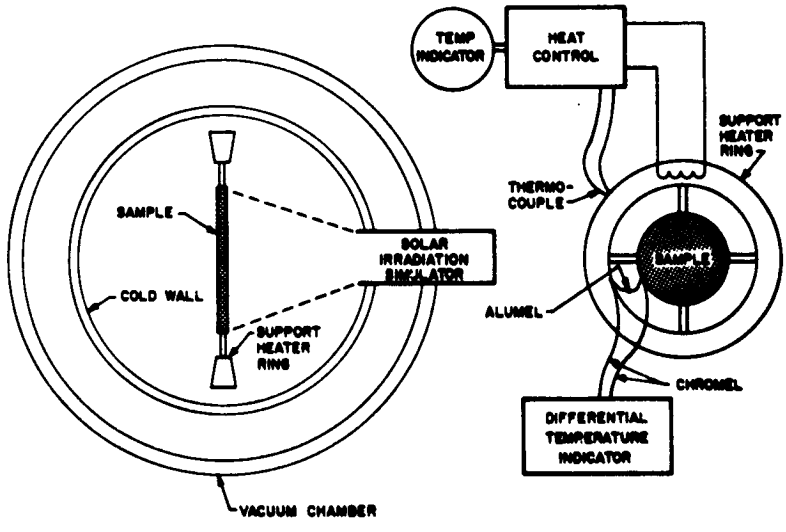

FIG. 6-3

MEASUREMENT OF $\frac{\alpha}{E}$ OF REFLECTIVE SURFACES

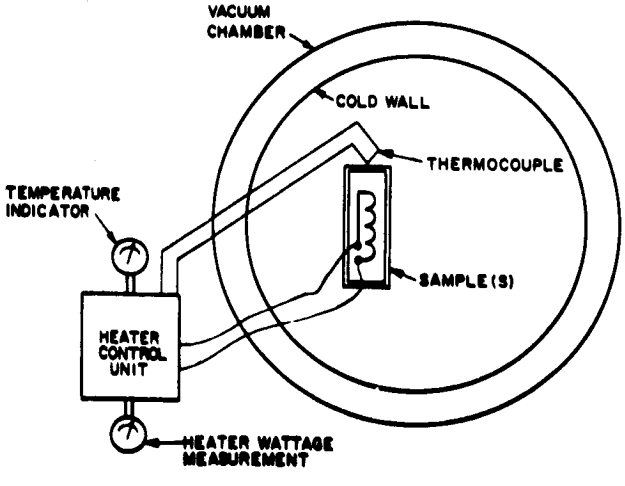

FIG. 6-4

MEASUREMENT OF EFFECTIVE EMISSIVITY (E) OF REFLECTIVE SURFACES

be used to measure the temperature of the sample. An external control unit will be required for adjusting heater power input to maintain the sample at a constant temperature level. A meter will be used for accurately measuring heater input power.

In addition to the above test setup requirements, facility for the inclusion of a reflectivity measurement should be considered, in the event that some unusual mirror degradation is found to occur in the execution of the described testing. Appropriate reflectivity measuring techniques are discussed in the later portion of this report concerning electro-magnetic radiation tests.

The following portion of the report describes the actual procedures to be used in the performance of these tests.

3. Test Conditions and Procedures

In the performance of the thermal conductivity measurements, a sample of known dimensions will be clamped into the test fixture and the vacuum chamber will be lowered into place. Upon producing the required level of pressure (approximately 10^{-6} torr), the heater will be turned on. When the differential temperature indicator has stabilized, its reading and the heater wattage reading will be recorded. A simple formula, shown below, can be used at this point to establish the thermal conductivity of the sample under test.

$$K = \frac{tH}{4.186\ A\ \Delta T}$$

where:

K = thermal conductivity (cal/sec/^{o}C)

t = thickness of sample (cm)

A = cross-sectional area (cm^2)

H = heater power input (watts)

ΔT = differential temperature

This test can first be performed on materials of known thermal conductivity to establish the reliability of the procedure.

The measurement of the ratio of absorptivity to emissivity may be performed by the following procedure. Two samples to be tested may be bonded back-to-back (or a single sample with a reflective surface on both faces may be used) and mounted within a support ring. Conducted heat losses to the support ring will be avoided by maintaining the ring temperature at the same level as the sample temperature by use of an electric heating element built into the ring. This is done by comparing these temperatures with a differential thermocouple device and adjusting heater power to maintain zero indication. The experiment is first placed into the vacuum chamber, which is evacuated to a pressure of approximately 10^{-6} torr. As solar type irradiation is applied, the temperature of the sample will rise to its thermal balance point. The support ring temperature, which is made to track the sample temperature, is measured as soon as a stable condition exists. The following calculations may then be used to determine α/ϵ.

$$\alpha AF = \epsilon 2A\sigma \left(T_s^4 - T_w^4\right)$$

where:

α = solar absorptivity

A = area of each face of the sample (cm^2)

F = irradiance of the source ($watts/cm^2$)

ϵ = effective emissivity

σ = Stefan-Boltzman constant $\left(\frac{watts}{^oC^4}\right)$

T_s = temperature of sample (^oC)

T_w = temperature of cold walls (^oC)

Since the temperatures are taken to the fourth power, the cold-wall temperature term becomes insignificant and may be dropped out leaving:

$$\alpha AF = \epsilon\ 2A\sigma\ T_s^4$$

or, since the A's cancel:

$$\frac{\alpha}{\epsilon} = \frac{2\sigma}{F} (T_s^4).$$

The spectral source will be carefully measured for level of irradiance. This leaves the sample temperature (or support ring temperature) as the only required data in establishing $\frac{\alpha}{\epsilon}$.

In determining the effective emissivity of a given sample, it may be heated internally with an electrical heating element. The input heating power is controlled only to maintain the sample at a constant temperature. The sample is suspended in a vacuum chamber at a pressure of approximately 10^{-6} torr, and surrounded by liquid-nitrogen cooled walls. When the temperature of the sample stabilizes, it is recorded along with the meter indication of the heater power being used. A simple formula given below provides easy calculation of the effective emissivity of the sample under test.

$$\epsilon = \frac{W}{4.186\ \sigma\ (T_s^4 - T_w^4)\ A}$$

where:

ϵ = emissivity

W = heater power (watts)

σ = Stefan-Boltzman constant ($5.67 \times 10^{-5} \frac{W}{{}^oC^4}$)

T_s = temperature of sample (^oC)

T_w = temperature of cold wall (^oC)

A = entire sample area (cm^2)

But since the temperature is increased to the fourth power, and since the temperature of the cold walls is so low, T_w can be dropped out of the equation, leaving:

$$\epsilon = \frac{W}{4.186\ \sigma\ T_s^4\ A}$$

Having established methods for determining $\frac{\alpha}{\epsilon}$ and ϵ for each of the specular samples to be tested, the determination of α becomes a simple matter of multiplying $\frac{\alpha}{\epsilon} \times \epsilon$. These resulting data will be used, as previously stated, in the thermal balance equations to more dependably define the required extreme temperature values to be used in the performance of the following tests.

4. Anticipated Meaningful Test Duration

This thermal testing portion of the ground simulation test program should not take particularly long compared to the typical test durations in the overall program. The greatest time consumption would occur in the preparation of the individual test setups and fixtures. The following estimates are on the basis of four samples each of twenty-five specular materials requiring study:

Conductivity Tests	
Preparation	4 weeks
Testing	1 week
Total Time	5 weeks
$\frac{\alpha}{\epsilon}$ Measurements	
Preparation	5 weeks
Testing	2 weeks
Total Time	7 weeks
ϵ Measurements	
Preparation	4 weeks
Testing	1 week
Total Time	5 weeks

Since the preparations for all three tests could take place concurrently, the total test duration would be about 8 weeks. This assumes the use of only one vacuum chamber.

6.3.2 Electromagnetic Radiation 50 Å - 23,000 Å

A discussion of the ground simulation facility required for duplicating solar electromagnetic radiation requires, in part, a subdivision into various spectral regions in order to present the sources, justifications, techniques and in general the rationale appropriate to each spectral region. From 23,000 Å to approximately 4,000 Å an arc source will be used. Another type of arc will be used for the 4,000 Å to 2,000 Å range while a pulsed plasma discharge will be used from 2,000 Å to 50 Å.

Each spectral range and appropriate source will be discussed with respect to: (1) purpose and justification, and (2) description of test set-up. Following the discussion of the spectral ranges and appropriate sources will be some remarks on test procedures and anticipated, meaningful test duration.

1. Spectral Ranges

a. 23,000 Å - 4,000 Å

(1) Purpose and Justification

Although the 23,000 Å - 4,000 Å range is ordinarily of concern because of thermal effects, it would seem wise to include a source for the spectral range in which 90 percent of the sun's radiation is found. This is because of possibly undiscovered degradation processes operating exclusively as a result of this particular radiation or acting as a combination process with another spectral region. The temperature of the samples will be separately controlable and will be entirely independent of irradiation. However a relatively simple extension of the solar simulator concept, so as to include cold, black surroundings would allow a dynamic investigation of mirror degradation. That is, the mutual interaction of changing temperatures and changing absorptivities could be observed in a true environmental situation. This unique capability would be a natural by-product of the exactness of the suggested solar source simulator and the intrinsic versatility of the test apparatus to be described. However, it is estimated that the ground testing required in conjunction with an actual flight test may be adequately performed with temperature separately controlled.

The inclusion of two sources in the range above 2,000 Å allows the investigator greater freedom in where to set the demarcation between the all-important ultraviolet and the visible-infrared region. Two physically separate sources in the 2,000 Å - 23,000 Å range allows separate variation of each in attempts to isolate causes of mirror degradation. There is no evidence that visible through infrared produces totally negligible effects for all materials. In particular absorbed energy per gram of absorbing material should be considered rather than absorbed energy as such. In this respect, ultraviolet-visible and infrared are potential sources of mirror degradation because of the opacity of mirror surfaces. Aluminum becomes totally transparent in the visible range for a few hundred Å aluminum film thickness. This means that the mass described by the depth is the mass in which the energy is dissipated. Even though reflectance is high over the visible and infrared for the mirror material chosen, the small spectral absorption factor is more than offset by the high concentration of energy in the solar visible-infrared spectral energy distribution.

It would also be unwise to consider that potentially harmful radiation would always strike the mirror surface and no other part of the mirror. Testing might require a mirror assembly that approximated the final space configuration in that it included some of the geometry and aluminum material of the nonreflecting, nonmetallic portion of the mirror structure. This might very possibly receive some direct degrading solar irradiation. In addition there is earth albedo present, very roughly, in proportions of 0.3, 0.4, and 0.5 of one solar constant for the infrared, visible, and ultraviolet respectively.

It should be remembered in the discussion of each of the three radiation sources that the mirror surface can never be considered a pure metal and thereby exempt from the usual nonmetal degradation effects. Some of the representative surfaces will be overcoated with SiO. Depending on the vacuum and rate of evaporation of the overcoat SiO, SiO_2, and Si_2O_3 will be present in varying proportions (Ref. 66).

It is well known that under certain common conditions of overcoating the spectral absorption of SiO begins to exert some appreciable weight in the blue and violet. It is also known that high purity fused silicon is necessary to avoid color center development with corresponding loss of transmission and that relatively little work has been done on coloration by wavelength below 3,000 Å in the presence of the longer wavelengths of sunlight. Also, the metal film itself will not be entirely free of contaminants, this too depending on the level of the vacuum and rate of evaporation as well as original purity of the metal.

The long wavelength limit chosen is the probable spectral absorption cut-off region for the relatively inexpensive glass optics to be used. The absorption itself is caused by water crystals present in the glass.

As mentioned before the short wavelength limit for this range would be dictated by the optimum solar match obtainable with the 2,000 Å - 4,000 Å source and the demarcation set thereby. Since the visible-infrared source recommended is a carbon arc there may be, for example, some benefits in including or excluding the cyanogen bands in view of the filter configurations available for the ultraviolet and visible-infrared regions and in view of the actual spectral energy distribution of the two sources determined experimentally. The solar spectrum to be matched and the carbon arc spectrum are given in Ref. 67.

(2) Description of Test Setup

A 120 amp, 5.8 volt Strong carbon arc would be used with cerium-cored electrodes and with the negative electrode offset so as to allow optimum radiation pickup by the condenser lens assembly. The radiation will be supplied by the positive crater and flame. For solar simulation purposes the cerium-core provides the best spectral match although further research in carbon cores by the National Carbon and Lorraine Carbon Companies is underway in an attempt to improve this match.

An all refractive, rather than catadioptoic, optical system is chosen primarily because it allows more space. More specifically, the source-condenser assembly can be situated a fairly large distance from the projection lens and chamber window, which would allow more space for the other source (See Fig. 6-5). The spectral range omits the 3,500 Å

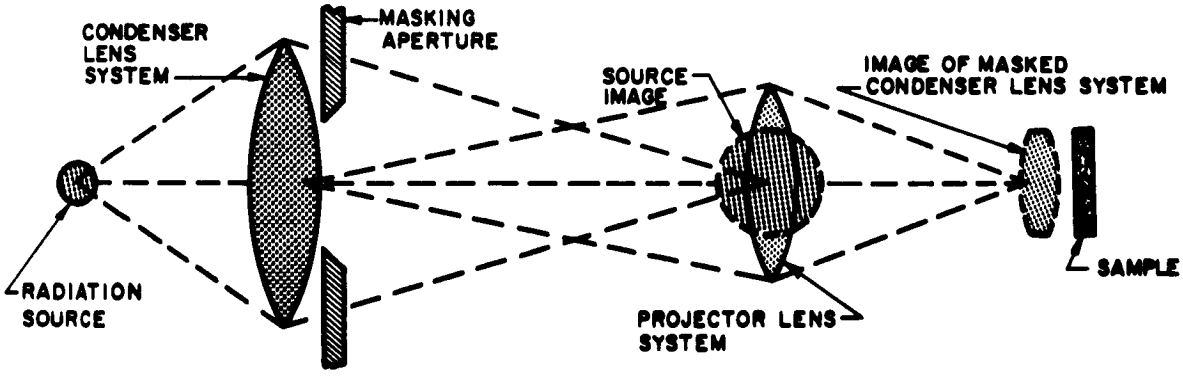

FIG. 6-5 SCHEMATIC OF CARBON ARC REFRACTIVE RADIATIVE TRANSFER SYSTEM

region in which the dispersion curve of glass is very steep. Therefore chromatic aberration is not quite so bad as it might be. It may be that, for reasons of chromatic aberration, the 2,000 Å - 4,000 Å source should be extended to longer wavelengths. That is, even less constraint would be put on the design of the glass optics for the visible infrared source if it operated in the 5,000 Å - 27,000 Å region. In addition the on-axis nature of an all refractive system facilitates alignment.

The projection principle will probably be that of a slide projector rather than the principle employed in the large commercial motion motion pictures. More particularly some optimum surface in the condenser assembly rather than the source itself will be focused on the target. Depending on the sophistication of the optics, an area of approximately 2 inches in diameter can be irradiated with ±5 percent uniformity with up to 64 solar constants. Since this high level of irradiance is not only unnecessary to anticipated accelerated testing but detrimental the optics will probably not be designed for optimum efficiency. The resultant saving in cost would be greater than designing a more efficient set of optics with a less powerful arc. Less powerful arcs, incidentally, that can match present requirements are nonexistent.

Different levels of irradiation might be supplied by an iris diaphragm at the projector lens or by operating the source at different power levels in view of the known absence of any first order effects on the visible-infrared spectrum. Irradiation could be attenuated by known amounts through the introduction of neutral density screens at an appropriate point in the optical path. There is no need to be concerned with the discontinuous nature of a screen causing discontinuous irradiation on the sample, because the screen image would not be placed at a conjugate focal point of the source. In order to supply different levels of irradiation another alternate approach is the use of several projector lenses with suitable focal lengths should be made available as well as appropriate masking apertures for the condenser assembly. The distance from projector lens to sample would be different for each. If feasible a simplified zoom concept might be considered.

The sample may possibly be irradiated at an angle to the sample normal because of spatial restrictions. Due consideration would have to be given to irradiance non-uniformities in such a case. (Ref. 68).

Arcs have been defined in the literature but two characteristics nearly all share are a negative, or practically zero, volt-ampere characteristic and a voltage at the cathode of the order of the minimum ionizing or exciting potential of the gas or vapor. The former necessitates a ballast resistance or reactance in series with the arc. The combined volt-ampere characteristic and resulting stability of the two in series has been well described by various workers. (Ref. 69).

The carbon arcs at one atmosphere of pressure can be classified as a high pressure arc. The boundary is determined by the pressure at which electrons and gas molecules approach thermal equilibrium, approximately 10 mm of mercury. The usual luminous and dark structured regions characteristic of lower pressure discharges merge and the discharge appears to consist entirely of a positive column. As a result the voltage gradient of a high pressure arc is much larger than the low pressure arc resulting in a much greater power input per unit length of the arc. The gas temperature in the compact arc is more uniformly distributed in an approximately cylindrical sense, between the two electrodes, the hottest regions in the more common arcs ranging from 5,500 ^{o}K - 8,000 ^{o}K. The temperature of the carbon arc positive crater has been determined to be about 4,000 ^{o}K.

The spectrum of the carbon arc in this case will be the spectrum of the incandescent positive carbon crater with the spectrum of the emitting atmospheric gas superimposed on it. The cyanogen bands around 3,850 Å are a noticeable feature of this spectrum. All regions except the ultraviolet can be expected to increase approximately linearly with the current while the ultraviolet increases more rapidly than the current.

b. 4,000 Å - 2,000 Å

(1) Purpose and Justification

Of the degrading effects that have been observed on materials exposed to simulated solar radiation, it is safe to say a majority have been attributable to this region of the spectrum. This is partially a result of a concentration of testing in this region of the spectrum to the exclusion of visible-infrared and vacuum ultraviolet irradiation. As mentioned before no new, first-order effects have been attributable exclusively to the visible infrared portions of the spectrum; however, vacuum ultraviolet radiation simulation presents many technical difficulties. The 2,000 Å - 4,000 Å regions comprise what is generally known as the near and far ultraviolet. Extreme or vacuum ultraviolet strictly extends from the Schumann-Runge oxygen absorption bands around 1,800 Å to the soft x-ray region around 50 Å.

The near and far ultraviolet comprise approximately 10 percent of the sun's electromagnetic radiation. This in addition to the general tendency of materials to become absorbing in this spectral region sets it as a region of potential importance for mirror degradation studies. Recent findings of Hass (Ref. 70) on the effects of ultraviolet irradiation on the ultraviolet reflectance of slowly deposited SiO aluminum mirror overcoatings indicate that much is still to be learned on radiation material interactions in this spectral region. Metals are not exempt from possible optically degrading effects. An example of findings of interest is the work of Ivanova et al who measured reflectance degradation of aluminum and rhodium mirrors for irradiation in the Schumann region of the spectrum (1100 Å - 1800 Å) under the action of ultraviolet light in a vacuum (Ref. 71). Some ultraviolet of longer wavelength was undoubtedly present in their test. As mentioned previously, earth albedo supplies a not insignificant portion of the ultraviolet. Much of the damage to non-metals such as mirror surroundings and mirror overcoating has been attributed to this region. Two likely sources for attaining the

required match are the zenon and mercury-xenon compacts arcs. The general filter configurations required for matching these sources to the solar ultraviolet spectrum are shown in Fig. 6-6. Data for the spectral output of these sources was supplied by the Englehard-Hanovia Industries compact arc catalog.

(2) Description of Test Setup

A xenon compact arc source is recommended for the near and far ultraviolet for several reasons. First it is a source with a continuous spectrum in the region of interest just as is the sun. When thermal considerations only are important, the adequacy of the final filtered source spectrum only makes sense in view of the anticipated number of different materials to be irradiated or in other words the anticipated materials show the greatest variation, (one from another), in spectral absorptivity provided of course that there is significant solar radiation present in these regions to begin with. One joule of radiation absorbed at 4,000 Å creates the same thermal effect as one joule absorbed at 2,000 Å. However quantized effects characterized by certain threshold wavelength regions begin to appear in the ultraviolet so that as close a match to the solar spectrum as is possible should be attempted.

The xenon arc is quickly reignited and can be considered to give its typical spectrum instantaneously upon ignition. Like the carbon arc the xenon arc approximates a point source. This approximation is fundamentally important to ease of radiative energy transfer in optical systems. In short, a compact arc reduces the size and simplifies the design of the optical elements.

The same collector-projector concept would be used in transferring radiation from the source to the sample as was used for the carbon arc. In particular, however, there will be an attempt to avoid refractive elements because of the rapidly changing slope of the quartz dispersion curve and the consequent difficulties with chromatic aberration. Ultraviolet achromats of any size are extremely expensive since they usually require correction by a sapphire lens. Reflectance of

SiO coated aluminum mirrors can be made to approach 90 percent through this entire spectral region. Ideally then this would suggest an off-axis collecting mirror (or a pair of such mirrors) possibly corrected for spherical aberration, which would transfer the magnified arc image to a projecting mirror (or mirrors) also corrected for spherical aberration (see Figs. 6-7 and 6-8). The projector mirror would then image the collecting mirror on the sample at a magnification of less than unity. The latter condition necessitates that the distance from target to projector element be small with respect to the distance from the collector element to the projector element. This is the same condition as was necessary with the carbon arc refractive system except in this case a doubling back is necessary because of the off-axis conditions dictated by the use of mirrors. Several solutions are available. However, it may be advantageous to use a reflective collector and a refractive suprasil quartz projector since field lenses are rarely ever achromatized and the projector in this case would be acting as a field lens. Such a design would ease the spatial constraints. Different levels of irradiation would be accomplished by the same methods as were listed for the carbon arc.

Ultraviolet sources call for extreme care in the determination of spectral energy distributions. Several factors contribute to this. First, there are no really satisfactory spectral intensity standards for this region of the spectrum, and virtually none at all in the vacuum ultraviolet (Ref. 72). Second, the use of prisms with their rapidly changing reciprocal linear dispersion present several difficulties in itself, most of which are related to the need for a constant spectral slit width (Ref. 73). Many lamp manufacturers use prism instruments in determining their source spectral energy distributions in order to cover as wide a spectral range as possible with their spectroradiometer. The results are erroneous spectral energy distributions. In addition the shorter wavelengths are much more susceptible to changes in intensity from

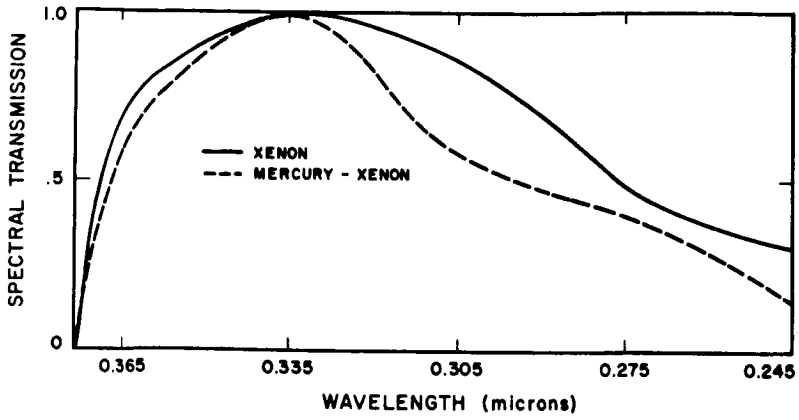

FIG. 6-6

SOLAR ULTRAVIOLET FILTER CONFIGURATIONS FOR XENON AND MERCURY XENON COMPACT ARCS

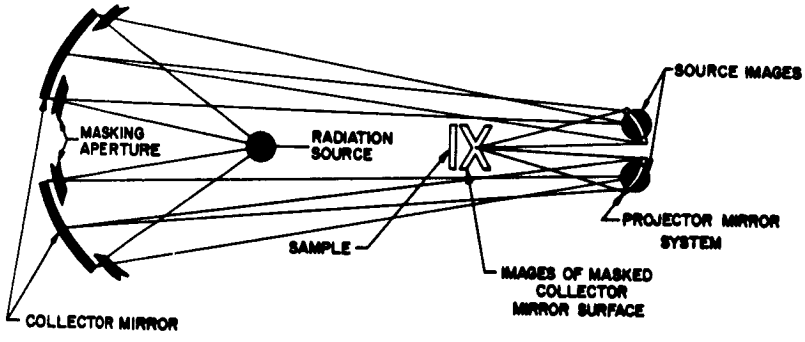

FIG. 6-7

SCHEMATIC FOR XENON ARC REFLECTIVE RADIATIVE TRANSFER SYSTEM

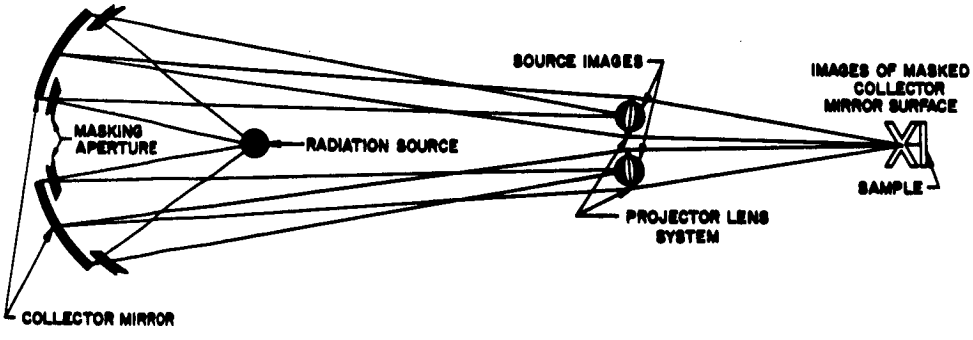

FIG. 6-8

SCHEMATIC OF XENON ARC CATADIOPTRIC RADIATIVE TRANSFER SYSTEM

temperature variations and therefore sources are more unstable for the shorter than for the longer wavelengths. This can be seen from an examination of the exponential dependence on temperature found in the Boltzmann equation. These considerations call for determinations of spectral energy distribution separate from those supplied by the lamp manufacturer.

The spectral radiance of a xenon arc operating at 20 atmospheres has been found to be considerably greater than that from the positive crater of a carbon arc (Ref. 74). The importance of this lies in the fact that a given optical system can produce a higher irradiance with a source of higher spectral radiance than with one of lower radiance. The most intense part of the xenon arc exceeds the carbon arc positive crater by a factor of 20 in radiance at 2500 Å. Moreover, the color temperature of the xenon arc, 6600°K, offers a convenient source to filter since filters tend to reduce the color temperature and the sun has an approximate color temperature of 5500°K in this region. Appropriate dichroic or absorption filters should be chosen only when the 2000 Å to 5000 Å source spectra have been adequately determined. Liquid filters offer some interesting spectral configurations for ultraviolet isolation more than for actual ultraviolet shaping.

Compact arc lamps require an rf starting circuit to initiate the arc and, as in the case of the carbon arc, a current limiting circuit element to maintain the arc at the desired level after the start.

The physics of the enclosed high pressure arc lamp is very similar to that of the carbon arc except that at pressures greater than one atmosphere the voltage drop across the arc increases even more with a given input wattage, and the size of the arc decreases to a still smaller diameter. Stark and pressure broadening increase line widths and there is also an increase in the level of the continuum relative to line radiation. The peak position of spectral lines is shifted generally toward longer wavelengths with higher pressure.

c. 2,000 Å - 50 Å

(1) Purpose and Justification

Electromagnetic radiation within the approximate spectral range of 2,000 Å to 50 Å may be referred to as the vacuum ultraviolet. Shorter wavelengths can be considered to lie in the soft x-ray region. Vacuum ultraviolet radiation is emitted when matter is excited into energy states between which transitions can occur and whose energy differences correspond to the frequencies involved.

Thus, using an electron volt-Angstrom conversion factor of 12,390 the energy equivalent of the 1500 Å to 50 Å wavelength range is 8 electron volts to 240 electron volts. The creation of excited states of matter with such high energies is equivalent to producing temperatures of the order 10^6 degrees Kelvin.

Because of the high level of absorption of most materials, including SiO, in the vacuum ultraviolet the mass absorptive rate in ergs/g-yr is potentially important (Ref. 75). Solar radiation of the wavelength range 500 Å to 1000 Å provides 10^8 ergs/cm^2-yr of ionizing radiation. Penetration ranges at 100 Å to 1000 Å are not well known but probably lie between 10^{-4} and 10^{-7} g/cm^2. The resulting ionization dose of 10^{12} to 10^{15} erg/g-yr will damage the thin layer reached by radiation and will very probably affect optical absorption. Electronic excitation, which is of concern from the vacuum ultraviolet up to 3000 Å, can also affect optical reflectivity. The mechanism for the ionization and excitation damage is roughly one of releasing electrons from their equilibrium positions in the crystal lattice resulting for some cases in trapped electrons and holes or color centers. The amount of radiation absorbed in a color center may be anywhere from 1/10 to 100 times that required to produce the center. Therefore, radiation below 3000 Å can effect the absorption of radiation at longer wavelengths.

Organic materials will also receive 10^{12} to 10^{15} erg/g-yr from sunlight of 100 Å to 1000 Å. Such doses will cause severe degradation to the properties of thin exposed layers of all known polymers. No experimental work has been conducted on polymers in the 100 Å to 1000 Å range and only limited work has been done in the 1000 Å to 3000 Å range.

Material degradation experiments conducted by Moore (Ref. 76) in the vacuum ultraviolet indicated the somewhat anomolous fact that for copper and gold reflecting surfaces overcoated with SiO less degradation in 2500 Å reflectance occurred for samples irradiated by vacuum ultraviolet radiation in a vacuum of 10^{-9} mm mercury than when the sample was exposed to vacuum alone. The previously mentioned, recent findings of Hass support these results at least partially by demonstrating that the reflectivity of SiO overcoated aluminum mirrors can be increased by depositing the film in the presence of ultraviolet radiation.

As mentioned before, some Russian investigators irradiated aluminum and rhodium mirrors with no overcoatings and found that irradiation in the 1700 Å to 1000 Å region caused a drop in reflectivity. Decrease in reflectivity was attributed to oxidation by residual oxygen in the apparatus where the measurements were made. Such a result might also indicate the need for a high vacuum as an environmental condition.

The most difficult potentially harmful region of the solar electromagnetic spectrum to simulate is undoubtedly the vacuum ultraviolet. Regardless of what type of source is chosen for this spectral region a general test configuration suggests itself. In providing radiation below 1050 Å the source precludes the use of any optics. This means not only that the source should be placed as close as possible to the sample, but that certain other precautions may have to be taken because no windows are permitted between source and sample. In particular, if the source requires for its ignition

the presence of a gas at a pressure significantly higher than the vacuum chamber pressure, suitable differential pumping and differential pumping slits must lie between the source and the index aperture to the sample vacuum tank. Such constraints designate the vacuum ultraviolet source as one that by necessity must lie close to the vacuum chamber.

(2) Description of Test Setup

A source developed by Moore seems to offer the advantages of a high, time-integrated source of vacuum ultraviolet radiation. In a WADD Technical Report 60-371 titled, A Source and Detector of Radiation in the Wavelength Region 1500 - 50 Å Suitable for Radiation Effects Studies on Materials in Vacuo, Dr. Moore describes several types of sources for vacuum ultraviolet radiation. The high voltage vacuum spark, the sliding vacuum spark, the gaseous discharge, the x-ray tube, the electron synchrotron, and the high current pulsed discharge. The following is an excerpt from the technical report in which the chosen source, the high current pulsed discharge, is discussed.

"If a large amount of capacitor stored energy is rapidly discharged through a confined tube containing low pressure gas, a strong continuous emission results known in the V.U.V. as the Lyman continuum (Ref. 77)."

"Anderson (Ref. 78) studied this type of continuous emission in the visible region of the spectrum and showed that current densities of order 30,000 amps per sq cm are required in the discharge tube. At shorter wavelengths the continuum has been observed by Rathenau (Ref. 79) and Worley (Ref. 80) to extend extend into the soft x-ray region at about λ100."

Details on the construction, operation and radiative output of the vacuum ultraviolet service will appear in the final report. This source represents an extensive development effort by EOS and was actually used to provide vacuum ultraviolet radiation in a series of space radiation degradation tests.

(3) Test Conditions and Procedures

The sample will be irradiated by the various sources at power levels and in configurations commensurate with spatial constraints and the necessary tank geometry. Suitable masking apertures will be used to avoid an undue level of scattered radiation in the vacuum tank. The sample temperature will be an externally controllable parameter and sample will be tested at suitably high, low, and mean temperatures with the sources' operating at various levels or irradiance both alone and simultaneously with the other radiation sources.

As an index to mirror degradation, absolute, specular, spectral reflectance tests will be conducted as a minimum experiment. The preferred experiment would determine the spectral index of refraction and spectral extinction coefficients referred to as the optical constants. In order to eliminate any effects due to atmospheric exposure following sample irradiation, the sample will be tested under vacuum, in the chamber itself. The minimum in-chamber test would determine absolute, specular, spectral reflectance, while the preferred in-chamber test would determine the optical constants. Data indicating degradation in specular reflectance determined in this manner could be supplemented by an out-of-chamber diffuse reflectance test for a more complete picture of reflectance degradation. An index to the effects of exposure to atmosphere necessary for a interpretation of the diffuse reflectance results could be estimated by following the in-chamber, specular reflectance test under vacuum with an in-chamber specular reflectance test under atmospheric conditions. The latter should of course involve a time delay so as to make the atmospheric specular reflectance test coincide as nearly as possible with the atmospheric diffuse reflectance test. Finally an out-of-chamber determination of the optical constants might be performed.

The out-of-chamber reflectance tests would be performed with a standard double-beam spectrophotometer used separately in the specular mode and diffuse mode. They would be made

absolute in nature by having a mirror surface of known spectral reflectance in the reference beam. The out-of-chamber determination of optical constants in the preferred experiment would be determined by the standard method of irradiating the sample at a known angle to the sample normal with radiation polarized in the plane of incidence and perpendicular to the plane of incidence. The same method would be used in the chamber.

For the in-chamber specular reflectance tests the normal source-detector combinations would be chosen for the various wavelength regions from 2000 Å to 25,000 Å. The light source for the 2000 Å to 2500 Å range may present some difficulty. The radiation will be chopped at the source, collimated, sent into chamber, reflected from sample, sent to focusing lens, and passed through a monochromator to a detector. The chopped radiation for the elimination of background radiation as well as to provide the usual advantages of an ac signal such as drift elimination and ease of amplification. The usual precautions on masking out stray radiation would also be necessary to avoid a strong dc base signal resulting in such difficulties as detector saturation.

The measurement is made absolute by mounting the irradiated sample with a shielded standard so that they may each be alternately measured. Care must be taken to insure the mechanical stability of such a mount, however, because an uncertainty in the deflection of the light beam from one test to the next would invalidate the results.

(4) Anticipated Meaningful Test Duration

As a practical limit up to 10 solar constants will be available depending upon the efficiency of the optics and size of the sample. Due regard should be taken with respect to violations of the reciprocity law (Ref. 81). That is the exposure of a sample to irradiation, defined by the product of the level of irradiance and the time during which the sample is exposed to the radiation, is not always a constant.

If the reciprocity law is assumed to hold and if the other electromagnetic and possibly particle sources can simultaneously supply flux densities of this level, the first test would run approximately three weeks at 24 hours per day. Such a test would hopefully allow degradation predictions to be projected up to at least a year for equivalent space exposures. During the simulated exposure the sources whose outputs are apt to vary with time will either be held constant through a control loop or will be monitored continuously in order that the time averaged outputs over long periods can be made equivalent by proper adjustments.

There is a possibility that electromagnetic flux and particle flux cannot be supplied simultaneously. Care must be taken to avoid overlooking any interactions between the two modes of irradiation. For instance, it is probable that the ultraviolet will strongly degrade organic substrate material over presently contemplated exposive periods. If this is accepted, it is clear that particle irradiation (particularly micrometeoroid) prior to electromagnetic radiation is potentially more harmful than reversing the sequence. It is also clear that a simultaneous irradiation by particle and electromagnetic fluxes will produce yet different results.

If it becomes clearly impossible to irradiate the samples with all fluxes simultaneously and if it is determined that discontinuous short periods or irradiation are equivalent to a continuous long period of irradiation, the samples may be alternately irradiated by particle and electromagnetic sources for successively shorter periods until an extrapolation to a condition of simultaneous irradiation is permitted.

Such a procedure would be inconvenient particularly if it were found important to maintain the sample continuously in a vacuum environment. Still it may also be difficult to have uninterrupted use of some of the particle sources for several weeks at a time.

Finally when degradation is detected in what is considered to be a suitable space environment, the sources will be eliminated, one by one, beginning with the most suspect in an attempt to isolate the causes.

6.3.3 Charged Particles

One of the most hazardous aspects of space flight, damaging to both men and materials, is the extremely high level of charged particle radiation surrounding the earth. These radiations exist primarily in the Van Allen Belts, within the magnetosphere, and in the solar space within the earth's orbit of the sun. Estimates of the flux levels of charged particle radiations and their quality have been collected in Subtask 1.1.

A summary of charged particles, energies, and flux levels in the worst situations that might be encountered by a satellite in an earth orbit has been drawn from Subtask 1.1 for quick reference and is given below in Table 6-1.

TABLE 6-1

CHARGED PARTICLES, ENERGIES, AND FLUX LEVEL SUMMARY

Radiation Type	Energy Range	Flux Part/cm^{2}sec	Orbit Earth Radii
Electrons	> 20 kev	10^{11}	3.5
Electrons	> 150 kev	10^{8}	3.5
Electrons	> 1.6 Mev	10^{5}	3.5
Electrons	> 20 kev	2×10^{10}	1.4
Electrons	> 600 kev	2×10^{8}	1.4
Protons	0.1 to 5 Mev	10^{8}	3.5
Protons	> 30 Mev	3×10^{4}	1.4

Highest levels of damage occur in circular orbits within the Van Allen Belts in an equatorial plane at a distance of 3.5 earth radii. In this orbit the total integrated flux of both electrons and protons experienced by a satellite on a one-year mission are extremely high. These figures are as indicated in Table 6-1.

Although some uncertainty exists, there is sufficient reason to believe there are proton and electron flux levels

in the earth-sun orbit at very low energies (0.5 to 20 kev) in the order of 10^8 to 10^{12} part/cm^2 sec. These fluxes may be encountered outside the protection of the geomagnetic field and in polar orbits.

It is clear from Table 6-1 that equipment for ground simulation of charged particle radiations must include means of reproducing electrons and protons within wide energy ranges and at high flux levels. The energy range for electrons lies between 20 kev and at least 1.6 Mev. The solar electron spectra during flares and steady state emissions are not well defined and cannot be considered at this time. When more data are available it is probable that the energy range will somewhat broaden the electron spectrum within the magnetosphere.

The picture for protons is not quite as simple from the point of view of ground simulation. Van Allen Belt energies range from 0.1 Mev to greater than 30 Mev. Radiations during solar flares are thought to extend into the Bev range. Highest energies within the magnetosphere are found in the inner Van Allen Belt where they have been measured to be greater than 30 Mev.

Choice of equipment for generation of charged particles is also affected by the desirability of performing sample irradiation on an accelerated basis. Irradiation times in the order of 10 hours would be desirable. During this period, the sample could receive an integrated dose equal to the maximum anticipated dose it could receive in space during one year of orbit under worst case conditions. The integrated flux levels encountered could be as high as 10^{19} electrons/cm^2 year and 10^{16} protons/cm^2 year. Equipment capability should provide a factor of 3 to 10 overlap for study purposes and to accommodate the possibility of new space research data yielding increased flux levels.

As a practical measure, consideration has been given to the relative effectiveness of proton-induced damage as a function of energy with a view to simplification of equipment without loss of rigor in the test data. In this program of study of reflecting surfaces

we are primarily concerned with effects that result in direct or indirect injury to the reflectance properties of the mirror. These effects are primarily surface or skin effects. The layer most susceptible to injury is the outermost surface, which is exposed to the full spectra of energies and intensities of the space radiations. This is particularly true when considering low energy charged particle radiations, which have low penetrability in solid materials and a high LET (linear energy transfer) or dE/dx value in the regions close to the surface. In the case of both the electrons and protons of space, the flux levels are highest for the low energy particles. The samples to be tested will have an overlay layer, reflecting layer, and substrate layer. Depending upon the thickness of the overlay, the reflecting layer will encounter a greater or lesser fraction of the radiant energy. Similarly, the substrate will be partially shielded against the soft radiations as a result of the first two layers. Bremsstrahlung radiation, generated in the earlier layers, will be experienced by the succeeding layers. This is a low energy photon radiation having more penetrability than the charged particles themselves. These radiations will penetrate into the substrate and thereby be less directly effective in damaging the reflective layer.

The most deleterious radiation, directly affecting the reflector, will be the low energy electrons and protons since they will deposit most of their energy in the first surfaces encountered. Protons with energies of 2 Mev have a range of about 40 microns. At 5 Mev the range is 300 microns, which is generally beyond the reflective layer and into the substrate. The dE/dx value for the first layers decreases with increasing energy. Since the effect of damage to the substrate on the reflective coating is indirect and coupled with this the fact that the flux rate for proton energies above 30 Mev is down by a factor of approximately 3,000, there is a measure of confidence in determining to neglect proton energies in the range above 5 Mev and even 2 Mev. Although, to be entirely rigorous, it is preferable to test with these high energy protons (> 2 Mev) the practical considerations of

equipment cost and availability of beam time at research centers may preclude testing within workable schedules. Existing accelerator facilities as noted in Table 6-1 are given in Ref. 82. Electrons and protons in the ranges below 5 Mev can be readily generated by more commonly available Van de Graaff particle accelerators or other types in use in various areas of the United States. These facilities are sometimes available on a service basis. In working with these outside facilities, there will be a high degree of inconvenience and lack of flexibility in instrumenting and scheduling. In view of the scope of the work anticipated, there is a good deal of justification for procurement of a particle accelerator specifically for preflight and postflight studies. In this way the work and cost of instrumenting, adapting, and interfacing of test fixtures with the accelerator can be reduced, together with a reduction in travel time, per diem, and transportation costs related to setting up at remote laboratories. For reasons previously given, it has been determined that this study should include tests of the cumulative effects of simultaneously applied electromagnetic and charged particle radiations on the sample materials. This will require the gathering together of a substantial amount of equipment and will necessitate special fixtures and adaptive devices to implement the test. A detailed discussion of this problem is given later in this report.

Special types of transducers and calibrating instruments will be required to accurately measure and record experimental data. Of particular interest in this section is the equipment used for accurately establishing energies and dose levels as required during the conduction of the experiments. Throughout the tests, the charged particle beams will be monoenergetic in origin from the accelerator. Kinetic energy developed by the particles is determined by the voltage potential through which the electron has fallen. Energy, then, is measured and controlled by the voltage settings established for the accelerator. The particle flux applied to the sample is measured by the beam current impinging on the sample. This will be determined by means of a Faraday cup

and electrometer to be provided as a part of the test apparatus. The electrometer output will be recorded against time during test runs to determine stability of the beam current and to determine average outputs during irradiation times.

1. Test Conditions and Procedures

To extract the maximum amount of useful data from the study, there are five types of tests planned for electron and proton damage effects. These are outlined as follows:

a. Damage as a Function of Dose Rate - Df(dI/dt)

This test should be performed first, to determine the validity of accelerated testing. Maximum integrated dose levels will be administered at a number of different dose rates under conditions of constant pressure and temperature (mean value), as previously established. Results of this test will be used to establish the maximum flux rate to be used for the remainder of the test program.

b. Damage as a Function of Energy - Df(E)

Tests will be conducted under pressure and temperature conditions previously established. The purpose of this test is to determine the most damaging energies. Full dose levels will be administered at each energy setting. Representative energy settings will be selected to give sufficient data and depict in graphic form damage versus energy. Information from this test will be basic to analysis of all ground and flight tests.

c. Damage as a Function of Angle of Incidence - $Df(\phi_I)$

The particle flux, as encountered by a surface in space in magnetic fields, will not always appear normal to the surface. This means that a flat surface can experience encounters with particles arriving with angles of incidence anywhere within a solid angle of 2π steradians. A test is planned in which damage is studied as a function of angle of incidence at full dose levels and at minimum, maximum, and mean energies. Degradation of surfaces due to sputtering is a function of angle of incidence.

d. Damage as a Function of Total Dose - Df(I)

Tests will be conducted under pressure and temperature conditions previously established. Dose levels between minimum and maximum limits will be administered to the samples and the extent of damage recorded and plotted as a function of the dose. This will be done at the energy determined under Subsection 1.a to be the most damaging and at a second energy calculated from existing data on space spectra as an average energy figure.

e. Damage as a Result of Full Spectrum, Full Dose Irradiation - $Df(\epsilon I_E)$

Assuming meaningful data are available describing the electron and proton spectra and absolute intensity values, a test can be conducted in which these spectra can be approximated by stepping the accelerator voltage (energy) and controlling intensity at each point. This could be done sequentially. A more desirable method is to modulate or program the applied voltage with time in such a way as to obtain the desired spectrum. This will require modification at the accelerator. This approach is being given further consideration. Successful reproduction of space spectra of electrons and protons would assure the experiments of being entirely rigorous.

Of interest in determining qualities of a reflector having maximum resistance to radiation would be a study of damage as a function of overlay thickness. Thickness of the reflective layer could also be worthy of investigation. Thickness of the substrates are considered to be of lesser importance except for the shielding effect of this layer, on the back side of the reflecting layer, from high energy radiations entering from the back side.

The data from all tests, Subsection 1.a to 1.e, will be used to predict results of flight testing and to correlate with preflight and postflight data.

2. Description of Test Setup

In order to provide the radiation environments as previously discussed and further summarized in Table 6-1, facilities will be required with energy and flux output capabilities as outlined in Table 6-2.

TABLE 6-2

ENERGY AND FLUX OUTPUT CAPABILITIES

Generator-Particle	Energy Range	Output Flux/Part/ cm^2/sec	Max Dose Flux/Part/ cm^2/year	Sample Exposure Time (hrs)
Van de Graaff electrons	10 - 100 kev	3×10^{13}	3×10^{18}	30
Van de Graaff electrons	0.100 - 2 Mev	3×10^{12}	3×10^{15}	0.3
Van de Graaff protons	0.100 - 5 Mev	3×10^{13}	3×10^{16}	0.3
Van de Graaff protons	5 - 30 Mev	No data available		
Cyclotron protons	>30 Mev	10^9	10^{12}	0.3

A Van de Graaff generator as pictured in Fig. 6-9 or similar equipment can be used for electrons and protons below 5 Mev. For practical reasons of availability and cost, and the fact that the 2-to-5 Mev energy range is down by several orders of magnitude from the fluxes in the 0-to-2 Mev range, a 2-Mev accelerator is considered the optimum choice. For similar reasons the use of a cyclotron for > 30 Mev protons has been eliminated. These energies are not found in the 3.5 earth radii orbit, which has been selected as the worst case situation.

In this phase of testing a single accelerator could serve to provide the electrons and protons alternately. These cannot be generated simultaneously by one accelerator. In anticipation of simultaneous

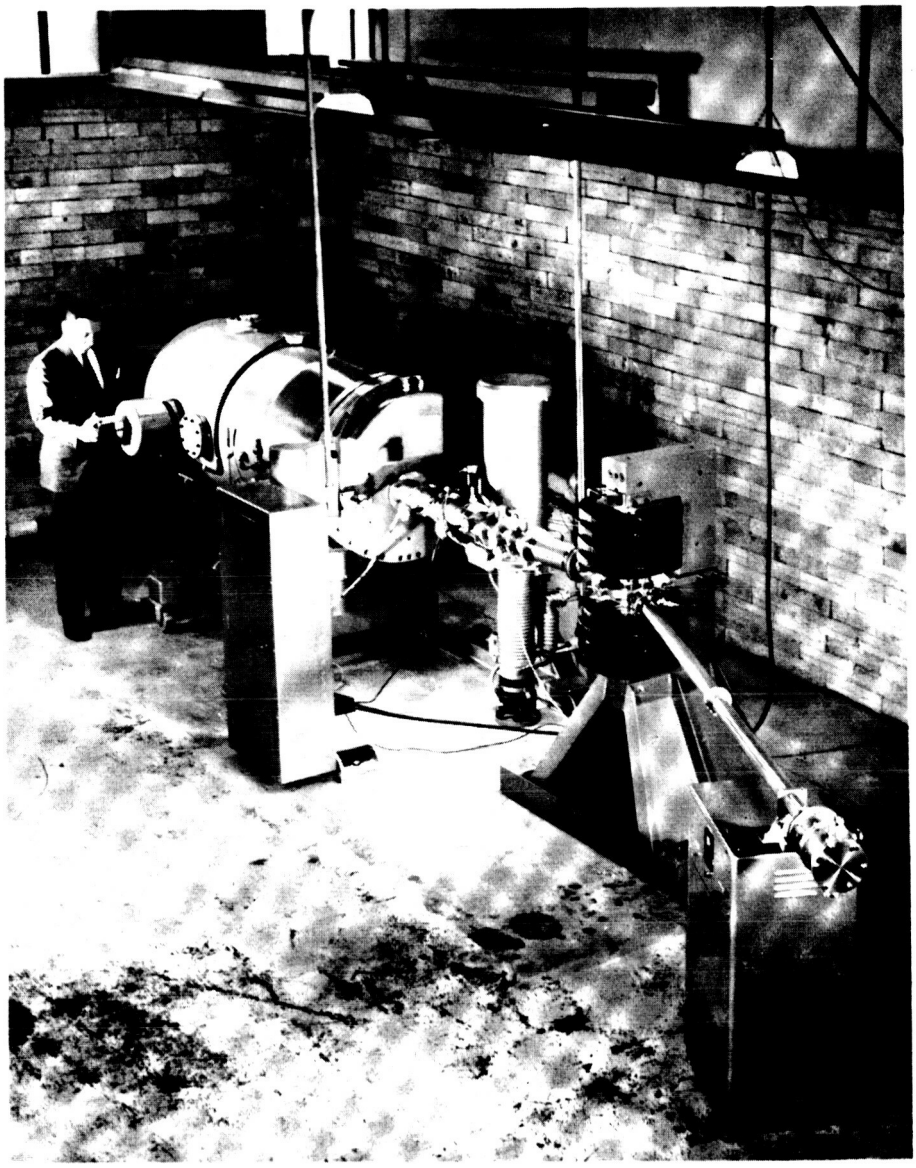

FIG. 6-9 TYPICAL PARTICLE ACCELERATOR EQUIPMENT AND INSTALLATION

generation of both protons and electrons, as described in Subsection 6.3.4, two generators have been shown, and arranged with respect to the sample and fixture, as schematically shown in Fig. 6-10.

Test fixtures will be arranged to provide support of the samples with respect to the accelerator output during the period of irradiation. Either of two methods can be used for analysis: In one instance the sample fixture is arranged for quick insertion and removal of the sample for alternately irradiating and analyzing it; the preferred method is a fixture or irradiation chamber that holds the sample as well as analytical instruments, internally or externally mounted as required for continuous or intermittent measurement and recording of damage as a function of exposure time. The fixture must be capable of holding a vacuum in the areas of 10^{-6} mm Hg and providing temperature control and stability to the samples. The internally mounted sample holder is powered to provide precise angular settings of the sample position within 360° of rotation about the vertical axis perpendicular to the particle beam axis. The vacuum chamber connects with the exit tube of the accelerator and operates at the same vacuum level. Reflective measurements are made with externally mounted sources and detectors. After each irradiation step the sample is re-positioned to the correct position for measurements of reflectance and then returned to its original position. This is done by a servo control externally operated.

During design and fabrication of the irradiation chamber the requirements of Subsection 6.3.4 will also be satisfied to avoid duplication of cost.

6.3.4 Combined EMR and Charged Particles

For reasons given in Subsection 6.2.2, it is desirable to achieve as closely as possible a true representation of the actual environment of an orbiting satellite.

In Subsections 6.3.1, 6.3.2, and 6.3.3, equipment and procedures have been described necessary to achieving thermal, pressure, micrometeoroid, EMR, and charged particle environments individually. As a final test following study of the individual variables it is felt desirable to combine the EMR and charged particle environments in one test. The micrometeoroid effect can be studied under these conditions as a parameter by using sample specimens which have been previously exposed to simulated levels of micrometeoroid bombardment at a number of representative levels. Conversely, samples exposed to the EMR and charged particle radiations can be exposed to various levels of micrometeoroid tests. If there are radical differences in degree of total damages in these two test results, it may be necessary to achieve micrometeoroid irradiation simultaneously with EMR and charged particles. This possibility will be studied further and reported on at a later time.

1. Description of Test Setup

The concept of the test apparatus is given schematically in Fig. 6-11. In addition to the equipment for generating EMR radiations in the region from 23,000 to 50 Å, two accelerators will be used; one for the proton flux and one for electrons. The flux field will be confined to an area of 1 cm^2 to 1 $inch^2$.

Two accelerators are recommended because of the need for simultaneous proton and electron fields. Each accelerator should be adapted so as to program the output beam energy and intensity so that the resultant spectrum closely approximates the actual orbital environment up to the 2 Mev limit of the generators.

Angle of incidence can also be simulated by rotating or rocking the sample surface through predetermined angles from 0° to 180° or even

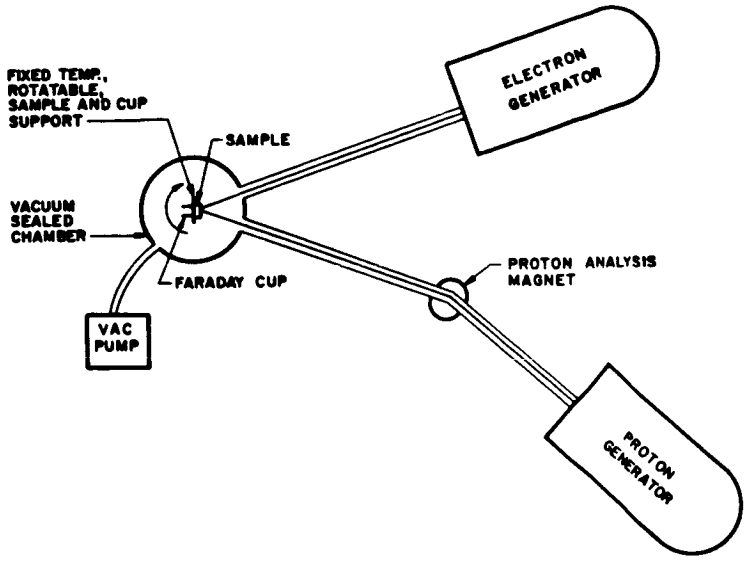

FIG. 6-10

CHARGED PARTICLE SAMPLE IRRADIATION TEST SETUP SCHEMATIC

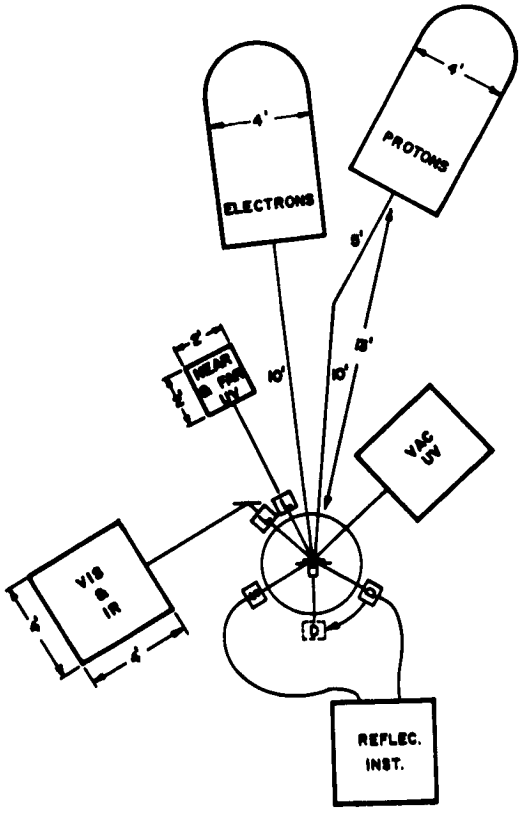

FIG. 6-11

COMBINED EMR CHARGED PARTICLE TEST SETUP (PLAN VIEW)

through 360° if closer investigations indicate this is desired. This rotation serves two purposes: It enables a convenient means of equipment setup so that all beams of particles and EMR radiation do not have to lie in a parallel line; a variation of angle of incidence more closely simulates the space environment. Although radiation in the Van Allen Belts is not isotropic it is only mildly unidirectional and normal to the magnetic lines of force. The effect of the satellite's motion in its orbit and possibly its own rotation, pitch, or yaw, will have the resultant effect on a surface of wide changes in incident angles of the radiations.

Combined electromagnetic radiation and particle tests can be discussed with respect to test equipment layout and anticipated tests. The carbon arc and condenser lenses can be up to 10 feet away from the projector lens. The latter must be fairly close to the chamber window (for instance, 2 feet to 1/2 foot). The carbon arc assembly itself can be considered a box 3 feet by 3 feet by 2 feet. The projector lens and mount would occupy about 1 cubic foot. Because of the relatively large distance between the condenser lens and the projector lens a folding mirror can be inserted, which would allow placement of the source at a fairly large angle to the sample surface normal.

The reflective condenser and refractive projector schematic for the xenon arc would not allow a folded section of the beam while the geometry of the all reflective system seems to create more problems than it solves. The later concept, however, should not be abandoned. The approximate volume for source and condenser is 2 cubic feet, although this will be a somewhat irregular shaped volume whose geometry can be changed if necessary. This volume will lie approximately 4 feet from a window in front of which is situated a projector lens occupying about 1 cubic foot.

The necessarily large component of the pulsed plasma discharge is a cylindrical capacitor approximately 3 feet in diameter and 3 feet high. It will lie on its side and there will be a 2- to 4-foot vacuum line and source extension centered coaxially on it.

2. Test Conditions and Procedures

Preliminary to testing, all source equipment will be calibrated and outputs adjusted so that total exposure of the samples to the correct energies and intensities, concurrently applied, will be accomplished within the period of the test. In instances where pulsed beams are required to control or deliver energies to the sample, the pulsing rate will be sufficiently rapid with respect to angular momentum of the rotating sample as to give representative average fluxes at all angles of incidence.

If spatial or other restrictions do not permit simultaneous irradiation by particle and electromagnetic radiation, the following sequence is suggested:

a. Irradiate first with particle sources and next with electromagnetic for a meaningful time.
b. Switch sequence in a.
c. If effects are noted in either or both a and b, then the possibility of interaction effects is suggested.
d. Since the spatial constraints do not permit simultaneous irradiation by the two types of sources, assume or verify that an interrupted test sequence is equivalent to a continuous test.
e. Next, irradiate the sample alternately with the particle and EMR sources for successively shorter duration periods of successively increasing number so as to keep exposure time constant. (This also calls for an assumption on a predetermined validity of the reciprocity law.)
f. A cautious and admittedly rough extrapolation to an infinite number of periods of infinitesimally short duration or simultaneous irradiation.

The most obvious particle-electromagnetic combination effects that could result from substrate exposure are:

a. Decomposition of polymer chains into smaller fragments giving loss of mechanical strength and elastic deflection as well as degradation of electrical properties.

b. Cross-linking of the chains (more important in space) that would increase mechanical hardness up to a point but would eventually reduce elastic deflection and embrittle other polymers to the point where surface flaking and fracture occur. In addition, the resultant free radicals have characteristic optical absorptions.

6.4 Summary and Conclusion

The purpose of this section is to report the results of the work performed in Task 3.1, Ground Simulation Test Definition. The resulting information has been a tentative outline of the ground testing program as visioned in terms of the data compiled and studies completed up to this time.

The program for ground testing has been outlined in a flow chart-type of schedule. This schedule is tentative but felt to be sound regarding sequence and relative test durations. The first testing phase will establish the temperatures to be used as reference levels during all subsequent testing. This is accomplished by determining the absorptivity, emissivity, and thermal conductivity of each sample type, and substituting these values into the thermal balance equations of Subtask 1.3.

The second phase of the ground test sequence is the performance of two types of tests to observe the resulting reflectivity degradation. One of these test categories is intended to reveal the magnitudes and characteristics of the deleterious effects of electromagnetic radiation upon various samples. The other test category is of equivalent purpose, where the effects of charged particle bombardment is studied. Within each of these categories, detailed tests are described which make possible the eventual analysis and classification of virtually any effect that might be observed. The electromagnetic studies stipulate spectral investigations ranging from the infrared (23,000 Å) to the gamma radiation frequencies. The charged particle studies include electron and proton irradiation in which both flux densities and energy levels are to be varied in order to perpetrate an entirely rigorous test.

A third testing phase is included which provides for simultaneously exposing samples to both categories of environment just discussed. This study should turn up any unusual deleterious effects

that occur in the presence of both environments but not in the presence of either environment separately. As an added note, this test will also reveal any degrading effects that might not occur in the presence of both environments, but do occur in the testing in the second phase previously described.

Additional tests have been discussed and considered desirable. These tests need not fall in the above sequence, but may be performed concurrently. The investigation of the effects of micrometeoroids is one of these. Also, certain protective coatings, which would sublime in space, could be evaluated for their possible usefulness in subsequent space missions requiring solar collectors.

7. FABRICATION PROGRAM

This section discusses the fabrication programs of both the preferred and minimum flight experiments. Both schedule and costing are included. The cost figures are more or less budgetary and are probably accurate to about 10-20% at this time.

7.1 Preferred Flight Experiment

Figure 7-1 shows the recommended schedule for the preferred flight experiment fabrication program and includes launch and early-time data acquisition and analysis. A ten month program is recommended with launch scheduled for nine months after initiation of the contract. The final report should be due at the end of the tenth month. Other reports such as monthly progress and interface reports should be provided where necessary. The list of tasks on the left side of Figure 7-1 is self-explanatory.

Table 7-1 shows the budgetary costing of the preferred flight experiment. The direct labor hours include all the tasks shown on Figure 7-1 and also the manhours for contractor program management, system analysis, and liaison with NASA (Scout office), LTV, and vendors. The cost includes the production of one prototype and three final-design satellites. The travel category assumes the contractor is located on the west coast and must travel to Wallops, Dallas, and the Washington area. The cost of the Scout vehicle is included as GFE.

7.2 Minimum Flight Experiment

The schedule for the minimum flight experiment should be about seven months from contract initiation to instrumentation delivery.

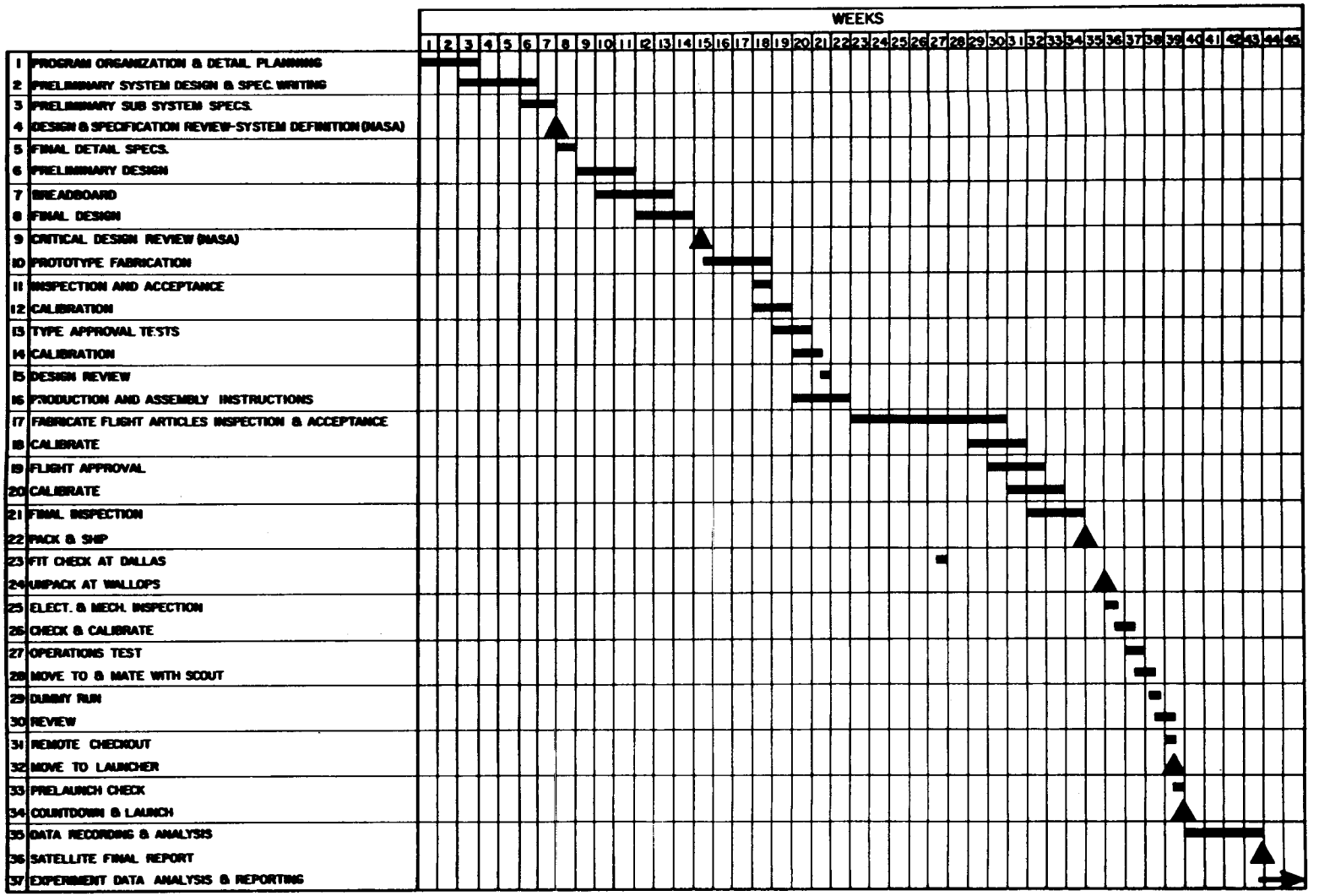

FIG. 7-1 SOLAR CONCENTRATOR REFLECTIVE SURFACE FLIGHT EXPERIMENT SCHEDULE (PREFERRED FLIGHT EXPERIMENT)

TABLE 7-1

PREFERRED FLIGHT EXPERIMENT COST

Direct Labor	61,200 hours	$ 283,000
Publications		7,000
Total Direct Labor		$ 290,000
Overhead (130%)*		$ 377,000
Material	$298,000	
Equipment	53,000	
Computer	6,000	
Travel and Field Services	25,000	
ODC	3,000	
	$385,000	385,000
		$1,052,000
	G&A (10%)*	105,200
		$1,157,200
	Fee (8%)*	92,600
Cost of three satellites, one prototype and services		$1,249,800
Cost of one Scout		$1,000,000

*These values are taken to be representative of the overhead, fee, and G&A of the industry.

The time of P-11 launch cannot be predicted at this time. The tasks on Figure 7-1 apply to the minimum flight experiment with the exception of tasks 23, 24, 28 and 32. The budgetary cost estimate for the minimum flight experiment is shown in Table 7-2. The manhours include the same items as those for the preferred experiment but are less since the minimum experiment involves only the instrumentation and not a complete satellite. Extra manhours were provided for P-11 interface purposes. The material includes one prototype and three flight instruments. The estimated cost of a modified P-11 is also given.

TABLE 7-2

MINIMUM FLIGHT EXPERIMENT COST

Direct Labor	31,600 hours	$147,000
Publications		6,000
Total Direct Labor		$153,000
Overhead (130%)*		$198,900
Material	$64,900	
Equipment	13,500	
Computer	6,200	
Travel and Field Service	12,000	
ODC	2,500	
	$99,100	$ 99,100
		$451,000
	G&A (10%)*	45,100
		$496,100
	Fee (8%)*	39,700
	Cost of three instruments, one prototype and services	$535,800
	Estimated cost of one modified P-11	$700,000

*These values are taken to be representative of the overhead, fee, and G&A of the industry.

8. SUMMARY OF RECOMMENDATIONS

A feasibility study of a flight experiment for accurate determination of the performance of the reflective properties of solar concentrators in space was conducted. A compilation of space environment data was performed and a selection of solar concentrator reflective samples, representative of present solar concentrator programs, was accomplished. Based upon the above, it is predicted that the reflectivity degradation due to the space environment is from less than 1 percent to about 30 percent per year for some samples. The upper value is uncertain because of the dearth of space environment data and ground simulation tests. It is felt that the most severe aspects of the space environment for reflective surfaces are low energy protons, solar ultraviolet radiation, and micrometeoroids. A program of continued ground simulation tests is recommended which should emphasize the above space environment aspects. In accordance with the program requirements a preferred and minimum (with respect to meaningful results and cost) flight experiment feasibility study was conducted. As a result of the study it is felt that both are feasible.

The preferred flight experiment uses the Scout as a launch vehicle with a due east launch from Wallops Island. The orbit has a 4,000 to 5,000 n. mi. altitude apogee, a 300 n. mi. altitude perigee with an angle of inclination of about 37 degrees. The high apogee is designed to expose the reflective samples to greater low-energy proton fluxes than exist at lower altitudes. The ideal exposure for this aspect of the space environment is at about 10,000 n. mi. altitude but the cost of attaining this altitude is prohibitive due to launch vehicle expense. The weight of the preferred experiment satellite is about 70-75 lb and its configuration in

prelaunch and in space, is essentially a cylinder 2 feet in diameter and about 8 inches long. The satellite is spin-stabilized and sun oriented by means of gas jets. The reflective samples (1.5 in. dia.) are mounted on the flat side of the satellite facing the sun. There are 25-28 samples which can be tested. Separation of effects of degradation is accomplished by occluding the sun from some samples so that essentially only particle radiation strikes them, covering other samples with fused quartz so that essentially only electromagnetic radiation strikes them, and exposing the other samples to the total space environment.

The samples are arranged in a circle at the center of which is a rotating arm which is a part of the reflectometer. This arm measures all samples plus 0% and 100% calibrate. The 0% calibrate is a cavity and the 100% calibrate is a fused quartz roof prism. The arm only rotates when measurements are performed and covers the calibrate positions in the standby mode thus leaving the samples exposed. The reflectometer uses a beam splitter and two light sources for redundancy. One light source is an incandescent filament and the other is the virtual image of the sun formed by a segment of a convex spherical reflector illuminated by the sun through a window in the satellite. Six detectors are used giving two broadband or white light reflection measurements (one for each light source) and four spectral measurements via a dispersing prism in the 0.35-2.8 micron region. The rotating bearing is sealed and the drive motor and gears are pressurized for long life. Sample temperature is measured to evaluate performance and to calculate α/ϵ and ϵ. Some of the particle and electromagnetic aspects of the space environment are also measured.

The telemetry system is PCM/FM with a transmitter power of about 50 milliwatts and a transmission bandwidth of 10kc. The power system uses solar cells with secondary batteries and has a minimum capability of 200 watt hours per orbit. Standard NASA tracking stations can be used for data acquisition. The duration of a measurement cycle is about

one minute or it could be longer if the ground station requires. Overall data accuracy should be about 1-2%. The frequency of measurements should be about once every orbit for the first few days of flight, then once per day for a month or so to cover rapid early-time degradation. After this, once a week probably would be sufficient to evaluate long term slopes and minimum experiment duration should be about one year. Since the measurement is performed on command from the ground the above frequencies can be altered to suit the degradations.

The minimum flight experiment uses the P-11 vehicle launched from the Agena. The apogee altitude is about 3,000 n. mi. and the perigee is about 210 n. mi. The angle of inclination and launch location depend upon the Agena. The P-11 has its own telemetry (FM/FM) and power system so only the instrumentation need be provided. Sample access to the skin of the P-11 is difficult since it is covered with solar cells and thermal control surfaces. Also, a protrusion from the P-11 is virtually impossible because of the Agena constraints in the stowed position. A total of ten samples could be mounted in a recessed circle on one of the outboard sections of the P-11. This would require a modification of the vehicle which would increase the cost. Essentially the same type of reflectometer should be used for the minimum experiment as is used for the preferred. Sample temperature measurements should be made and probably some space environment measurements. The exact character of the instrumentation for the P-11 is difficult to define because of the large number of interfaces with this existing vehicle and the modifications required by the instrumentation. The P-11 has a design life of 6 months and will not be actively sun oriented. However, if properly launched the samples can be exposed to the sun for the 6 months lifetime. Overall data accuracy for the minimum experiment is about 5%.

The overall cost of the preferred flight experiment is roughly $2,250,000 which includes launch vehicle, satellite and all necessary services up to launch. The program duration should be about 8-12 months

minimum to launch. The overall cost of the minimum flight experiment is about $1,236,000 which includes the launch vehicle (P-11 only), instrumentation and all necessary services up to launch. This figure is not as accurate as the above because of the uncertainty of the modification costs of the P-11. The program duration for the instrumentation should be about 6 to 8 months but launch dates are strictly a function of available Agena launchings.

REFERENCES

1 U. S. Standard Atmosphere, 1962

2 L. D. Jaffe and J. B. Rittenhouse, Behavior of Materials in Space Environments, TR 32-150, Nov 1961

3 D. D. Carlson, Space Environments and Simulation Requirements, AEDC TDR 62-209, Nov 1962

4 Astronautics, Vol. 7, No. 8, 1962, pp. 54-61

5 R. Jastrow, Inter-Planetary Environment / Lectures in Aerospace Medicine, Jan 1962 (B.A.F.B. School of Aerospace Medicine)

6 B. J. O'Brian, "Review of Studies of Trapped Radiation with Satellite-Borne Apparatus," Space Science Reviews, 1962-1963, pp. 415-484

7 A. C. B. Lovell, Meteor Astronomy, Oxford University Press, 1954

8 F. L. Whipple, J. of Geophys. Res., Vol. 68, No. 17, Sep 1963, pp. 4929-4939

9 Herbert Friedman, "Rocket Spectroscopy," Space Science, John Wiley, 1963, pp. 549-627

10 J. H. Shaw, "Results of Scientific Research in Space," J. Applied Optics, Mar 1962, pp. 87-95 (paper presented at NASA)

11 J. E. Naugle, Proceedings of the Conference on Space-Age Planning (paper presented in Chicago at NASA conference, May 1963)

12 State University of Iowa, Publication No. 1079, Jun and Aug 1962

13 L. A. Frank and J. A. Van Allen, J. of Geophys. Res., Vol. 68, No. 17, Sep 1963

14 B. J. O'Brian, "Radiation Belts," Scientific American, Vol. 208, No. 5, May 1963, pp. 84-96

15 W. P. Saylor, et al., Space Radiation Guide, AMRL-TDR-62-86, 1962

REFERENCES (contd)

16 D. P. Le Galley, Space Science, John Wiley, 1963

17 C. G. S. Goetzel, Lockheed Missiles and Space Company, Space Materials Handbook, Contract AF 04(647)-673, Jan 1962

18 J. A. Van Allen, "Brief Note on the Radiation Belts of the Earth," T.I.D. 7652, Book 1, Nov 1962 (given at a symposium on Protection Against Radiation Hazards in Space)

19 Cain, Chapman, J. of Geophys. Res., Vol. 67, No. 7, Jul 1962

20 J. A. Van Allen, Space Science, John Wiley, 1963, p. 226

21 Alan Rosen, Space Science, John Wiley, 1963, p. 275

22 L. A. Frank, J. Van Allen, W. Whelpley, J. D. Craven, J. of Geophys. Res., Vol. 68, No. 6, pp. 1573, Mar 1963

23 L. R. Davis and J. M. Williams, "Low Energy Trapped Protons," Space Research III, 1962, pp. 365-375

24 J. W. Freeman, "Detection of Low Energy Protons or Ions Trapped in the Inner Radiation Zone," J. of Geophys. Res., Vol. 67, No. 3, Mar 1962, p. 921

25 L. J. Gringuaz, and S. M. Balinda, "On Results of Experiments with Charged Particle Traps in the Second Radiation Belt - Space Research," 1962, pp. 432-437

26 J. Van Allen and Frank Macagno, J. of Geophys. Res., Vol. 68, No. 6, Mar 1963

27 B. J. O'Brian, "Lifetime of Outer Zone Electrons and Their Precipitation into the Atmosphere," J. of Geophys. Res., Vol. 67, No. 10, Sep 1962, pp. 3687-3706

28 B. J. O'Brian, Private Communication, Sep 1963

29 G. S. Hawkins, "The Statistics of Meteors in the Earth's Atmosphere," 1956

30 F. Kreith, "Radiation Heat Transfer for Spacecraft and Solar Power Plant Design," International Textbook Company, Scranton, Penna., 1962, pp. 74-79

REFERENCES (contd)

31 Emerson and Cuming, Inc., Tech. Bull., 6-2-1B, Eccofoam SH

32 E. I. du Pont de Nemours and Co. (Inc.), Tech. Rpt., TR-1 on Properties of Mylar

33 R. E. Gaumer, "Materials for Solar-Energy Systems," Space/Aeronaut. Oct 1961, p. 62

34 E. H. Davison and P. C. Winslow, "Space Debris Hazard Evaluation," NASA Tech. Note, D-1105, 1961

35 R. D. Collins and W. H. Kinard, "The Dependency of Penetration on the Momentum per Unit Area of the Impacting Projectile and the Resistance of Materials to Penetration," NASA Tech. Note, D-238, 1960

36 F. L. Whipple, "The Meteoric Risk to Space Vehicles," Vista in Astronaut., Vol. 1, Pergamon Press, New York, 1958, pp. 115-124

37 R. S. Barnes, "The Effect of the Radiations Encountered by Materials in Space," J. Brit. Interplanetary Soc., Vol. 18, 1962, pp. 377-381

38 R. J. Eichelberger and J. W. Gehring, "Effects of Meteoroid Impacts on Space Vehicles," J. ARS, No. 32, 1962, pp. 1583-1591

39 A. B. Thompson and C. F. Gell, "Meteoroids as a Hazard in Space Flight," (presented at ARS Space Flight Report to the Nation, New York, Oct 1961)

40 J. E. Duberg, "The Meteoric Hazard in the Environment of a Satellite," NASA Tech. Note, D-1248, 1962

41 M. Dubin and C. W. McCracken, "Measurements of Distributions of Interplanetary Dust," Astron. J., Vol. 67, 1962, pp. 248-256

42 F. L. Whipple, "On Meteoroids and Penetration," Adv. in Astron. Sci., Vol. 13, 1963, pp. 590-598

43 W. H. Kinard and R. D. Collins, "An Investigation of High-Velocity Impact Cratering into Nonmetallic Targets and Correlation of Penetration Data for Metallic and Nonmetallic Targets," NASA Tech. Note, D-726, 1961

44 D. L. Anderson, "Ion Bombardment and Its Effects on the Optical Properties of Metals," (paper presented at the American Vacuum Society Meeting, Boston, Mass., Oct 16-18, 1963)

REFERENCES (contd)

45 D. L. Anderson and G. J. Nothwang, "Effects of Sputtering with Hydrogen Ions on Total Hemispherical Emittance of Several Metallic Surfaces," NASA Tech. Note, D-1646, Jan 1963

46 The Boeing Company, Photovoltaic Concentrator Development, Interim Report No. 1, Jul 1962, JPL Contract 950270 (Subcontract under NASA, Contract NAS7-100)

47 C. B. Neel, "Measurement of Thermal-Radiation Characteristics of Temperature-Control Surfaces During Flight in Space," (paper presented at the Ninth National Aerospace Instrumentation Symposium, San Francisco, May 8 1963)

48 C. B. Neel, "Measurement of Thermal-Radiation Characteristics of Temperature-Control Surfaces During Flight in Space," (paper presented at the Ninth National Aerospace Instrumentation Symposium, San Francisco, May 8 1963)

49 C. B. Neel, NASA-Ames Research Center, (private communication)

50 R. Tousey, "Optical Problems of the Satellite," J. Opt. Soc. Am., , Vol. 47, 1957, p. 261

51 L. Page, "Introduction to Theoretical Physics," 3rd Ed., N.Y., 1952

52 W. R. Smythe, "Static and Dynamic Electricity," McGraw-Hill, 2nd Ed., 1950, p. 417

53 Sabersky, "Engineering Thermodynamics," McGraw-Hill, Fig. C-3, 1957

54 Den Hartog, "Mechanical Vibrations," 4th Ed., p. 443

55 Roark, "Formulas for Stress and Strain," 3rd Ed.

56 Jaffe and Rittenhouse, "Behavior of Materials in the Space Environment," JPL TR 32-150

57 R. W. Astheimer, R. DeWaard, and E. A. Jackson, "Infrared Radiometric Instruments on Tiros II," J. Opt. Soc. Am., Vol. 5, Dec 1961

58 P. Hrycak, et al., "The Spacecraft Structure and Thermal Design Considerations," Bell System Tech. J., Vol. 42, Jul 1963, pp. 973-1005

REFERENCES (contd)

59 J. A. Zoutendyk, et al., "Mariner 2 Solar Panel Design and Flight Performance," Transcript of the Photovoltaic Specialists Conference, Vol. II, Interagency Advanced Power Group, PIC-SOL 209/3.1, Jul 1963

60 H. E. Montgomery and S. J. Paddack, "EGO Orbital Parameters and Heat Inputs," NASA Goddard Space Flight Center, Report No. X-643-63-61, Apr 1963

61 G. A. McCue, "Program for Determining the Thermal Environment and Temperature History of Orbiting Space Vehicles," ASD Tech. Note, 61-83, Mar 1962

62 T. O. Thostesen, Jet Propulsion Laboratory, (Private Communication)

63 "Advances in Hypervelocity Techniques," Plenum Press, New York, 1962, M. Krill, Ed.

64 J. Friichtenicht, "Two-Million-Volt Electrostatic Accelerator for Hypervelocity Research," Rev. Sci. Instr., Vol. 33, 1962, pp. 209-212

65 Dr. B. Hammermesh, Space Technol. Lab., Inc., (Private Communication)

66 G. Hass, J. Opt. Soc. Am., Vol. 53, 1963, p. 1096

67 D. W. Gibson, "Studies of the Spectral Energy Distribution of Different Light Sources in Connection with Solar Simulation," (J. Weinard 1962 Proceedings of the Institute of Environmental Sciences)

68 K. T. Compton, J. AIEE, Vol. 46, 1927, p. 1192

69 P. Copeland and W. H. Sparing, J. Applied Phys., Vol. 16, 1945, p. 302

70 G. Hass, J. Opt. Soc. Am., Vol. 53, 1963, p. 1096

71 M. K. Ivanova, et al., "Optika y Spektroskopiya," Vol. IV, 1958, p. 535

72 A phone conversation with Dr. Mostrup of Space Technol. Lab. indicated development of a pulsed vacuum ultraviolet spectral intensity standard.

73 M. Dalton, Applied Optics, (to be published)

REFERENCES (contd)

74 W. A. Baum and L. Dunkelman, J. Opt. Soc. Am., Vol. 40, 1950 p. 782

75 Jet Propulsion Laboratory Technical Report No. 32-150, p. 42

76 WADD Technical Report No. 60-371

77 Jet Propulsion Laboratory Technical Report

78 T. Lyman, "The Reversal of the Hydrogen Series in the Extreme Ultraviolet," Science, Vol. 64, 1926, p. 89

79 J. A. Anderson, "Spectral Energy Distribution of the High-Current Vacuum Tube," Astrophy J., Vol. 75, 1932, p. 394

80 G. Rathenau, "Untersuchung am Absorptionsspektrum von Wasserdumpf und Kohlendioxyd im Gebiet unter 2000 Å," Zeit fur Physik, Vol 87, 1933, p. 32

81 R. E. Worley, "An Improved Source for the Lyman Continuum in the Vacuum Ultraviolet," R.S.I., Vol. 13, 1942, p. 67

82 "World-wide List of Accelerators," American Institute of Physics Handbook, McGraw-Hill, 2nd Ed., pp. 8-176 to 8-221

APPENDIX A

SOLAR COLLECTOR TEST SATELLITE

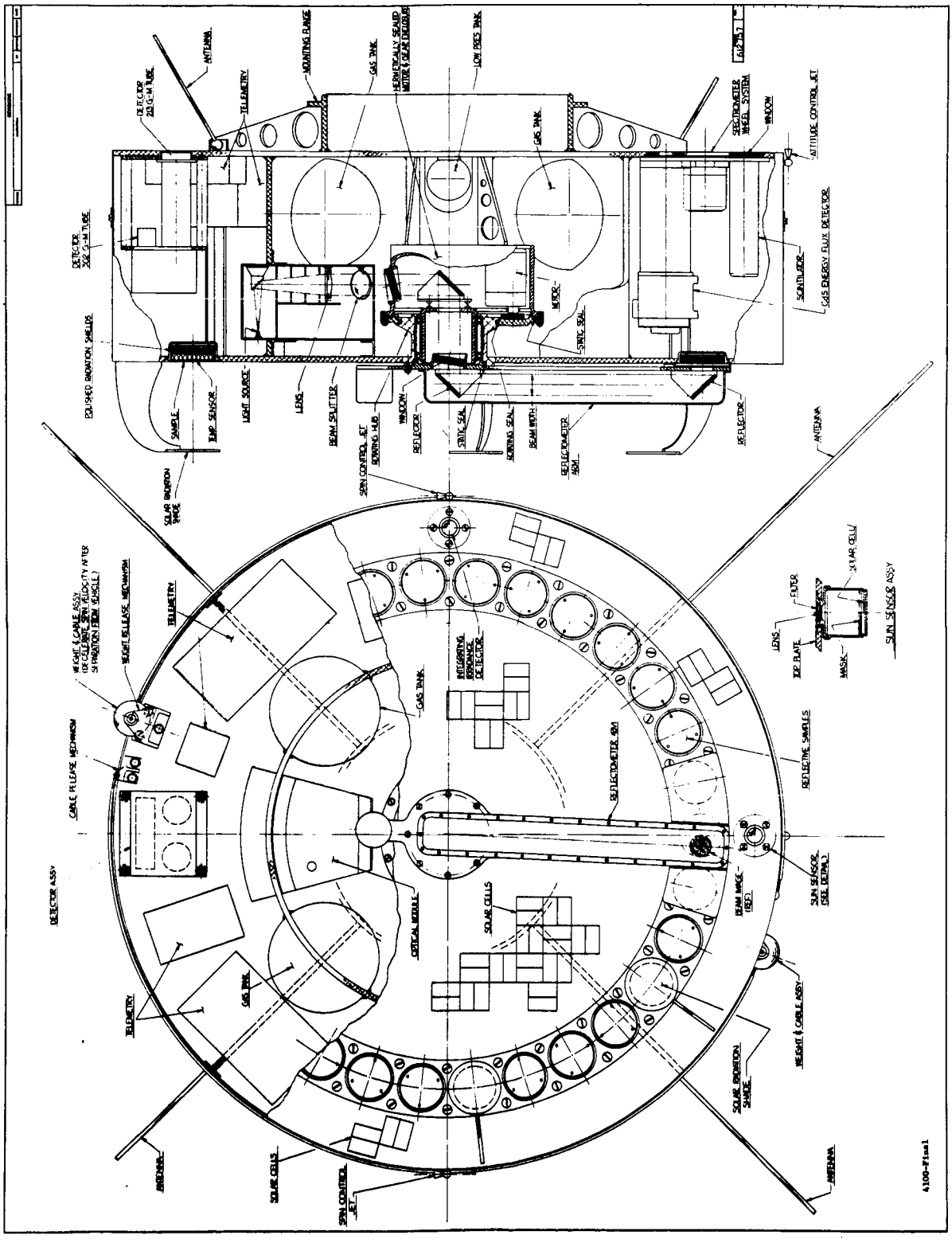

Figure A-1.- Solar collector test satellite.

APPENDIX B

ELECTRICAL INTERCONNECTIONS BETWEEN SUBSYSTEMS

SUBSYSTEM	MODULE	FUNCTION NAME	INPUT/OUTPUT CHARACTERISTICS	MODULE	SUBSYSTEM
Instrument	Det. assy.	28 vdc switched	840 mw during exp.	Pwr. prog.	Telemetry
"	"	Common	---	Battery	Power
"	"	Det. No. 1	0-20 mv into 10 K	Mast.mult.	Telemetry
"	"	Det. No. 2	"	"	"
"	"	Det. No. 3	"	"	"
"	"	Det. No. 4	"	"	"
"	"	Det. No. 5	"	"	"
"	Int. irr. det.	+28 vdc	500 mw continuous	28 vdc reg.	Power
"	"	+28 vdc switched	280 mw during exp.	Pwr. prog.	Telemetry
"	"	Common	---	Battery	Power
"	"	Int. irrad. front	0-20 mv into 100 K	Mast.mult.	Telemetry
"	"	Int. irrad. back	"	"	"
"	Lamp assy.	28 vdc switched	1 watt during exp.	Pwr. prog.	"
"	"	28 vdc	0.3 watts continuous	+28 vdc reg.	Power
"	"	Common	---	Battery	"
"	Inst. motor	28 vdc switched	5 watts during exp.	Pwr. prog.	Telemetry
"	"	Common	---	Battery	Power
"	Inst. sync. gen.	28 vdc switched	84 mw during exp.	Pwr. prog.	Telemetry
"	"	Instrument sync.	5v 2ms into 100 K	Mast.timer	"

SUBSYSTEM	MODULE	FUNCTION NAME	INPUT/OUTPUT CHARACTERISTICS	MODULE	SUBSYSTEM
Instrument	Sample temp.	+28 vdc switched	1.4 watts during exp.	Pwr. prog.	Telemetry
"	"	Common	---	Battery	Power
"	"	Sample No. 1 temp.	0-5 vdc into 100 K	Sub-multip.	Telemetry
"	"	" No. 2 "	"	"	"
"	"	" No. 3 "	"	"	"
"	"	" No. 4 "	"	"	"
"	"	" No. 5 "	"	"	"
"	"	" No. 6 "	"	"	"
"	"	" No. 7 "	"	"	"
"	"	" No. 8 "	"	"	"
"	"	" No. 9 "	"	"	"
"	"	" No. 10 "	"	"	"
"	"	" No. 11 "	"	"	"
"	"	" No. 12 "	"	"	"
"	"	" No. 13 "	"	"	"
"	"	" No. 14 "	"	"	"
"	"	" No. 15 "	"	"	"
"	"	" No. 16 "	"	"	"
"	"	" No. 17 "	"	"	"
"	"	" No. 18 "	"	"	"
"	"	" No. 19 "	"	"	"
"	"	" No. 20 "	"	"	"

SUBSYSTEM	MODULE	FUNCTION NAME	INPUT/OUTPUT CHARACTERISTICS	MODULE	SUBSYSTEM
Instrument	Sample temp.	Sample No. 21 temp.	0-5 vdc into 100 K	Sub-multip.	Telemetry
"	"	" No. 22 "	"	"	"
"	"	" No. 23 "	"	"	"
"	"	" No. 24 "	"	"	"
"	"	" No. 25 "	"	"	"
	"				
Telemetry	Sub-multip.	Sample No. 1 temp.	0-5 vdc into 10 meg.	Sample temp.	Instrument
"	"	" No. 2 "	"	"	"
"	"	" No. 3 "	"	"	"
"	"	" No. 4 "	"	"	"
"	"	" No. 5 "	"	"	"
"	"	" No. 6 "	"	"	"
"	"	" No. 7 "	"	"	"
"	"	" No. 8 "	"	"	"
"	"	" No. 9 "	"	"	"
"	"	" No. 10 "	"	"	"
"	"	" No. 11 "	"	"	"
"	"	" No. 12 "	"	"	"
"	"	" No. 13 "	"	"	"
"	"	" No. 14 "	"	"	"
"	"	" No. 15 "	"	"	"
"	"	" No. 16 "	"	"	"

SUBSYSTEM	MODULE	FUNCTION NAME	INPUT/OUTPUT CHARACTERISTICS	MODULE	SUBSYSTEM
Telemetry	Sub-mult.	Sample No. 17 temp.	0-5 vdc into 10 meg.	Sample temp.	Instrument
"	"	" No. 18 "	"	"	"
"	"	" No. 19 "	"	"	"
"	"	" No. 20 "	"	"	"
"	"	" No. 21 "	"	"	"
"	"	" No. 22 "	"	"	"
"	"	" No. 23 "	"	"	"
"	"	" No. 24 "	"	"	"
"	"	" No. 25 "	"	"	"
"	"	Solar panel temp.	"	Solar panel	Power
"	"	Battery temp.	"	Battery	"
"	"	Transmitter temp.	(Within subsystem)	Transmitter	Telemetry
"	"	Back panel temp.	0-5 vdc into 10 meg.	Back panel	Vehicle
"	"	Spare temp.	"	---	---
"	Inst. and tm. prog.	+28 vdc switched	1.4 watts during exp.	Sample temp.	Instrument
"	"	"	5 watts during exp.	Refl. motor	"
"	"	"	840 mw during exp.	Refl. det. assy.	"
"	"	"	1 watt during exp.	Refl. lamp assy.	"
"	"	"	280 mw during exp.	Int. irrad. det.	"
"	"	"	84 mw during exp.	Inst. sync. gen.	"

SUBSYSTEM	MODULE	FUNCTION NAME	INPUT/OUTPUT CHARACTERISTICS	MODULE	SUBSYSTEM
Telemetry	Inst. and tm. prog.	+28 vdc switched	140 mw during exp.	302 gm tube	Env. Inst.
"	"	"	"	213 gm tube	"
"	"	"	"	"(#2)	"
"	"	"	"	Scint.count.	"
"	"	"	60 mw during exp.	CdS XTAL	"
"	"	"	300 mw during exp.	H.V. supply	"
"	"	"	700 mw peak (10% duty C.) during exp.	Step. motor	"
"	Mast. mult.	Det. No. 1	0-20 mv into 10 meg.	Refl. det. assy.	Instrument
"	"	Det. No. 2	"	"	"
"	"	Det. No. 3	"	"	"
"	"	Det. No. 4	"	"	"
"	"	Det. No. 5	"	"	""
"	"	High-E particles	"	302 gm tube	Env. inst.
"	"	Low-E particles	"	213 gm tube	"
"	"	Medium-E particles	"	"(#2)	"
"	"	Scint. (D.C.)	"	Scint.count.	"
"	"	Scint. (pulse)	"	"	"
"	"	CdS XTAL	"	CdS XTAL	"
"	"	Battery volts check	"	Battery	Power

SUBSYSTEM	MODULE	FUNCTION NAME	INPUT/OUTPUT CHARACTERISTICS	MODULE	SUBSYSTEM
Telemetry	Mast. mult.	Panel volts check	0-20 mv into 10 meg.	Solar panel	Power
"	"	(Spare)	"	---	---
"	"	(Spare)	"	---	---
"	"	+28 vdc check	"	28 vdc reg.	Power
"	"	+13 vdc check	"	13 vdc reg.	"
"	"	Int. irrad. front	"	Int. irrad. det.	Instrument
"	"	Int. irrad. back	"	"	"
"	"	High volts check	"	H.V. supply	Env. inst.
"	"	Xmtr. pwr. out.	(Within subsystem)	Transmitter	Telemetry
"	"	(Spare)	"	"	"
"	Sync.logic	Instrument sync.	5 v 2 msec into 1 meg.	Ins. sync. gen.	Instrument
"	Xmtr. pwr. prog.	+28 vdc	2.2 watts during track	28 vdc reg.	Power
"	Cut-off timer	+28 vdc	40 mw during exp.	"	"
"	Inst.and tm pwr. prog.	+28 vdc	22.9 watts during exp.	"	"
"	"	Common	---	Battery	"
"	Xmtr.	R.F. output	136 mcs PCM-FM, 50 mw, 50 ohms	Antenna	---

SUBSYSTEM	MODULE	FUNCTION NAME	INPUT/OUTPUT CHARACTERISTICS	MODULE	SUBSYSTEM
Telemetry	Com. rcvr.	+13 vdc	100 mw continuously 1.3 watts during command (1/2 sec.)	13 vdc reg.	Power
"	Com. dec.	Common	---	Battery	"
Env. Inst.	302 gm tube	+28 vdc switched	140 mw during exp.	Pwr. prog.	Telemetry
"	"	Common	---	Battery	Power
"	"	High-E particles	0-20 mv into 100 K	Mast.mult.	Telemetry
"	213 gm tube	+28 vdc switched	140 mw during exp.	Pwr. prog.	"
"	"	Common	---	Battery	Power
"	"	Low-E Particles	0-20 mv into 100 K	Mast.mult.	Telemetry
"	"(#2)	+28 vdc switched	140 mw during exp.	Pwr. prog.	"
"	" "	Common	---	Battery	Power
"	" "	Medium-E particles	0-20 mv into 100 K	Mast.mult.	Telemetry
"	Scint.cntr.	+28 vdc switched	140 mw during exp.	Pwr. prog.	"
"	"	Common	---	Battery	Power
"	"	Scint. (D.C.)	0-20 mv into 100 K	Mast.mult.	Telemetry
"	"	Scint. (pulse)	0-20 mv into 100 K	"	"
"	CdS Xtal.	+28 vdc switched	60 mw during exp.	Pwr. prog.	"
"	"	Common	---	Battery	Power
"	"	CdS Xtal.	0-20 mv into 100 K	Mast.mult.	Telemetry
"	H.V. supply	+28 vdc switched	300 mw during exp.	Pwr. prog.	"

SUBSYSTEM	MODULE	FUNCTION NAME	INPUT/OUTPUT CHARACTERISTICS	MODULE	SUBSYSTEM
Env. Inst.	H.V.supply	Common	---	Battery	Power
"	"	H.V. check	0-20 mv into 100 K	Mast.prog.	Telemetry
"	Step.mtr.	+28 vdc switched	700 peak (10% duty cycle) during exp.	Pwr. prog.	"
"	"	Common	---	Battery	Power
Orientation	Attitude ckt.	+28 vdc	280 mw continuously	28 vdc reg.	Power
"	"	Common	---	Battery	"
"	Sol. driver	+28 vdc unreg.	56 watts (0.005% ave. duty cycle)	"	"
"	Att. solenoid	Common	---	"	"
"	Centr. sw.	+28 vdc unreg.	56 watts (2-3, secs 2-3 times/year)	"	"
"	Cw.solenoid	Common	---	"	"
"	Ccw. solenoid	Common	---	"	"
Power	Battery	+28 vdc unreg.	56 watts (0.005% ave. duty cycle)	Sol. driver	Orientation
"	"	"	56 watts (2-3 secs 2-3 times/year)	Centr. sw.	"
"	"	Common	---	Att. ckt.	"
"	"	"	---	Att. sol.	"
"	"	"	---	Cw. sol.	"

SUBSYSTEM	MODULE	FUNCTION NAME	INPUT/OUTPUT CHARACTERISTICS	MODULE	SUBSYSTEM
Power	Battery	Common	---	Ccw. sol.	Orientation
"	"	"	---	302 gm tube	Env. inst.
"	"	"	---	213 gm tube	"
"	"	"	---	"(#2)	"
"	"	"	---	Scint.ctr.	"
"	"	"	---	CdS Xtal.	"
"	"	"	---	H.V.supply	"
"	"	"	---	Step.mtr.	"
"	"	"	---	Lamp assy.	Instrument
"	"	"	---	Inst.motor	"
"	"	"	---	Sample temp.	"
"	"	"	---	Det. assy.	"
"	"	"	---	Int. irr. det.	"
"	"	"	---	Pwr. prog.	Telemetry
"	"	"	---	Com. rcvr.	"
"	"	Battery temp.	0-5 vdc into 100 K	Sub-mult.	"
"	"	Battery volts check	0-20 mv into 100 K	Mast.mult.	"
"	+28 vdc reg.	+28 vdc	280 mw continuously	Att. ckt.	Orientation
"	"	"	300 mw continuously	Lamp assy.	Instrument
"	"	"	500 mw continuously	Int. irr. det.	"

SUBSYSTEM	MODULE	FUNCTION NAME	INPUT/OUTPUT CHARACTERISTICS	MODULE	SUBSYSTEM
Power	+28 vdc reg.	+28 vdc	2.2 watts during track	Xmtr. pwr. prog.	Telemetry
"	"	"	40 mw during exp.	Cut-off timer	"
"	"	"	22.9 watts during exp.	Pwr. prog.	"
"	"	+28 vdc check	0-20 mv into 100 K	Mast.mult.	"
"	+13 vdc reg.	+13 vdc	104 mw continuously 1.3 watts during command (1/2 sec.)	Com. rcvr.	"
"	"	+13 vdc check	0-20 mv into 100 K	Mast.mult.	"
"	Solar panel	Solar panel temp.	0-5 vdc into 100 K	Sub-mult.	"
"	"	Panel volts check	0-20 mv into 100 K	Mast.mult.	"